The role of mitochondrial metabolism during recombinant protein production in CHO cells

A dissertation submitted for the degree of Ph.D.

by

Antonio Alarcón Miguez, M.Sc.

The work here described was conducted under the supervision of

Dr. Donal O'Gorman

Prof. Niall Barron (National Institute for Bioprocessing Research and Training, University College Dublin)

National Institute for Cellular Biotechnology

School of Biotechnology

Dublin City University

JUNE 2022

Declaration

I hereby certify that this material, which I now submit for assessment on the programme of study leading to the award of PhD is entirely my own work, and that I have exercised reasonable care to ensure that the work is original, and does not to the best of my knowledge breach any law of copyright, and has not been taken from the work of others save and to the extent that such work has been cited and acknowledged within the text of my work.

Signed:

Antonio Alarcón Miguez

ID No.: 15212056

Date: 9th June 2022

Table of contents

Declaration i

Table of contents iii

List of Figures and Tables viii

Abbreviations xiv

Publications xviii

Acknowledgments xix

Abstract 1

CHAPTER 1 3

1.1. Chinese Hamster Ovary cell lines as Biopharmaceutical production host. 4

1.2. Cell metabolism and the Warburg effect during recombinant protein production. 6

1.3. Engineering of CHO metabolism. 8

1.3.1. Control of nutrients and metabolites. 8

1.3.1.1 Control of nutrients and metabolites input in the culture. 8

1.3.1.2. Control of cell culture environment. 12

1.3.2. Engineering the expression of key metabolic genes. 14

1.3.2.1. The nuclear genome of CHO cells: engineering key metabolic genes. 15

1.3.2.2. Lactate dehydrogenase and Warburg effect. 19

1.4.Mitochondria as targets for cell line optimisation. 21

1.4.1. Engineering of nuclear-encoded mitochondrial genes 23

1.4.1.1. Peroxisome proliferator-activated receptor-gamma coactivator-1 alpha (PGC1α) 24

1.4.1.2. Dynamin-Related Protein 1 (DRP1) 26

1.4.1.3. Adenine Nucleotide Translocator Isoform 1 (ANT1) 27

1.4.2. Mitochondrial Heteroplasmy 28

1.4.2.1. Characteristics of heteroplasmy 28

1.4.2.2. Heteroplasmy in CHO cells. 33

1.5. Aims and objectives. 35

CHAPTER 2 36

2.1. Cell culture techniques: 37

2.1.1. General cell culture laboratory practices. 37

2.1.2. Cell-Line sub-culturing. 37

2.1.3. Cell density and viability determination. 39

2.1.3.1. Trypan Blue exclusion method 39
2.1.3.2. Flow cytometry (Guava Easycyte™) 39
2.1.3.3. Calculation of growth rate: 40
2.1.4. Cryopreservation of cells. 40
2.1.5. Revival of cryopreserved cells. 41
2.1.6. Transfection of plasmids and siRNA into the CHO cells. 41
2.1.7. Evaluation of transfection efficiency. 42
2.1.8. Generation of stable cell lines 42
2.1.9. Limited dilution cloning. 42
2.2. Molecular biology techniques: 43
2.2.1. RNA extraction and isolation with TRIzol reagent. 43
2.2.2. DNA isolation with Purification kits (Gene Jet, Qiagen, etc). 44
2.2.3. Nucleic acid quantification 45
2.2.3.1. Nanodrop® Spectrophotometer. 45
2.2.3.2. Qubit Fluorometric Quantification 45
2.2.4. Nucleic acid amplification assays. 46
2.2.4.1. Bacterial Transformation 46
2.2.4.2. Primer design and testing 46
2.2.4.3. Routine PCR 47
2.2.4.4. High-Fidelity PCR 48
2.2.5. Gene expression assays 48
2.2.5.1. cDNA synthesis 48
2.2.5.2. Real-time quantitative PCR 49
2.2.6. Next-Generation sequencing. 50
2.2.6.1. Mitochondrial DNA purification 50
2.2.6.2. Library generation 51
2.2.6.3. Next-Generation sequencing 53
2.2.7. Protein expression analysis 54
2.2.7.1. Mitochondrial isolation 54
2.2.7.2. Bradford Assay 55
2.2.7.3. LICOR Western Blot assay 55
2.2.8. ELISA assays 56
2.2.8.1. IgG ELISA quantitation 56
2.2.8.2. hEPO ELISA quantitation. 57
2.2.8.3. Calculation of specific productivity 58
2.3. Metabolism evaluation techniques 58

2.3.1. OROBOROS/OXgraph-2k 58
2.3.2. High-throughput metabolic activity analysis. 59
2.3.2.1. Seahorse XF-96 59
2.3.2.2. Instrument setup 61
2.3.2.3. Seahorse metabolic phenotype assay. 62
2.3.2.4. Seahorse mitochondrial stress assay 62
2.3.2.5. Seahorse glycolytic rate assay 64
2.4. In silico data analysis tools. 66
2.4.1. Plasmid cloning/Maps. 66
2.4.2. Primer generation tools. 66
2.4.3. Gene alignment and sequence homology tools 66
2.4.4. Statistical analysis. 66
CHAPTER 3 68
3.1. Introduction: 69
3.2. Results: 72
3.2.1. Growth and productivity of a set of CHO cell clones exhibiting heteroplasmic variants in mitochondria-encoded CYTB and COX2 72
3.2.1.1. CHO clones differences in growth patterns, growth rate, and viability does not necessarily correlate with mitochondrial content 74
3.2.1.2. Recombinant protein titer of CHO clones does not correlate with the growth phenotype 82
3.2.1.3. The transcript levels of mitochondrial protein-encoding genes in CHO clones does not relate to either heteroplasmy or growth phenotype. 85
3.2.1.4. ``In vivo´´ analysis of both oxidative and glycolytic metabolism using an XF-Flux analyzer reveals similarities in the metabolism of the set of CHO clones 90
3.2.1.5. ``In vivo´´ analysis of glycolytic metabolism using an XF-Flux analyzer Glycolytic Rate assay kit reveals higher glycolytic levels among the SGPCs from the panel of CHO clones. 95
3.2.1.6. Summary of the analysis performed in the panel of CHO clones. 99
3.2.2 Temperature shift influence in the metabolism of CHO cell clones with different heteroplasmy variants. 101
3.2.2.1. Growth arrest and long-term viability increases in a panel of CHO cell clones after the temperature shift. 102
3.2.2.2. Post-temperature shift metabolic analysis of the metabolism reveals changes in the metabolism of SPGCs from the panel of CHO clones. 106
3.2.3. Influence of the growth media used in the metabolism and growth of CHO cell clones with different heteroplasmy variants. 112
3.2.3.1. The influence of the growth media on max viable cell density and viability is significantly more acute in SGPCs from the CHO clone panel. 112

3.2.3.2. Influence of the growth media in the metabolism of the panel of CHO cell clones. 115
3.2.3.3. Summary of media adaptability experiment results. 120
3.3 Discussion. 121
CHAPTER 4 129
4.1 Introduction: 130
4.2. Evaluation of evolution of heteroplasmy in CHO clones derived from CHO-520F 132
4.2.1. Generation of new clones by limited dilution cloning results in changes in heteroplasmy over 20 passages. 132
4.2.1.1. Amplification and purification of mtDNA. 132
4.2.1.2. Analysis of output from mtDNA library sequencing 140
4.2.2. Phenotypical differences found in clones #5 and #6 after 24 passages. 158
4.3. Discussion. 161
CHAPTER 5 167
5.1. Introduction. 168
5.2. Overexpression of PGC1a and DRP1 in CHO-K1-EPO cells. 171
5.2.1. Transient transfection of PGC1a and DRP1 impacts the growth of CHO-K1-EPO cells. 171
5.2.2 Generation of CHO-K1-EPO cell lines stably overexpressing PGC1a and DRP1. 174
5.2.3 Stable overexpression of DRP1 and PGC1a influences growth, viability, and mitochondrial content of CHO-K1-EPO cells. 175
5.2.4 Generation of new CHO-K1-EPO-PGC1α cells to ensure the stable overexpression of PGC1α. 179
5.2.5 Stable overexpression of DRP1 leads to extended viability in CHO-K1-EPO cells in CHO-S-SFMII media, but not in CHO-BalanCD media. 180
5.2.6. PGC1α and DRP1 overexpression induce changes in the recombinant protein titre of transfected CHO-K1-EPO cells. 189
5.3. ANT1 silencing in CHO-K1-EPO cells. 191
5.3.1. Silencing of ANT1 CHO-K1-EPO cells does not significantly change the recombinant protein titre. 195
5.4. Discussion. 195
CHAPTER 6 201
6.1. Reducing leachables and extractables in Single-use bioreactors 202
6.1.1.Introduction: 202
6.2. Different SUB materials impact in CHO-K1 and CHO-DP12 cells. 203
6.2.1 The different E&L released by SUBs have different impacts on CHO cell growth and viability. 203

6.2.2 The different E&L released by SUBs have different impacts on CHO cell metabolism. 206

6.2.3. The different E&L released by SUBs have different impacts on CHO cell glycolytic metabolism. 210

6.3. Combined knockdown of the four pyruvate dehydrogenase complexes and LDHA eliminates lactate production by CHO cells. 214

6.3.1. Introduction: 214

6.4. Analysis of the phenotype and metabolism of Zero Lactate (ZeLa) CHO cells. 215

6.4.1. ZeLa CHO cells exhibit increased oxidative metabolism and diminished glycolytic metabolism compared with wild-type CHO cells. 215

6.4.2. Glycolytic metabolism of the ZeLa CHO cells is confirmed to be diminished compared with the wild-type CHO cells. 218

6.5. Discussion 220

6.5.1. The different E&L released by SUBs negatively impact the growth, viability, and metabolism of CHO cells. 220

6.5.1. The Zero Lactate Cells (ZeLa) show increased oxidative metabolism and reduced media acidification. 221

CHAPTER 7 223

7.1. Conclusions: 224

7.1.1: Evidence of the influence of heteroplasmy in the metabolism of the evaluated CHO clones was not obtained. 224

7.1.2: Heteroplasmy of CHO cells was observed to change throughout passages. 225

7.1.3: Overexpression of DRP1 improved CHO cells culture performance, while overexpression of PGC1α or ANT1 knockdown was detrimental. 227

7.1.4: New model plastic bioreactors can improve the general culture performance of CHO cells. 229

7.1.5: Warburg-Null CHO cells showed decreased lactate generation. 229

7.2. Future Work 230

7.2.1: Future work on heteroplasmy assessment: 230

7.2.2: Future work on heteroplasmy variability over passages : 230

7.2.3: Future work on transfections : 231

7.2.4: Future work on Bioreactor E&L : 231

7.2.5: Future work on Warburg-Null (Zero Lactate) cells : 232

Bibliography and references 233

Annex 1: Supplemental Figures 260

List of Figures and Tables

Figures:

Figure 2. 1. Representation of a functioning Seahorse plate + sensor cartridge. Image from David A. Ferrik et al 2008.---------- 60
Figure 2. 2. Typical profile obtained using Seahorse Mito Stress test kit. Image obtained from Agilent website.---------- 63
Figure 2. 3. Typical profile obtained using Seahorse Glycolytic Rate Assay kit. Image obtained from Agilent website.---------- 65
Figure 3. 1. Heteroplasmy variants found by Kelly et al. 2017 in the panel of 22 CHO clones at genes Cox2 and Cob (CYTB). The figure shows the degree of heteroplasmy corresponding with every mitDNA position in percent of mutant mitochondrial DNA copies over the total mitDNA sequenced. 70
Figure 3. 2. Heteroplasmic variants present in the selected clones. Each bar represent the percent of mtDNA mutant copies containing each variant in the different CHO clones..... 73
Figure 3. 3. Growth profile of CHO clones over the course of 168 hours. Cells were cultured in suspension culture in 5mL of CHO-SFMII media. Each bar represent the average Viable cell density at a given time of biological triplicates measured in triplicates using Guava Easycite cytometer ± SD. Significance was tested using a one-way ANOVA with a <0,05, represented as * in the figure. 76
Figure 3. 4. Viability profile of CHO clones over the course of 168 hours. Cells were cultured in suspension culture in 5mL of CHO-SFMII media. Each bar represent the average viability at a given time of biological triplicates measured in triplicates using Guava Easycite cytometer ± SD. Significance was tested using a one-way ANOVA with a <0,05..... 77
Figure 3. 5. Relative mitochondrial content of CHO clones over the course of 140 hours. Cells were cultured in suspension culture in 5mL of CHO-SFMII media. Each bar represent the average relative mitochondrial content at a given time of biological triplicates measured in triplicates using Guava Easycite cytometer ± SD. Significance was tested using a one-way ANOVA with a <0,05, intra-group significant differences are marked with #, while inter-group significant differences are marked with *. 78
Figure 3. 6. Protein titre from clones after 96 hours in culture. Each bar represent the average protein titre of biological triplicates measured in duplicate by ELISA ± SD. Significance was tested using 1-way ANOVA with a< 0,05..... 84
Figure 3. 7. Relative expression of mitochondrial genes COX1, COX2 and NaD5 in the CHO clones. Each bar represents the RQ for a given gene, calculated using the 2ΔΔcT formula. 87
Figure 3. 8. Relative expression of mitochondrial genes CYTB in the CHO clones. Each bar represents the RQ of CYTB in a certain clone. RQ was calculated using the 2ΔΔcT formula**.** 88
Figure 3. 9. Oxygen consumption rate (OCR) from the CHO clones after 96 hours of culture in each of the three different media tested. Each bar represents the average OCR level of biological triplicates measured in 7 technical replicates using Seahorse XF-96 analyser ± SD. Significance was tested using one-way ANOVA with a<0.05, represented by * in the figure. 92
Figure 3. 10. PER from CHO clones after 96 hours of culture. Each bar represents the average PER of biological replicates measured in 7 technical replicates with Seahorse XF-96 glycolytic rate assay ± SD. Significance was tested using a one-way ANOVA with a <0,05, represented in the figure by *. 97

FIGURE 3. 11. VIABLE CELL DENSITY OF CHO CLONES AFTER 48 (LEFT) AND 72 (RIGHT) HOURS OF CULTURE. CELLS WERE CULTURE IN SUSPENSION CULTURE IN A SHAKER INCUBATOR IN 5ML OF CHO-SFMII MEDIA AT 37ºC OR 31ºC RESPECTIVELY. EACH COLUMN REPRESENTS THE AVERAGE VIABLE CELL DENSITY OF BIOLOGICAL TRIPLICATES MEASURED IN TRIPLICATES USING GUAVA EASYCITE CYTOMETER ± SD. SIGNIFICANCE WAS TESTED USING A ONE-WAY ANOVA WITH A <0,05, MARKED WITH * IN THE FIGURE. 103

FIGURE 3. 12. VIABLE CELL DENSITY OF CHO CLONES AFTER 48 (LEFT), 96 (CENTRE) AND 144 (RIGHT) HOURS OF CULTURE. CELLS WERE CULTURED IN SUSPENSION CULTURE IN A SHAKER INCUBATOR IN 5ML OF CHO-SFMII MEDIA AT 37ºC OR 31ºC RESPECTIVELY. EACH COLUMN REPRESENTS THE AVERAGE VIABLE CELL DENSITY OF BIOLOGICAL TRIPLICATES MEASURED IN TRIPLICATES USING GUAVA EASYCYTE CYTOMETER ± SD. SIGNIFICANCE WAS TESTED USING A ONE-WAY ANOVA WITH A <0,05, MARKED WITH * IN THE FIGURE. 105

FIGURE 3. 13. OXYGEN CONSUMPTION RATE (OCR) FROM CHO CELL CLONES AFTER 48 HOURS OF CULTURE. EACH BAR REPRESENTS THE AVERAGE OCR LEVEL OF BIOLOGICAL TRIPLICATES MEASURED IN 7 TECHNICAL REPLICATES USING SEAHORSE XF-96 ANALYSER ± SD. SIGNIFICANCE WAS TESTED USING ONE-WAY ANOVA WITH A<0.05, REPRESENTED BY * IN THE FIGURE. 107

FIGURE 3. 14. OXYGEN CONSUMPTION RATE (OCR) FROM CHO CELL CLONES AFTER 48 HOURS OF CULTURE. EACH BAR REPRESENTS THE AVERAGE OCR LEVEL OF BIOLOGICAL TRIPLICATES MEASURED IN 7 TECHNICAL REPLICATES USING SEAHORSE XF-96 ANALYSER ± SD. SIGNIFICANCE WAS TESTED USING ONE-WAY ANOVA WITH A<0.05, REPRESENTED BY * IN THE FIGURE. 109

FIGURE 3. 15. VIABLE CELL DENSITY OF CHO CLONES AFTER 72 (LEFT) AND 96 (RIGHT) HOURS OF CULTURE. CELLS WERE CULTURE IN SUSPENSION CULTURE IN A SHAKER INCUBATOR AT 37ºC IN 5ML OF EITHER CHO-SFMII MEDIA OR CHO-BALANCD MEDIA RESPECTIVELY. EACH BAR REPRESENTS THE AVERAGE VIABLE CELL DENSITY OF BIOLOGICAL TRIPLICATES MEASURED IN TRIPLICATES USING GUAVA EASYCITE CYTOMETER ± SD. SIGNIFICANCE WAS TESTED USING A ONE-WAY ANOVA WITH A <0,05, MARKED WITH * IN THE FIGURE. 114

FIGURE 3. 16. OXYGEN CONSUMPTION RATE (OCR) FROM CHO CELL CLONES AFTER 72 HOURS OF CULTURE. EACH BAR REPRESENTS THE AVERAGE OCR LEVELS DURING BASAL AND SPARE RESPIRATION OF BIOLOGICAL TRIPLICATES MEASURED IN 7 TECHNICAL REPLICATES USING SEAHORSE XF-96 ANALYSER MITOCHONDRIAL STRESS ASSAY KIT ± SD. SIGNIFICANCE WAS TESTED USING ONE-WAY ANOVA WITH A<0.05, REPRESENTED BY * IN THE FIGURE. 116

FIGURE 3. 17. EXTRACELLULAR ACIDIFICATION RATE (ECAR) FROM CHO CELL CLONES AFTER 72 HOURS OF CULTURE OVER THE COURSE OF THE ANALYSIS. EACH BAR REPRESENTS THE AVERAGE ECAR LEVEL OF BIOLOGICAL TRIPLICATES MEASURED IN 7 TECHNICAL REPLICATES USING SEAHORSE XF-96 ANALYSER GLYCOLYTIC STRESS ASSAY ± SD. SIGNIFICANCE WAS TESTED USING ONE-WAY ANOVA WITH A<0.05, REPRESENTED BY * IN THE FIGURE. 119

FIGURE 4. 1. THE MITOCHONDRIAL DNA AMPLIFICATION AND THE PRIMERS USED. PRIMER SEQUENCE WAS OBTAINED FROM KELLY ET AL 2014. PRIMERS WERE DESIGNED TO AMPLIFY OVERLAPPING SECTIONS OF THE MTDNA, ENSURING THAT THE TOTAL SEQUENCE IS PRESENT IN THE FINAL SAMPLE. SUBSEQUENTLY, THE REACTION WITH THE BIGGEST PRODUCT (BLUE) WAS NAMED REACTION 1 AND THE REACTION WITH THE SMALLER PRODUCT (GREEN) WAS NAMED REACTION 2. 134

FIGURE 4. 2. AGAROSE 1% GEL CONTAINING THE AMPLICONS OBTAINED FROM A HIGH-FIDELITY PCR AMPLIFICATION OF DNA SAMPLES FROM CHO CLONES USING THE PRIMERS CORRESPONDENT WITH REACTION 1. SAMPLES WERE RUN AT 180V FOR A TOTAL TIME OF 1 HOUR AND 30 MINUTES TO ENSURE PROPER RUN AND SEPARATION. 135

FIGURE 4. 3. PCR AMPLICONS OBTAINED FROM EACH CLONE AFTER PURIFICATION WITH MAGNETIC BEADS. REACTIONS 1 AND 2 SHOULD YIELD AN AMPLICON OF 8814BP AND 7702 BP CORRESPONDINGLY. SAMPLES WERE RUN IN A 1% AGAROSE GEL AT 180V FOR A TOTAL TIME OF 1 HOUR AND 30 MINUTES TO ENSURE

PROPER RUN AND SEPARATION. THIS FIGURE SHOWS ONLY ONE EXAMPLE OF THE MULTIPLE GELS THAT WERE RUN, SPECIFICALLY, SAMPLES FROM THE FOURTH PASSAGE (P4). 136
FIGURE 4. 4. MTDNA FRAGMENT ANALYSIS PERFORMED USING A TAPESTATION DNA SCREENTAPE SYSTEM. THE MOLARITY AND THE AVERAGE FRAGMENT SIZE OF THE MTDNA SAMPLES OBTAINED AFTER TAGMENTATION, AMPLIFICATION AND PURIFICATION OF THE DNA, CALCULATED WITH THE INSTRUMENT, CAN BE SEEN IN THE IMAGE. AS REQUIRED FOR THE LIBRARY GENERATION, THE ANALYSIS OF FRAGMENT SIZE AND MOLARITY WAS LIMITED TO THOSE FRAGMENTS BETWEEN 200-1000 BP. 138
FIGURE 4. 5. MTDNA FRAGMENT ANALYSIS PERFORMED USING A TAPESTATION DNA SCREENTAPE SYSTEM PERFORMED TO ENSURE THE PRESENCE OF THE MTDNA SEQUENCES CORRESPONDING TO THE HIGH-FIDELITY PCR AMPLIFICATION PREVIOUSLY PERFORMED IN THE SAMPLES. 139
FIGURE 4. 6. READ MAPPING OF CHO MTDNA SEQUENCE FROM SAMPLES OF 12 DIFFERENT CLONES AT TWO DIFFERENT TIMEPOINTS (P4 OR P20). EACH BAR REPRESENT THE NUMBER OF READS PER SAMPLE, WITH A COLOR CODE REPRESENTING THE UNIQUE (GREEN), DUPLICATE (BLUE) OR UNMAPPED SECTIONS READ. 140
FIGURE 4. 7. AVERAGE DEPTH OF SEQUENCING, PERFORMED WITH ILLUMINA ISEQ FOR EACH CHO CLONE SAMPLE. 142
FIGURE 4. 8. COVERAGE PER BASE OF MTDNA SEQUENCE FOR EACH CLONE AND TIMEPOINT 143
FIGURE 4. 9. DISTRIBUTION OF ALLELE FREQUENCY IN THE CHO CLONES. THE MINIMUM ALLELE FREQUENCY CALLED WAS 2%. 145
FIGURE 4. 10. PREDICTED NUMBER OF IMPACTFUL VARIANTS PER GENE IN THE CHO CLONES. EACH BAR REPRESENT THE NUMBER OF PREDICTED VARIANTS FOR A GIVEN GENE. ANALYSIS PERFORMED USING SNPEFF ANALYSIS SOFTWARE. 146
FIGURE 4. 11. FREQUENCY OF HETEROPLASMY VARIANTS OF MITOCHONDRIAL RRNA-S, TRNA-VAL AND RRNA-L SEQUENCES FOUND IN THE CHO CLONES USING ISEQ INSTRUMENT AFTER 4 PASSAGES) OR 20 PASSAGES CORRESPONDINGLY. THE COLOUR OF THE HIGHLIGHTED POSITIONS INDICATES THE PREDICTED IMPACT OF THE HETEROPLASMIC MUTATION. 149
FIGURE 4. 12. FREQUENCY OF HETEROPLASMY VARIANTS OF MITOCHONDRIAL NADH3 SEQUENCE FOUND IN THE CHO CLONES USING ISEQ INSTRUMENT AFTER 4 PASSAGES OR 20 PASSAGES CORRESPONDINGLY. THE COLOUR OF THE HIGHLIGHTED POSITIONS INDICATES THE PREDICTED IMPACT OF THE HETEROPLASMIC MUTATION..... 151
FIGURE 4. 13. FREQUENCY OF HETEROPLASMY VARIANTS OF MITOCHONDRIAL COX1 AND COX 2 SEQUENCES FOUND IN THE CHO CLONES USING ISEQ INSTRUMENT AFTER 4 PASSAGES OR 20 PASSAGES CORRESPONDINGLY. THE COLOUR OF THE HIGHLIGHTED POSITIONS INDICATES THE PREDICTED IMPACT OF THE HETEROPLASMIC MUTATION. 153
FIGURE 4. 14. FREQUENCY OF HETEROPLASMY VARIANTS OF MITOCHONDRIAL CYTB SEQUENCE FOUND IN THE CHO CLONES USING ISEQ INSTRUMENT AFTER 4 PASSAGES OR 20 PASSAGES CORRESPONDINGLY. THE COLOUR OF THE HIGHLIGHTED POSITIONS INDICATES THE PREDICTED IMPACT OF THE HETEROPLASMIC MUTATION..... 156
FIGURE 4. 15. VIABLE CELL DENSITY OF THE CHO CLONES OVER THE COURSE OF 196 HOURS. CELLS WERE CULTURED IN SUSPENSION CULTURE IN 5ML OF CHO-SFMII MEDIA. EACH LINE REPRESENT THE AVERAGE VIABLE CELL DENSITY OF BIOLOGICAL TRIPLICATES MEASURED IN TRIPLICATES USING GUAVA EASYCITE CYTOMETER ± SD. SIGNIFICANCE WAS TESTED USING A ONE-WAY ANOVA WITH A <0,05..... 159
FIGURE 4. 16. PROTEIN TITRE FROM CLONES AFTER 96 HOURS IN CULTURE. EACH BAR REPRESENT THE AVERAGE PROTEIN TITRE OF BIOLOGICAL TRIPLICATES MEASURED IN DUPLICATE BY ELISA ± SD. SIGNIFICANCE WAS TESTED USING 1-WAY ANOVA WITH A< 0,05. 160
FIGURE 5. 1. PERCENT OF FLUORESCENT CHO-K1-EPO CELLS AFTER TRANSFECTION. EACH LINE REPRESENT THE AVERAGE GREEN FLUORESCENCE OF BIOLOGICAL TRIPLICATES MEASURED IN TRIPLICATE USING GUAVA EASYCYTE CYTOMETER AND EXPRESSPLUS SOFTWARE..... 172

FIGURE 5. 2. VIABLE CELL DENSITY OF THE TRANSIENTLY TRANSFECTED CHO CELLS OVER THE COURSE OF 144 HOURS. CELLS WERE CULTURED IN SUSPENSION CULTURE IN 5ML OF CHO-SFMII MEDIA. EACH LINE REPRESENT THE AVERAGE VIABLE CELL DENSITY OF BIOLOGICAL TRIPLICATES MEASURED IN TRIPLICATES USING GUAVA EASYCITE CYTOMETER ± SD. SIGNIFICANCE WAS TESTED USING A ONE-WAY ANOVA WITH A <0,05. 173

FIGURE 5. 3. VIABLE CELL DENSITY OF THE STABLY TRANSFECTED CHO CELLS OVER THE COURSE OF 144 HOURS. CELLS WERE CULTURED IN SUSPENSION CULTURE IN 5ML OF CHO-SFMII MEDIA. EACH LINE REPRESENT THE AVERAGE VIABLE CELL DENSITY OF BIOLOGICAL TRIPLICATES MEASURED IN TRIPLICATES USING GUAVA EASYCYTE CYTOMETER ± SD. SIGNIFICANCE WAS TESTED USING A ONE-WAY ANOVA WITH A <0,05 (* IN THE FIGURE)..... 176

FIGURE 5. 4. RELATIVE MITOCHONDRIAL CONTENT OF CHO CLONES AFTER 72 HOURS OF CULTURE. EACH BAR REPRESENT THE AVERAGE MITOCHONDRIAL CONTENT OF BIOLOGICAL TRIPLICATES MEASURED WITH A FLOW CYTOMETER (GUAVA EASYCYTE) AFTER BEING INCUBATED WITH MITOTRACKER GREEN DYE. SIGNIFICANCE WAS TESTED USING A ONE-WAY ANOVA WITH A <0,05 (* IN THE FIGURE). 177

FIGURE 5. 5. RELATIVE EXPRESSION PGC1A IN THE TRANSFECTED CHO CELLS. EACH BAR REPRESENTS THE RQ FOR GIVEN SAMPLE, CALCULATED USING THE 2ΔΔCT FORMULA. FOR EACH SAMPLE, BIOLOGICAL TRIPLICATES WERE MEASURED IN TRIPLICATES. 180

FIGURE 5. 6. VIABLE CELL DENSITY OF THE STABLY TRANSFECTED CHO CELLS OVER THE COURSE OF 120 HOURS. CELLS WERE CULTURED IN SUSPENSION CULTURE IN 5ML OF CHO-SFMII MEDIA. EACH LINE REPRESENT THE AVERAGE VIABLE CELL DENSITY OF BIOLOGICAL TRIPLICATES MEASURED IN TRIPLICATES USING GUAVA EASYCYTE CYTOMETER ± SD. SIGNIFICANCE WAS TESTED USING A ONE-WAY ANOVA WITH A <0,05 AND HIGHLIGHTED WITH * IN THE FIGURE. 182

FIGURE 5. 7. VIABLE CELL DENSITY OF THE STABLY TRANSFECTED CHO CELLS OVER THE COURSE OF 264 HOURS. CELLS WERE CULTURED IN SUSPENSION CULTURE IN 5ML OF CHO BALANCD MEDIA. EACH LINE REPRESENT THE AVERAGE VIABLE CELL DENSITY OF BIOLOGICAL TRIPLICATES MEASURED IN TRIPLICATES USING GUAVA EASYCYTE CYTOMETER ± SD. SIGNIFICANCE WAS TESTED USING A ONE-WAY ANOVA WITH A <0,05 AND HIGHLIGHTED WITH * IN THE FIGURE. 183

FIGURE 5. 8. RELATIVE EXPRESSION OF PGC1A IN THE TRANSFECTED CHO CELLS (CHO-K1-EPO-PGC1A-AT#4). EACH BAR REPRESENTS THE RQ FOR GIVEN SAMPLE, CALCULATED USING THE 2ΔΔCT FORMULA. FOR EACH SAMPLE, BIOLOGICAL TRIPLICATES WERE MEASURED IN TRIPLICATES. NUMBERS IN BRACKETS REPRESENT THESE DIFFERENT CELL POPULATIONS. 185

FIGURE 5. 9. RELATIVE EXPRESSION OF PPARD IN THE TRANSFECTED CHO CELLS. EACH BAR REPRESENTS THE RQ FOR GIVEN SAMPLE, CALCULATED USING THE 2ΔΔCT FORMULA. FOR EACH SAMPLE, BIOLOGICAL TRIPLICATES WERE MEASURED IN TRIPLICATES. 187

FIGURE 5. 10. RELATIVE EXPRESSION OF MNF1 IN THE TRANSFECTED CHO CELLS. EACH BAR REPRESENTS THE RQ FOR GIVEN SAMPLE, CALCULATED USING THE 2ΔΔCT FORMULA. FOR EACH SAMPLE, BIOLOGICAL TRIPLICATES WERE MEASURED IN TRIPLICATES. 188

FIGURE 5. 11. PROTEIN TITRE FROM STABLY TRANSFECTED CHO-K1 CELLS. EACH BAR REPRESENT THE AVERAGE PROTEIN TITRE OF BIOLOGICAL TRIPLICATES MEASURED IN DUPLICATE BY ELISA ± SD. SIGNIFICANCE WAS TESTED USING 1-WAY ANOVA WITH A< 0,05 AND HIGHLIGHTED WITH * IN THE FIGURE. 190

FIGURE 5. 12. RELATIVE EXPRESSION OF ANT1 IN THE CHO CELLS TRANSFECTED WITH SIRNA. EACH BAR REPRESENTS THE RQ FOR GIVEN SAMPLE, CALCULATED USING THE 2ΔΔCT FORMULA. FOR EACH SAMPLE, BIOLOGICAL TRIPLICATES WERE MEASURED IN TRIPLICATES. 192

FIGURE 5. 13. VIABLE CELL DENSITY OF THE SIRNA TRANSFECTED CHO CELLS OVER THE COURSE OF 96 HOURS. CELLS WERE CULTURED IN SUSPENSION CULTURE IN 5ML OF CHO SFMII MEDIA. EACH LINE REPRESENT THE AVERAGE VIABLE CELL DENSITY OF BIOLOGICAL TRIPLICATES MEASURED IN TRIPLICATES USING GUAVA EASYCYTE CYTOMETER ± SD. SIGNIFICANCE WAS TESTED USING A ONE-WAY ANOVA WITH A <0,05 AND HIGHLIGHTED WITH * IN THE FIGURE. 193

FIGURE 5. 14. PROTEIN TITRE FROM SIRNA TRANSFECTED CHO-K1 CELLS. EACH BAR REPRESENT THE AVERAGE PROTEIN TITRE OF BIOLOGICAL TRIPLICATES MEASURED IN DUPLICATE BY ELISA ± SD. SIGNIFICANCE WAS TESTED USING 1-WAY ANOVA WITH A< 0,05 AND HIGHLIGHTED WITH * IN THE FIGURE. 194
FIGURE 6. 1. VIABLE CELL DENSITY OF CHO-K1 CELLS AFTER 96 HOURS OF CULTURE. CELLS WERE CULTURED IN SUSPENSION CULTURE IN 5ML OF THE CORRESPONDING MEDIA. EACH LINE REPRESENT THE AVERAGE VIABLE CELL DENSITY OF BIOLOGICAL TRIPLICATES MEASURED IN TRIPLICATES USING GUAVA EASYCYTE CYTOMETER ± SD. SIGNIFICANCE WAS TESTED USING A ONE-WAY ANOVA WITH A <0,05 AND HIGHLIGHTED WITH * IN THE FIGURE. 204
FIGURE 6. 2.) VIABLE CELL DENSITY OF CHO- DP12 CELLS AFTER 96 HOURS OF CULTURE. CELLS WERE CULTURED IN SUSPENSION CULTURE IN 5ML OF THE CORRESPONDING MEDIA. EACH LINE REPRESENT THE AVERAGE VIABLE CELL DENSITY OF BIOLOGICAL TRIPLICATES MEASURED IN TRIPLICATES USING GUAVA EASYCYTE CYTOMETER ± SD. SIGNIFICANCE WAS TESTED USING A ONE-WAY ANOVA WITH A <0,05 AND HIGHLIGHTED WITH * IN THE FIGURE. 205
FIGURE 6. 3. OXYGEN CONSUMPTION RATE (OCR) FROM CHO-K1 AFTER 96 HOURS OF CULTURE IN EACH OF THE THREE DIFFERENT MEDIA TESTED. EACH BAR REPRESENTS THE AVERAGE OCR LEVEL OF BIOLOGICAL TRIPLICATES MEASURED IN 9 TECHNICAL REPLICATES USING SEAHORSE XF-96 ANALYSER ± SD. SIGNIFICANCE WAS TESTED USING ONE-WAY ANOVA WITH A<0.05, REPRESENTED BY * IN THE FIGURE. 208
FIGURE 6. 4. OXYGEN CONSUMPTION RATE (OCR) FROM CHO-DP12 AFTER 96 HOURS OF CULTURE IN EACH OF THE THREE DIFFERENT MEDIA TESTED. EACH BAR REPRESENTS THE AVERAGE OCR LEVEL OF BIOLOGICAL TRIPLICATES MEASURED IN 9 TECHNICAL REPLICATES USING SEAHORSE XF-96 ANALYSER ± SD. SIGNIFICANCE WAS TESTED USING ONE-WAY ANOVA WITH A<0.05, REPRESENTED BY * IN THE FIGURE. 209
FIGURE 6. 5. GLYCOPER FROM CHO-K1 AFTER 96 HOURS OF CULTURE IN EACH OF THE THREE DIFFERENT MEDIA TESTED. EACH BAR REPRESENTS THE AVERAGE GLYCOPER LEVEL OF BIOLOGICAL TRIPLICATES MEASURED IN 9 TECHNICAL REPLICATES USING SEAHORSE XF-96 ANALYSER ± SD. SIGNIFICANCE WAS TESTED USING ONE-WAY ANOVA WITH A<0.05, REPRESENTED BY * IN THE FIGURE. 211
FIGURE 6. 6. GLYCOPER FROM CHO-DP12 AFTER 96 HOURS OF CULTURE IN EACH OF THE THREE DIFFERENT MEDIA TESTED. EACH BAR REPRESENTS THE AVERAGE GLYCOPER LEVEL OF BIOLOGICAL TRIPLICATES MEASURED IN 9 TECHNICAL REPLICATES USING SEAHORSE XF-96 ANALYSER ± SD. SIGNIFICANCE WAS TESTED USING ONE-WAY ANOVA WITH A<0.05, REPRESENTED BY * IN THE FIGURE. 212
FIGURE 6. 7. VIABLE CELL DENSITY OF ZERO LACTATE (ZELA) AND WT CHO CELLS AFTER 96 HOURS OF CULTURE. CELLS WERE CULTURED IN SUSPENSION CULTURE IN 5ML OF CD-CHO MEDIA. EACH BAR REPRESENT THE AVERAGE VIABLE CELL DENSITY OF BIOLOGICAL TRIPLICATES MEASURED IN TRIPLICATES USING GUAVA EASYCYTE CYTOMETER ± SD. SIGNIFICANCE WAS TESTED USING A ONE-WAY ANOVA WITH A <0,05 AND HIGHLIGHTED WITH * IN THE FIGURE. 216
FIGURE 6. 8. OXYGEN CONSUMPTION RATE (OCR) FROM ZERO LACTATE (ZELA) AND WT CHO CELLS AFTER 96 HOURS OF CULTURE. EACH BAR REPRESENTS THE AVERAGE OCR LEVEL OF BIOLOGICAL TRIPLICATES MEASURED IN 15 TECHNICAL REPLICATES USING SEAHORSE XF-96 ANALYSER ± SD. SIGNIFICANCE WAS TESTED USING ONE-WAY ANOVA WITH A<0.05, REPRESENTED BY * IN THE FIGURE. 217
FIGURE 6. 9. GLYCOPER FROM ZERO LACTATE (ZELA) AND WT CHO CELLS AFTER 96 HOURS OF CULTURE. EACH BAR REPRESENTS THE AVERAGE GLYCOPER LEVEL OF BIOLOGICAL TRIPLICATES MEASURED IN 15 TECHNICAL REPLICATES USING SEAHORSE XF-96 ANALYSER ± SD. SIGNIFICANCE WAS TESTED USING ONE-WAY ANOVA WITH A<0.05, REPRESENTED BY * IN THE FIGURE. 219

Tables:

TABLE 1. 1. PROTEIN-ENCODING MITOCHONDRIAL GENES AND THEIR POSITIONS WITHIN THE MITOCHONDRIAL GENOME. 22

TABLE 2. 1. VOLUMES USED ON ROUTINE ADHERENT CULTURE. VOLUMES INCLUDE, FROM LEFT TO RIGHT, DMEM-F12 CULTURE MEDIA VOLUME USED FOR CULTURE, PBS VOLUME USED FOR WASH, TRYPSIN-EDTA VOLUME USED TO DETACH THE CELLS FROM THE FLASK, AND THE DMEM-F12 CULTURE MEDIA VOLUME ADDED TO THE TRYPSIN AFTER INCUBATION TO INHIBIT IT..... 38

TABLE 2. 2. EXAMPLE OF TYPICAL ROUTINE PCR TEMPLATE TO PREPARE THE REACTION. THE DNA VOLUME USED DEPENDED ON THE DETAILS OF THE EXPERIMENT BEING PERFORMED. NUCLEASE-FREE WATER WAS ADDED TO MAKE THE TOTAL VOLUME EQUAL TO 25μL..... 47

TABLE 2. 3. PCR CONDITIONS USED FOR TAQ 2X PCR. THE ANNEALING TEMPERATURE WAS DETERMINED FOR EVERY REACTION DEPENDING ON THE DNA TEMPLATE AND THE PRIMERS USED**.**..... 47

TABLE 2. 4. EXAMPLE OF TYPICAL HF-PCR TEMPLATE TO PREPARE THE REACTION. THE MTDNA VOLUME USED DEPENDED ON THE LOWEST CONCENTRATED SAMPLE. NUCLEASE-FREE WATER WAS ADDED TO MAKE THE TOTAL VOLUME EQUAL TO 25μL OR 50μL**.**..... 48

TABLE 2. 5. PCR CONDITIONS USED FOR HIGH-FIDELITY PCR..... 48

TABLE 2. 6. EXAMPLE OF TYPICAL RT-PCR TEMPLATE TO PREPARE THE REACTION MIX..... 49

TABLE 2. 7. PCR CONDITIONS USED FOR RT-PCR REACTIONS**.**..... 49

TABLE 2. 8. EXAMPLE OF TYPICAL RT-QPCR TEMPLATE TO PREPARE THE REACTION MIX..... 50

TABLE 2. 9. PCR CONDITIONS USED FOR RT-PCR REACTIONS..... 50

TABLE 2. 10. PCR REACTION SETUP FOR INDEXED DNA AMPLIFICATION..... 52

TABLE 3. 1. CLASSIFICATION OF THE CHO CLONES IN ``FAST´´ OR ``SLOW´´ GROWTH CLONES DEPENDING IN THEIR SPECIFIC GROWTH RATE. CLONES WITH LESS THAN 0,023 CELL DIVISIONS/HOUR WERE CONSIDERED ``SLOW PHENOTYPE ´´ WHILE CLONES WITH MORE THAN 0,023 CELL DIVISIONS/HOUR WERE CONSIDER HAVING A ``FAST PHENOTYPE´´. 74

TABLE 3. 2. GROWTH RATE (CELL DIVISIONS/HOURS), DOUBLING TIME (HOURS) AND NUMBER OF DUPLICATIONS CALCULATED FOR THE EVALUATED PANEL OF CHO CLONES FROM THE GROWTH DATA SEEN IN FIGURE 3.9 (LOWER HALF). THESE PARAMETERS WERE CALCULATED TAKING INTO ACCOUNT THE FIRST 96 HOURS OF CULTURE. 79

TABLE 4. 1.SAMPLES SELECTED FOR THE SEQUENCING EXPERIMENT. EACH SAMPLE CORRESPOND TO A WHOLE MTDNA SEQUENCE OBTAINED AFTER MIXING THE TWO PCR REACTIONS PERFORMED PER CLONE, WEEK AND PASSAGE NUMBER. THESE SAMPLES WERE NORMALIZED TO 1 NG/ μL AND USED TO PREPARE THE INDEXED MTDNA LIBRARY USING THE NEXTERA XT DNA LIBRARY PREP KIT. 137

Abbreviations

- **ALT1:** Alanine Aminotransferase I.
- **ANT1:** Adenine Nucleotide Translocator isoform 1.
- **BalanCD:** BalanCD CHO Growth A.
- **BAT:** Brown Adipose Tissue.
- **BER:** Base-excision repair.
- **bDtBPP:** tris 2,4-di-tert-butyl phenyl-phosphite.
- **CCF:** CO_2 Contribution Factor.
- **CCL:** Continuous Cell Line.
- **CHO cell:** Chinese Hamster Ovary cell.
- **CHO-S-SFM:** CHO-S-Serum Free Media II.
- **COX1/COX2:** Mitochondrial Cytochrome c Oxidase gene 1 or 2.
- **CRISPR**: Clustered Regularly Interspaced Short Palindromic Repeats.
- **CYTB/CYB gene:** mitochondrial cytochrome b gene.
- **DCA:** dichloroacetate.
- **DFHR:** Dihydrofolate reductase.
- **2-DG:** 2-Deoxy-D-glucose.
- **DRP1:** Dynamin Related Protein 1.
- **DTE protein:** Difficult to Express protein.
- **E&L:** Extractables and Leachables**.**
- **ECAR:** Extracellular Acidification Rate.
- **ER:** Endoplasmic Reticulum.
- **ERR*α*:** Estrogen-Related Receptor α.

- **ETS:** Electron Transport System.
- **FA:** Fatty Acids.
- **FCCP:** Carbonyl cyanide 4-(trifluoromethoxy)phenylhydrazone.
- **FGPC**: Fast Growth Phenotype CHO cell clone.
- **GALK1:** Galactokinase 1.
- **GS:** Glutamine synthetase.
- **GLUT**: Glucose Transporters.
- **IFN:** Interferon.
- **IgG:** Immunoglobulin G.
- **LDH:** Lactate Dehydrogenase.
- **LHON:** Lieber Hereditary Optic Neuropathy.
- **LHP:** Length heteroplasmy.
- **mAB:** Monoclonal Antibody.
- **MAF:** Minor Allele Frequency.
- **MELAS:** Mitochondrial encephalomyopathy and lactic acidosis with stroke-like episodes.
- **MERRF:** Myoclonic Epilepsy and ragged red fiber.
- **MFA:** Metabolic Flux Analysis.
- **miRNA:** micro RNA.
- **MMEJ:** microhomology-mediated end joining.
- **MPA:** Metabolic Phenotype Assay.
- **MPC:** Mitochondrial pyruvate carrier.
- **mtDNA:** mitochondrial DNA.
- **mtRNA:** mitochondrial RNA.

- **NGS:** Next Generation Sequencing.
- **NIAS:** Non-Intentionally Added Substance.
- **NPCs:** Normal Proliferating Cells (as opposed to Cancer cells).
- **NRF:** Nuclear Respiratory Factor.
- **OCR:** Oxygen Consumption Rate.
- **OXPHOS:** Oxidative Phosphorylation.
- **PDH:** Pyruvate Dehydrogenase.
- **PER:** Proton Efflux Rate.
- **PDK/PDHK:** Pyruvate Dehydrogenase Kinase.
- **PGC1α:** Peroxisome proliferator-activated receptor-gamma coactivator-1 alpha.
- **PGC1β:** Peroxisome proliferator-activated receptor-gamma coactivator-1 beta.
- **Phe:** Phenilalanine.
- **PHP:** Point Heteroplasmy.
- **PCR (gene):** PGC-1-Related Coactivator.
- **PCR (assay):** Polymerase Chain Reaction.
- **Pro:** Proline.
- **PYC2:** Pyruvate Carboxylase gene.
- **ROS:** Reactive Oxygen Species.
- **Rot/AA:** Rotenone/Antimycin A.
- **ROX:** Residual Oxygen Consumption.
- **R-Protein:** Recombinant Protein.
- **rRNA:** ribosomal RNA.
- **SEAP:** Secreted Alanine Phosphatase.
- **SD:** Standard Deviation.

- **SGLT:** Sodium-like Glucose Transporters.
- **SGPC:** Slow Growth Phenotype CHO cell clone.
- **SGR**: Specific Growth Rate**.**
- **siRNA:** Small interfering RNA.
- **SLC25A4:** Solute Carrier Family 25 member 4. Another name for ANT1.
- **SNP:** Single Nucleotide Polymorphism.
- **S-rRNA:** small ribosomal RNA.
- **SUB:** Single-use bioreactors.
- **TALENS:** Transcription activator-like effector nuclease.
- **TAUT:** Taurine Transporter.
- **TCA:** Tricarboxylic Acid Cycle.
- **TFAM:** Mitochondrial Transcription Factor A.
- **tPA:** tissue Plasminogen Activator.
- **tRNA:** transfer RNA.
- **UPR genes**: Unfolded Protein response genes.
- **Val:** Valine.
- **WAT:** White Adipose Tissue**.**
- **WT:** Wild-type.
- **XF:** Extracellular Flux.
- **ZeLa:** Zero Lactate cells.
- **ZFN:** Zinc-finger nuclease.

Publications

-*Capella Roca, B., Alarcón Miguez, A., Keenan, J., Suda, S., Barron, N., O'Gorman, D., Doolan, P., & Clynes, M. (2019).* Zinc supplementation increases protein titer of recombinant CHO cells. Cytotechnology, 71(5), 915–924.

-*Kelly, P. S., Alarcon Miguez, A., Alves, C., & Barron, N. (2018).* From media to mitochondria–rewiring cellular energy metabolism of Chinese hamster ovary cells for the enhanced production of biopharmaceuticals. Current Opinion in ChemicalEngineering, 22, 71–80.

-*Kelly, P. S., Dorival-García, N., Paré, S., Carillo, S., Ta, C., Alarcon Miguez, A., Coleman, O., Harper, E., Shannon, M., Henry, M., Connolly, L., Clynes, M., Meleady, P., Bones, J., & Barron, N. (2019).* Improvements in single-use bioreactor film material composition leads to robust and reliable Chinese hamster ovary cell performance. Biotechnology Progress, 35(4), 1–17.

Scientific talks and Posters

•European Society for Animal Cell Technology (ESACT) - 25th biennial meeting, Laussane.

I presented a research poster focused on a part of my thesis titled: ``Studying mitochondrial metabolism in CHO cell clones containing different heteroplasmy variants´´ at this prestigious animal cell technology conference.

•ESACT Frontiers Retreat 2018, Zagreb, Croacia. I presented a research-based lecture focused on a part of my thesis titled: ``Effects of mitochondria related genes PGC1α and DRP1 in recombinant protein expression in CHO cells´´.

Acknowledgments

First and foremost, I would like to thank my supervisors, Professors Niall Barron and Donal O'Gorman, whose expertise, knowledge, patience, and kind guidance have been invaluable to me during this PhD process. Since I stepped into DCU, they have helped me not only to grow as a scientist, but also as a person, and they were always there when to help anything they could.

Appreciations also to Mairead Callan, Gillian Smith, Anita White, and James Spalding for all their technical assistance. You were always there for either a nice chat or technical assistance and this project will have not been the same without you.

I would also like to thank all the nice people on the first floor, namely Ali Coyle, Charles Doherty, Nicola Gaynor, Neil Conlon, Sambhavi Priyadarshini, and Shannon Nelson. Special mention goes to John Noone, whose help and friendship were invaluable to this project.

I must of course thank my dear friends from DCU, Ricardo Valdes-Bango, Jesus Martinez, Berta Capella, Krishna Motheramgari, Prashant Kaushik, Peter Berry, Teresa Lauria, Giuseppe Avella, Julie Brueckner, Karmel Gkika, Ares Varvarezos, Peter Brennan, and Simon Creane. The experiences we have shared, all the coffee, the beers, and, of course, the research will not be forgotten. I would always hold them in my heart.

A million thanks go also to Mr. Damian O'Donohue, whose wisdom guide me when I arrived in Dublin like a lost child and never failed to provide new stories full of both wisdom and entertainment.

I could never forget the kind guidance and friendship of Doctor Ioanna Tzani, from UCD whose experience and teachings helped me with the sequencing experiments.

Obviously, I can't forget about the support and love of my family, including my former girlfriend, now wife, Paloma Ozores, which love, support and understanding have gone me through my darkest hours.

I must express my most sincere gratitude to Dr. Ana Terres and her lovely family. Without her friendship, guidance, kindness, and an impressive amount of patience, I may have never stepped into Ireland nor completed this PhD. I wish I could repay so much kindness someday.

Finally, I must thank the IRC for giving me the extraordinary opportunity to perform my research in Ireland, providing financial support to carry out this research project.

The role of mitochondrial metabolism during recombinant protein production in CHO cells.

Antonio Alarcón Miguez

Abstract

Chinese Hamster Ovary cells (CHO cells) are recombinant protein-producing cells widely used to produce biopharmaceutical products. Improving the recombinant protein production efficiency of CHO cells has been the subject of many studies over the last decade, due to its capacity to produce complex recombinant proteins of interest with human-like post-translational modifications. However, CHO cells are less efficient and more costly than bacteria and yeast-based expression systems. While many engineering methods have been previously described, the delicate balance between oxidative metabolism and glycolytic metabolism, which promotes protein production and cell proliferation respectively, remains a challenge. Recent sequencing studies performed on CHO cells mitochondria, the powerhouse of the cell, and the center of oxidative metabolism, have provided a deeper understanding of the mechanism underlying CHO cell metabolism. These studies have shown the existence of heteroplasmic mutations within CHO cell mitochondrial DNA, which have a potential impact on cell metabolism. In this study, the engineering of CHO cell metabolism was attempted by focusing the efforts on the mitochondria and oxidative metabolism, aiming to increase recombinant protein production by CHO cells. The potential influence of heteroplasmy variants previously found in CHO cells was evaluated to establish the future potential of creating ``de novo´´ heteroplasmic variants that will improve the recombinant protein production of the cell. The evolution of heteroplasmy over time in CHO cells was also assessed by performing deep sequencing on 12 different newly generated CHO clones at different time points. Additionally, genes closely related to mitochondrial metabolism, biosynthesis, and fission, including PGC1α, DRP1, and ANT1, were overexpressed or knocked down in CHO-K1-EPO cells. This approach aimed to increase the number of mitochondria, potentially promoting an increase in oxidative metabolism and recombinant protein production. Finally, the effect of modern, alternative approaches to metabolic engineering of cell culture performance, with a special focus on oxidative metabolism, was evaluated with promising results.

CHAPTER 1
Introduction

Disclaimer: This introduction is based on the review ``*From media to the mitochondria-rewiring cellular energy metabolism of Chinese hamster Ovary cells for the enhanced production of biopharmaceuticals´´*(Kelly *et al.*, 2018), which was co-authored by the author of the present study.

1.1. Chinese Hamster Ovary cell lines as Biopharmaceutical production host.

During the last three decades, the biopharmaceutical industry has used mainly mammalian cells to produce high-quality recombinant proteins for therapeutic ends. Among mammalian cells, Chinese Hamster Ovary cells (CHO-cells) remain the most commonly used line in the Biopharmaceutical Industry, with around 84% of monoclonal antibody (mAb) products (57 of 64) being produced in CHO systems in 2018 (*Walsh, 2018*). This extensive use has earned CHO cells the status of ``Biological workhorse´´ of the biopharmaceutical industry.

CHO cells were first derived by Theodore Puck in 1958 (*Puck 1958*), during a characterization study on somatic mammalian cells. Chinese Hamster Ovary cells were grown over 9 months and were seemingly immortalized at this moment. This means CHO cells were not designed nor intended to be used for recombinant protein production but rather were being used to investigate chromosomal dynamics when the immortalization occurred (*Wurm and Wurm, 2021*).

In 1963, Ham reported mutant CHO cells lacking Proline synthesis, which could spontaneously revert to their original phenotype. In 1966, Kao, a Puck collaborator, reported that the Proline minus CHO cells as a new cell line, a trait shared by all successive CHO cell lines (*Kao and Puck, 1967*) At the time, different CHO cell lines were being derived from the CHO Pro (-) line. An example of these newly derived lines was CHO-K1, which was generated from a single clone (*Kao 1968*). Another example is the CHO-S line, consisting of CHO cells capable of growing in suspension culture, derived from a variant of CHO-K1 (*Thompson and Baker, 1973).*

From CHO-K1, the CHO-DBX line was isolated using deoxyuridine and methotrexate as selective agents (*Urlaub and Chasin, 1980*) this cell line was created in hopes of performing cancer metabolic studies related to chemotherapy and paving the way to the industrial applications of CHO cells. Additionally, this line raised the interest in the potential of CHO cells deficient in dihydrofolate reductase for genetic studies, this caused the generation of CHO-DG44 line when an MTX resistant-CHO mutant had both dihydrofolate reductase alleles mutated using radiation (*Urlaub et al., 1983*).

Years later, in 1986, the first CHO cell line used for manufacturing recombinant proteins was derived from the CHO-DBX11 line by Genentech, to produce human tissue plasminogen activator (tPA) with what was considered high efficiency at the time. The reason behind CHO-DBX being selected as recombinant protein producer cells was precisely their DFHR mutation, which allowed transfection of the gene of interest in conjunction with a functional DFHR gene, which allowed selection of recombinant cells based on DFHR activity (*Scahill et al., 1983)*.

The different CHO cell lines have been kept and maintained by numerous laboratories all over the world. While several, well-established CHO lines have been described in this text, some authors like Wurm (*Wurm and Wurm, 2021*) argue that CHO cell line classification is nowadays not correct, due to the high capability of adaptation shown by CHO cells increasing the diversity in the subpopulations of CHO cells. The genetic diversity observed in CHO cells, at both the nuclear (*Wurm, 2013*) and mitochondrial level (*Kelly et al., 2017)* has led to CHO cells being described as ``Quasi-Species´´, a term meaning that no CHO cell line or clone is the same and, consequently, they can have unique phenotypes and different metabolic demands (*Wurm and Wurm, 2017*). These underlying differences in supposed clones can involve changes in phenotype and metabolism which will difficult considerably the study of the CHO cells. (*Wurm and Wurm, 2021*).

Regardless, CHO cells are nowadays widely used by the biopharma industry mainly for general characteristics shared by CHO cell lines. These characteristics include:

1. The CHO cell's adaptability and flexibility, which allow them to be grown in suspension culture and serum-free chemically defined media.

2. The CHO cell's ability to produce high-quality proteins with human-like post-transcriptional modifications, such as glycosylation (*Sarantos and Cleo, 2013; McDonnell, 2015).*

3. Reduced risk of viral contaminations, as human viruses are not able to propagate as easily in CHO cells as in other cell lines, such as BHK cells *(Berting, Farcet, and Kreil, 2010)*

4. Several well-established gene amplification systems exist within CHO cells, such as the DFHR system or the GS system.

These characteristics are the reason that CHO cells remain nowadays the main platform for the production of therapeutic human recombinant glycoproteins. For this reason, research on new CHO lines with a focus on generating more productive phenotypes has been extensive during the last decades. (*Fischer, Handrick and Otte, 2015*).

1.2. Cell metabolism and the Warburg effect during recombinant protein production.

Observations of the metabolism of CHO cells and other immortalized Continuous Cell Lines (CCLs) have paralleled that of observations of cancer cells concerning their need for constant availability of nutrients and compounds such as carbon, nitrogen, or ATP to sustain their metabolic functions. One of the most remarkable parallelisms between cancer cells and CCLs metabolism is their preference for glycolysis to sustain their cell growth, even in aerobic conditions (*Young, 2013*).

This phenomenon, known as the Warburg Effect, involves the conversion of glucose to lactate by diverting pyruvate from the Tricarboxylic Acid Cycle (TCA) and fermenting it to lactate by the action of the Lactate Dehydrogenase (LDH) enzyme, a metabolic process which, in normal conditions, only occurs during oxygen deprivation conditions. This results in lactate accumulation in the media, contributing to the acidification of the media. (*Mulukutla et al., 2015*) This accumulation of lactate can compromise the purity of the final product in bioreactors, and the acidification of the media can compromise the growth and viability of the cells. (*Möller et al., 2021*).

It is still not clear why the Warburg Effect occurs in certain types of cells at their early phases, as at first sight involves switching to a much less efficient metabolism in terms of energy generation. While glycolysis occurs at a much faster rate than the complete oxidation of glucose in the mitochondria (Roughly, 10-100 times faster), this process is also much less energetically efficient, with glycolysis producing 2ATPs per molecule of glucose, while the oxidative pathway produces 36 ATPs per molecule of glucose (*Heiden, Cantley, and Thompson, 2009*) Regardless, both cancer cells and immortalized cells have been observed to resort to aerobic glycolysis during the early phases of growth. For this reason, this phenomenon has intrigued both cancer and immortalized cell researchers for

decades, as these types of cells are using an, apparently, energetically wasteful metabolism.

Over the years, several hypotheses tried to explain the Warburg effect. One popular hypothesis suggested the cells repurpose their mitochondria during the early growth stages, switching from a predominantly catabolic ATP producing engine to an anabolic metabolism supplying biosynthetic intermediates for the synthesis of new cell components. This way, the mitochondria will be used to provide, for example, carbon supply for lipid biosynthesis, aminoacids for the synthesis of nucleotides, etc, and will be unable to perform oxidative metabolism (*Young, 2013*). Although the energy generation of the cell is on average much lower in these conditions, the commitment of the TCA intermediates to the synthesis of cell components makes rapid cell growth much more efficient. For this reason, it is commonly believed that cell growth and r-protein-specific productivity are mutually exclusive, but recent studies using molecular markers have failed to find a straightforward correlation between these two parameters (*Edros, McDonnell, and Al-Rubeai, 2013).*

Other hypotheses proposed about the origin of the Warburg Effect include a mechanism of response to Reactive Oxygen Species (ROS) accumulation in cancer cells (*Murphy, 2009)* faster generation of ATP (*Locasale and Cantley, 2011*) or to acidify the media, creating an acid microenvironment to promote the growth of tumor cells *(Estrella et al., 2013)*. A recent study (*H. Sun et al., 2019*) highlights differences between cancer cells and normal proliferating cells (NPCs) concerning the Warburg effect. While Sun and collaborators observed the Warburg effect being common to both types of cells, they concluded the Warburg effect occurs for different reasons in each cell type: In cancer cells, Warburg will be used to regulate the internal pH of the cell, generating protons that neutralize the constant flux of cytosolic OH^- generated by reactions caused by ROS. In NPCs, Warburg related acidification will be used to maintain the acidic pH conditions optimal for ribosomal activity (H. Sun *et al.*, 2019). All these hypotheses are very interesting and provide different insights into the Warburg effect. However, to date, none of the hypotheses has been proven, and all of them have their own problems or unanswered questions (*Liberti and Locasale, 2016)*.

On the other hand, recombinant protein production is known to increase with higher mitochondrial oxidative activity *(Templeton et al., 2013*), which is likely related to the

very high energy-demanding process of protein folding in the Endoplasmic Reticulum (ER) *(Kaufman and Malhotra, 2014*). This reveals a dichotomy in recombinant-protein producer cell lines: two different metabolic programs coexist within these cells. During the early stages of growth, the cells adopt a glycolytic metabolism, releasing lactate to the media and promoting cell growth. in the late exponential phase, the cells resort to oxidative metabolism, which promotes recombinant-protein production, until death. While the mechanism of the shift is currently not completely understood, the Warburg effect must be considered when attempting to engineer the CHO cells' metabolism. The next section expands the different attempts at controlling the CHO cells (and other recombinant-protein producer immortalized cell lines) metabolism and the metabolic shift caused by the Warburg effect.

1.3. Engineering of CHO metabolism.

Over the years, many different strategies have been employed by CHO cell biologists to control cellular energy metabolism through different means. These approaches include both non-genetic of the cells and genetic intervention of the CHO cells.

1.3.1. Control of nutrients and metabolites.

The non-genetic interventions in CHO cells metabolism in the context of biomanufacturing are normally focused on either manipulating the input of supplements and nutrients to the cell culture media or the culture environment conditions, such as the temperature.

1.3.1.1 Control of nutrients and metabolites input in the culture.

The control of glucose and glutamine input in bioreactor cultures, aiming to reduce the accumulation of wasteful subproducts of the cell metabolism, such as lactate and ammonia, has dominated most of the media and process development platforms. The in-media lactate levels are normally monitored in industrial processes in the biopharmaceutical industry, as lactate is a critical metabolite of culture mammalian cells. (*Rafferty et al., 2020*). Lactate is typically produced in high amounts during the early exponential growth phases, due to Warburg Effect (*Mulukutla et al., 2015*) and it is often subsequently consumed during the stationary phase, although not all the cell lines and/or

subclones possess the ability to consume the lactate previously produced (*Zagari et al., 2013)*.

Lactate production is strongly influenced by the availability of glucose in the culture media, while lactate consumption is induced by the presence of glutamine (*Zagari et al., 2013)*. Generally, cells utilize glucose more readily as its cellular uptake is accelerated by two types of monosaccharide transporters, the Glucose transporters (GLUT) (*Joost and Thorens, 2001)* and the sodium-glucose linked transporters (SGLT) (*Takasu et al., 2019)*. Alternatively, cells may use different carbohydrates as carbon sources, such as galactose, fructose, and mannose. These carbohydrates have reduced permeability through the phospholipid layer and their availability is directly related to the availability of transporter proteins, used to internalize these carbohydrates , which are also used to internalize glucose, which depending on the cell or the tissue has a much higher affinity for the transporter (*Altamirano et al., 2000; Leong et al., 2017, 2018)*

A metabolic shift from lactate production to lactate consumption can promote extended cell longevity and can improve productivity by reducing the levels of this toxic metabolite in the media (*Martínez et al., 2013*). Many of the strategies to develop CHO cells with decreased lactate production are focused on controlling the levels of glucose and/or glutamine in the media, as both are known to be key metabolites in the metabolism of lactate, acting as the main carbon sources for lactate production *(Torres, Altamirano and Dickson, 2018*).

Glucose control is a popular way to control lactate levels in the media. The development of a system called High-End pH-controlled delivery of glucose (HIPDOG) was proven successful in improving the cell culture conditions by having the addition of glucose controlled by a pH probe. (*Gagnon et al., 2011)*. More recently, the use of Raman spectroscopy probes (RSP) to monitor fed-batch cultures levels of glucose and lactate and control the glucose input at certain lactate levels was successful in maintaining lactate levels lower than during routine cultures, which increased both the cell viability and the recombinant protein titer (*Matthews et al., 2016*). Lactate accumulation has been observed, in large-scale reactors, to be dependent not only on glucose levels but also on parameters such as pH, osmolarity, pCO_2, and the stirring speed of bioreactors (Xu *et al.*, 2018).

Glutamine control also constitutes a useful mechanism to control the metabolic switch from lactate production to consumption. Feeding glutamine to CHO cells is known to promote cell division, but also to increase lactate production and delay the switch to lactate consumption (*Zagari et al., 2013)* additionally, the metabolization of glutamine causes the accumulation of ammonia in the culture, which has been observed to reduce the maximum viable cell density (but not the viability) and the quality of the glycosylation patterns of the recombinant-protein produced by the cells (*Synoground et al., 2021*). However, it is not so easy to control the shift by depriving mammalian cells of glutamine. Firstly, glutamine constitutes a major source of energy and nitrogen for the cells and the low levels of endogenous synthesis on mammalian cell cultures make these cells very reliant on external glutamine supplies. Secondly, glutamine deprivation has been observed to induce autophagy in some mammalian cell cultures, such as CHO cells (*Shanware et al., 2014)*. Reduced concentrations of glutamine have been observed in previous studies to successfully reduce the concentration of ammonia in the media *(Rajendra et al., 2012)*. However, even low levels of ammonia in the culture are known to have a detrimental effect on the culture cells (*Synoground et al., 2021*). For this reason, strategies for developing CHO cells that can survive without relying upon glutamine have been studied over the last years. While several strategies have focused on genetic engineering of genes related to glutamine metabolism which will be discussed later in this section, CHO cells have been successfully adapted to growth on glutamine-free media without the use of genetic engineering, namely a one-step glutamine reduction strategy, removing the glutamine supplementation to the culture altogether, resulting in a significant reduction of the ammonia levels (*Kaushik et al., 2020*).

Other supplementation strategies include early feeding of lactate to the cells (*Freund and Croughan, 2018)*, the substitution of glucose and/or glutamine by other sources of carbon, such as galactose (*Torres et al., 2019*) or maltose (*Leong et al., 2018)*. While these methods are commonly successful in reducing lactate and ammonia accumulation in the media, a reduction of the viable cell growth rate is also noted when these alternative nutrients are supplemented.

Aside from primary carbon sources, the supplementation of other animal-derived products, such as carrier proteins, vitamins, aminoacids, or trace elements can be used to support CHO cell growth. Yeast hydrolysates have been observed to enhance the growth

and productivity of a β-Interferon producing CHO cell line (*Rodriguez et al., 2005; Spearman et al., 2014)*. More recently, supplementation with protein hydrolysates from Flaxseed Oil Cake has been observed to increase the cell density in culture and is speculated to exert some kind of protective effect on the cells (*Logarušić et al., 2021*). However, the supplementation of hydrolysates often has reproducibility issues, with results varying greatly in different CHO cell lines and with different hydrolysates. For this reason, the use of hydrolysates is not common in newer processes.

Amino acids play a central role in CHO cells metabolism and are common to have them supplemented to CHO cell cultures based on their rate of consumption *(Salazar, Keusgen, and Von Hagen, 2016*). As many amino acids, such as leucine or tyrosine, have low solubility, it is common to use amino acids derivatives instead to facilitate their integration into cell metabolism (*Schmidt et al., 2021*). The addition of amino acids or derivatives has the problem of increasing the concentration of ammonia in the media as a subproduct of its processing, which has a detrimental effect on both the cells and the quality of the recombinant protein (*Synoground et al., 2021*).

The presence of trace metals in the culture such as Cooper (*Yuk et al., 2014*), Zinc *(Capella Roca et al., 2019*), and Iron (*Graham et al., 2021)* play a critical role in metabolism. Iron injections have been observed by Graham and collaborators (*Graham et al., 2021)* to increase the titer and glycosylation of monoclonal antibodies (mAB) in CHO cells. Effects of Zinc supplementation were tested by Capella and collaborators *(Capella Roca et al., 2019*)and compared with the effects of copper supplementation. While both Zinc and Copper supplementation was observed to result in a titer increase and a reduction of the Viable cell density, the increase in titer caused by Zinc supplementation was significantly higher than the increase caused by copper. Additional approaches on supplementation of mammalian cell cultures include chemicals such as dichloroacetate (DCA), which inhibits Pyruvate Kinase and could be used to reduce lactate production (*Buchsteiner et al., 2018*) or supplementation with Tricarboxylic Acid Cycle (TCA) intermediates, such as malic acid and succinic acid (*Zhang et al., 2020*), which increase the lactate consumption of the cells and, subsequently, the recombinant protein titer.

While there are many studies and different approaches to engineering CHO cell metabolism by modifying the nutrient supplementation, the applications of this

knowledge are not often this simple. These approaches often require complex process development, including approaches such as the design of experiments to optimise the media and feed ingredients and timing. For this reason, most companies choose to move to a platform approach where they choose the clones that best suit a media and process. Additionally, the variability of CHO cell lines, which earned CHO the definition of ``quasi-species´´ as previously commented, often implies that each particular CHO cell line needs a culture media specifically tailored to the metabolic needs of the cells, which makes the application of the metabolic engineering using nutrient very difficult to apply universally.

For these reasons, an important amount of effort has been invested in the research of different mechanisms to change and control the metabolism of CHO cells and other mammalian continuous cell lines.

1.3.1.2.Control of cell culture environment.

Manipulation of the bioreactor temperature, pH conditions, and/or the concentration of oxygen dissolved in the media are some examples of the methods reported in the literature to manipulate the metabolic transition in mammalian cell cultures via environmental conditions control.

The use of mild hypothermic conditions (31-35ºC) is a common process control strategy to increase the lifespan of the cells and induce the metabolic shift towards the oxidative metabolism, increasing recombinant protein production (*Fox et al., 2005; Robinson, Picken and Coopman, 2014)*. In the study performed by Fox and collaborators in 2005 (*Fox et al., 2005*), the cells were allowed to grow exponentially during the initial phase of the culture, after which they were shifted to the 32ºC temperature and their growth was observed to halt, but their r-protein production improved significantly. Similarly, a more recent study performed by Torres and collaborators (*Torres et al., 2018*) shows CHO-DG44i cells grown at 37ºC, 33ºC, or 31ºC correspondingly. The cell viability was observed to be greatly increased by the lower temperatures compared with the control, prolonging the growth phase and both the viable cell density long-term and the r-protein titer obtained from the cells.

The reasons behind these changes in the cell behavior are still unknown, although several studies have suggested many potential explanations, such as decreased apoptosis (*Moore*

et al., 1997) and cell cycle arrest at G1/G0 (*Yoon, Song and Lee, 2003*), which could lead to the extended viability and the prolonged growth phase previously commented. Additionally, mild hypothermic conditions are known to improve not only the recombinant protein titer of complex r-proteins, such as β-interferon (*Sunley, Tharmalingam and Butler, 2008)* but also the transcription and stability of the r-proteins genes (*Kou et al., 2011*). Dynamic Metabolic Flux Analysis (MFA) of CHO cell cultures after a temperature shift has demonstrated a reduced utilization of nutrients such as glucose, glutamine, and serine, which are typically associated with accumulation of lactate, which suggest a switch from a fast-growing phenotype to a productive phenotype *(Martínez et al., 2015*). Recently, a study performed by Torres and collaborators showed the upregulation of the unfolded protein response pathway genes (UPR-genes) and transcription factors related to the Endoplasmic Reticulum (ER) when CHO cells are grown in low-temperature cultures (*Torres et al., 2021)*, potentially explaining the upregulation of the r-protein titer and quality observed in other studies.

The control of pH and dissolved oxygen concentration levels are frequently monitored during bioprocesses, as changes in these parameters can be detrimental to the cells in the culture (H. Sun *et al.*, 2019). For this reason, pH and dissolved oxygen are frequently monitored in bioreactors, and during the last years, a body of research has been dedicated to the development of monitoring tools, such as optical sensors to control both pH and dissolved oxygen in bioreactors (*Naciri, Kuystermans and Al-Rubeai, 2008*) or the use of Magnetic sector gas analyzers (*Floris et al., 2020*). Research into new systems to control the pH of the bioreactor cultures by sparging gases, without the addition of bases to the culture, which may change osmolarity, has also recently been reported by Hoshan and collaborators (*Hoshan et al., 2019*).

An excessively low or high dissolved oxygen concentration level in bioreactors has been reported to lead to impaired glycosylation activity and a decrease in the viable cell density of CHO cells (*Restelli et al., 2006*). This decrease is suspected to be related to the lack of oxygen, in the case of low dO_2 concentration or to the generation of Reactive Oxygen Species (ROS) in the case of high dO_2 concentration. Control of ROS, normally generated by the r-protein producer cells in great amounts during bioreactor culture has been also the subject of a good body of research. Chevallier and collaborators (*Chevallier, Andersen and Malphettes, 2020)* highlighted in their last review several strategies against ROS

generation, such as the addition of thiol compounds or molecules such as ketoacids to the cell culture media.

Finally, a recent approach to improvements in the culture environment is to improve the composition of the bioreactors. Plastic bioreactors are nowadays integral devices for biopharmaceutical production, but they are known to release plastic leachables to the culture media, which are highly toxic to the cells. For this reason, new generation bioreactors, with a minimum leachable release, are being designed to improve the performance of r-protein-producing cell lines in culture (Kelly *et al.*, 2019).

Like in the case of media supplementation, the engineering of CHO cells by exerting control over the cell culture environment is often very specific. Cells shifted from their regular conditions without being previously adapted may respond differently to the new conditions. To achieve a change in the cell metabolism with changes in the culture environment, a period of adaptation to generate CHO cells adapted to the new temperature is normally required. Additionally, maintaining these conditions often requires having complex monitoring systems in place to ensure these conditions remain in a controlled interval for the duration of the process.

For this reason, while the non-genetic interventions are still nowadays the most used system for CHO cell process development, the interest in genetic engineering of CHO cells has gained interest during the last decades.

1.3.2. Engineering the expression of key metabolic genes.

The natural alternative to process and media development is the genetic engineering of CHO cells. The genetic engineering of mammalian cells used in r-protein production processes has been often focused on the goals of reducing the toxic metabolic by-products such as lactate and ammonia while other strategies have focused on anti-apoptotic engineering (*Cost et al., 2010*), high cell density/proliferation (*Wilkens and Gerdtzen, 2015*) or reprogramming CHO cells metabolism to increase their reliance on the oxidative metabolism, increasing their recombinant protein titer *(Seth et al., 2006)*. The publication of the CHO-K1 genome in 2011 (*Xu et al., 2011)* and the mitochondrial sequence of Chinese Hamster in 2007 *(Partridge, Davidson and Hei, 2007)* constituted a major inflexion point for the genetic interventions in CHO cells, as the availability of the

sequences greatly facilitates genetic engineering strategies. Proteomic analysis of CHO cells has been performed to identify several genes involved in sustained protein productivity (*Meleady et al., 2011*). Additionally, a recent multi-omics study performed by Hefzi and collaborators (*Hefzi et al., 2016*) resulted in a reconstruction of the CHO cell metabolism at genome-scale. This metabolic model included 1766 genes and 6663 reactions, showing how complex the functional networks of CHO are, and was used to make predictions on CHO cells phenotypes successfully. Subsequently, a genome-scale model for CHO secretory pathway was reconstructed by the same group (*Gutierrez et al., 2020*) to predict metabolic cost and maximum productivities of r-protein in CHO cells, identifying potential targets for CHO cell genetic engineering.

The current advanced genome editing techniques will likely create the next major jump in CHO cell productivity. The recent advances in gene-editing technology allow any gene to be either edited or deleted using nuclease systems. Further, the discovery of the CRISPR-Cas9 tool, guided by RNA, enables relatively easier editing of the tool to target the gene of interest compared with classic nucleases or TALENs systems (*Gupta and Shukla, 2017).* Moreover, further challenges arising in the CHO cell productivity process landscape, such as hard to express proteins, different glycoforms, clone stability, or HCP contaminants, make the genetic interventions an interesting way of looking for desirable phenotypes to solve these different issues.

1.3.2.1.The nuclear genome of CHO cells: engineering key metabolic genes.

As commented before, the genes related to metabolism represent the main targets of interest for the genetic engineering of CHO cells. The relationship between oxidative metabolism and r-protein production (*Templeton et al., 2013*) makes the genes related to oxidative metabolism interesting targets for genetic engineering. Additionally, due to the waste by-products, such as lactate, generated by CHO cells during the glycolytic metabolism (*Mulukutla et al., 2015),* the editing genes related to the glycolytic route have been the focus of research over the last 10 years.

The use of galactose as an alternative source of carbon (*Altamirano et al., 2000; Torres et al., 2019)* was reported to decrease lactate levels, but also peak viable cell density. However, cultures containing both glucose and galactose as carbon sources have been seen to produce lactate again, as the metabolism associated with galactose is far slower

than glucose. This will lead to decreased levels of lactate compared with glucose-only cultures, as when the glucose is consumed, pyruvate will be slowly produced due to the slow metabolism of the galactose, leading to lactate consumption (*Wilkens, Altamirano and Gerdtzen, 2011*). In this context, using genetic engineering to promote the overexpression of both the galactose transporter gene *Slc2a8* (GLUT8) and Galactokinase 1 (GALK1) can increase cell growth while maintaining a low lactate production rate in CHO cell cultures containing both galactose and glucose (*Jiménez, Wilkens and Gerdtzen, 2011)*. Moreover, recently the same group generated a CHO-GalK1 line, overexpressing the GALK1 gene, able to survive using galactose as the primary carbon source, reducing significantly the lactate production and increasing the specific growth rate of the cells by 34% (*Jiménez, Martínez and Gerdtzen, 2019*).

Other studies have achieved improved metabolism and reduced lactate production through the stable expression of a fructose transporter gene (SLC2A5 gene which translates into the fructose transporter GLUT5) and pyruvate carboxylase (PYC2). These cells achieved higher cell densities and prolonged lifespan when cultured in fructose in absence of glucose (*Wilkens and Gerdtzen, 2015*). Metabolic Flux Analysis (MFA) was performed on the dual-engineered cells, demonstrating that these CHO cells have higher metabolic fluxes in glycolysis and TCA cycle while consuming more fructose, which supports higher cell density. The study of mTOR pathways has revealed potential genetic engineering targets known to regulate the recombinant protein-specific productivity levels (*Edros, McDonnell and Al-Rubeai, 2014; Jossé et al., 2016)*.

The control of the metabolic shift itself has been also widely attempted in literature, the mitochondrial pyruvate levels being one of the common targets to control the metabolic shift. The overexpression of yeast cytosolic pyruvate carboxylase (PYC2) in CHO cells has been demonstrated to augment pyruvate flux towards the TCA cycle, which reduces fourfold the lactate accumulation in the culture and increases about 70% the r-protein production (*Gupta et al., 2017*). Similarly, the overexpression of the mouse mitochondrial pyruvate carrier (MPC), achieved by simultaneous overexpression of the two subunits of the carrier, MPC1, and MPC2, has been observed to reduce the Warburg effect without compromising the glucose consumption on the cells, which increased the specific growth rate and viable cell concentration around 40% while simultaneously reducing the lactate yield by approximately 50% (Bulté *et al.,* 2020a).

Research in the upregulation of membrane transporters to mediate the uptake of nutrients is, of course, not limited to pyruvate and fructose transporters. The overexpression of the taurine transporter (TAUT) was observed to delay apoptosis, extend the cell culture period and decrease the lactate production of the cells, overall increasing the r-protein production of the cells (*Tabuchi et al., 2010*). However, this method had the disadvantage of producing alanine as a by-product, which caused accumulation of ammonia late in the culture as the glutamine consumption increased. For this reason, Tabuchi and collaborators explored new strategies to improve their method, using the co-expression of Alanine aminotransferase I (ALT1) which further enhanced cell proliferation and achieved higher r-protein productivity in half of the time by catalyzing the reversive transamination between alanine and 2-oxoglutarate to form pyruvate and glutamate. (*Tabuchi and Sugiyama, 2013*). Glutamine synthase expressing CHO cells, which can utilize glutamate instead of glutamine, have also been engineered, reducing the levels of ammonia in the culture (*Zhang et al., 2006)*.

Although the mitochondrion plays a central role in energy metabolism, its role as a major gateway controlling intrinsic cell death must also be taken into account. Cell loss due to programmed cell death is one of the biggest limitations to maintaining high viable cell densities and, therefore, high r-protein titer in CHO batch cultures. A common approach to limit cell death consists in the overexpression of anti-apoptotic genes, such as the genes from the Blc2 family. Overexpression of genes from this family, such as Bcl-X_l in CHO-K1-EPO cells (*Kim et al., 2009*) or Bcl-2Δ in CHO-S cells (*Templeton et al., 2014*) has demonstrated increased biomass yield, peak viable cell density, and extended culture longevity. Curiously, Bcl-2Δ overexpression was also observed to reduce the lactate accumulation in the culture, as Bcl-2Δ overexpression not only decreased the caspase 3/7 activity but also altered the pyruvate metabolic destiny towards mitochondrial oxidation, which promoted lactate consumption. The overexpression of both Bcl-X_l and Mcl-1 anti-apoptotic in CHO cells was reported to significantly increase antibody production and cell viability. Curiously, overexpression of Bcl-X_l was observed to increase the antibody production by 82%, while the overexpression of Mcl-1increased the production by 34%. Comparatively, Bcl-X_l showed more effectiveness (X. Zhang *et al.*, 2018).

An alternative strategy to regulate cell death is to knock down pro-apoptotic genes. Two classical targets to this approach are the genes Bak and Bax, which belong to the Blc2

family. Lim and collaborators studied the generation of siRNA constructs to simultaneously silence both Bak and Bax genes in CHO-K1 Interferon (IFN) producing cells, leading to resistance against UV radiation and cytotoxic lectins induced apoptosis, as well as extended culture viability and a 35% increase on IFN titer (*Lim et al., 2006)*. Cost and collaborators deleted both Bak and Bax genes from CHO-K1 cells using Zinc-Finger Nucleases (ZFN) followed by inaccurate DNA repair, which resulted in CHO-K1 cells being resistant to apoptosis under stress conditions, such as starvation or the presence of staurosporine and sodium butyrate (*Cost et al., 2010*). Recently, the CRISPR interference (CRISPRi) system has been used to downregulate three pro-apoptotic genes, namely Bak, Bax, and Cas3, in CHO-S cells. In addition to the decrease in apoptosis and increase in peak viable cell density, the mitochondrial membrane integrity was observed to improve and the caspase activity to decrease (*Xiong et al., 2019*).

In the last decade, microRNAs (miRNAs) have become promising candidates to engineer the metabolism and bioprocessing characteristics of CHO cells (*Kelly et al., 2014; Valdés-Bango Curell and Barron, 2018)*. miRNAs have been reported to regulate many of the key enzymes involved in the Warburg-like metabolism (*Jin and Wei, 2014*), which further highlights the potential of these small molecules for CHO cell metabolic engineering.

Ectopic expression of miR-34, a known tumor suppressor miRNA, successfully inhibited the growth and decreased the viability of CHO-SEAP cells, proving the miRNAs can be used to modify and improve CHO cell performance (*Kelly, Gallagher, et al., 2015)*. The depletion of several miRNAs has been reported by several studies to successfully induce metabolic reprogramming in CHO cells. miR-23 is known to regulate the Glutaminase enzyme (*Gao et al., 2009)*, which is involved in the glutaminolysis process, converting glutamine into glutamate, which is then converted by the glutamate dehydrogenase into α-ketoglutarate, supplementing the TCA cycle. The depletion of miR-23 in CHO cells reportedly achieved a three-fold increase in volumetric productivity without affecting cell growth, this increase was related to an increase in the activity of mitochondrial complexes I and II (*Kelly, Breen, et al., 2015)*. The identification of miR-7 in CHO cells as miRNA differentially expressed in CHO cells subjected to a temperature shift (*Barron et al., 2011)* allowed the subsequent stable depletion of mir-7 in r-protein producing CHO cells, which

reportedly enhance the r-protein production and peak viable cell densities (*Sanchez et al., 2014*).

More miRNAs have been recently reported in the literature to be useful for CHO cell engineering. Stable inhibition of miR-466h increases the transcript levels of anti-apoptotic genes (*Druz et al., 2013*). Overexpression of miR-495 can delay starvation-related autophagy, extending the lifespan of the cells (*Li et al., 2016*). miR-557 can improve the r-protein titer of CHO cells producing difficult to express (DTE) proteins, enhancing the production without negatively impacting growth or product quality, while also slightly decreasing lactate production of CHO cells (*Fischer et al., 2017*).

A recent study described the role of miR-31* in the cellular process of a CHO-DP12-SEAP (*Martinez-Lopez et al., 2021)*. In this study, cells with miR-31* overexpression were observed to show increased r-protein expression but decreased cell growth, similar to the cell growth arrest showed by CHO cells during temperature shifts to 31ºC. Moreover, this study characterized the proteins upregulated and downregulated in CHO-DP12-SEAP cells overexpression miR-31*, providing a list of potential engineering targets for CHO cell line development.

miRNAs have come out as an alternative to genetic engineering by the use of siRNAs due to its ability to regulate several genes at once without adding an excessive translational burden to the cell (*Valdés-Bango Curell and Barron, 2018*) and has already shown enough promised to be one of the new-generation tools for genetic engineering of r-protein producing cells, such as CHO cells.

1.3.2.2.Lactate dehydrogenase and Warburg effect.

During the few last years, studies about CHO cell engineering have focused on the control of the metabolic shift to lactate, with the ultimate goal of engineering high r-protein-producing CHO cells without lactate production and/or detrimental effects to viable cell density or cell viability: Warburg-null CHO cells. Apart from the previously mentioned engineering, which focused on the CHO cells accepting new nutrients, membrane transporters, and apoptosis control, two particular enzymes, which are the key to the lactate metabolic shift, have been the main subject of many CHO metabolic studies: Lactate Dehydrogenase (LDH) and Pyruvate Dehydrogenase (PDH).

Lactate dehydrogenase is an obvious choice for engineering as it is capable to consume or produce lactate in a single reaction. There are three known LDH genes, LDHA, LDHB, and LDHC. LDHA gene encodes for the LDH-M protein, with has a higher affinity for pyruvate, and preferentially catalyzes the conversion of pyruvate to lactate. LDHB gene encodes the LDH-H protein, which has a higher affinity for lactate and preferentially catalyzes the conversion of lactate to pyruvate. Finally, the LDHC gene is believed to be germline-specific *(Valvona et al., 2016; Hartley et al., 2018*). The presence of LDH isozymes can vary among tissues, and there is no consensus available for the predominant form in CHO cells. However, it must be noted that a good number of studies have reported LDHA transcripts in CHO cells (*Jeong et al., 2001; Odet et al., 2008; Ross et al., 2010; Qian et al., 2011),* which means the presence of this isozyme of LDH is likely to be highly represented in CHO cells.

LDHA subunit activity is known to be increased in cancer cells, and inhibition of this isozyme has been reported to cause an increase of the oxidative metabolism in cancer cells (*Le et al., 2010*), making LDHA a very interesting target for metabolic engineering. However, despite the down-regulation of LDHA and LDHB levels been observed in human disease (*Maekawa et al., 1990; Wakabayashi et al., 1996*), and the fact that down-regulation of LDHA can reportedly be used as means to engineer CHO metabolism towards the oxidative pathway (*Jeong et al., 2006; Kim and Lee, 2007; Zhou et al., 2011*), the efforts to achieve the complete deletion of LDHA gene have been, up to date, notably unsuccessful, most likely due to the relationship between LDH enzyme and NAD^+ regeneration *(Yip et al., 2014; Lee et al., 2015*).

For this reason, during the last decades, there have been different attempts to generate r-protein producer cells unable to produce lactate by simultaneous downregulation of the LDHA gene and other genes related to glycolytic metabolism. As previously commented, pyruvate is a key metabolite for the Warburg effect, and research efforts have been dedicated to pyruvate flux control for this reason. At the branching point in which the metabolism can be directed to either fermentation to lactate or the TCA cycle sits the Pyruvate dehydrogenase enzyme (PDH), capable of converting the pyruvate into Acetyl-CoA performing the pyruvate decarboxylation, connecting this way the glycolysis and the TCA cycle. The PDH enzyme is regulated by 4 different kinases, named pyruvate dehydrogenase kinases (PDKs from 1 to 4), which are regulated themselves by the ratios

of different key metabolic molecules, such as ADP/ATP; NAD^+ /NADH or Acetyl-CoA /CoA ratios, and can inhibit PDH when activated (*Roche et al., 2001; Möller et al., 2021)*. The simultaneous downregulation of PDKs 1, 2, and 3 and LDHA using siRNAs has been reported to decrease lactate production and increase r-protein titer without any detrimental effect on cell growth or viability (*Zhou et al., 201*1). However, the simultaneous knockout of LDHA in a PDKs 1, 2, and 3 knockdown CHO cell line is reportedly lethal to CHO cells (*Yip et al., 2014)*.

Apart from PDKs knockdown, different genes have been the target of simultaneous engineering with LDHA. The overexpression of glycerol-3-phosphate dehydrogenase (GPDH), an enzyme capable of oxidizing NADH like the LDHA enzyme, and simultaneous knockdown of LDHA gene in CHO DHFR- cells successfully decreased lactic acidosis and r-protein production but also generated high levels of oxidative stress (*Jeong et al., 2006*). Wilkens and collaborators performed a study that highlights the use of the CRISPR-Cas9 tool to selectively knockout one allele of the LDHA, obtaining an LDHA single-allele knockout CHO cell clone, which redirected the cell energy into the oxidative metabolism, greatly improving the recombinant protein production, but decreasing cell growth, which supports the idea of LDHA being critical to lactate generation in CHO cells (*Wilkens et al., 2019)*. Supporting this data, a recent study by Mazzio and collaborators has achieved, in a human colon cancer line, the generation of a Warburg-null line by both double knockouts of LDHA and LDHB or single knockout of the Glucose-6-phosphate isomerase, which completely inhibits glycolysis. This resulted in a glycolysis and Warburg null line which showed high production of ATP and increased mitochondrial functions, but with a slower proliferative rate (*Mazzio et al., 2020*). These findings support the hypothesis of the Warburg effect being dispensable to immortalized cells and LDH being a key enzyme in the metabolic shift (*Ždralević et al., 2018*).

1.4. Mitochondria as targets for cell line optimisation.

In the previous sections, the use of several powerful and revolutionary genetic engineering tools, such as CRISPR-Cas9 or the miRNAs, in CHO cells has been commented on, and there is no doubt about the present and future usefulness of these genetic engineering tools for the task of improving CHO cell performance in the context of biopharmaceutical r-protein production, which has been already demonstrated in some

examples. As many of these engineering efforts are directed to direct the cells towards a specific metabolic pathway, generally the TCA cycle and the oxidative pathway, as previously seen, a greater focus in the mitochondria itself has raised during the last years.

Mitochondria are double membrane-bound organelles, commonly found inside the cells of most eukaryotic organisms. These organelles constitute the location of many energy-generating reactions and the major source of energy within the cells, which has earned them the popular nickname ``the powerhouse of the cell´´. Mitochondria matrix is the site where main metabolic reactions like the TCA cycle and oxidative phosphorylation occur, generating 36 ATP per molecule of glucose, consuming oxygen, and releasing CO_2.

While roughly 99% of the mitochondrial associated genes are encoded by the nuclear genome, the mitochondria itself contains a 16.5 kb circular genome (mtDNA) in which 37 of these genes are located (*Kelly et al., 2017*). Of these genes, 2 genes are known to encode for the mitochondrial rRNAs, 22 genes encode for the mitochondrial tRNAs and 13 genes are protein-encoding (**Table 1.1**), with the resulting proteins having a role within the respiratory chain complexes.

Gene	Region
NADH1	2733-3687
NADH2	3898-4930
COX1	5310-6854
COX2	6994-7677
ATP8	7746-7949
ATP6	7907-8587
COX3	8587-9370
NADH3	9439-9786
NADH4L	9857-10153
NADH4	10147-11524
NADH5	11721-13541
NADH6	13525-14049
CYTB	14123-15265

Table 1. 1. Protein-encoding mitochondrial genes and their positions within the mitochondrial genome.

Therefore, these genes constitute potential targets for metabolic engineering of r-protein-producing cell lines, given the previously discussed relationship between higher oxidative activity and high r-protein titers *(Templeton et al.,* 2013). However, until recently, the mitochondria previously had little attention in the area of biomanufacturing, which is due to several reasons. First, cancer cells and immortalized mammalian cell lines, like CHO, are known to rely heavily upon metabolic pathways of ATP. Secondly, mitochondrial engineering has proven challenging, and to date, no reports of CHO-specific mitochondrial engineering exist.

The relationship between cellular mitochondrial content and r-protein production capacity of cells has been explored using mitochondrial-specific dyes, e.g. Mitotracker™ in a panel of CHOK1SV clones expressing cB72.3 protein. No correlation between mitochondrial content, r-protein synthesis, and growth of the cells was found (*O'Callaghan et al., 2015)*, which suggests that mitochondrial efficiency and/or functionality, rather than mitochondrial abundance, could play a role in specific productivity. Mitochondrial membrane potential and has been also reported to correlate with glucose uptake rate, making it a useful tool to perform CHO clone cell sorting, selecting the clones with the lower glucose consumption and, subsequently, the clones with lower lactate production (*Hinterkörner et al., 2007; Chakrabarti et al., 2019*). The manipulation of genes related to the mitochondria, either nuclear or mitochondrial encoded, has also been the subject of research in recent decades.

1.4.1. Engineering of nuclear-encoded mitochondrial genes

As mentioned, mitochondria constitute a very interesting target to engineer the metabolism of cells. For this reason, interest in the manipulation of mitochondrial-related genes has increased in the last few years. However, as previously described, most mitochondrial-related proteins are encoded in the nucleus, which makes these genes potential targets for metabolic control through genetic manipulation.

A common target for this kind of engineering is genes that encode mitochondrial transcription factors. Some transcription factors, like FOXM1, are known to be critical for cancer progression and regulation of the balance between glycolytic and aerobic metabolism. FOXM1 inhibits oxidative phosphorylation and promotes glycolysis in a process dependent on nuclear transcription in human cells *(Cui et al., 2014; Black et al.,*

2020), which makes FOXM1 a candidate for CHO mitochondrial engineering through the downregulation of its expression on the nuclear genome. The overexpression of mitochondrial Transcription Factor A (TFAM) in transgenic mice leads to an increase of mtDNA copies by 2-fold in cardiac cells while limiting mitochondrial oxidative stress caused by ROS (*Ikeda et al., 2015*). While these genes constitute only a few interesting examples of metabolic engineering by targeting mitochondrial genes that are nuclearly encoded, the rest of this section will be dedicated to the genes examined in the present study: PGC-1α (From the PGC1 family), DRP1, and ANT1. The main reason for these particular genes to be selected over others is their direct relationship with the regulation of the mitochondria in response to changes in oxidative metabolism. The following sections will be dedicated to explaining these genes and how the engineering of these genes may be of particular interest for the improvement of CHO cell metabolism.

1.4.1.1. Peroxisome proliferator-activated receptor-gamma coactivator-1 alpha (PGC1α)

The transcriptional coactivators of the Peroxisome proliferator-activated receptor-gamma coactivator-1 (PGC1) family are commonly referred to as the master regulators of mitochondrial biogenesis and metabolism. This family of transcriptional coactivators comprises three different members: PGC1α, PGC1β, and PRC (*Scarpulla, Vega and Kelly, 2012)*.

Peroxisome proliferator-activated receptor-gamma coactivator-1 β (PGC1β) is a known stimulator of mitochondrial biogenesis and respiration, similar to PGC1α, and it is known to be highly expressed in high-energy tissues, like brown adipose tissue as well as heart and skeletal muscle (*Y. Zhang et al., 2018)*. While PGC1β and PGC1α perform similar functions, several differences between these two coactivators exist. These differences are mainly tissue-specificity and expression in response to stimuli. PGC1β expression is not upregulated in brown adipose tissue (BAT) in response to cold, obesity, or exercise, while overexpression of PGC1α is observed under the same circumstances, suggesting that PGC1β may play a role in adrenergic-independent mitochondrial biogenesis, while the role of PGC1α is focused on the adrenergic-dependent process (*Meirhaeghe et al., 2003*).

The PGC-1-Related Coactivator (PRC), like PGC1α and PGC1β, can bind to transcription factors related to mitochondrial activity, exerting metabolic regulation functions

(*Scarpulla, Vega and Kelly, 2012)*, as well as regulation of mitochondrial biogenesis by activation of the ERRα gene (*Mirebeau-Prunier et al., 2010*) and microglial activation (*Mou et al., 2015*). It is believed that, in contrast to PGC1α and PGC1β, PRC is essential for early embryonic development (*He et al., 2012*).

Finally, the last member of this family is PGC1α, also known as the Peroxisome proliferator-activated receptor-gamma coactivator-1 α, a known stimulator of mitochondrial biogenesis, respiration, and adaptative thermogenesis. PGC1α was the first member of the PGC1 family to be discovered, being identified during a study of cold-induced thermogenesis, during which it was found to be associated with the PPARγ gene. (*Puigserver et al., 1998*). PGC1α is highly expressed in adipose tissue, liver, pancreas, kidney, the skeletal and cardiac muscles, and the brain (*Dillon, Rebelo and Moraes, 2012; Besseiche et al., 2015*) where is known to induce changes in response to adrenergic stimuli.

PGC1α can bind to transcriptions factors from the PPAR family, such as PPARγ, PPARβ, and PPARα, enhancing peroxisome abundance in the cell and ultimately leading to an increase in Fatty Acid (FA) oxidation levels (*Huang et al., 2017*). PGC1α also has an important role in the response to stress stimuli, such as exercise, being able to elevate the energy available to muscle cells by increasing the browning of White Adipocytes (WAT) by overexpression of the Uncoupling Protein 1 (UCP1) (*Sandri et al., 2006*). PGC1α also aids in exercise by increasing mitochondrial biogenesis and angiogenesis in response to exercise (*Chinsomboon et al., 2009*).

PGC1α also binds to Nuclear Respiratory Factors 1 and 2 (NRF-1 and NRF2) Estrogen-Related Receptor α (ERRα) and the mitochondrial Transcription Factor A (TFAM), which bind themselves to the promoter region of mitochondrial genes, such as β-ATP synthase, cytochrome c or cytochrome c oxidase unit (*Gleyzer, Vercauteren and Scarpulla, 2005; Dillon, Rebelo and Moraes, 2012)*. This binding greatly increases both the activity and the gene expression of NRF-1, NRF2 and TFAM, additionally, PGC1α also coactivates the transcriptional activity of NRF-1 in particular (*Cheng, Ku and Lin, 2018)*. This upregulation of mitochondrial transcription factors increases mtDNA replication, facilitating mitochondrial biogenesis, as well as the expression of genes from the respiratory chain, thus increasing oxidative metabolism. PGC1α is also known for protecting mitochondria from ROS damage and increasing the cells' lifespan, although to

a limited extent (*Karlsson et al., 2019*). Cancer cells use this mechanism to develop resistance to chemotherapeutic drugs (*M. J. Sun et al., 2019*).

All these facts point to PGC1α being an interesting target for metabolic engineering in r-protein-producing cell lines, as overexpression of PGC1α has been described to increase mitochondrial biogenesis and improve mitochondrial oxidation while simultaneously protecting the cells from ROS related damage.

1.4.1.2. Dynamin-Related Protein 1 (DRP1)

The members of the dynamin family of proteins are key components of mitochondrial dynamics. Among them, The Dynamin Related Protein 1, also known as DRP1, is a key protein for the mitochondrial fission process (Elena Smirnova *et al.*, 2001). DRP1 is, evolutionarily speaking, a very conserved protein, present mainly in the cytosol, but also located in the mitochondrial microtubules pooled in spots that normally correspond with future fission points (*Chan, 2006*). DRP1 is able to self-assemble at the fission sites in the inner mitochondrial membrane into large multimeric spirals, mediating the process of mitochondrial fission through constriction of the mitochondria, which is dependent on the DRP1 subunit containing a GTPase effector domain. *(Frank et al.*, 2001; *Chan, 2006*).

The mitochondrial fission process has a fundamental role in the induction of apoptosis and mitophagy in cells. (*Cassidy-Stone et al., 2008; Pascucci et al., 2021)* which exerts a protective effect on the cell against damaging compounds such as ROS or 3-chlorpropane-1,2-diol (*Jin et al., 2020*). DRP1 is a fundamental component of mitochondria, and the knockdown of this protein causes mitochondrial dysfunction and severe muscle atrophy *(Dulac et al.*, 2020). On the other hand, overexpression of DRP1 can produce an excess of mitochondrial fission in certain tissues, causing metabolic disorders in humans. One example of this is diabetes: deletion of DRP1 in the podocytes of mice suffering diabetic nephropathy was able to successfully rescue the pathological features of the cells (*Ayanga et al., 2016).*

The relationship between DRP1 and protection against the aging process related to ROS was described by Rana and collaborators, who found that induction of DRP1 expression in midlife *Drosophila melanogaster* significantly increased their lifespan (*Rana et al., 2017).* The mitochondria of the flies were observed to take on a less rounded, more elongated shape with aging, making the mitochondria less functional. The induction of

mitochondria fission by DRP1 overexpression successfully restored these mitochondria to the more rounded, functional state, additionally increasing mitochondrial respiration and reducing ROS levels. Therefore, the induction of DRP1 expression in r-protein producing cell lines, such as CHO cells, may have the potential to increase the long-term viability of the cells without compromising the r-protein titer, overall increasing the final product yield of the cells.

1.4.1.3. Adenine Nucleotide Translocator Isoform 1 (ANT1)

ANT is an integral protein located in the mitochondrial membrane, with a structure similar to other mitochondrial solute carriers. This protein facilitates the exchange of cytosolic ADP for mitochondrial ATP, coupled with ATP synthesis (*Erich Pfaff, Hans Walter Heldt and Martin Klinenberg 1969; Brenner et al., 2011)*. However, the transport efficiency of ANT is quite low, being a potential limiting step in the energy generation processes in mitochondria (*Klingenberg, 2008)*. ANT has four different isoforms, with tissue-specific expression.

ANT1 is a member of the mitochondrial carrier subfamily which is expressed in skeletal/heart muscle and brain. Its function is to translocate ADP from the cytoplasm into the mitochondrial matrix and ADP from the mitochondrial matrix into the cytoplasm (*Brenner et al., 2011*). It is also known as SLC25A4 (Solute Carrier Family 25 member 4).

Knock-down of ANT1 in mouse skeletal muscle has been reported to lead to mitochondrial hyperproliferation in diabetic mice (*Morrow et al., 2017)*. During this process subunit V of the respiratory chain, ATPase, partially uncouples from the electron transport chain through not well-understood means, leading the cell to a constant maximum Electron Transport System (ETS) state, in which the cells achieve their maximum OXPHOS (Oxidative Phosphorilation) potential, but are totally uncoupled from ATPase activity, partially inhibiting ATP production. Recently, the mitochondrial uncoupling process has been described as a naturally-caused state of respiration, and not mitochondrial dysfunction as previously believed, designed to regulate many biological processes in cells (*Demine, Renard and Arnould, 2019*). Therefore, it could be that the increase in oxidative activity caused by knock-down of ANT1 may cause a corresponding increase in r-protein production in producing cell lines, such as CHO cells, as oxidative

phosphorylation and r-protein production are known to be correlated (*Templeton et al., 2013)*.

1.4.2. Mitochondrial Heteroplasmy

1.4.2.1.Characteristics of heteroplasmy

As previously described, mitochondria contain their own DNA, a 16.5 kb circular genome commonly known as mtDNA in which 37 genes are located (*Kelly et al., 2017*). Each mitochondrion contains 2-10 copies of mtDNA, capable of autonomous replication. This genome, like its nuclear counterpart, is susceptible to mutations, which tend to accumulate over time, as the mitochondrial polymerases lack efficient proof-reading systems, although the polymerase POLG is believed to perform proof-reading to some extent (*Trifunovic et al., 2004*). Genomic repair mechanisms in the mitochondria are not well understood and believed to be less numerous than in the nucleus, involving mainly base-excision repair (BER) and microhomology-mediated end joining (MMEJ) (*Alexeyev et al., 2013; Krasich and Copeland, 2017; Zinovkina, 2018)*, making the mitochondrial genome more prone to accumulating mutations than the nuclear genome.

As each mitochondrion can contain several copies of mtDNA accumulated mutations may be different on each genome copy. This coexistence of two or more different mtDNA molecules in the same mitochondrion is referred to as ``heteroplasmy´´ (*Smeitink, Van Den Heuvel and DiMauro, 2001; Just, Irwin and Parson, 2015)*. The mitochondrion can possess mtDNA sequences that differ in their length, which is defined as ``Length Heteroplasmy´´ (LHP) or, alternatively, may differ at a single nucleotide position, which is then defined as ``Point Heteroplasmy´´ (PHP) (*Just, Irwin and Parson, 2015*). Where all the mtDNA copies inside a given mitochondrion are identical this is referred to as homoplasmy. (*Stewart and Chinnery, 2015*).

As the mtDNA encodes important subunits of the respiratory chain complexes, mutations can exert a significant influence on cellular energetics. However, the degree of heteroplasmy is important here as mitochondria may simultaneously possess enough wild-type mtDNA copies to maintain normal mitochondrial activity. Only if enough mutant copies are present will there be an impactful metabolic impact. The percentage of mutant mtDNA copies necessary to exceed this ``biochemical threshold´´ and cause

changes in the respiratory chain is commonly very high: an average of 80% of mtDNA must possess the mutation to cause an observable metabolic effect, suggesting most heteroplasmic mutations tend to either accumulate or disappear due to their neutral impact in the mitochondrial metabolism. *(Durham et al., 2007; Stewart and Chinnery, 2015; van den Ameele et al., 2020)*.

Heteroplasmy is known to be quite ubiquitous, with pathogenic mtDNA variants believed to be more common than expected in humans (*Elliott et al., 2008)*. Most heteroplasmic mutations do not lead to an actual disease, being either neutral or even potentially conferring an advantageous trait to the cell or organism in question, should the mutant mtDNA molecule numbers be high enough to surpass the biochemical threshold (*van den Ameele et al., 2020)*. The level of pathogenicity caused by deleterious mtDNA mutations is mainly determined by the relative abundance and the nature of the mutation (*Grady et al., 2018*). Most deleterious mtDNA mutations are considered ``recessive mutations´´, because the frequencies of these mutations are normally not high enough to exceed the biochemical threshold, even if these mutations are commonly found at low frequencies in a given population (*Elliott et al., 2008; Stewart and Chinnery, 2015; van den Ameele et al., 2020)*.

Despite this, mitochondrial heteroplasmy is known to be associated with several hereditary human diseases, some examples include Lieber Hereditary Optic Neuropathy (LHON) *(Yu et al., 2012; Reddy et al., 2015; Jankauskaitė, Bartnik and Kodroń, 2017)*, Mitochondrial encephalomyopathy and lactic acidosis with stroke-like episodes (MELAS) (*Chinnery et al., 1997; Rahman et al., 2001; El-Hattab et al., 2015)*, Myoclonic Epilepsy and ragged red fiber (MERRF) (*Chinnery et al., 1997; Blakely et al., 2014*), Alzheimer's disease *(Corral-Debrinski et al., 1994; Keogh and Chinnery, 201*5) and Parkinson's disease (*Bender et al., 2006; Keogh and Chinnery, 2015*). There are approximately 200 different known mtDNA mutations associated with human metabolic disorders, which indicates changes in heteroplasmy happening both over the generations and with time.

Changes in heteroplasmy can come from various sources. A known source of random and abrupt changes in heteroplasmy is the phenomenon commonly known as the "mitochondrial bottleneck´´ which occurs in germline cells. The bottleneck results in an unequal, random distribution of the mitochondria, and with them, the mtDNA within

them, from the primordial maternal cells after division, in which mtDNA replication does not occur, to the primary oocytes. Each of the primary oocytes will receive random copies of mtDNA coming from the primordial cell, which may be either mutant mtDNA, wild-type DNA, or a mix of both, changing the proportion between the mutant and the wild-type variants. Then the oocytes rapidly replicate the mtDNA, further increasing the number of mutant mtDNA copies if there are any present. This process can result in secondary oocytes containing only wild-type mtDNA, only mutant mtDNA, or, like the parent, a mix of both (*Shoubridge and Wai, 2007*). While the exact mechanism behind the segregation of mtDNA to the oocytes is not fully understood, several proposals other than random drift, like the mtDNA being separated in clusters in the primordial cells before division, have been described in the literature (*Diot et al., 2016*). This mechanism has been also theorized to have a protective function against deleterious mtDNA mutations, which may be selected against in a later stage of the development, as has seen observed in mice (*Fan et al., 2008; Zhang, Burr and Chinnery, 2018)*. However, this mechanism also can cause the congenital transmission of hereditary metabolic disorders from healthy mothers carrying a mutation to the offspring. (*Diot et al., 2016*).

Beyond the germline, heteroplasmic mutations are also known to appear with time in somatic cell lines. The gradual increase of inherited mtDNA mutations during development and aging is known to be the cause of most late-onset human mitochondrial disorders *(van den Ameele et al., 2020*). This makes the prediction of human mitochondrial diseases quite hard, due to the unpredictable nature of the segregation. Furthermore, it is suspected that in the case of some metabolic degenerative diseases, such as Alzheimer, Parkinson or diabetes, the accumulation of novel mtDNA mutations, which appear with aging, may be the root of these diseases (*Keogh and Chinnery, 2015; Stewart and Chinnery, 2015; van den Ameele et al., 2020)*.

Some somatic mitochondria mutations, like the common m3243 A > G mutation in the tRNA for leucine, are well known and characterized. In the case of said mutation, the mutant mtDNA copies tend to accumulate in the muscle tissue as the patient ages, while disappearing from the hematopoietic lineage (*Rajasimha, Chinnery and Samuels, 2008; Monnot et al., 2011)*. Rajasimha and collaborators suggested the proliferating stem cells be more vulnerable to the negative effects of dysfunctional mitochondria, which resulted in the observed exponential decrease in mutated hematopoietic cells. (*Rajasimha,*

Chinnery and Samuels, 2008). Other mutations have been reported in the literature to follow a similar pattern concerning blood cells and muscle tissue *(Larsson et al., 1990; Jacobi et al., 2001*). Despite this, this tissue-dependent segregation has not been observed for all the notorious detrimental mtDNA mutations: for example, the m.8344A mutation in the tRNA for lysine does not show any decrease in blood cells with aging (*White et al., 1999*). In addition, variants with no measurable effect in mitochondria-related metabolism have also been observed to follow a non-random segregation pattern across different tissues (*Battersby, Loredo-Osti and Shoubridge, 2003*).

As previously mentioned, new mitochondrial mutations can also arise during aging and development. These causes mosaicism among the cells of proliferating tissue such as the gut (*McDonald et al., 2006*), skin fibroblast, and hematopoietic cells (*Taylor et al., 2003; Greaves et al., 2006; Kang et al., 2016)*. While the proliferating cells mostly tend to accumulate point mutations, post-mitotic cells have been reported to be more prone to mtDNA deletions. Accumulation of somatic deletions is common in the context of the natural aging process (*Keogh and Chinnery, 2015; van den Ameele et al., 2020*), but also human neurodegenerative diseases, such as Alzheimer *(Corral-Debrinski et al., 1994*) or Parkinson (*Bender et al., 2006*).

The segregation of somatic heteroplasmy is theorized to occur through different mechanisms. Some examples of which will be provided

The first proposed mechanism is the potential replication selection of mutant mtDNA versus wild-type mtDNA. The replication of the mtDNA is believed to be a ``relaxed replication´´, this is a replication-independent from the nuclear replication or any other genome in the cell, similar to DNA plasmids (*Chinnery and Samuels, 1999*), which means any mtDNA variants somehow favored by the replication process can accumulate over time even in cells not actively performing replication. While this may seem obvious for positive or neutral variants, some harmful or detrimental variants are known to offer a replicative advantage, engaging a ``selfish´´ behavior and being able to displace the regular wild-type genomes and eventually taking over the cells (*Ma and O'Farrell, 2016*). The mtDNA variant leading to MELAS, m.3243A > G, is known to possess this kind of replicative advantage despite being a detrimental variant (*Yoneda et al., 1992*).

A second proposed mechanism is a variability caused by mitochondria biogenesis and the repair mechanism of the mitochondria. The mtDNA replication in post-mitotic cells is

proposed to be dependent on the amount of mutant and healthy mtDNA molecules inside the cell, with the mtDNA replication increasing to keep the number of healthy mtDNA copies within a minimum threshold at which the mitochondria can work normally despite possessing dysfunctional mtDNA molecules (*Chinnery and Samuels, 1999; Johnston et al., 2015)*. If the number of dysfunctional mitochondria is high enough, a signal is sent to the nucleus, which triggers the biosynthesis of new mitochondria to compensate for the decrease in mitochondria-generated energy, using the previously mentioned PGC1 family members to activate the transcription factors involved in mitochondria synthesis (*Hock and Kralli, 2009*). If the number of mutant mtDNA copies is high enough, this will result in constant replication cycles and accumulation of mutant mtDNA in the cell (*Chinnery and Samuels, 1999; van den Ameele et al., 2020*).

Finally, the third proposal suggests mitochondrial dynamics to be behind the segregation of the mtDNA. These dynamics include processes such as selective mitochondrial degradation, mitochondria fusion, and the mitochondria fission processes. The degradation of mitochondria is a process believed to target dysfunctional and/or old mitochondria. Mitochondria degradation is believed to occur through a process named mitophagy, which consists of a specific autophagy process capable of removing blocks of old or dysfunctional mitochondria, along with their mtDNA (*Pickles, Vigié and Youle, 2018)*. This mechanism will shift heteroplasmy towards wild-type mtDNA, in the case of the mutant mtDNA being detrimental to mitochondrial metabolism, by eliminating the dysfunctional mitochondria, preventing the mutant mtDNA from such mitochondria from spreading. Mitochondrial fusion and fission processes are also known to have a strong impact on the mtDNA content (*Tam et al., 2015*). A recent study performed in *Drosophila* by Kandul and collaborators reported a significant increase of fusion/fission transitions to result in a significant increase in mtDNA clearing (*Kandul et al., 2016*). This data support previous observations in patients afflicted with Charcot-Marie-Tooth disease, which is linked to a mutation in the MFN2 gene a mitochondria fusion factor, which is reported to prevent mitochondrial fusion and increase the number of mtDNA mutations (*Rouzier et al., 2012*).

It is worth noting that while deletions seemingly accumulate over time in post-mitotic cells, they tend to quickly disappear in dividing cells from the same tissue. For example, a patient with the Kearns-Sayre syndrome, a disease caused by the accumulation of a

deletion in muscle tissue, was reported to show accumulation of such deletions in post-mitotic muscle cells, but no deletion was found in cultures of proliferating myoblasts from the same patient. (*Moraes et al., 1989; Clark et al 1997)*. An interesting explanation for this phenomenon is the existence of a ``somatic bottleneck´´ during asymmetric cell divisions, comparable to the ``mitochondrial bottleneck´´ from the germline, resulting in smaller daughter cells receiving fewer mtDNA copies, which will result in a restriction of heterogeneity and lead to rapid segregation of mtDNA. Supporting this theory, the asymmetric segregation of mtDNA has been described in mammalian cells, which is believed to be required to maintain the stemness of stem cells (*Katajisto et al., 2015*).

1.4.2.2.Heteroplasmy in CHO cells.

Heteroplasmy adds another layer of variability to the already diverse CHO cells. The main regulator pharmacological agencies, such as the FDA in the United States or the EMA in Europe include in their guidelines and regulations the need to generate producer cell lines with consistent behaviour, which is normally referred to as ``phenotypic stability´´. As the presence of mutant mtDNA can potentially interfere with the metabolic activity of the cell, and consequently with the phenotypic stability of the clones, analysis of the underlying heteroplasmy in CHO cells may help to understand and/or prevent potential undesirable metabolic shifts.

An ultra-deep next-generation sequencing (NGS) study comparing 22 CHO cell lines was performed, discovering widespread genetic heterogeneity across all the cell lines (*Kelly et al., 2017)*. In this study, the NGS was performed at an average depth of coverage of 4000X, identifying genetic heteroplasmy in all the cell lines, which were then compared to the Chinese Hamster mitochondria reference genome. The mutations were observed to occur at an allele frequency of between 1 and 99% heteroplasmic variants to full heteroplasmic changes. Some of the homoplasic (mutations with a frequency of nearly 99% were considered homoplasic) and the heteroplasmic variations identified were observed to be specific to certain lineages, such as CHO-K1.

A total of 197 variants at 130 nucleotide positions were identified with shared heteroplasmic mutations. At least one heteroplasmic variant in each cell line resulted in a predicted amino acid change, which illustrates the potential for impact due to heteroplasmy in CHO mitochondrial function. Additionally, the heteroplasmic mutations

were observed to propagate independently and at a different rate in a panel of CHO cell clones derived from a single cell line development (cloning) project. An example of this was in the cytochrome b (CYTB) gene, in which the parental sequence reflected the Chinese hamster reference, while the clones presented a deletion (m.14136delA) predicted to cause a frameshift mutation, with a minor allele frequency (MAF) ranging from 7.7% to 52%, which could potentially play a role in the varying degrees of cell growth rate previously observed in these clones.

As previously mentioned, mitochondrial heteroplasmy can propagate under the radar if it has no discernible phenotypic effects, for example, if the load of mutant mtDNA is not high enough to exceed the biochemical threshold and cause observable changes in metabolism. . Kelly and collaborators' study also highlighted the mitochondria as a new source of phenotypic variability in CHO cells, adding a new layer to the recognised genetic instability of CHO but also constituting a source of clonal variation at the level of genetic programming.

The present study is the natural continuation of Kelly and collaborators' study, aiming to better understand the phenotypic effects of heteroplasmy on the metabolism of CHO clones (if any) and to evaluate the frequency and rate of change in heteroplasmy levels in CHO clones over time.

1.5. Aims and objectives.

The aims and objectives of the present study were the following:

1. To evaluate the impact of heteroplasmy on bioprocess-relevant phenotypes of CHO cells.
2. To evaluate whether potential improvements in CHO cell culture performance can be achieved by selecting CHO clones with different mitochondrial heteroplasmy.
3. To investigate the evolution of heteroplasmy in CHO cells over the course of several passages.
4. To study the potential of several mitochondrial-related nuclear-encoded genes to engineer mitochondrial metabolism in a way that benefits the culture performance and the r-protein productivity of CHO cell clones.
5. To evaluate the potential of alternative methods of metabolic engineering to improve CHO cell culture performance and mitochondrial-related metabolism.

CHAPTER 2

MATERIALS AND METHODS

2.1. Cell culture techniques:

2.1.1. General cell culture laboratory practices.

All the cell culture work described in this study was performed in negatively pressured rooms and inside Class II Laminar Flow Cabinets (Class II-LFC). This includes the preparation and/or formulation of all reagents that require sterile conditions. The LFC was allowed a warm-up time before use, of roughly 15 minutes. After the warm-up time, the LFC was cleaned using a 70% Industrial Methylated Spirits (IMS) solution and a wipe. All and every item introduced on the LFC were also promptly cleaned with 70% IMS before being introduced into the cabinet. This included the hands of the operator, always properly covered by nitrile protective gloves. The LFC was fully cleaned and disinfected once every 2 weeks using Virkon and IMS in succession. Additionally, LFCs were annually qualified and maintained to ensure the proper function of the cabinets.

Cell culture work was routinely performed handling only a single cell type at any time to avoid cross-contamination. Additionally, when work with two different cell types was performed the LFC was fully cleared in between work with the two cell types, which included a cabinet clean-up and a warm-up time of 15 minutes between the work performed with every cell type.

2.1.2. Cell-Line sub-culturing.

Routinely, cells were grown in suspension culture. However, eventually, some cells were grown in adherent culture.

For routine suspension culture, cells were incubated in 50mL vented cap spin tubes (TPP) in 5 mL of cell culture media. Alternatively, cells were incubated in 250mL vented cap flask (Corning) for cultures ranging between 20 and 60 mL of cell culture media. Additionally, cells were occasionally incubated in 24-well suspension plates (Corning), normally during transfection or cloning experiments, in 1mL of cell culture media. All cells in suspension culture were grown in a Kühner Climo-Shaker ISF1-X incubator set up at 37ºC, 80% humidity, 5% CO_2, and 170 rpm. Routinely, these cells were grown on either CHO-S-SFMII media (Gibco) with 1% Poly-vinyl alcohol (PVA) as an anti-clumping agent. Several cell types and/or experiments required the use of different media, such as BalanCD CHO Growth A (Irvine Scientific) supplemented with L-glutamine (4 mM) or CD-CHO media (Gibco). The cells were routinely seeded at $2x10^5$ cells/mL and

passaged every 72-96 hours depending on the cell type to maintain them growing and in the mid-exponential phase of growth.

For Adherent culture, cells were grown on a Tissue culture flask (25 cm^2 or 75 cm^2) in Dulbecco's Modified Eagle Medium: Nutrient Mixture F-12 (DMEM-F12) with 5% Fetal Bovine Serum (FBS) and incubated in a static incubator at set up at 37ºC, 80% humidity and 5% CO_2. Cells were allowed to grow to approximately 80% of confluence and were routinely passed about twice a week (every 96 hours). The passage was performed by removing the cell culture media, washing with 5-10 mL of Phosphate Buffer Saline (PBS) depending on the size of the flask, and trypsinizing the flask using a 4-8mL of a trypsin-EDTA solution, incubated 8 minutes at 37ºC. Fresh warm culture media containing FBS, in equal volume to the trypsin solution, was added to inhibit the trypsin and the cell suspension was recovered in a centrifuge tube, which was centrifuged at 1000g for 5 minutes. The supernatant containing trypsin was then discarded and the cell pellet resuspended in fresh DMEM-F12 media. Flask was then seeded, typically mixing 9:10 parts in volume of fresh media and 1:10 parts in volume of cell suspension.
The volumes used for each different flask or plate can be seen in **Table 2.1.**

Flask	DMEM-F12 (culture)	PBS (wash)	Trypsin-EDTA (detach)	DMEM-F12 (Trypsin Inhibition)
T25	4mL	5mL	2mL	2mL
T75	8mL	10mL	4mL	4mL
24-well plate	1mL	1.5 mL	0.5mL	0.5mL

Table 2. 1. Volumes used on routine adherent culture. Volumes include, from left to right, DMEM-F12 culture media volume used for culture, PBS volume used for wash, Trypsin-EDTA volume used to detach the cells from the flask, and the DMEM-F12 culture media volume added to the trypsin after incubation to inhibit it.

2.1.3. Cell density and viability determination.

Cell density and viability of the cells were routinely determined using two different systems depending on the number of samples to be evaluated.

2.1.3.1. Trypan Blue exclusion method

Cells were evaluated using a haematocytometer and trypan blue for staining. An aliquot of 10 µL of cell sample was taken and mixed with 10 µL of Trypan blue (Gibco) in a 1:1 dilution. The dilution was well mixed and loaded into the chamber of a haematocytometer. The cells on the 4 big squares (composed of 16 smaller squares) of the grid were counted, including the cells located in the outer border of the squares, but not the cells located in the inner borders of the squares. Cells seen as clear or ``white´´ were identified as viable cells, while cells seen as dark or ``blue´´ were considered dead cells.

After counting, the average of the 4 big squares was calculated for both viable cells and total cells (viable + dead cells), then the following formulas were used to calculate the viable cell density, the total viable cells, and viability.

1. $Viable\ cell\ density = Average\ viable\ cells\ x\ dilution\ factor\ x\ 10000$
2. $Total\ viable\ cells = Viable\ cell\ density\ x\ Volume\ of\ cell\ suspension$
3. $Total\ cell\ density = Average\ Total\ cells\ x\ dilution\ factor\ x\ 10000$
4. $Total\ cell\ number = Total\ cell\ density\ x\ Volume\ of\ cell\ suspension$
5. $$Viability = \frac{Viable\ total\ cells\ x\ 100}{Total\ cells\ number}$$

2.1.3.2. Flow cytometry (Guava Easycyte™)

For large amounts of cells, both cell density and viability were measured using a Guava Easycyte™ bench-top-flow-cytometer (Merk). For routine cell counting, The Viacount® assay was used. The Viacount® dye was prepared in house in an LFC using the following formula:

For 100mL of Viacount® Dye:

- 100mL of sterile PBS.
- 200µL of LDS-751 (Invitrogen)
- 400µL of Propidium Iodide

The Viacount® dye was always protected from light and was stored at 4ºC after preparation. Samples for the Viacount® assay were prepared in U-shaped bottom 96-well plates. A small aliquot of cell culture suspension was diluted with PBS up to 100 µL in the well, after which 100 µL of Viacount® dye were added into the well, obtaining a 1:1 dilution. The initial dilution of the cell suspension made on PBS depended on the number of cells roughly expected, as the Viacount® assay needs the samples to fit between 10-500 cells/ µL to ensure the accuracy of the counting. A typical example of dilution for day 3 cells was to dilute 20 µL of cell suspension in 80 µL of PBS, then adding 100 mL of Viacount® dye, obtaining a final cell dilution of 1:10. The Viacount® software was then run and the cells were counted by the instrument.

2.1.3.3.Calculation of growth rate:

Growth rate µ [1/d] was calculated according to the following equation (*Zboray et al., 2015)* where X [cells] represents the total viable cell number and t [d] the time in days.

$$\mu = \ln(X1/X0) * 1/(t1 - t0)$$

2.1.4. Cryopreservation of cells.

For the cryopreservation of the cells, cells were split into 20mL of media and cultured as routinely. After 72 hours of culture, freezing media, containing 20% DMSO, was formulated, after which cells were counted as previously described. Then cells were centrifuged and resuspended in fresh, cold (4ºC) culture media. The volume of media used for resuspension depended on the cell density obtained, with 1mL of media being used for every $15x10^6$ cells to be thawed. For each cryovial, 0.5mL of cell suspension was added, which were topped and mixed with 0.5mL of freezing media. Final concentrations on each cryovial were 10% DMSO and approximately $7x10^6$ cells/mL. Cryovials were then stored in a polystyrene box and placed into the -20ºC freezer for 2 hours. After the 2 hours have passed, the cryovials were moved into a -80ºC freezer. After

3 days of storage on the -80ºC, roughly ¼ of the cryovials were moved into liquid nitrogen storage to preserve a stock of the cells, while the other vials remained on the freezer (-80ºC) for routine use and mid-term storage.

2.1.5. Revival of cryopreserved cells.

To revive the cells stored in either the -80ºC freezer or in the liquid nitrogen tank, some warm, fresh culture media, roughly 5mL, was first prepared in a centrifuge tube. Then the corresponding cryovial was carefully recovered from the corresponding storage and warmed up slightly in a hot water bath until the frozen media detached from the bottom of the vial. The cryovial was then introduced into the LFC and the thaw content was recovered into the centrifuge tube with media using a sterile plastic Pasteur pipette. The same pipette was used to wash the vial with fresh, warm media to fully thaw the content of the media and ensure the recovery of the maximum number of cells. The cell suspension was then centrifuged at 1000g for 5 minutes and the pellet was resuspended into 5mL of fresh culture media. The cells were then counted and seeded correspondingly.

2.1.6. Transfection of plasmids and siRNA into the CHO cells.

To perform transfections, the TransIt-X2 Dynamic Delivery System (Mirus Bio) was used. Transfections were performed in non-treated 24-well plates for suspension culture. 24 hours before the transfection, the cells to be transfected were moved into fresh media at a density between 0,5-2 million cells/mL and incubated overnight. On the day of the transfection, fresh, non-supplemented media was warmed up and used to pre-complex the corresponding DNA to be transfected and the TransIT-X2 reagent. For the pre-complexing process, 2 µL of TransIt-X2 were used for every 1 µg of DNA, taking into account that a rough average of 500 µg of DNA were used per $1x10^6$ cells transfected, the precomplex solution was incubated for 20 minutes at Room Temperature.

Cells were then counted and $1x10^6$ cells were plated per well, suspended 900 µL of fresh, warm, fully supplemented media. Then 100 µL of complexed DNA were added to each well. The 24-well plate was then cultured as previously described in **section 2.2.2**.

The process used to integrate siRNA into the cells was roughly the same. Before the complexing step, siRNA was diluted to a 20nM concentration in ultra-purified, nuclease-free water. Before the complexing step, the siRNA dilution was warmed at room temperature for 5 minutes. 1.54 µL of siRNA per every, 2 µL of TransIt-X2 reagent were

used for the pre-complexing process, after which the process continued exactly as described before for DNA transfection.

2.1.7. Evaluation of transfection efficiency.

To evaluate the efficiency of the transfection process (% of transfected cells), a plasmid containing a GFP reporter gene was used as a positive control in all the transfection experiments. The Guava Easycyte™ bench-top-flow-cytometer was used for this purpose, using the Expressplus software of the instrument to measure cell fluorescence. The fluorescence gate for dark, non-fluorescent cells was defined using control, non-transfected cells, while the gate for bright, fluorescent cells was defined using positive control cell populations. The same settings were used to analyse all the populations to maintain comparability of results. To perform the analysis, the cells were diluted in PBS to an appropriate concentration (10-500 cells/µL as previously seen) and plated in U-shaped bottom 96-well plates. Typically, 5000 cells were analysed per sample.

2.1.8. Generation of stable cell lines

From the transiently transfected cells generated as described in the 2.2.6 section, stable cell lines were generated by selecting the transfected cells using the corresponding antibiotic. Three pools of transfected cells, coming from three separated wells of a transfection process, were seeded into adhesion culture in three T25 flasks as described in section 2.2.2. The DMEM-F12 culture media used was supplemented with an appropriate amount of the corresponding selection antibiotic. For each batch of selection, three T25 flasks containing non-transfected cells were also seeded and cultured with the DMEM-F12 containing antibiotic as a negative control. These cells were expanded under antibiotic selective pressure up to a T75 flask. This process normally took around two weeks of time, depending on the growth speed of the cells. At this point, the cells were moved into suspension culture and, on the first passage, a cryo-bank of the new, stably transfected cells was generated as described in section 2.2.4. Before experimental use, the cells were adapted to suspension culture for at least three total passages and after the observation of a stable, solid growth pattern.

2.1.9. Limited dilution cloning.

Limited dilution cloning was used to obtain single clone cells from a parental clone. Before the procedure was performed, conditioned media was obtained. Briefly, Parental clone cells were incubated for 48 hours. Then the cells were centrifuged at 1000gs for 10

minutes and the media supernatant recovered. The media was then filtered through a sterile 0.45 µm filter. Finally, the conditioned media was stored at 4ºC until the day of the limited cloning dilution.

For the dilution cloning, parental clone cells were cultured for 72 hours, after which these cells were counted 6 times on the flow cytometer to ensure the maximum accuracy on the counting. Cells were then serially diluted to 5 cells/mL in 50mL of media. The media used on the last dilution was made by mixing 20mL of conditioned media with 80 mL of fresh media. Then, 100 µL of the cell suspension were seeded per well in a tissue-treated 96-well plate, aiming to seed approximately 1 cell per every 2 wells. The cells were then incubated for 10 days, after which wells containing single-cell colonies were screened, selected, and marked. The media was then replaced by fresh media, the cells expanded and the cells from the 24 marked wells were expanded into a tissue treated 24-well culture plate.

2.2. Molecular biology techniques:

2.2.1. RNA extraction and isolation with TRIzol reagent.

RNA was isolated using the TRIzol® to separate cells into different phases containing RNA, DNA, and protein respectively. The reagent in question, TRIzol® reagent (SIGMA-ALDRICH®, T9424). is a ready-to-use reagent, consisting of a monophasic solution of phenol, guanidine isothiocyanate, and other components to facilitate the isolation of RNA species, thus employed for the extraction of high-quality total RNA samples. TRIzol® reagent inhibits RNase activity, disrupts the cells, and dissolves cell components.

The extraction of RNA using TRIzol was routinely performed by adding 1mL of TRIzol® per $5x10^6$ cells. The TRIzol® solution could then be frozen at -80ºC until the protocol could be continued. If frozen, samples of cells in TRIzol® were allowed to thaw in ice and then rest at room temperature before continuing with the RNA extraction. Cells were then mechanically disrupted by pipetting the TRIzol® solution up and down with a 1000 µl pipette. After homogenizing, samples were incubated for 5 minutes at room temperature. Then 200 µl of chloroform per mL of TRIzol® were added to the solution and the solution was vigorously shaken and incubated again at RT for 3 minutes. Samples

were then centrifuged at 12000gs for 15 minutes at 4ºC. As a result, the TRIzol® solution was separated into three different phases, of which the aqueous phase contained the RNA.

The aqueous phase (from now on, RNA solution) was then recovered into a new centrifuge tube, taking care of not mixing it with the other phases. 500 µl per mL of TRIzol® used were added to the RNA solution to precipitate the RNA, the solution was then incubated for 10 minutes at RT and then centrifuged again at 12000gs for 15 minutes at 4ºC. The supernatant was carefully discarded and the pellet was washed twice with 1mL of 75% ethanol per mL of Trizol initially used was added to wash the pellet. The sample was then briefly vortexed and then centrifuged at 75000gs for 5 minutes at 4ºC. The supernatant was discarded and samples were left to air dry for approximately 10 minutes. The RNA was finally resuspended in RNAse-free water, which was previously pre-warmed up to 55ºC to facilitate the resuspension of RNA. The RNA samples obtained this way were stored short term at -20ºC or long term at -80ºC.

2.2.2. DNA isolation with Purification kits (Gene Jet, Qiagen, etc).

The DNA isolation kits, which use purification columns and a series of reagents to purify small circular DNA, were used following the manufacturer's protocol mainly to isolate plasmids from bacterial cultures. The same protocols were also used to purify mtDNA according to the works of Quispe-Tintaya (2013).

To recover isolate plasmids from bacterial cultures, the following steps were followed:

First, the bacteria, pelleted, were resuspended in 250µL of resuspension buffer and transferred to a microcentrifuge tube. The bacteria solution was then mixed with 250µL of lysis buffer and incubated for a minimum of 3 minutes and no more than 5 minutes to avoid denaturalization of the plasmid, the lysis was stopped by the addition of 350µL of Neutralization Buffer to the solution, which was mixed by inverting the tube. The solution was then centrifuged (5 min, 12000 rpm) to pellet cell debris and chromosomal DNA. The supernatant was moved into a purification column, included in the kit, taking care not to disturb the waste pellet. The column was placed in a collection tube and centrifuged, after which the flow-through was discarded. 500µL of washing buffer was then added to the column, which was centrifuged again for 60s at 12000 rpm, the flow-through was again discarded. The washing step was repeated twice, after which one

additional centrifugation was performed to get rid of the ethanol residues on the sample. Finally, the column was moved into a fresh 1.5mL centrifuge tube and 20-50 µL of Elution buffer was added to the center of the column to elute the DNA. The column was incubated for 2 minutes at Room Temperature and then centrifuged at 120000rpm for 2 minutes.

To purify mt-DNA, several changes were made to the protocol and extra steps were taken:

Before starting the process, a 24-well plate with attached CHO cells, media was carefully removed and cells were washed with 2 mL of sterile PBS to ensure full removal of the media. Then, 150 µL of 0,01% SDS lysis buffer were added to each well and distributed on the surface to ensure cell lysis. Then the plate was frozen at -80ºC until use.

On the day of the mt-DNA extraction, the plate was thaw in ice and the protocol was performed as described above, skipping the resuspension buffer step and starting with the lysis buffer step. Additionally, two elution steps were performed instead of one, each of them using 10µL of Elution Buffer, obtaining mtDNA diluted in 20 µL of Elution buffer.

2.2.3. Nucleic acid quantification

2.2.3.1. Nanodrop® Spectrophotometer.

The Nanodrop® Spectrophotometer was used to quantify DNA and RNA samples. The instrument was cleaned and initialized using a drop of water. Then, a Blank sample, consisting of Nuclease-Free Water or Elution buffer correspondingly was measured to establish the 0. The samples were then measured loading 1µL of sample on the Nanodrop and reading it. Normally, each sample was read three times to ensure accuracy and the average was calculated.

2.2.3.2. Qubit Fluorometric Quantification

The Qubit 4 Fluorimeter instrument was used to accurately quantify mtDNA samples of with low DNA concentrations with a fluorometric assay. First, the standard two samples were prepared by mixing 190 µL of Qubit Buffer with 10 µL of Qubit Standard sample. The standard sample was read and the instrument calibrated. Then, mtDNA samples were prepared to be read in the Qubit instrument by mixing 198 µL of Qubit buffer with 2 µL of mtDNA sample, previously well mixed. The sample was then read on Qubit, using the dsDNA setting for this purpose.

2.2.4. Nucleic acid amplification assays.

2.2.4.1. Bacterial Transformation

For plasmid amplification, bacterial transformations were performed. A 1.7 mL microcentrifuge tube containing 30-100 µL of Competent DH5alpha Sub Cloning Efficiency E. coli (Invitrogen), +10% of the volume of the ligation reaction or 1% of the volume was used for pure plasmid amplification. The mix was incubated in ice for 30 minutes. Then, the mix was subjected to a heat shock at 42ºC for 40 seconds in a water batch and incubated again in ice for 2 minutes. 300-500 µL of S.O.C. medium (Invitrogen) were added to the mix. The transformed cells were incubated for 1 hour at 37oC in a shaken platform at 220 rpm. The samples were then centrifuged at 4.000 rpm for 5 minutes. All the Supernatant, but 50-100 µL was discarded, and cell pellets were re-suspended in the remaining medium. The obtained bacterial suspensions were plated in pre-warmed LB-Agar containing the corresponding selection antibiotic, by spreading 5-50 µL of the bacterial suspension. The plates were incubated overnight at 37ºC, lid down to avoid condensation drops falling on the agar surface. Colonies could be observed after the incubation, and plates could be stored at 4ºC for up to 2 weeks.

2.2.4.2. Primer design and testing

To amplify sequences of interest inside a gene or to quantify gene expression, primers were designed using in silico-tools like the primer blast tool (https://www.ncbi.nlm.nih.gov/tools/primer-blast/) from the National Center for Biotechnology Information (NICB) or the Primer3 software (http://primer3.ut.ee). Normally, 2-3 pairs of primers were designed and ordered to Integrated DNA Technologies (IDT). Primers were resuspended in Nuclease Free water and well mixed making a stock concentration of 100µM upon arrival, according to IDT instructions, and stored at -20ºC until use. Before use, primers were thawed in ice and diluted 1:10 to a work concentration of 10µM when no working solution was available. The primers at working dilution were also stored at -20ºC after use.

Every pair of primers was tested prior to its use on experimental PCR assays. The testing was done by performing a PCR reaction on cDNA samples using the same conditions that

will be used for later assays (such as qPCR assays). The product of the PCR reaction was analysed by Agarose Electrophoresis and the pairs of primers yielding a single band of the expected size were selected. Optimization, when required, was done the same way.

2.2.4.3.Routine PCR

For routine analysis of nucleic acids and testing of the primers, PCR reactions were made using the MyTaq2x kit (Bioline). The primer concentration used ranged from 0.2µM to 1µM. Similarly, the DNA template concentration used ranged normally between 20-200ng, depending on the experiment. All the reactions were prepared in ice and done following the following formula seen in **Table 2.2.**

My Taq 2x reaction template	
Reagents	**Reaction**
MyTaq Mastermix (2X)	12.5µl
Primer forward (10 µM)	1µl
Primer reverse (10 µM)	1µl
Nuclease-free water	X
DNA template	X
Total volume	25µl

Table 2. 2. Example of typical routine PCR template to prepare the reaction. The DNA volume used depended on the details of the experiment being performed. Nuclease-free water was added to make the total volume equal to 25µL.

The PCR conditions included standardized temperatures for Denaturation and Extension and a user-determined Annealing temperature, which was changed depending on the DNA template/fragment to be amplified. These conditions can be seen in **Table 2.3.**

Step	*Temperature*	*Time*	*Cycles*
Initial Denaturation	95℃	1 min	1
Denaturation	95℃	15 s	25-40
Annealing	User determined	15 s	
Extension	72℃	10 s	

Table 2. 3. PCR conditions used for Taq 2X PCR. The annealing temperature was determined for every reaction depending on the DNA template and the primers used.

2.2.4.4.High-Fidelity PCR

For High-fidelity amplification of mitochondria DNA, the Platinum Taq High-fidelity Polymerase (Life technologies 11304-011) was used. The primer concentration used for these reactions was set at 0.2µM in the final reaction. The mtDNA template concentration used ranged normally between 20-200ng depending on the amount of mtDNA available for the lowest concentrated sample, being normally of around 100ng whenever possible. All the reactions were prepared in ice and done following the following formula seen in **Table 2.4.** The conditions used for the HF-PCR process can be seen in **Table 2.5**.

Platinum high fidelity PCR			
Reagent	*volume (µl) for 25ul*	*volume (µl) for 50ul*	*Final Concentration*
HF buffer	2.5	5	1X
50mM MgSO4	1	2	2 mM
10mM Dntp MIX	0.5	1	0.2mM
10 µM Primer Forward	0.5	1	0.2µM
10 µM Primer Reverse	0.5	1	0.2µM
HF polimerase	0.4	0.8	1U/rxn
DNA template	X	X	<500ng
Nuclease-free H_2O	X	X	
Total volume	25	50	

Table 2. 4. Example of typical HF-PCR template to prepare the reaction. The mtDNA volume used depended on the lowest concentrated sample. Nuclease-free water was added to make the total volume equal to 25µL or 50µL**.**

Platinum high fidelity PCR		
Steps	*Temperature*	*Time*
Initial denaturation	94ºC	2 min
25 cycles	94ºC	30 s
	55ºC	30 s
	68ºC	9 min
Final extension	68ºC	10 min

Table 2. 5. PCR conditions used for High-fidelity PCR.

2.2.5. Gene expression assays

2.2.5.1.cDNA synthesis

To quantify the gene expression, the total RNA (extracted as described on 2.2.1) must be transcribed to cDNA. This transcription was done by performing a Reverse-transcriptase

reaction using the High-Capacity cDNA Transcription kit (Applied Biosystems). This kit relies on random primers to generate single-strand cDNA molecules. All the reactions were prepared in ice and done following the following formula seen in **Table 2.6.** Additionally, the conditions used for the RT-PCR process can be seen in **Table 2.7**.

RT-PCR mix	
Reagents	***Reaction***
100mM dNTPs	0.8 µL
Multiscribe	1 µL
10X RT buffer	2 µL
Random primers	2 µL
RNAse inhibitor	1 µL
Nuc. Free water	3,2 µL
RNA template (2 µg)	10 µL
Total	20 µL

Table 2. 6. Example of typical RT-PCR template to prepare the reaction mix.

RT-PCR settings		
Steps of the reaction	***Temperature***	***Time***
STEP 1	25℃	10 min
STEP 2	37℃	120 min
STEP 3	85℃	5 min
STEP 4	4℃	Hold

Table 2. 7. PCR conditions used for RT-PCR reactions**.**

2.2.5.2.Real-time quantitative PCR

To quantify the gene expression the cDNA obtained with the RT-PCR was amplified using the Fast SYBR® Green Master Mix (Applied Biosystems) and the primers previously designed and tested for the target genes. Additionally, control primers (typically housekeeping genes such as GAPDH or β-Actin) were included together with the target genes. This allowed to analyse the qPCR data, obtain a relative quantification of the genes of interest for the different target genes selected and assess that roughly the

same volume of sample and cDNA template was loaded in all the wells. All the reactions were prepared in ice and done following the following formula seen in **Table 2.8.** Additionally, the conditions used for the RT-PCR process can be seen in **Table 2.9**.

Real Time qPCR reaction mix template	
Reagents	***Reaction***
FAST SYBR® GREEN Master Mix	10 µl
Primer Forward (10 µM)	0.5 µl
Primer Reverse (10 µM)	0.5 µl
Nuclease-free H_20	8 µl
cDNA (20ng)	1 µl
Total reaction volume	20 µl

Table 2. 8. Example of typical RT-qPCR template to prepare the reaction mix.

Real Time qPCR reaction settings			
Step	***Temperature***	***Time***	***Cycles***
Fast DNA Polymerase Activation	95℃	20 s	Hold
Denaturation	95℃	3 s	40
Annealing / Extension	60℃	30 s	

Table 2. 9. PCR conditions used for RT-PCR reactions.

2.2.6. Next-Generation sequencing.

2.2.6.1.Mitochondrial DNA purification

The mitochondria DNA amplified by High-fidelity PCR (section 2.2.4) was purified, cleaning it from primers and other small DNAs using a purification protocol with magnetic beads. AMPpure XP beads (Beckman Coulter). The beads were shaken well and, per every mtDNA sample, 20µL of beads were added to 36µL of the sample solution in a 96-well plate. The solution was pipette-mixed 20 times until it looked homogeneous and then incubated 5 minutes at RT. After this, the plate containing the reactions was placed into a magnetic plate for 2 minutes, during which the beads were attached to the walls of the wells by the magnetic attraction, forming a ``ring´´. The supernatant was removed, leaving 5 µL behind, taking care of not disturbing the bead ring. The beads were then washed by adding 200 µL of 70% ethanol to each well, which was then removed

without leaving supernatant behind, this washing process was repeated twice. The bead was then air-dried for 2 minutes, taking care not to leave them to air dry for more than 5 minutes, as the beads could then crack and mtDNA could be lost. The plate containing the beads was then removed from the magnetic plate and 40 µL of elution sample was added per well, mixing with the pipette 10 times until the bead ring was dissolved into the elution buffer. The plate was then placed back into the magnetic plate and incubated for a minute, after which the supernatant was recovered in a new 1.5 mL centrifuge tube, taking care not to disturb the beads.

2.2.6.2.Library generation

Libraries of indexed-paired end sequences were generated using the mtDNA samples obtained after the purification process to be used in the mtDNA sequencing experiment. First, samples were thawed on ice and the mtDNA concentration of each individual sample was measured using Qubit (2.2.4) and samples were diluted to a concentration of 2 ng/µL. At this point, the corresponding mtDNA samples, divided into two different reactions per sample, each of which covered roughly half of the mtDNA-sequence, were pooled together to ensure the presence of a full mt-genome. The pooled reactions were measured again using Qubit and the mtDNA samples were diluted to a final volume of 10 µL and a final concentration of 0.2 ng/ µL of DNA.

From this point onwards, the Nextera XT DNA Sample Preparation kit (Illumina) was used for the library generation process. The first step on this kit was the tagmentation process, consisting in using an engineered transposon able to simultaneously fragment and tag the DNA, adding unique adapter sequences during the process. These adapter sequences will be used in a limited-cycle PCR reaction to amplify the DNA, while simultaneously adding index sequences in both ends of the DNA, enabling the dual-indexed sequencing of the pooled library on the Illumina Iseq system.

- **Tagmentation**

To perform the tagmentation of the mtDNA samples, first, the samples and reagents were ice-thawed. One microcentrifuge tube per sample was prepared, and 10 µL of Tagmentation DNA Buffer (TD) was added to each tube. After this, 5 µL of each mtDNA sample was added into each microcentrifuge tube. As the mtDNA sample was diluted to a concentration of 0.2 ng/ µL, 1 ng of total mtDNA was added per sample. Finally, 5 µL

of Amplicon Tagment Mix (ATM) were added to each sample and mixed well using a pipette.

Samples were then centrifuged at 280g for 1 minute and placed in a thermocycler, which was run using the following program:

- 55ºC for 10 minutes
- Hold at 10ºC

As soon as the samples reached 10ºC, 5 µL of Neutralize Tagment Buffer (NT) were added to each sample and pipette-mixed, taking care of changing pipettes in between samples. Finally, the samples were then centrifuged again at 280g for 1 minute and incubated at RT for 5 minutes.

- **PCR amplification.**

The next step in the library generation procedure was to index the tagmented mtDNA samples using a PCR reaction. The PCR reagents were thawed and prepared. Then, 15 µL of Nextera PCR MasterMix (NPM) were added to each sample. After carefully mixing, every sample was added the corresponding 5 µL Index 2 (S5XXX) and 5 µL of the corresponding Index 1 (N7XXX) to Index the samples (f.e. Parental sample was added indexes N703 and S504, while sample P4C10 was added Indexes N701 and S502, which will be used during the sequencing process to identify each corresponding sample). Each reaction was mixed using a pipette 5 times and centrifuged at 280gs for 1 minute. The PCR was then performed using the conditions described in **Table 2.10.**

Step	*Temperature*	*Time*	*Cycles*
Step 1	72℃	3 min	-
Step 2	95℃	30 s	-
Step 3	95℃	10 s	12
	55℃	30 s	
	72℃	30 s	
Step 4	72℃	5 min	-
Step 4	10℃	Hold	-

Table 2. 10. PCR reaction setup for indexed DNA amplification.

- **DNA purification**

After the PCR amplification, the resulting DNA samples were purified using AMPure XP beads as described before in this section. For each sample, 30 µL of AMPure beads were added to 50 µL of mtDNA sample. Other than that, the process was made identically as previously described and samples were in the end resuspended in 50µL of Resuspension Buffer (RSB).

- **Sample normalization.**

To normalize the samples, the protocol described on the Nextera XT kit was not followed, instead, samples were normalized by calculating the molarity of the samples with the base on the mtDNA concentration of the sample and the average fragment size, after which the samples were normalized to 2nM and pooled together in a library.

First, the fragment size was calculated using a Tapestation instrument (Agilent), an automated quick electrophoresis instrument. To prepare the samples to be analysed on the Tapestation, the concentration of the samples was measured using Qubit, and samples were diluted to 0.5 ng in 2 µL (1 ng total DNA). The diluted samples were mixed with 2 µL of Tapestation Loading solution and loaded into the instrument. The result of the Tapestation electrophoresis provided the average fragment size (in Base Pairs) for each sample.

The molarity of the samples was then calculated using the following formula:

$$\text{Molarity (nM)} = \left(\frac{Sample\ mtDNA\ concentration\ (^{ng}/_{\mu L})}{\text{Average fragment size x } 660} \right) \text{x } 1\text{x}10^{6}$$

The molarity of all the samples was calculated, after which all samples were diluted to a concentration of 2nM and pooled into a library. The library was then sequenced as described in the next section.

2.2.6.3.Next-Generation sequencing

To initiate the sequencing process on the iSeq (Illumina) instrument, an Iseq cartridge was thawed in a water bath 12 hours before the process and then left at RT during the preparations. On the day of the sequencing, the library was diluted to 1nM in 20 µL of

total volume in a low-binding centrifuge microtube using RSB as diluent. After this, the library was diluted to Loading concentration by mixing 15 µL of the 1nM library with 85 µL of RSB. At this point, PhiX was prepared. PhiX is a small pre-ready library with balanced nucleotide representation, used to provide additional metrics and nucleotide representation during sequencing analysis, improving the output. 1 nM PhiX was prepared by mixing 5 µL of 10 nM PhiX and 45 µL of RSB, after which PhiX was diluted to a working concentration of 100pM by mixing 10 µL of 1nM PhiX with 90 µL of RSB. Finally, 10 µL of PhiX 100pM were added to the library to generate a 10% spike-in during the sequencing process. Samples were then centrifuged (280gs x 1 minute) and the library was left in ice till used.

The Iseq Cartridge was then taken out of the bag and inverted 5 times to mix the reagents inside. The reservoir of the cartridge was open and 20 µL of the prepared library were carefully added to the bottom of the reservoir. The Flow Cell optical sensor was then carefully loaded into the cartridge, avoiding touching the electronic interface. The cartridge was loaded into the Iseq instrument. Local Run Manager was selected on the Iseq software and the ``Sequence´´ option was used with ``FastQ workflow ´´sequencing. The indexing of the samples was input and 151 cycles were selected. The samples were then sequenced. All the samples were sequenced twice using the same library to increase the number of reads and the depth of coverage. Additionally, a new library containing only the parental samples was generated and sequenced, aiming to increase the quality and coverage of the sequencing on those specific samples.

2.2.7. Protein expression analysis

2.2.7.1. Mitochondrial isolation

Intact mitochondria were isolated using a Mitochondrial Isolation kit for cultured cells (Thermo Scientific, #88794) in accordance with the manufacturers' specifications. A maximum of 6 samples were processed at any one time with 2 x 10^7 cells being the processing limits. Following the reagent-based method, 2 x 10^7 cells were pelleted by centrifugation ~850 g for 2 min and the supernatant was discarded. 800 µL of Mitochondria Isolation Reagent A was added and vortexed at medium speed for 5 seconds followed by a 2-minute incubation in ice. 10 µL of Mitochondria Isolation Reagent B was

added and vortexed at maximum for 5 seconds followed by incubation on ice for 5 min with vortexing at maximum every minute. 800 µL of Mitochondria Isolation Reagent C was added followed by inversion of samples. Samples were centrifuged at 700 x g for 10 min at 4°C. The supernatant was transferred to a new 2 mL tube and centrifuged at 12,000 x g for 15 min at 4°C. This contains mitochondria, lysosomes, and peroxisomes (3,000 x g for 15 min at 4°C to further reduce by >50%). Transfer the supernatant (cytosol fraction) to a new tube. The pellet contains isolated mitochondria. 500µL Mitochondria Isolation Reagent C was added to the pellet and centrifuged at 12,000 x g for 5 min. The supernatant was discarded. Pellet was maintained in ice until required. Freeze-thawing may compromise mitochondria integrity.

2.2.7.2.Bradford Assay

A BSA standard was serially diluted using UHP from a 2 mg/mL stock of Quick start™ Bovine Serum albumin Standard (Bio-Rad, #500-0206) starting with 1 mg/mL and spanning 0.5, 0.25, 0.125 and 0 mg/mL. Standards and samples were measured in triplicates at least by pipetting 5 µl of each into the corner of the base of a well in a 96-well plate. 250 µL of Quick start™ Bradford 1X Dye Reagent (Bio-Rad, #500-0205) to each well and incubated in the dark for 10-15 min. Absorbance readings were measured on a benchtop spectrophotometer at a wavelength of 595 nm.

2.2.7.3.LICOR Western Blot assay

Proteins for analysis by Western Blotting were resolved using SDS-polyacrylamide gel electrophoresis (SDS-PAGE). 1/10 diluted RIPA Lysis buffer was added to the cell pellet. Cell lysis was carried out for 20 min on ice and following vortex, the lysate was spun at 4°C for 15 min at maximum speed to remove insoluble debris.

Protein samples were normalized by dilution in 4X Laemlli buffer (which contains loading dye, Sigma-Aldrich, S#3401) and corresponding volumes of lysis buffer. Before loading into the gel, a reducing agent was added to the samples, which were warmed up in the heating block at 70ºC for 10 minutes and spinned down quickly. 5 µg of protein and the molecular weight marker (New England Biolabs) were loaded onto a 4-12%

NuPAGE Bis-Tris precast gradient gel (Life Technologies, NP0322BOX). The electrophoretic transfer was carried running at 100V for 90 minutes. Membranes and filter paper were equilibrated 20 minutes in Pierce 1-step transfer buffer (Thermo-fisher #84731) and samples were then blotted in a Pierce fast western blot transfer machine at 50V for 7 minutes.

Membranes were then blocked with Odyssey Blocking Buffer for at least 2 hours at 4ºC and the membrane was incubated with the primary antibody of choice (1:1000 in Odyssey Blocking Buffer containing 1XPBS-0, 1% Tween) overnight at 4ºC. The primary antibody is recovered and recycled afterward. An anti-mouse GAPDH monoclonal antibody (Abcam, #ab8245) was used as an endogenous control.

Membranes are then washed 4 times with 1XPBS-0, 1% Tween. Then the membrane was incubated for 1 hour with the secondary antibody (1:5000 dilution 800 green anti-rabbit goat Odyssey antibody in Odyssey Blocking Buffer containing 1XPBS-0, 1% Tween). After repeating the washing step, the membrane was analyzed using Odyssey Licor Imager.

2.2.8. ELISA assays

2.2.8.1. IgG ELISA quantitation.

To quantify the titre of human IgG produced by CHO cells, the Human IgG ELISA quantitation set (Bethyl Laboratories) was used.

First, the Goat-Anti-human IgG antibody (1mg/mL) was diluted at 1:100 in coating buffer. 100µL of this coating solution were added to a 96-well ELISA plate (Nunc) and incubated at Room Temperature for 60 minutes. The coating solution was removed and the plate was washed five times with ELISA washing solution. Then 200µL of blocking solution were added to each well and the plate was incubated for 30 minutes at room temperature. The blocking solution was removed and the plate was once again washed five times with washing solution. The standards (IgG) were serial diluted 1:2 in Sample/Conjugate diluent solution in 9 different centrifuge tubes, with concentrations ranging from 500 ng/mL to 7.8 ng/mL and including a blank (0 ng/ml) sample. The samples were diluted to 1:200 and 1:300 in Sample/Conjugate diluent solution and 100µL of either standard or sample were added to the corresponding wells. The plate was then

incubated for 60 minutes at room temperature and washed 5 times with ELISA washing solution. The Detection antibody (HRP conjugated) was then diluted 1:100000 in Sample/Conjugate diluent and 100 µL of the dilution were added per well, after which the plate was incubated for 60 minutes at room temperature and later washed 5 times. After the incubation, 100 µL of ready-to-use TMB solution were added to each well and incubated in dark at room temperature for 15 minutes. After 15 minutes, the reaction was stopped by adding 100 µL of ELISA stop solution to each well. The plate was gently tapped to mix the wells and the optical density was measured at 450nm using a PowerWave Microplate Spectrophotometer linked to a PC running Gen5 software (BioTek). IgG concentration was calculated from the absorbance using a four-parameter logistic curve as recommended by the manufacturer of the kit.

2.2.8.2.hEPO ELISA quantitation.

A volume of 100µl monoclonal anti-human EPO antibody (R&D Systems Monoclonal anti-human EPO antibody MAB287) at a final concentration of 2µl/ml was added to each well of Nunc 96-well plates and incubated at 4°C for 16 hours (overnight). This coating antibody solution was then discarded and plates were washed with wash buffer 200µl wash buffer three times. Plates were blotted dry and 200µl of blocking solution was added to each well and the plate was incubated for 60 minutes. During the 60 minutes incubation time, standards and samples were prepared. Commercially available recombinant human EPO protein produced in CHO cells (Merck Millipore 329871, Erythropoietin, Human, Recombinant, CHO Cells) was used as a standard. The EPO standard was made in serial dilution ranging from 0-8,000pg/ml. Subsequently, medium samples were prepared with a dilution of up to 1:10,000. Pure Epo test samples were diluted in Sample/Conjugate diluent solution. After an hour of incubation at room temperature, the blocking solution was discarded and 100µl diluted samples (diluted to 1:2000 and 1:3000) and standards were loaded to triplicate wells, and plates were incubated for 90 minutes at 37°C on a shaking incubator at 165 rpm. The liquid in each well was then discarded and wells were washed three times with wash buffer and blotted dry. Detection antibody (R & D Systems Rabbit Polyclonal anti-human EPO antibody AB-286-NA) was prepared in Sample/Conjugate diluent solution to a final concentration of 400ng/ml. 100µl detection antibody solution was added to each well and plates were incubated at room temperature for 1.5 hours. The liquid was then discarded from each well and wells were washed three

times with washing buffer and the plate was blotted dry. Goat anti-rabbit IgG antibody-peroxidase conjugate (secondary antibody) was diluted 1:2,000 with dilution buffer. 100µl of the secondary antibody dilution were added to each well and plates were incubated at room temperature for 1 hour. The liquid was discarded and wells were washed three times with wash buffer and blotted dry. 100µl of ready-to-use TMB development solution was added to each well and plates were incubated in the dark, wrapped with aluminum foil, at room temperature for 30 minutes. The reaction was stopped by the addition of 100µl Stop Buffer to each well. The optical density was measured at 450nm using a PowerWave Microplate Spectrophotometer linked to a PC running Gen5 software (BioTek, Bedfordshire, U.K.). EPO concentration was calculated from the absorbance using a four-parameter logistic curve as recommended by the manufacturer of the kit.

2.2.8.3.Calculation of specific productivity

Specific productivity qP [pg/cell/day] was calculated according to the following equation (*Zboray et al., 2015)* where P [pg] represents the product amount and X [cells] the total viable cell number.

$$qP=((P1-P0)/(X1-X0)) * \mu$$

2.3. Metabolism evaluation techniques

2.3.1. OROBOROS/OXgraph-2k

The OROBOROS/Oxgraph-2k, a two-chambered respirometer equipped with a Peltier thermostat and integrated electromagnetic stirrers, was used to determine respirometric measurements. The oxygen concentration was recorded using the software DatLab (OROBOROS instruments) and specific oxygen consumption rates were represented as (pmol O_2/s/106 cells). Measurements were performed using 1 x 106 cells/mL in 2 mL of CHO-S-SFMII at 37 ˚C with continuous stirring. Cells were seeded and allowed to grow 24 hours before the analysis. The following substrate-uncoupler-inhibitor-titration (SUIT) protocol was applied. Oxygen consumption was allowed to stabilize upon inoculation and sealing of the chambers which resulted in the acquisition of routine respiration (R). Leak respiration (L) was established upon inhibition of ATP synthase through the addition of Oligomycin (2 µg/mL). Oligomycin inhibits ATP synthase by blocking the subunit F0 proton channel, inhibiting ATP synthesis. Oligomycin does not,

however, stop the proton gradient or the electron flow, as protons can travel back to the mitochondrial matrix through uncoupling proteins, leading to a Leak state of respiration. Maximum respiratory capacity in an uncoupled state was achieved through the addition of FCCP (0.2 µM). FCCP, also known as Carbonyl cyanide 4-(trifluoromethoxy) phenylhydrazone is a potent uncoupler of mitochondrial oxidative phosphorylation. FCCP can dissipate the proton gradient (and membrane potential) by catching and transporting protons across the mitochondrial inner membrane. The cells will then reach the maximum respiration state, attempting to restore the proton gradient. This respiration state is known as the maximum ETS (Electron Transport System) state.

Once cells reached their maximum ETS capacity, oxygen flux was left to stabilize. Complexes I and III were then inhibited by adding 5µl Rotenone and 1µl of Antimycin A respectively, allowing to observe residual oxygen consumption. Rotenone is a crystalline isoflavone, normally used as a pesticide. It inhibits Complex I by preventing the transfer of electrons from Complex I iron-sulfur centers to Ubiquinone. Stopping the electron transport chain, which leads to the production of oxygen radicals inside the mitochondria. Antimycin A is a secondary metabolite produced by *Streptomyces* bacteria. It is a strong inhibitor of Complex III, binding to the Qi site of Cytochrome c reductase, which should bind Ubiquinol. This disrupts the Quinone cycle, as Ubiquinol could not be oxidized back to ubiquinone, and stops the electron transport chain. The addition of Rotenone and Antimycin A following the previous additions of Oligomycin and FCCP completely stops OXPHOS in the cells. However, some oxidation side reactions will still take place inside the cell. This respiration is known as Residual respiration or ROX. ROX will be used to correct Routine, Leak, and ETS respiration data

2.3.2. High-throughput metabolic activity analysis.

2.3.2.1.Seahorse XF-96

Seahorse Extracellular Flux Analysers (the model used in this study was Seahorse XF 96,) greatly facilitates obtaining data about metabolic function in a short amount of time. XF analyzer can measure two major parameters of cell metabolism, glycolysis, and respiration, by measuring extracellular pH and oxygen consumption as explained in the previous section using fluorescent biosensors. These analyzers can be used to analyze the metabolism in real-time while keeping the cells intact and still suitable for certain

experiments, such as Bradford (but not for culture). A variable number of cells in a small number (200µl in the case of XF 96) are plated into a special 96-well plate, attaching and constituting a monolayer. Then a cartridge containing solid-state sensors is placed above the plate and measured in the XF (**figure 2.1**).

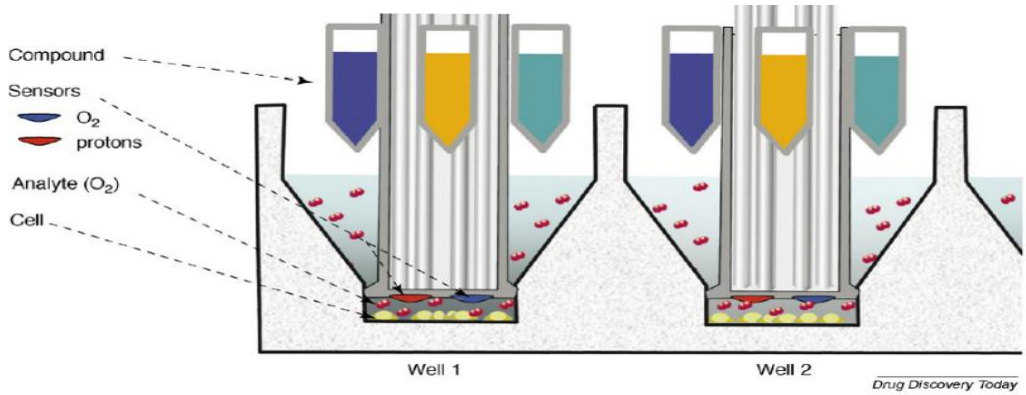

Figure 2. 1. *Representation of a functioning Seahorse plate + sensor cartridge. Image from David A. Ferrik et al 2008.*

The XF-96 analyzer can complete analysis cycles every 5-9 minutes, allowing for the quick collection of a considerable amount of replicates and data just using one assay. In every cycle, the media is first mixed and then both pH and oxygen consumed are measured for a few minutes, normally depleting oxygen level within the well by around 20-30% and lowering the pH by 0,1-0,2 units according to the manufacturer instructions. After every cycle, the sensor is retired from the well for a moment, allowing new oxygen to access the well, before mixing the media again and performing a new cycle.

Typically, for phenotypic assays, baseline metabolism is measured 4-5 times before adding substrates, such as Olygomicyn and FCCP, and reading again. These substrates will change the metabolism of the cell and allow the observation of the relationship between ECOR and ECAR. ECOR or oxygen consumption is measured in pmol of oxygen /minute and ECAR is measured in mpH /min. XF assay media, a bicarbonate-free media depleted of most nutrients is used for XF assays. Before this media can be used it is necessary to add the desired substrates (such as glucose) and to adjust the pH of the media to 7.4 after adding such compounds. As the assay keeps the cells alive, multiple measurements can be performed in one run. Also, the possibility of performing different

assays on the cells after completing a run on the XF, such as a Bradford assay to quantify protein levels, represents an interesting advantage of using the XF96 machine.

2.3.2.2.Instrument setup.

- **Initializing the instrument**

The Seahorse XF-96 analyzer required setup before being used. One day, or at least 8 hours before starting the experiment, a sensor cartridge was placed in a utility plate containing 200µl per well of XF calibration buffer. This cartridge was incubated overnight in a non-CO_2 incubator, as any CO_2 that may fixate to the sensor or the plates could cause undesired changes in the pH of the assay media. Also, the Seahorse XF-96 machine itself was turned on and Wave software was initiated at least 12 hours before the assay to ensure the desired temperature was reached before the assay was performed.

- **Preparing the cells for the assay.**

As the cells analyzed were cells growth in suspension culture, a special coating called Cell-tak was first applied on the Seahorse assay plate. Cell-Tak is a formulation of polyphenol proteins extracted from the marine mussel *Mytilus Edulis* designed to be used as a coating on a substrate to immobilize cells or tissues and is provided in a solution of 1.33mg/ml in 5% acetic acid. For XF assay plates, the concentration recommended by the manufacturer is 22,4ug/ml. Filter-sterile sodium bicarbonate pH 8.0 was recommended by the manufacturer to dissolve cell-tak. For every plate, 100ul of cell-tak were mixed with 1,9ml of filter-sterile sodium bicarbonate pH 8.0, then 20ul of the cell-tak mix were plated per well in sterile conditions and incubated in a non- CO_2 incubator for at least 1 hour. Meanwhile, 50 ml of Seahorse media were prepared by adding glucose, pyruvate, and L-glutamine to the media, up to 10mM each. After that, the media was warmed in a water bath to 37ºC and the pH was adjusted to 7.4 adding NaOH and HCl until the desired pH was achieved. Media was incubated in a water bath at 37ºC. After this, Cell-tak was removed from the coated plate, washed with 37ºC Ultra-purified sterile water (2 washes of 200ul), and left to air dry for 30 minutes -1hour.

Cells were then counted with Guava Easycyte Cytometer and plated in 50 µl XF assay media per well at a concentration of 20000 cells per well. The plate was afterward centrifuged at 200 g for 1 minute and 130 µl of XF assay media were carefully added to

every well. Cells are left 30 minutes to ensure total attachment and observed later under the microscope to check for proper attachment. Finally, depending on the assay to be performed, the corresponding drugs were loaded into the sensor cartridge, as described in the next sections.

2.3.2.3.Seahorse metabolic phenotype assay.

After the plate with the cells was ready as described in the previous sections, Oligomycin and FCCP were loaded into the well ``A´´ of the sensor cartridge correspondingly. Oligomycin and FCCP were firstly prepared at a concentration of 1mM each in Seahorse Media previously prepared as described before. Then 20 µL of Olygomycin + FCCP solution were pipetted into each well labeled ``A´´ of the sensor cartridge.

After finishing the preparations, the sensor cartridge resting on the utility wells was introduced at the XF-96 machine for equilibration and calibration of the sensor. After finishing the calibration, XF-96 returns the utility plate only, the cell plate was then placed on the Seahorse XF analyzer. In the case of the phenotypic assay, the Seahorse runs 3 cycles first, after which it is automatically injected into the wells containing the cells the Olygomicyn + FCCP solution previously loaded into the ``A´´ wells of the sensor cartridge. This injection causes the uncoupling of ATP synthase and puts the cells into an ETS state, which were measured for another 5 cycles more. Results are displayed after the run is finished.

2.3.2.4.Seahorse mitochondrial stress assay

Seahorse Mitochondria stress assay works similarly to the phenotype assay, but with this test, different parameters can be calculated, such as the non-mitochondrial oxygen consumption of the cells or ATP-linked respiration and spare respiration capacity of the cells. The main differences in the set-up of the assay were the number of cycles and the drugs added on the sensor cartridge. A total of 12 cycles were run (3 per respiration state to be measured) and 4 different drugs were added. **Figure 2.2** shows the typical profile obtained with this assay.

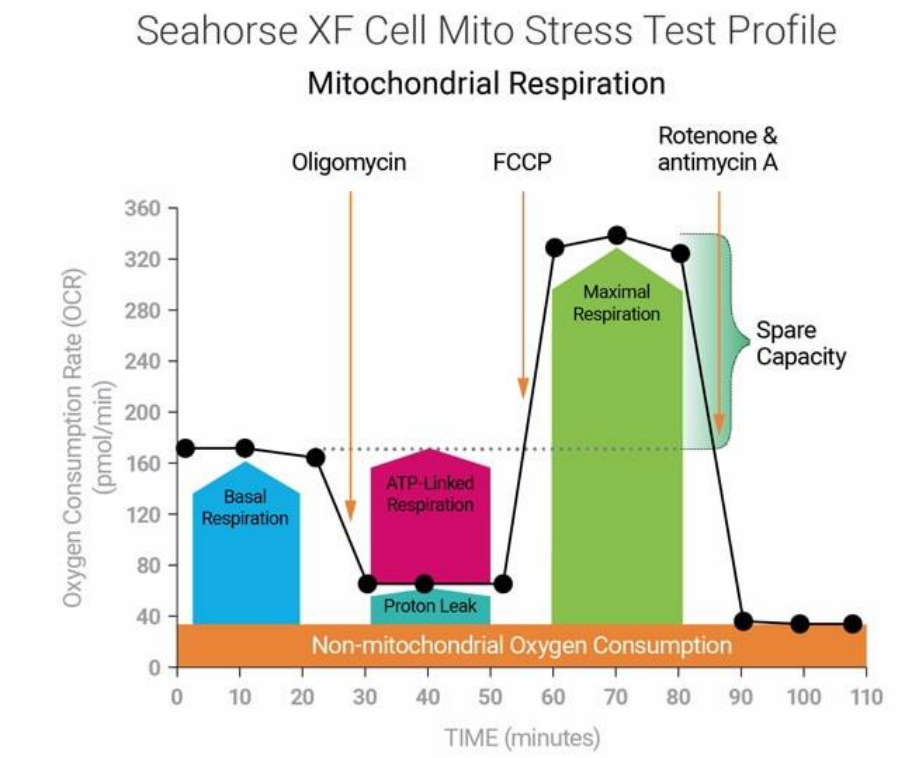

Figure 2. 2. Typical profile obtained using Seahorse Mito Stress test kit. Image obtained from Agilent website.

After the plate with the cells was ready as described in the previous sections 1mM Oligomycin was loaded into the well ``A´´ of the sensor cartridge, 1 mM FCCP was loaded into the well ``B´´ of the sensor cartridge and a mix of 0.5 mM of both Rotenone and Antimycin-A was loaded into the well ``C´´ of the sensor cartridge. To this end, the drugs were firstly prepared at a concentration of 1mM and 0.5 mM correspondingly in Seahorse Media. Then 20 µL of each drug were pipetted into their corresponding wells in the sensor cartridge.

After finishing the preparations, the sensor cartridge resting on the utility wells was introduced at the XF-96 machine for equilibration and calibration of the sensor. After finishing the calibration, XF-96 returns the utility plate only, the cell plate was then placed on the Seahorse XF analyzer. In the case of the Mitostress assay, three cycles were run, then Oligomycin was (automatically) added into the cells by the instrument, blocking the activity of ATP synthase (subunit V) by blocking the subunit F0 proton channel, which inhibits ATP synthesis. However, inhibition of the proton gradient and the electron flow is not stopped by the inhibition of ATP synthase, and the proton gradient continues to operate through uncoupling proteins, leading to a Leak state of respiration. The difference

between basal respiration and leak respiration corresponds with ATP-linked respiration. After measuring the leak respiration during three cycles, FCCP was injected into the wells with cells by the instrument. FCCP dissipates the proton gradient by catching and transporting protons across the mitochondrial inner membrane, causing the cells to reach a maximum respiration state (Max Electron Transport System potential or Max ETS) in an attempt to restore the proton gradient. The cells were measured during three cycles while in the ETS state. The difference between the Basal oxygen consumption and the consumption observed during the ETS is known as ``Spare respiration´´. Finally, Rotenone and Antimycin-A were injected into the wells with cells by the instrument. Rotenone inhibits Complex I of the respiratory chain and Antimycin A is a strong inhibitor of Complex III, as explained in detail in section 2.3.1. The addition of Rotenone and Antimycin-A at this point completely stopped the oxidative phosphorylation in the cells. However, some oxygen consumption still remained in the cells. This Non-mitochondrial oxygen consumption was measured during the last three cycles and was used as a correction factor of the previously analysed types of mitochondrial respiration.

2.3.2.5.Seahorse glycolytic rate assay

Seahorse Mitochondria stress assay works in a similar way to the phenotype assay, but with a focus on the glycolytic activity of the cells rather than the respiration. This assay was used in this study to accurately measure the acidification of the media related to the glycolytic activity, getting rid of the bias caused by the CO_2 acidification of the media caused by the oxidative metabolism of the cells. The main difference with the previously described assays is the drugs used and the number of cycles: instead of using drugs to influence the oxidative metabolism of the cell at different stages, Rotenone and Antimycin were injected early to completely stop the oxidative phosphorylation process. 11 cycles are run in this assay.

After the plate with the cells was ready as described in the previous sections, 0.5 mM of Rotenone/Antimycin-A were loaded in the cell ``A´´ of the sensor cartridge, 50 mM of 2-Deoxy-D-Glucose (**2-DG**) were loaded into the well ``B´´ of the sensor cartridge. To this end, the drugs were firstly prepared at a concentration of 0.5 mM and 50 mM correspondingly in Seahorse Media. Then 20 µL of each drug were pipetted into their corresponding wells in the sensor cartridge.

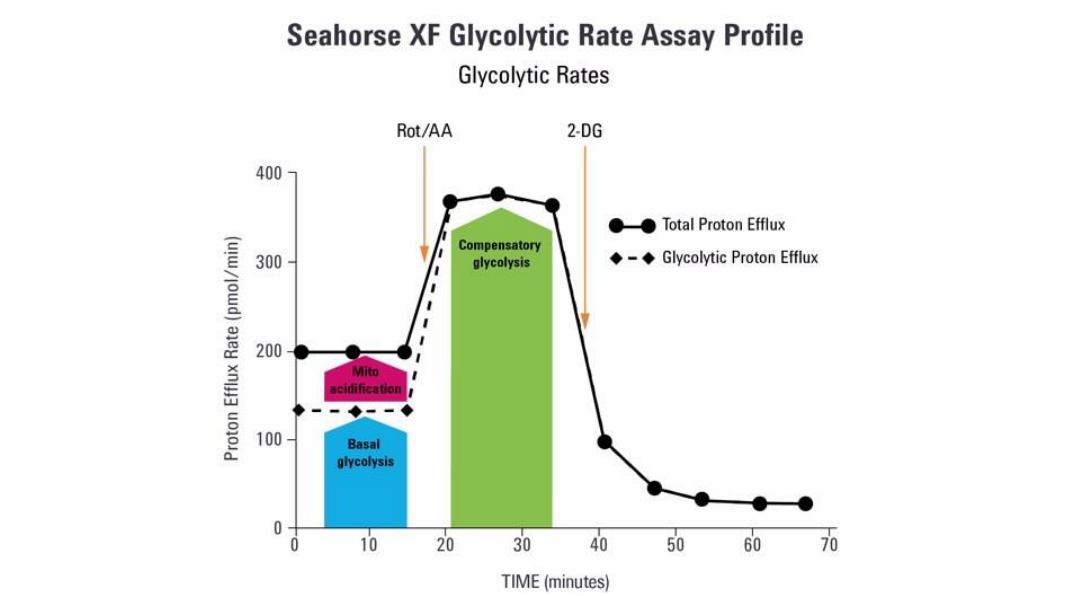

Figure 2. 3. Typical profile obtained using Seahorse Glycolytic Rate Assay kit. Image obtained from Agilent website.

After finishing the preparations, the sensor cartridge resting on the utility wells was introduced at the XF-96 machine for equilibration and calibration of the sensor. After finishing the calibration, XF-96 returned the utility plate only, the cell plate was then placed on the Seahorse XF analyzer. In the case of the Glycolytic rate assay, three initial cycles were run to measure the basal metabolism of the cells. After this, the instrument injected the Rot/Ant-A mix into the wells with the cells, inhibiting the oxidative metabolism and starting a compensatory glycolysis state on the cells. Three cycles were run to measure the compensatory glycolysis state. After these three cycles, the 2-DG was injected into the wells with the cells by the instrument. 2-DG inhibits glycolysis by competitively inhibiting the Glucose-6-phosphate isomerase enzyme, which normally interconverts Glucose-6-phosphate into Fructose-6-phosphate, but is unable to convert the 2-DG due to the presence of a hydroxyl group in position number 2, halting the glycolysis process. The glycolysis was this way inhibited by adding 2-DG and measured during 5 cycles to calculate the Extracellular Acidification Rate (**ECAR**) non-related to either glycolysis or the CO_2 generated by the oxidative metabolism. This allowed to correct the rest of the ECAR measures by deducting the acidification non-related to the glycolysis process itself. Then the Proton Efflux Rate (**PER**), measured in pmol H^+ /min is calculated and the glycolytic Proton Efflux Rate (**GlycoPER**) is calculated from it.

The instrument automatically calculated both total PER and GlycoPER from the data of this assay using the following formula:

$$PER\ (pmol\ H^+/min\ ) = ECAR\ (mpH/min\ )x\ BF\ (mmol/L/pH)\ x\ Geometric\ Volume\ (\mu L)x\ Kvol$$

Where:

- **ECAR:** Extracellular Acidification Rate. Data measured during the assay, corresponding with the rate of change on mpH/min in an assay well. Measured in mpH/min.
- **BF:** Buffer Factor. According to Agilent PER quick reference guide, the buffer factor is the measure of the in-situ buffer capacity obtained in XF instruments, which accounts for the buffer capacity of both medium and sensor systems. It is measured in mmol/L/pH
- **Geometric volume:** The physical volume of the measurement microchamber, assuming it is completely sealed. It is measured in µL
- **Kvol:** Empirically-derived scaling factor used to account for total proton production in the measurement chamber. Has no units.

2.4. In silico data analysis tools.

2.4.1. Plasmid cloning/Maps.

SnapGene Viewer License-free software was used to generate the plasmid maps.

2.4.2. Primer generation tools.

NCBI primer designing tool (https://www.ncbi.nlm.nih.gov/tools/primer-blast/) was used to generate primer candidates for the amplification of the genes of interest.

2.4.3. Gene alignment and sequence homology tools

BLAST tool (https://blast.ncbi.nlm.nih.gov/Blast.cgi) was used to check the homology between sequences from different species and to predict the target regions of the primers designed.

2.4.4. Statistical analysis.

SPSS statistics tool (https://www.ibm.com/es-es/products/spss-statistics) was used to perform the statistical analysis. ANOVA analysis was performed to assess the significance of the differences between different samples. This analysis normally

consisted of one-way ANOVA analysis followed with two different posthoc analyses, HSD Tukey or Games-Howell, depending on the result of Levene's test.

CHAPTER 3

Investigating the impact of mitochondrial heteroplasmy on CHO cell growth and productivity

3.1. Introduction:

A considerable amount of effort has been dedicated to engineering the metabolism of CHO cells to achieve desirable phenotypes. These efforts are often focused on increasing the recombinant protein production of the CHO cells, which has been associated with oxidative metabolism (*Templeton et al., 2013*).

Among these studies, it is common to find approaches focused on nuclear genome-located genes related to the glycolytic and oxidative pathways. Some examples include the overexpression of Galactose kinase *(Jiménez, Martínez and Gerdtzen, 2019)*, which was reported to accelerate metabolism by increasing galactose consumption, or the most recent study on the overexpression of the Mitochondrial Pyruvate carrier (Bulté *et al.*, 2020b), which was shown to increase oxidative metabolism without impairing cell growth, challenging the Warburg effect present in the CHO cells.

Consequently, interest in mitochondrial DNA and heteroplasmy has been raised in recent years not only for clinical purposes but also for process engineering purposes. The careful observation of heteroplasmy in relevant recombinant-protein-producing cell lines may lead to the development of new, more efficient clones. Identification of heteroplasmic mutations leading to an increase in oxidative metabolism, and consequently to an increase in recombinant protein yield, can open the pathway of direct CHO cell mitochondrial genome engineering using editing systems such as TALENS (*Bacman et al., 2013*).

On this line of thinking, the mitochondrial genome of a panel of 22 CHO cell clones was sequenced using ultra-deep sequencing technologies (*Kelly et al., 2017*). The analysis identified different heteroplasmy variants among the CHO cell clones.

Among the numerous variants observed, described in Chapter 1, a heteroplasmic variant was consistently observed in 9 of the CHO clones, although varying in the degree of heteroplasmy. This variant corresponds to position 14136 of the mitochondrial DNA, which is in the sequence encoding a subunit of Cytochrome B protein – part of respiratory complex III. The clones containing this variant were originally provided by Pfizer to Kelly and collaborators and were originated from CHO-K1 cells in two different cell lines development projects originally named CLD1 and CLD2 (**Figure 3.1**). The cell lines (clones) used were generated in an industrial cell line development campaign having been

single-cell cloned from a stably transfected parental population. They were chosen based on a range of phenotypic characteristics including productivity and cell growth/viability. All these clones produce mAb (IgG protein).

The variant found at position 14136 resulted in a sequence frameshift. This frameshift was predicted to lead to a non-functional cytochrome b subunit which, we hypothesized, may compromise the correct function of complex III and, therefore, the correct function of the respiratory chain.

		mitDNA position										
Kelly et al 2017	*Name in this thesis*	14136	14311	14339	14378	14835	14849	15031	15035	15136	15183	15209
ATCC CHO-K1	**CHO-K1-Parental**	41%										
Pfizer CHO-K1-CLD1 #1	**CHO-513F**	16%			22%							
Pfizer CHO-K1-CLD1 #2	**CHO-516F**	16%			20%							
Pfizer CHO-K1-CLD1 #3	**CHO-520F**	8%			36%							
Pfizer CHO-K1-CLD1 #4	**CHO-522F**	15%			11%							
Pfizer CHO-K1-CLD1 #5	**CHO-111S**	37%		17%			32%					
Pfizer CHO-K1-CLD2 #1	**CHO-10122S**	51%					53%					
Pfizer CHO-K1-CLD2 #2	**CHO-596S**	27%										
Pfizer CHO-K1-CLD2 #3	**CHO-792S**	50%				3%	52%					
Pfizer CHO-K1 114	**CHO-114**											
Pfizer CHO-K1 2B6	**CHO-2B6**										6%	
DCU CHO-K1-SEAP	**CHO-K1-SEAP**											
DCU miR23 Sponge #1	**m23sp-c4**											
DCU miR23 Sponge #2	**m23sp-c6**											
DCU Control Sponge #1	**mNC-sp-c11**											
DCU Control Sponge #2	**mNCsp-c2**											
Biogen CHO-K1	**CHO-K1Bio**											
ATCC DG44	**CHO-DG44**								12%			
Biogen DG44 #1	**DG44-5L11Bio**									19%		22%
Biogen DG44 #2	**DG44-ED003Bio**							11%				
ATCC CHO-S	**CHO-S**											
Biogen CHO-S	**CHO-S 2D2**		100%									
		CYTB										

		mitDNA position				
Kelly et al 2017	*Name in this thesis*	6996	7162	7166	7226	7364
ATCC CHO-K1	**CHO-K1-Parental**					3%
Pfizer CHO-K1-CLD1 #1	**CHO-513F**	26%				
Pfizer CHO-K1-CLD1 #2	**CHO-516F**	21%				
Pfizer CHO-K1-CLD1 #3	**CHO-520F**	17%				
Pfizer CHO-K1-CLD1 #4	**CHO-522F**	14%				
Pfizer CHO-K1-CLD1 #5	**CHO-111S**					
Pfizer CHO-K1-CLD2 #1	**CHO-10122S**					
Pfizer CHO-K1-CLD2 #2	**CHO-596S**					
Pfizer CHO-K1-CLD2 #3	**CHO-792S**					
Pfizer CHO-K1 114	**CHO-114**					
Pfizer CHO-K1 2B6	**CHO-2B6**					
DCU CHO-K1-SEAP	**CHO-K1-SEAP**					
DCU miR23 Sponge #1	**m23sp-c4**					
DCU miR23 Sponge #2	**m23sp-c6**					
DCU Control Sponge #1	**mNC-sp-c11**		2%			
DCU Control Sponge #2	**mNCsp-c2**					
Biogen CHO-K1	**CHO-K1Bio**					
ATCC DG44	**CHO-DG44**					
Biogen DG44 #1	**DG44-5L11Bio**				17%	
Biogen DG44 #2	**DG44-ED003Bio**			32%		
ATCC CHO-S	**CHO-S**					
Biogen CHO-S	**CHO-S 2D2**					
		COX2				

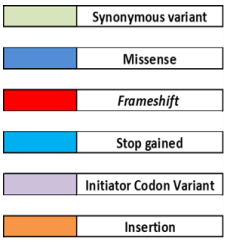

Figure 3. 1. Heteroplasmy variants found by Kelly et al. 2017 in the panel of 22 CHO clones at genes Cox2 and Cob (CYTB). The figure shows the degree of heteroplasmy corresponding with every mitDNA position in percent of mutant mitochondrial DNA copies over the total mitDNA sequenced.

Additionally, the variant found at position 14136 was observed at a higher degree of presence in CHO clones previously classified as ``slow growth clones´´. The influence of the variant found at position 14136 in these ``growth phenotypes´´ was to be determined.

Further interesting heteroplasmy variants were identified only in CHO cell clones previously classified as ``fast-growth phenotype´´ clones. A stop codon variant was observed at position 14378 of the mitochondrial genome. This position corresponds to a region encoding a subunit of Cytochrome b protein, which is part of respiratory complex III. Therefore, the mutation introduced by this variant has the potential to introduce changes to the oxidative metabolism of these CHO cells. As this mutation was found in conjunction with the Frameshift variant of position 14136, the influence of these mutations in oxidative metabolism was theorized to be potentially cumulative.

Finally, an initiator codon variant *m.6996G>A* variant was observed at position 6996 of the mitochondrial genome of these clones, which is part of a region encoding a subunit of COX2 protein, part of the respiratory complex IV. This mutation was hypothesized to lead to the production of non-functional or impaired COX2 subunits, hindering the electron transport chain.

The goal of this part of the study was to determine if these heteroplasmic variants described in *Kelly et al. 2017* have a relevant impact on the general metabolism of the clones.

For this purpose, cell growth and viability, protein titer, mitochondrial content, gene expression, and oxidative metabolism of the clones were evaluated.

3.2. Results:

3.2.1. Growth and productivity of a set of CHO cell clones exhibiting heteroplasmic variants in mitochondria-encoded CYTB and COX2

From the panel of CHO cell clones studied in *Kelly et al 2017*, nine clones were observed to have potentially significant heteroplasmic variants. The heteroplasmic mutations observed in these nine clones were predicted to cause frameshift mutations that have the potential to impact protein expression and thus the oxidative metabolic activity of the cells.

As previously described, these 9 CHO cell clones shared a common trait: they have a frameshift heteroplasmic mutation at position 14136 of the mitochondrial genome (*m.14136delA* variant, corresponding with CYTB, a gene encoding a subunit of Cytochrome B, belonging to Complex III of the respiratory chain).

The heteroplasmy degree of this frameshift mutation varies greatly among the clones. This can be seen in **Figure 3.2**. Some clones, such as the Clone CHO-111S, showed a high heteroplasmy degree, with 36% of the mitochondrial genome copies having the frameshift mutation at position 14136. in the other hand, some other clones, like clone CHO-520F, showed a very low heteroplasmy degree, with only 7% of the mitochondrial genome copies having the frameshift mutation at position 14136.

Differences in the heteroplasmy content between clones with the same growth phenotype were also observed. The *m.14136delA* variant was observed to have a frequency of 50% in Clone CHO-792S; 26,5% for Clone CHO-596S and, as previously mentioned, 36% in Clone CHO-111S. While sharing the growth phenotype, the differences in the heteroplasmy degree of this variant were notable. Despite these differences observed, all the ``slow´´ growth clones had a higher frequency of position 14136 frameshift variant than any of the ``Fast´´ growth clones. Clones CHO-520F and CHO-513F were observed to possess a heteroplasmy degree of 7% and 15% respectively for the frameshift variant.

These observations alone seemed to establish a correlation between the degree of heteroplasmy and the growth phenotype observed in the clone. ``Slow´´ clones, such as CHO-111S were observed to have a higher heteroplasmy degree than ``Fast´´ clones, such as CHO-520F. As it has been previously established in the literature that, to have a

phenotypic effect, the heteroplasmy degree must reach a certain threshold, known as the ``metabolic threshold´´, the apparent correlation between higher heteroplasmy degree and ``slow´´ growth phenotypes was hypothesized to be due to a negative effect of the heteroplasmy after either surpassing such threshold.

Finally, some of the ``fast´´ clones showed additional heteroplasmic mutations of potential interest, such as a stop codon variant at position 14378 of the mitochondrial genome (also within the CytB gene) or *m.6996G>A* variant (in the COX2 gene). These mutations were predicted to result in loss of expression of the proteins potentially resulting in metabolic changes in the cells. However, it must be noted that the sequencing performed in the original study was done in populations of cells, and not in single cells. Therefore, it is unknown whether these mutations are present together in all the cells in a population or correspond to a subset of cells from that population.

A subset of 5 of these CHO cell clones showing heteroplasmic variants of interest was selected based on their degree of heteroplasmy and corresponding growth phenotype.

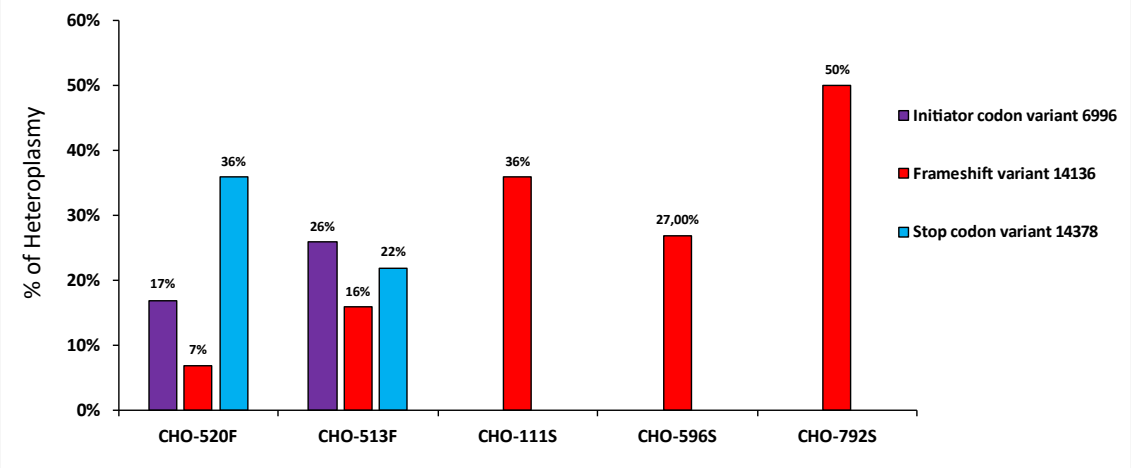

Figure 3. 2. Heteroplasmic variants present in the selected clones. Each bar represent the percent of mtDNA mutant copies containing each variant in the different CHO clones.

The 5 CHO cells clones selected from the 24-clone panel were originally classified as either ``Fast´´ (Fast Growth Phenotype CHO cell clones or FGPC) or ``Slow´´ (Slow Growth Phenotype CHO cell clones or SGPC) growth Clones depending on their Specific Growth Rate (*SGR*) (**Table 3.1)**. Finding an existing relationship, if any, between the heteroplasmy variants and the growth phenotype was the main goal of the project. It is worth noting that only those clones classified as ``Fast ´´ growers (*SGR* > 0,025

divisions/hour) presented the variants at position 6996 (initiator codon variant in COX2 gene) and the variant at position 14378 (Stop codon variant at Cob gene).

Clone	Phenotype	Specific growth rate
CHO-520F	*Fast*	*> 0.025 cell divisions/hour*
CHO-513F	*Fast*	*> 0.025 cell divisions/hour*
CHO-111S	*Slow*	*< 0.023 cell divisions/hour*
CHO-596S	*Slow*	*< 0.023 cell divisions/hour*
CHO-792S	*Slow*	*< 0.023 cell divisions/hour*

Table 3. 1. Classification of the CHO clones in ``Fast´´ or ``Slow´´ growth clones depending in their specific growth rate. Clones with less than 0,023 cell divisions/hour were considered ``Slow phenotype ´´ while clones with more than 0,023 cell divisions/hour were consider having a ``Fast phenotype´´.

3.2.1.1.CHO clones differences in growth patterns, growth rate, and viability does not necessarily correlate with mitochondrial content.

The original hypothesis of this study was that there is a relationship between the heteroplasmic variants observed and the growth phenotype of the clones. Therefore, the starting point for the study was to determine if the CHO cell clones could still be classified as either FGPC or SGPC in standard batch culture conditions in the lab.

The original media in which these clones were grown was unavailable at the time. For this reason, CHO-S-SFMII media, supplemented with 2%PVA, was used instead as described in *Chapter 2: Materials and methods 2.2.2.*

Cell growth was evaluated using a cytometry assay (Guava Viacount) over days. A growth curve and a viability curve were drawn for every clone.

Additionally, the mitochondrial content of the cells was evaluated using the fluorescence probe ``Mitotracker Green dye™´´. Mitotracker probes consist of dye molecules that are captured by ``active´´ mitochondria, meaning mitochondria actively perform mitochondrial respiration. Inside the mitochondria, the molecules become fluorescent after being oxidized.

Mitotracker assays were performed using Mitotracker™ Green dye. Cells were incubated for 30 minutes in media containing the dye, washed twice with PBS, and read using Guava ExpressPlus.

The Mitotracker system allowed us to determine the relative mitochondrial content of each CHO cell clone with respect to the others. Any differences in the mitochondrial content of the cells can have an impact in further assays, for example, western blot and qPCR of mitochondrial genes. Therefore, the mitochondrial content of the clones should be considered before performing any further experiments.

Changes in mitochondrial content may also be related to the heteroplasmy variants. For example, clones with a high number of harmful heteroplasmic variants might react by increasing their mitochondrial content. An increase in mitochondrial content would increase the number of functional wild-type mitochondrial DNA copies, thus maintaining mitochondrial respiration despite the presence of mutant mtDNA copies.

Firstly, the growth, viability, and mitochondrial content from five clones from the 22-clone panel described in *Kelly et al 2017* were assessed. The clones selected for the assay were two FGPC clones (CHO-520F and CHO-513F) and three SGPC (CHO-111S; CHO-596S and CHO-792S). These clones were seeded at 2 x 10^5 cells/mL in a 5mL flask. Then the clones were grown over a total time of 168 hours in batch culture, being counted every 24 hours.

The mitochondrial content assay was done after 96 hours and 120 hours, as these points were observed in the previous experiment to correspond with a peak of the mitochondria content of the cells and correspond to points in time at which differences between the clones were observed (**Figure 3.3)**.

The five CHO cell clones were then seeded at 2*10^5 cells/mL in three vented cap tubes containing 5 ml of media per clone and grown over 168 hours. Cells were counted every 24 hours using Guava Viacount as described above.

As can be seen in **Figure 3.3.**, up to 72 hours of culture, most of the clones did not show significant differences in growth, the only exception being CHO-596S, which had significantly lower growth than the rest of the clones. However, clones CHO-520F and CHO-513F growth peaks after 144 hours of culture, with 2.8 x10^6 cells/ml and 3.4 x10^6 cells/ml respectively. These numbers are relatively high when compared with the other clones, which have their growth peaks at 2.5 x10^6 cells/ml (CHO-720S), 2 x10^6 cells/ml (CHO-111S), and 1.5 x10^6 cells/ml (CHO-596S).

Clones originally classified as FGPC, namely clones CHO-513F and CHO-520F were observed to have significantly higher cell densities than clones originally classified as SGPC, in particular, CHO-111S and CHO-596S after 96 hours of culture and onwards

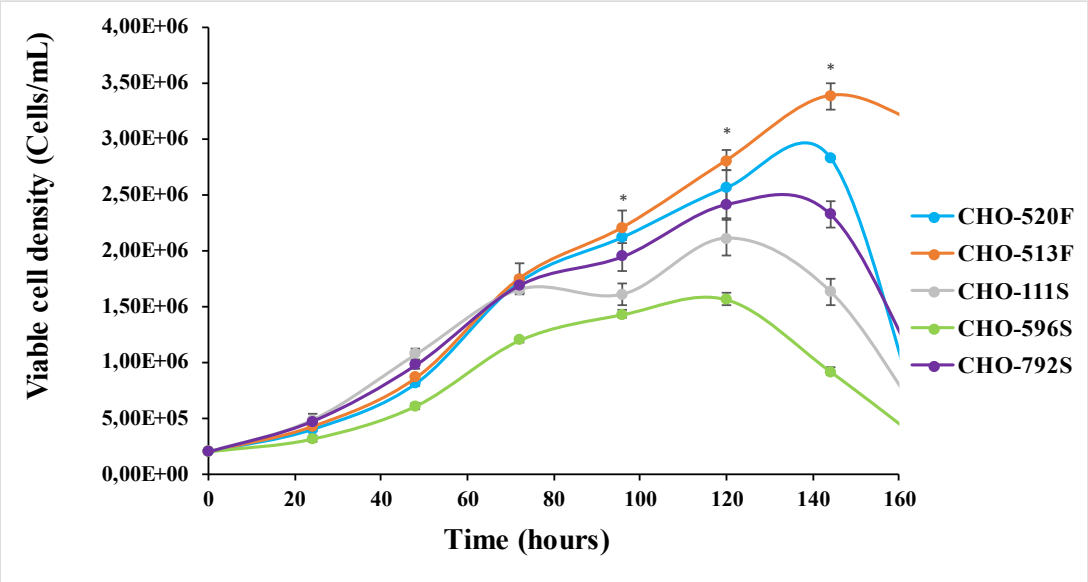

Figure 3. 3. Growth profile of CHO clones over the course of 168 hours. Cells were cultured in suspension culture in 5mL of CHO-SFMII media. Each bar represent the average Viable cell density at a given time of biological triplicates measured in triplicates using Guava Easycite cytometer ± SD. Significance was tested using a one-way ANOVA with α <0,05, represented as * in the figure.

CHO-792S behaviour was somewhere in between SGPC and FGPC. While the data in **Figure 3.3.** shows clone CHO-792S to have a lower peak density than clones CHO-513F and CHO-520F only after 144 hours of culture while keeping a growth pattern generally similar to the FGPC clones until then.

Figure 3.4. shows the viability of the five CHO cell clones over time. While overall the viability of the clones remained similar over the 168 hours of culture, there are some points at which differences were observed, most notably CHO clone 596S which had significantly lower viability than the rest of the clones.

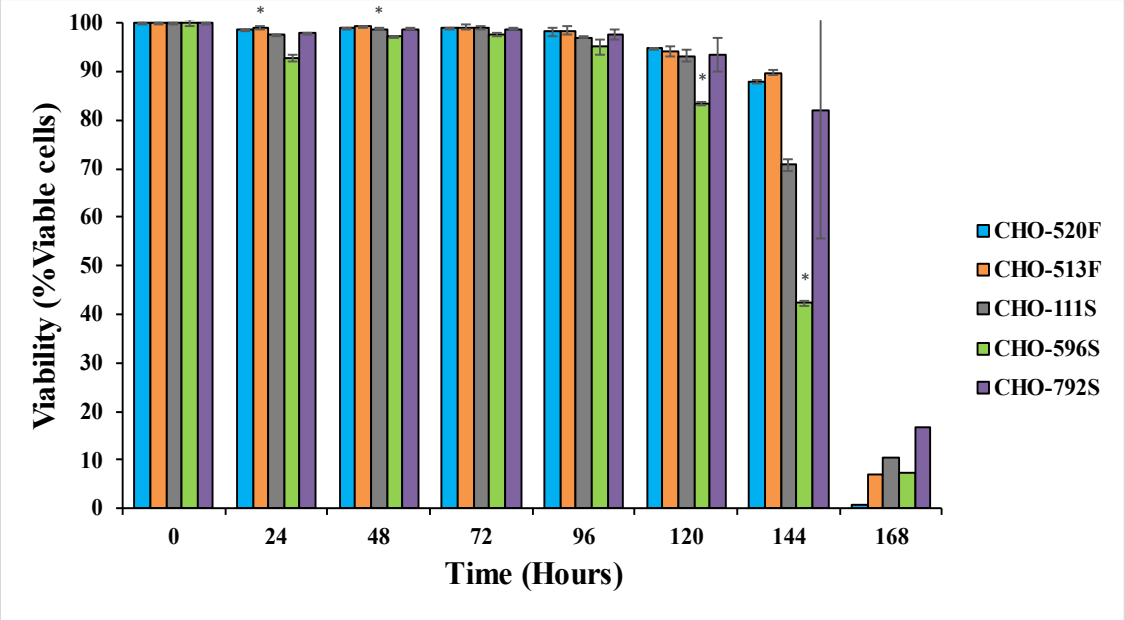

Figure 3. 4. Viability profile of CHO clones over the course of 168 hours. Cells were cultured in suspension culture in 5mL of CHO-SFMII media. Each bar represent the average viability at a given time of biological triplicates measured in triplicates using Guava Easycite cytometer ± SD. Significance was tested using a one-way ANOVA with $\alpha < 0{,}05$.

In summary, overall FGPCs CHO-520F and CHO-513F remained viable slightly longer than the SGPCs. Additionally, CHO clone CHO-596S showed considerably decreased viability when compared with the rest of the clones.

The relative mitochondrial content of the clones was evaluated after 96 hours and 120 hours of culture, which corresponds with the early stationary and stationary phase of growth as seen before in **Figure 3.3**.

Firstly, an increase in mitochondrial content over time was observed in every clone (**Figure 3.5**.). However, this amplitude of the increase varied somewhat for each clone. In clones CHO-520F, CHO-792S, and CHO-111S mitochondrial content increased by approximately 25% at 120hrs compared to 96hrs. Clone CHO-513F increased around 30% and, finally, clone CHO-596S fluorescence increased nearly 40% (from 32 to 55).

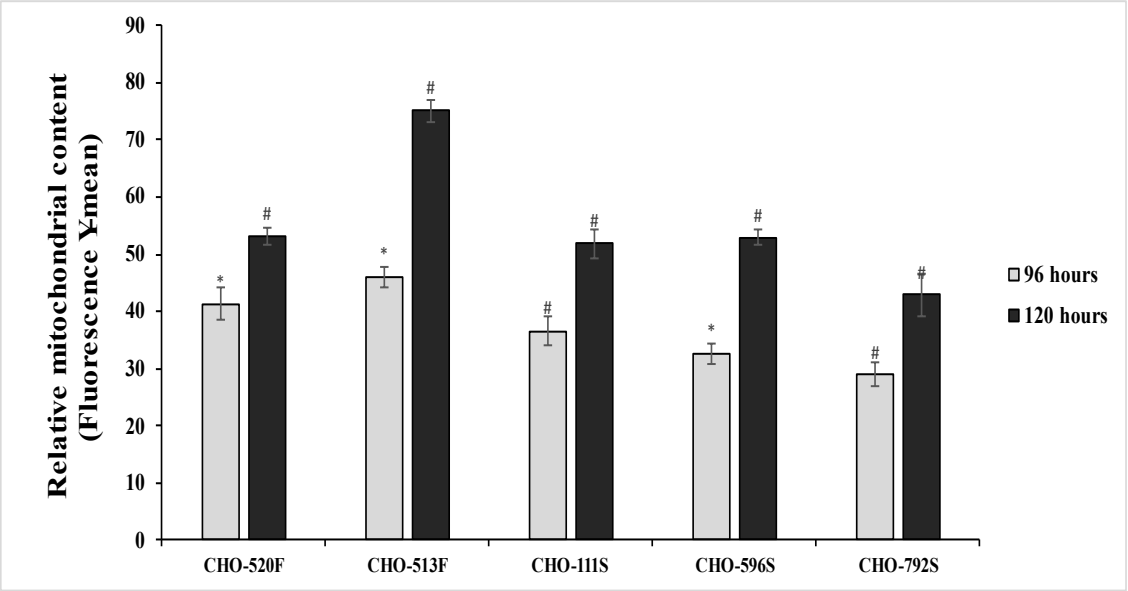

Figure 3. 5. Relative mitochondrial content of CHO clones over the course of 140 hours. Cells were cultured in suspension culture in 5mL of CHO-SFMII media. Each bar represent the average relative mitochondrial content at a given time of biological triplicates measured in triplicates using Guava Easycite cytometer ± SD. Significance was tested using a one-way ANOVA with α <0,05, intra-group significant differences are marked with #, while inter-group significant differences are marked with *.

Differences between the mitochondrial content of the different clones were also observed. For clarity, differences between the clones have been highlighted in the figure. When the clones were observed to have statistically significantly different mitochondrial content than a clone from the same group (For example, CHO-520F, had higher mitochondrial content than CHO-792S) they were marked with an asterisk (*). Similarly, when significant differences between clones classified within the same group (CHO-520F vs CHO-513F for example) were noticed, these clones were marked with a pound (#).

At 120 hrs of culture, CHO-513F mitochondrial content was observed to be significantly higher than any other clone except for clone CHO-520F.

Clone CHO-111S had similar mitochondrial content to both clone CHO-520F and CHO-596S after 96 hours of incubation. This similarity in mito-content levels is also present among these three particular clones after 120 hours of culture. Despite this, the growth of these three clones was previously seen to be quite different.

Clone CHO-792S had significantly lower levels of mitochondrial content among all the clones after both 96 and 120 hours of culture. The lower mitochondrial content did not seem to have a significant impact on the overall culture performance of CHO-792S, as it was previously observed to reach higher cell densities than both CHO-111S and CHO-596S.

Finally, the higher mitochondrial content of CHO-513F seemed to correlate with the growth and viability observations. Despite attaining higher cell densities than most of the clones, clone CHO-513F was observed to maintain high viability compared with the other clones even at late stages of the culture, which hints at a relationship between a higher mitochondrial content and good culture performance. This relationship will be discussed later.

Clone	Growth rate (cell divisions/hour)	Doubling time (h)	Total duplications
CHO-520F	*0.033*	*21.13*	*3.41*
CHO-513F	*0.033*	*20.78*	*3.47*
CHO-111S	*0.029*	*23.94*	*3.01*
CHO-596S	*0.027*	*25.36*	*2.84*
CHO-792S	*0.032*	*21.92*	*3.29*

Table 3. 2. Growth rate (cell divisions/hours), doubling time (hours) and number of duplications calculated for the evaluated panel of CHO clones from the growth data seen in Figure 3.9 (Lower half). These parameters were calculated taking into account the first 96 hours of culture.

Overall, the results did not demonstrate a clear correlation between the mitochondrial content of the clones and their original FGPCs and SPGCs classification or with their observed growth performance.

The results described in this set of assays provided an interesting picture of the general phenotype of the set of five CHO cell clones selected.

Firstly, the cell growth data aligned reasonably well with the original classification, although rather than as a distinct division between FGPCs and SGPCs, it appeared to manifest as more of a gradation or range of growth phenotypes, from faster to slower clones (**Figure 3.3**). This division became more evident after 72 hours of culture, with clones CHO-520F and CHO-513F reaching much higher densities than the other clones. It is also worth pointing out that CHO-596S showed a significantly lower growth than the rest of the clones over all the culture processes.

Intra-group differences were also observed with, for example, CHO cell clone CHO-513F achieving higher cell densities than clone CHO-520F. Differences were also evident between SGPCs even early in time due to the low growth of clone CHO-596S but became more evident after 96 hours of incubation as mentioned before. It is worth noting that SGPC clone CHO-792S growth pattern was observed to be more similar to the pattern of both FGPCs than the pattern of SGPCs during most of the culture time.

Growth rate (μ), doubling time, and the number of total duplications was calculated for this set of clones (**Table 3.2**). In all cases, the growth Rate obtained was over 0,025 divisions/hour, which will classify all the clones as FGPCs following the original classification. Both clones CHO-520F and CHO-513F showed a higher growth rate, approximately 0.033 cell divisions/hour, than any of the clones formerly classified as SGPCs, which have a growth rate of approximately 0.027-0.029. This result further supports the theory of adaptation of the cells to the new media and culture, as the cells' growth rate was seemingly changed. Nonetheless, as previously mentioned, the clones previously classified as FGPCs were still growing at a faster rate and to higher densities than those previously classified as SGPCs.

Secondly, the viability data did not reflect the pattern seen in the previous figure. More similarities than differences among the different CHO cell clones were observed over time in the viability of the clones. The viability of both CHO-520F and CHO-513F was also observed to decline later, but more sharply than the viability of the rest of the clones. Clone CHO-596S stood out as different from the rest of the CHO cell clones, with its viability declining faster than the viability of the other clones. This way, this data seemingly explained why clone CHO-596S, despite showing a higher Growth rate than CHO-792S and CHO-111S, reached lower viable cell densities than those SGPCs clones.

Finally, the mitochondrial content showed significant changes over time, with average mito-content increasing sharply over time. The levels of mito-content in the CHO cell clones were observed to be much higher after 120 hours of culture than after 96 hours of culture in all clones, despite their original growth phenotype classification.

As commented before, differences were also observed among the panel of clones. These differences were observed among clones with little to no regard for their classification as either FGPCs or SGPCs. These differences in mitochondrial content were independent of

the growth phenotype of the cells, as clones with similar mitochondrial content showed significant differences in cell density when examined at a given point in time.

CHO-513F stands out from the others, with the mitochondrial content being significantly higher than the others after both 96 and 120 hours of growth. As previously mentioned, this seems to correlate with higher cell density and viability over time. While no significant differences between the cell density, growth rate, or viability of clones CHO-520F and CHO-513F were found at these particular points in time, both the cell density and viability of CHO-513F was later observed to be significantly higher than in CHO-520F. This output seemingly points to the higher density of mitochondria observed in CHO-513F being beneficial to this clone.

Oppositely, CHO-792S mitochondrial content was observed to be significantly lower than any other clone, as mentioned above. However, CHO-792S maintained an overall high cell density and very high viability over time, remaining similar to both CHO-520F and CHO-513F after 120 hours of culture. While the CHO-792S growth rate was lower than the growth rate of the FGPCs, the high viability seemingly helped CHO-792S to maintain a cell density equivalent to such clones. Additionally, CHO-792S was observed to be the clone with the highest viability after 168 hours of culture.

The phenotype data obtained in these growth and mitochondrial content experiments provided some evidence of a potential relationship between the observed phenotypes and the heteroplasmy previously observed in the set of CHO cell clones. SGPC's growth and viability performance seemed, at first sight, to correlate with a higher frequency of the *m.14136delA* variant in the CYTB mitochondrial gene. Similarly, CHO-513F, possessing almost double the frequency of this variant than CHO-520F, showed improved performance. Regardless of FGPCs possessing lower frequencies of the frameshift variant, they were observed to grow to high cell densities than any of the SGPCs. This may be a consequence of the unique heteroplasmy variants observed in FGPCs, such as the initiator codon variant at position 6996 or the stop codon variant at 14378.

While these results suggest the existence of a potential link between the heteroplasmy and the clone’s growth behaviour, another important trait that could be impacted is productivity. Therefore, the recombinant protein titer of the clones was evaluated.

3.2.1.2. Recombinant protein titer of CHO clones does not correlate with the growth phenotype

In the previous section of this chapter, the growth phenotype and mitochondrial content of the clones have been analyzed and evaluated. Yet another important parameter of the phenotype remained to be evaluated: the capabilities of the different CHO clones from the panel to produce recombinant protein. Recombinant protein production and oxidative metabolism have been previously described as closely related, with peak recombinant protein production being related to peak oxidative activity within the CHO cells (*Templeton et al., 2013*). Therefore, as heteroplasmy potential influence over the clones, if any, will manifest through changes in the oxidative metabolism, the recombinant protein production will be impacted by heteroplasmy.

An ELISA targeting human IgG antibody was performed to investigate whether there was any correlation between the titer and the other parameters measured to see if any correlation exist. Clones CHO-520F, CHO-111S, CHO-513F, and CHO-596S were selected from the panel to perform this assay, as they all can produce human-like IgG. CHO-792S did not grow in the culture at the time and was not included.

Media samples were collected from cell culture in suspension after 96 hours of culture and quantified as described in **Section 2.2.8 from chapter 2**.

The analysis showed a higher titer of IgG protein in clones CHO-520F and CHO-111S when compared with the others (**Figure 3.6**). Both clones showed a protein titer of approximately 120 µg/mL and qPs (Specific productivity) of around 30 pg/cell/day. Clone CHO-513 produced approximately 75 µg/mL while CHO-596S was lowest at 42 µg/mL. Curiously, both clones showed similar qPs with CHO-513 having a qPs of 18,6 pg/cell/day. and CHO-596S having a qPs of 15,1 pg/cell/day. Although the variance of the samples was high for protein titre in µg/mL, ANOVA analysis showed significant differences between clones CHO-513F and CHO-596S and the rest of the clones.

The recombinant protein titer and specific productivity observed in clones did not appear to have a clear relationship with the previous observations. Clones CHO-520F and CHO-111S showed very similar specific productivity and recombinant protein titre, which may relate to their also similar mitochondrial content. However, their growth rate and density were completely different. Oppositely, CHO-513F was similar to CHO-520F in culture

in growth rate and with the highest mitochondrial content among the panel, showed a relatively low r-protein titre and specific productivity compared with both CHO-520F and CHO-111S. Finally, CHO-596S was seen to underperform in both r-protein titre and specific productivity levels compared with the other clones. This was not surprising, given CHO-596S also underperforms in general culture performance.

This data demonstrated that the mitochondria number alone not being the definite factor for recombinant protein production in this panel of clones. Differences in protein production observed between clones with similar mitochondria numbers were hypothesized to be related to other factors. This data also supported the hypothesis of CHO-513F high mitochondrial content being related to oxidative performance problems, which may be related to the heteroplasmy variants found within this clone.

With both the growth and recombinant protein titer of the clones being established, the existence or the absence of a relationship between the observed phenotype of the clones and the heteroplasmy remained to be proven. To obtain more evidence to support or refute the potential relationship between heteroplasmy and these phenotypes, the next logical step was to check if the heteroplasmy found in the clones had any effect on the expression of the mitochondrial protein-encoding genes of interest, namely, CYTB and COX2.

The levels of mRNA transcribed from the corresponding mitochondrial protein-encoding genes are known to not necessarily correlate with the final levels of protein expression. For this reason, both transcript levels and protein expression levels of the set of CHO cell clones were evaluated separately, starting with the transcript levels.

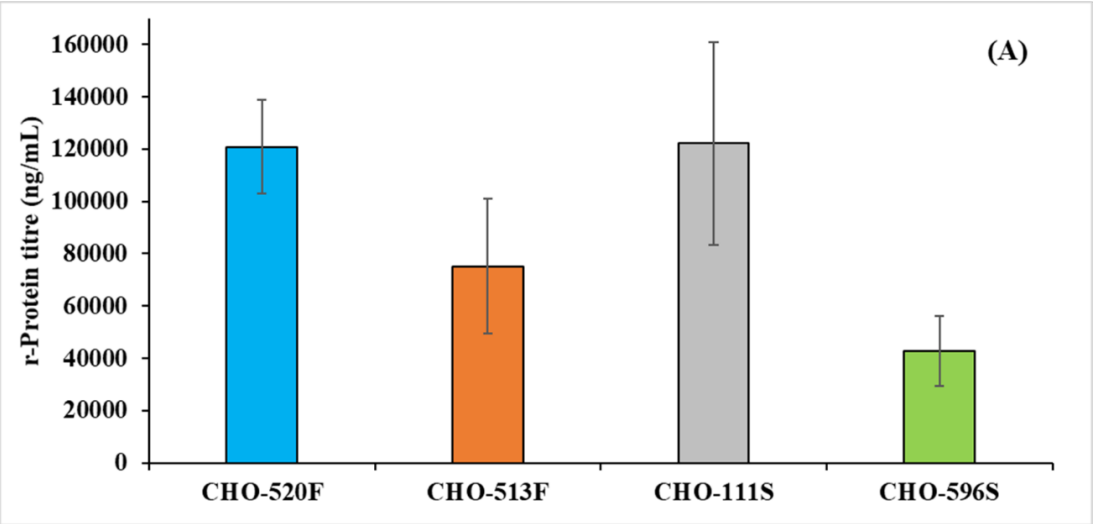

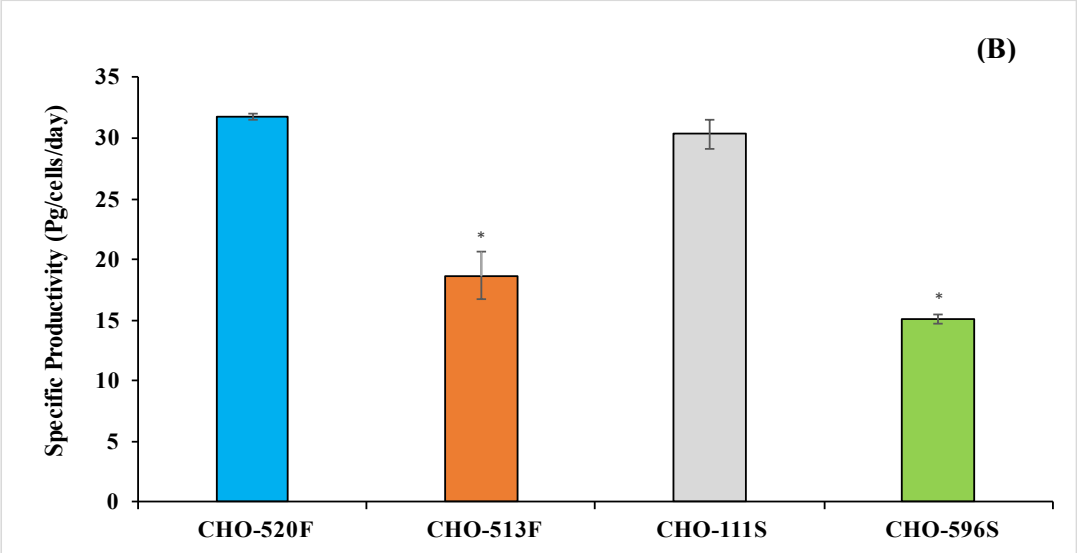

Figure 3. 6. (A) Protein titre from clones after 96 hours in culture. Each bar represent the average protein titre of biological triplicates measured in duplicate by ELISA ± SD. Significance was tested using 1-way ANOVA with $\alpha < 0,05$.

(**B)** Specific productivity (qP) of the clones measured over 96 hours of culture. Each bar represent the average qP of biological triplicates measured in duplicate by ELISA ± SD. Significance was tested using 1-way ANOVA with $\alpha < 0,05$.

3.2.1.3. The transcript levels of mitochondrial protein-encoding genes in CHO clones does not relate to either heteroplasmy or growth phenotype.

As briefly described in the previous section, to obtain evidence supporting or refuting the relationship between heteroplasmy and the phenotype of the evaluated set of CHO cell clones, an analysis of mRNA levels of mitochondrial protein-encoding genes was performed.

The mutations previously observed in the clones of interest were predicted to lead to the expression of non-functional versions of the proteins they encode, which could have an impact on mitochondrial oxidative metabolism.

Nevertheless, these mutations were also observed to represent only a varying percentage of the total mtDNA inside the cell, ranging from 7% to 50 %, which means there is a high number of wild types mtDNA molecules without those mutations contained inside the cells. Therefore, these wild-type copies may be enough to maintain regular mitochondrial oxidative metabolism, despite the presence of the mutant mtDNA molecules. To exert major changes on the metabolism of the cell the degree of heteroplasmy present in the mitochondria, this is the number of mtDNA copies with the mutation, must surpass the metabolic threshold, which means being present in a number high enough to become the main mtDNA type in the cell, changing the metabolism depending in the mutations present.

For this reason, we wished to first establish whether the presence of heteroplasmy observed to different degrees in FGPCs and SGPCs may lead to observable differences at the transcriptomic level. The presence of mutant mtDNA copies in high numbers was expected to lead to an overexpression of the wild type mtDNA copies to compensate for the presence of transcripts encoding non-functional versions of the protein, overall mtRNA levels would increase as the PCR primers used do not differentiate between mutant and wild type transcripts.

Primers targeting the following mitochondrial encoded genes were designed:

- **NAD5** (Subunit of respiratory complex I).
- **CYTB** (Subunit of Cytochrome C, part of complex III).
- **COX1** (Subunit of Cytochrome C Oxidase, complex IV)
- **COX2** (Subunit of Cytochrome C Oxidase, complex IV)

CYTB and COX2 genes were the two mitochondrial genes affected by the heteroplasmic mutations previously described in this chapter. While NaD5 and COX1 were found in previous studies to have minor heteroplasmic variants, those genes were included as a control of mitochondrial gene expression for genes belonging to the respiratory chain and not showing relevant heteroplasmy variants.

RNA was extracted from the cells using the TRIzol Reagent method (**Section 2.2.1**). The obtained RNA was then normalized and reverse transcribed into cDNA.

The obtained cDNA was used first to check if the primers produce the expected product size in all the clones (**Supplementary data 1.1)**.

For the first qPCR assay, primers targeting COX1, COX2, and NaD5 were used in the qPCR experiment. Beta-actin was used as an endogenous control (**Figure 3.7**).

COX1 expression was seen to vary greatly among the CHO cell clones. Compared to the wild-type reference sample, clone CHO-DG44i-ED003, COX1 expression increased to 2-fold in clone 520F, to 3,4-fold in clone CHO-111S, and 4-fold in clone CHO-513F. These data seemingly reveal differential expression of a mitochondrial gene not showing heteroplasmy in the different clones.

NaD5 followed a similar pattern to that observed for COX1. Compared to the reference sample CHO-DG44i-ED003, NaD5 expression increased to 2-fold in clone CHO-520F, to 3-fold in CHO cell clone CHO-111S, and 2.5-fold in CHO cell clone CHO-513F. These data reveal the natural variation in expression of a mitochondrial gene not showing heteroplasmy in the different CHO cell clones.

The levels of COX2 were lower in CHO-520F, CHO-111S, and CHO-513F compared to the wild-type clone. The data also suggested differences in COX 2 expression between clones CHO-520F, CHO-111S, and CHO-513F. However, the range of this difference

was relatively small, being around 0,3-0,4 RQ, which is close to the range of variation of the qPCR techniques (± 0,2 RQ).

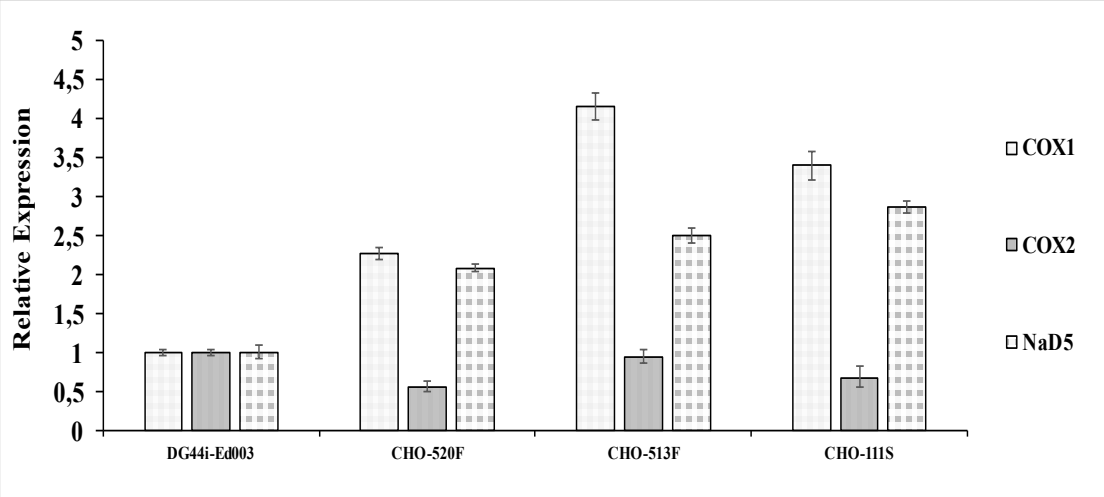

Figure 3. 7. Relative expression of mitochondrial genes COX1, COX2 and NaD5 in the CHO clones. Each bar represents the RQ for a given gene, calculated using the 2ΔΔcT formula.

The second qPCR experiment measured CYTB expression. In this case, CHO-520F was used as the reference sample instead of CHO-DG44i-ED003. This change was done for several reasons: First, to accommodate the samples of all the 5 CHO cell clones in the same qPCR plate. Secondly, CHO-520F had the lowest frequency of the *m.14136delA* variant in the CYTB gene. Finally, the change itself did not impede establishing a comparison between the different CHO cell clones, as the experiment was set for ``relative quantification´´ of the expression.

The analysis revealed a degree of variation in CYTB transcript levels detected across the samples (**Figure 3.8**). In particular, CHO-792S and CHO-596S displayed much lower and higher levels, respectively, than the other three clones. Conversely, similar CYTB expression was seen in CHO-520F, CHO-111S, and CHO-513F.

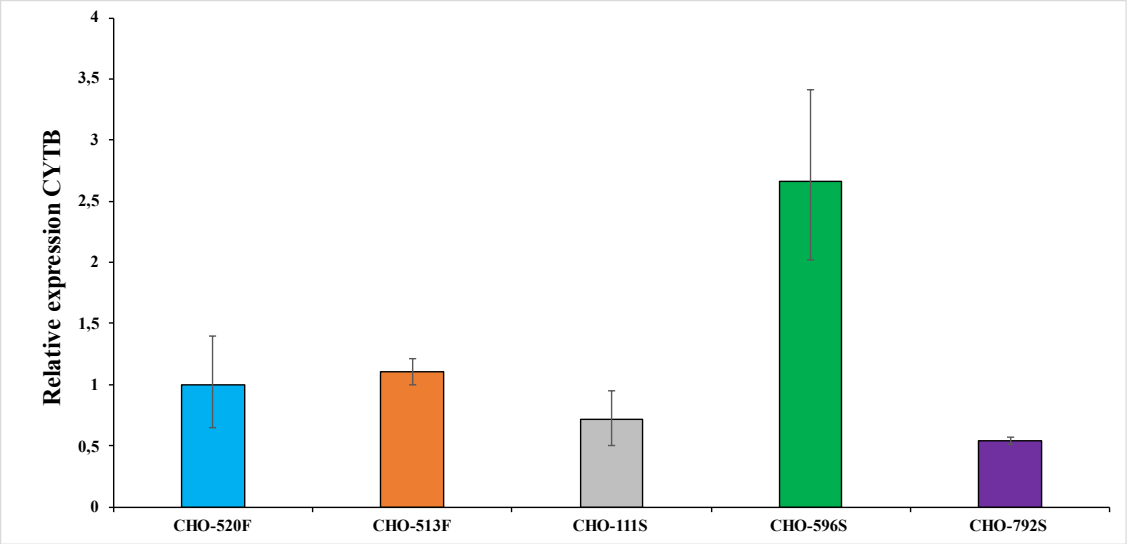

Figure 3. 8. Relative expression of mitochondrial genes CYTB in the CHO clones. Each bar represents the RQ of CYTB in a certain clone. RQ was calculated using the 2ΔΔcT formula**.**

Both CHO-520F and CHO-513F were classified originally as FGPCs, possess the same heteroplasmic variants (although to a different degree), and have been observed to possess similar growth rates and viability. However, CHO-513F was previously seen to have a much higher mitochondrial content than CHO-520F and, despite this, the transcript levels for both CYTB and COX2 remained similar in both clones. The CYTB *m.14136delA* variant and the COX2 *m.6996G>A* variant have both been observed to have higher frequencies in 513F than in 520F (about 10% more). Therefore, the higher mitochondrial content of CHO-513F could be related to the heteroplasmy: the higher number of mutant mtDNA copies may promote the synthesis of more mitochondria, containing enough wild-type mtDNA to compensate for non-functional transcripts.

Despite the differences in phenotype observed, despite lacking the heteroplasmic mutations found in the FGPCs and showing a much higher frequency in the CYTB *m.14136delA* variant, CHO-111S transcript levels were also observed to be similar to both CHO-520F and CHO-513F. This result, together with the similar mitochondrial content of CHO-520F and CHO-111S suggests the differences between CHO-111S and the ``fast´´ clones could be unrelated to the heteroplasmy observed in COX2 and CYTB mitochondrial genes.

CHO-596S showed the highest levels of CYTB transcript observed in the panel of clones. The growth, viability, and growth rate of CHO-596S were known to be the lowest of the clones analyzed. However, the mitochondrial content of CHO-596S was similar to other clones like CHO-520F and CHO-111S. Several explanations about these apparent contradictions were hypothesized. If CHO-596S was a clone with a high recombinant protein titer, this may lead to low growth and viability, but higher mitochondrial activity, leading to the high expression seen in the assay. Another potential explanation could be related to the heteroplasmy: as the frameshift variant may produce non-functional proteins, the transcription and expression of mitochondrial genes were increased by the cell in an attempt to compensate for this deficit.

Finally, CHO-792S was observed to have both low levels of transcript and low levels of mitochondrial content among all the clones of the panel. Regardless, CHO-792S showed the highest growth and viability among the SGPCs. The CYTB heteroplasmy degree for the frameshift *m.14136delA* variant in CHO-792S was also the highest from the panel (50%). Despite this, and differently from CHO-596S, the high heteroplasmy frequency found in CHO-792S seemed to not have a dramatic impact on the performance of the clone. Interestingly, both CHO-111S and CHO-792S were previously described in Kelly et al 2017 to have a Missense variant in mtDNA position 14849, corresponding with the CYTB gene too, which CHO-596S and both FGPCs lack. This mutation was reported to be found in very high frequencies in CHO-792S and could explain the differences observed among the SGPC clones.

Therefore, despite some differences between the expression of CYTB in different clones being observed, it remained unclear whether these differences are clone-specific or if CYTB expression varies greatly between different cells from the same clone group.

The data obtained by qPCR only covers the potential influence of heteroplasmy at the transcriptomic level and not the protein. The presence of heteroplasmic variants of CYTB and COX2 genes may not change the number of transcripts produced by the cell but may have influenced the quantity of the final product: the protein. Consequently, the next step taken was to analyze the proteins related to the heteroplasmic genes. This was attempted by Western Blot analysis.

However, the Western blot analysis were not successful, as CHO specific antibodies targeting CYTB and COX2 were not commercially available and the time. Moreover, the

CYTB antibody used in the experiments, which targeted human mitochondrial CYTB, seemed to be tissue-specific, as only human kidney protein lysate samples gave back a signal, while the human lung lysates failed to show a signal in western blot. These results can be found in the Supplemental figures of this study.

Given the difficulties in determining whether the heteroplasmic variants found in the clones may cause differences at either transcript level or protein expression level, the decision was made to focus instead on the phenotypic effects of heteroplasmy.

For this reason, it was decided to perform further metabolic measurements using a different system: an extracellular flux analyzer, an instrument capable of measuring both oxidative and glycolytic metabolism simultaneously over a short time.

3.2.1.4. ``In vivo´´ analysis of both oxidative and glycolytic metabolism using an XF-Flux analyzer reveals similarities in the metabolism of the set of CHO clones.

An extracellular flux analyzer was used to measure the whole picture of the metabolism in the CHO cell panel. Extracellular flux analyzers obtain metabolic data from a set of target cells arranged in a 96-well plate by measuring two different parameters.

The first parameter measured is the oxygen consumption of the cells over a set period, which is referred to as the OCR (Oxygen Consumption Rate).

The second parameter is the acidification of the media, which relates to the glycolytic metabolism of the cells, this parameter is referred to as ECAR (Extracellular Acidification Rate).

Three different protocols for metabolic analysis were used during this study. The standard protocol on the Seahorse XF-96 analyzer, known as the ``metabolic phenotype assay´´ (**MPA**), was the most frequently used. Differences between assays are related to the drugs added to the cells and will be described in detail in the relevant experiments.

Cells were maintained in suspension culture for 96 hours. Then, a 96-well XF cell culture microplate was treated with Corning Cell-Tak to ensure the adherence of the cells to the bottom of the wells. Finally, $2x10^4$ cells per well were seeded in each well, except for the wells in the corners of the plate, which remained as Blank controls.

As every plate can hold up to four samples with approximately 24 replicates, with a minimum size of 7-12 replicates to have an accurate reading according to the

manufacturer advice, four CHO cell clones, CHO-520F, CHO-111S, CHO-513F, and CHO-596S, were selected to be used in the analysis. CHO-792S stocks were not available at the time of this experiment and it was for this reason left out.

Firstly, the Seahorse XF-96 MPA kit was used to determine whether the clones show a metabolic tendency towards the oxidative phenotype or the glycolytic phenotype. When performing the metabolic phenotype assay two drugs were added to the media to achieve the ETS state. The drugs used were Oligomycin first and FCCP afterward. Such drugs are added into the wells automatically by the instrument at a previously set point of the assay. The action of both drugs together uncouples the electron transport chain from Complex V or ATP-synthase. Now free of limitations, the cells can achieve the maximum electronic transport state (**ETS**), also known as maximum respiration state or ``stressed´´ state. The maximum oxygen consumption potential of the cells can this way be evaluated.

When Baseline ECAR was analyzed in the clones, it was found to be similar apart from CHO-596S, which displayed a lower rate of acidification of the media, indicating reduced lactic acid secretion, and thus lower glycolytic activity (**Figure 3.9**). Analysis of the Stressed ECAR showed the same pattern, with CHO-596S displaying a lower acidification rate than the rest of the clones.

The ECAR rate in clones CHO-520F and CHO-513F ranged between 68 and 73 mpH/min during the stressed state while the CHO-111S ECAR rate was observed to be closer to 80 (78mpH/Min). As previously mentioned, the ECAR rate of clone CHO-596S was shown to be significantly diminished when compared to the ECAR rate of all the other clones in both basal and stressed states. The ECAR ratio of clone 596S was 45 mpH/min in the stressed state, equal to approximately half of the ECAR ratio of the other clones. The relatively low ECAR levels demonstrated by CHO-596S matched well the growth phenotype of this clone, as a decreased glycolytic metabolism is normally associated with slower growth rates. However, the CHO-111S ECAR rate was similar, with a tendency to high ECAR scores, to the rate of both CHO-520F and CHO-513F, which seemingly contradicts the classification of CHO-111S as an SGPC.

The ECAR ratio was observed to experience a 3x increase in the stressed state compared to the basal state in all clones. This uniform increase in ECAR Ratio is just an indirect consequence of the increase in OCR.

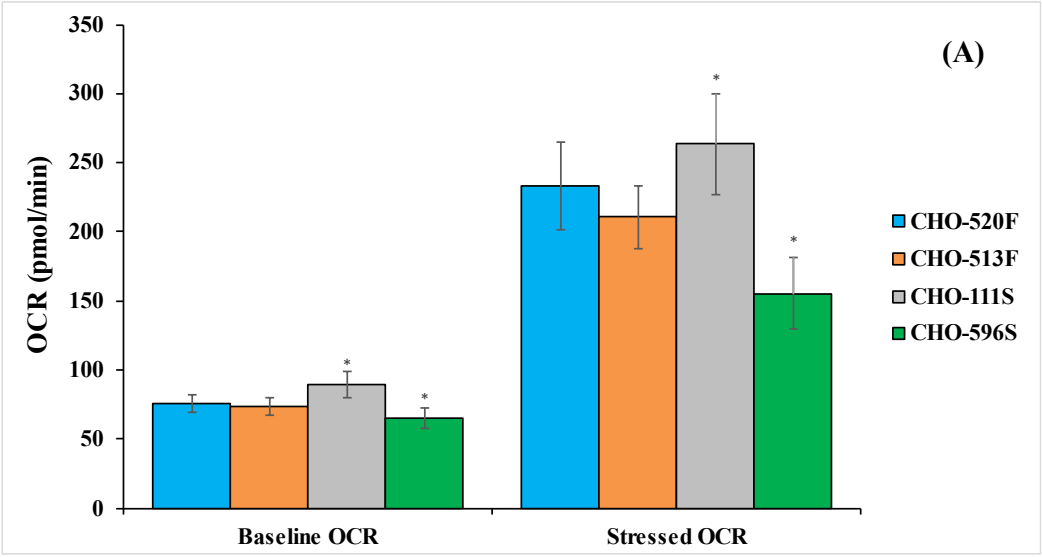

Figure 3. 9. (A) Oxygen consumption rate (OCR) from the CHO clones after 96 hours of culture in each of the three different media tested. Each bar represents the average OCR level of biological triplicates measured in 7 technical replicates using Seahorse XF-96 analyser ± SD. Significance was tested using one-way ANOVA with $\alpha<0.05$, represented by * in the figure.

(B) Extracellular Acidification Rate (ECAR) from the CHO clones after 96 hours of culture in each of the three different media tested. Each bar represents the average ECAR level of biological triplicates measured in 7 technical replicates using Seahorse XF-96 analyser ± SD. Significance was tested using one-way ANOVA with $\alpha<0.05$, represented by * in the figure.

The analysis of Oxygen consumption rate data (OCR) showed a similar pattern. Firstly, no significant differences between the OCR rate of clones CHO-520F and CHO-513F were observed, either during basal state or stressed state. OCAR levels ranged between 210 and 230 pmol/min after Oligo/FCCP injection. Oligomycin is an inhibitor of ATP-synthase, which blocks the proton channel subunit of the protein. FCCP is a potent uncoupler of mitochondrial oxidative phosphorylation which can dissipate the proton gradient (and membrane potential) by catching and transporting protons across the mitochondrial inner membrane. The addition of these two drugs causes the cells to reach the maximum respiration state while attempting to restore the proton gradient. This respiration state is known as the maximum ETS state.

Secondly, the OCR rate of clone CHO-596S was shown to be diminished when compared to the OCR rate of the other clones, although only during the stressed state, during which showed an OCR ratio of 150 pmol/min. Finally, the OCR rate of clone CHO-111S was observed to be significantly higher than the OCAR rate of the rest of the clones, reaching a peak of 263 pmol/min.

These results seemed to differ from what was expected to be seen in the metabolism of the different CHO cell clones. The extracellular flux analysis found no significant differences between FGPCs growth phenotype clones. However, differences between the two SGPCs growth phenotype clones were larger than the differences observed between FGPCs and SGPCs.

The data obtained in this experiment showed differences with the data obtained respirometry assay. Mainly, respirometry data showed CHO-520F oxygen consumption levels to be lower than the other clones, while the data obtained with the XF-Analyser showed CHO-520F OCR to be similar to both CHO-111S and CHO-513F.

These differences may be explained by the cells for both analyses being analyzed at different time points, as the respirometry assays were performed during the early exponential phase (24 hours after being seeded) while the XF analysis was performed during the late exponential phase (96 hours after being seeded). However, performing an extracellular flux analysis at such an early time point was discarded for two different reasons:

First, the sheer quantity of cells needed to get a reliable result was deemed too high. Each well should contain $2*10^4$ cells at least to get the maximum oxygen consumption possible, as determined by experimental observation in the laboratory. Additionally, a minimum amount ranging between 7-12 wells per sample, meaning technical replicates of the sample, was recommended by the manufacturer to achieve an accurate reading. This dramatically increased the number of cells required for the experiment.

Secondly, the heteroplasmic mutations are located in genes encoding subunits of the respiratory chain. Because of this, it was expected to observe the effect of these mutations mainly in the oxidative metabolism of the cell, as CHO cell lines are known to shift from glycolytic metabolism to oxidative during the late exponential phase and keep it up from that moment onwards.

For these reasons, early exponential phase cells were not analyzed in the XF analyzer. Therefore, a comparison between the data obtained within the respirometry assay and the data obtained with the XF analyzer is not meaningful. However, it was considered that the higher precision of the method and the higher number of samples made those data obtained by the extracellular flux analysis method more accurate compared with the respirometry data.

The data obtained from the metabolic phenotype assay provided no observable evidence of heteroplasmy influencing the metabolism of the different clones. However, the metabolic phenotype assay is unable to provide a 100% accurate picture of the glycolytic metabolism by itself. The Seahorse XF-96 analyzer measures the ECAR ratio by measuring the acidification ratio of the media, which has a fixed initial pH of 7.4. However, the CO_2 generated as a by-product during oxidative metabolism also contributes to the acidification of the media.

Therefore, to accurately measure potential differences in glycolytic metabolism, a further assay using the Seahorse XF 96 instrument was performed: The Glycolytic rate assay.

3.2.1.5.``In vivo´´ analysis of glycolytic metabolism using an XF-Flux analyzer Glycolytic Rate assay kit reveals higher glycolytic levels among the SGPCs from the panel of CHO clones.

Briefly, during this assay the oxidative respiration is inhibited completely by adding rotenone to the cell media, then glycolysis is also inhibited to measure the acidification of the media non-related to the glycolysis. This assay takes place in three different stages.

During the first stage, the cells' general metabolism is measured without the addition of any drug. This will allow calculating later the influence of the oxidative metabolism in the acidification of the media.

During the second stage, rotenone and actinomycin A is added to the media. Rotenone inhibits the transfer of electrons from Complex I to Complex II. Antimycin A binds to complex III (cytochrome c reductase), disrupting the enzyme Q cycle. The addition of these two drugs stops oxidative metabolism completely. At this stage, the general contribution of the glycolytic metabolism to the media is measured. The potential bias introduced by the CO_2 generated as a by-product during the oxidative metabolism is absent, measuring the acidification rate (ECAR) more accurately than in the previously described assay in the previous section.

Finally, during the third and final step, 2-Deoxy-D-glucose (**2-DG** from now on) is added into the media. **2-DG** can be taken by the glucose transporters into the cell, but cannot be incorporated into glycolysis, as it has the 2-hydroxyl group replaced by hydrogen, inhibits glycolysis by binding competitively to glucose hexokinase, the first enzyme in the glycolytic pathway. This results in a decrease in the acidification of the media, as the acidification related to glycolysis disappears. This decrease provides valuable information about the real influence of the glycolysis acidification ratio. This final acidification rate can be used to confirm if the acidification observed at stage 2 depended solely on glycolysis.

The acidification ratio of the growth media is calculated as Proton Efflux Rate (PER from now on). The contribution of mitochondrial oxidative metabolism to PER in form of CO_2 (mito PER) is calculated by the instrument during the assay using an empirically calculated value provided by the manufacturer (CO_2 Contribution Factor or CCF).

According to the manufacturer's website, the CCF for the instrument used in this study, the Seahorse XF-96 analyzer, is 0.61± 0.13.

With this data and using the ECAR and OCR values described in the previous section as the base for the calculations, the instrument can provide information about the PER caused by the glycolytic metabolism of the cell. The output value, known as glycoPER, represents ``the rate of protons extruded into the extracellular medium during the glycolysis´´ as it is defined by the user's manual provided by the manufacturer, Agilent. Changes in glycoPER reflect this way changes in the glycolytic metabolism of the cells.

The percent of PER corresponding to the glycolytic pathway in the basal state was this way analyzed (Figure 3.10A). The basal state corresponds to the state of the cells in culture with no drugs capable of altering the metabolism being added into the media. Most clones show a similar percent of PER corresponding to glycolysis, of approximately 85-90%. However, clone CHO-596S showed a diminished percent of glycolysis-dependent PER, corresponding to only 73,7% of the total PER.

The PER data corresponding to the glycolysis during the Basal state, Compensatory glycolysis stage, and post-glycolysis inhibition acidification stage was analyzed and calculated as glycoPER (PER related to glycolysis exclusively). The corrected glycoPER in pmol/min was calculated during the three stages described for each clone. (**Figure 3.10**).

The data obtained for CHO-596S during the first stage, Basal glycolysis, showed this clone to have a diminished glycolytic activity, with a low glycoPER level (100 pmol/min) compared with the other clones, which glycoPER ranges around 200-250 pmol/min. This result seemed to confirm the previous observations in clone CHO-596S ECAR rate, which was lower than in the other clones. Additionally, CHO-111S was observed to have higher levels of glycoPER (271 pmol/min) during the basal state than any other clone. CHO-111S results obtained during the metabolic analysis were also showing higher levels of glycolysis than in CHO-596S, which seemingly contradicted the expected metabolism of an SGPC.

Furthermore, during the present assay, CHO-111S demonstrated significantly higher glycoPER levels than both CHO-520F and CHO-513F, which as FGPCs would be expected to have higher levels of glycolysis.

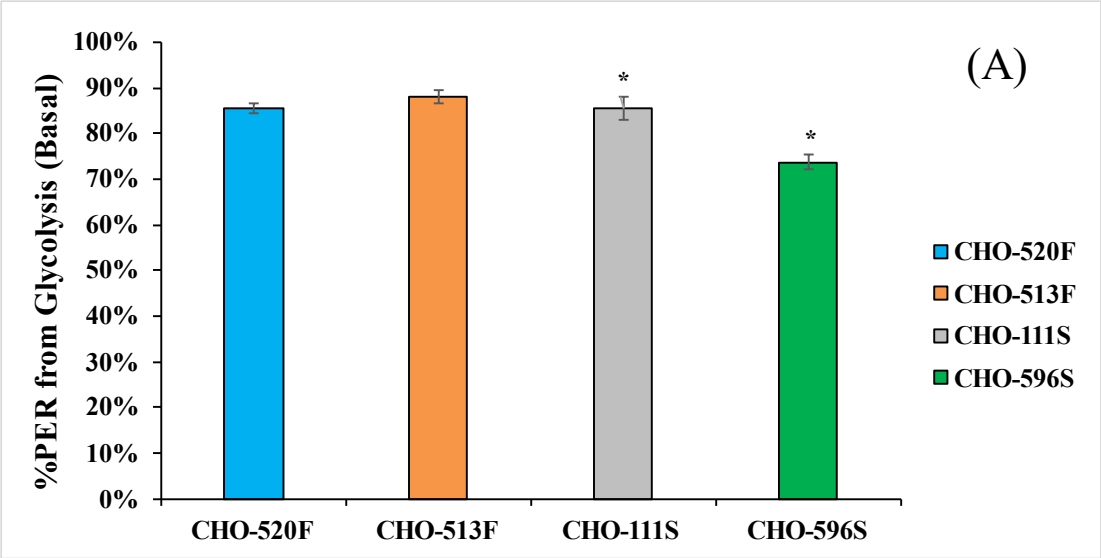

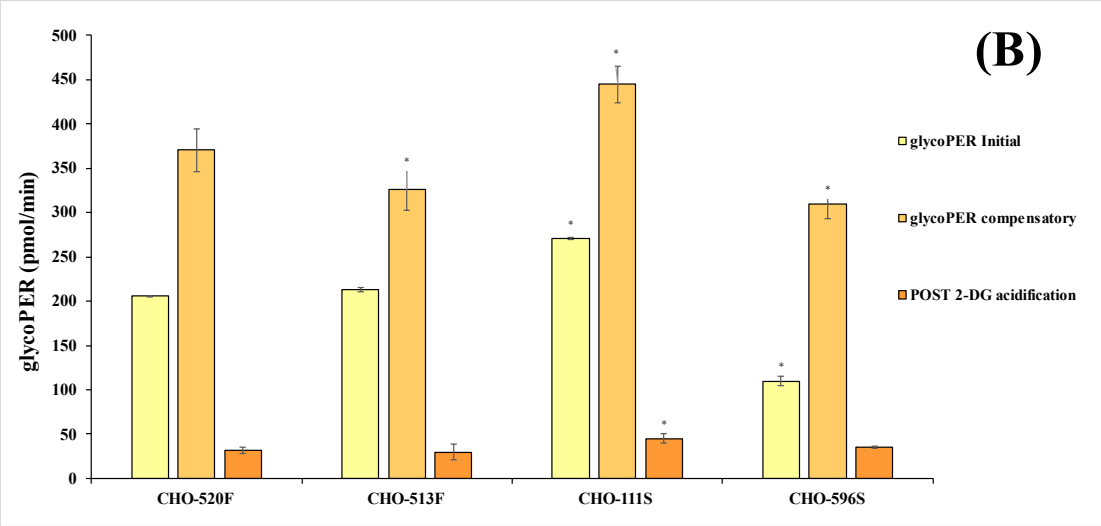

Figure 3. 10. (A) PER from CHO clones after 96 hours of culture. Each bar represents the average PER of biological replicates measured in 7 technical replicates with Seahorse XF-96 glycolytic rate assay ± SD. Significance was tested using a one-way ANOVA with α <0,05, represented in the figure by *.

(B) GlycoPER from CHO clones after 96 hours of culture. Each bar represents the average GlycoPER at different points in time of biological replicates measured in 7 technical replicates with Seahorse XF-96 glycolytic rate assay ± SD. Significance was tested using a one-way ANOVA with α <0,05, represented in the figure by *.

This trend was observed to continue during the Compensatory Glycolysis stage, caused by the addition of Rot/AA to the media. During this stage, CHO-111S reached much higher levels of glycoPER (444 pmol/min) than any other clone. Meanwhile, Clones CHO-520F and CHO-513F differentiated, with the former reaching higher levels of glycoPER (370 pmol/min) than the latter (320pmol/min). This result was also contradictory, as CHO-513F was previously observed to grow to higher densities than CHO-520F. The clone CHO-596S performance was observed to greatly improve during this stage, reaching glycoPER levels almost equal to CHO-513F (309 pmol/min). Regardless, CHO-596S remained as the clone with the lowest glycolytic activity from the panel. This data showed differences not seen during the previous assay between clones CHO-111S, CHO-520F, and CHO-513F. Notably, CHO-596S was observed in both assays to be the clone performing worst in glycolysis.

Finally, the Post-2-DG acidification (acidification non-related to glycolysis) was observed to be similar in all clones bar CHO-111S, which showed a slight yet significant increase.

These results confirmed the previous observations about CHO-596S glycolysis levels and added an extra layer of information about the rest of the clones. Differences between the glycolytic metabolism of clone CHO-111S and the glycolytic metabolism of the fast clones, previously hinted in the metabolic phenotype assay but not clearly observed, were shown. In addition, differences between the FGPCs were also clearly observed during the Compensatory glycolysis.

The XF-analyser assays provided useful insight into the metabolism of the panel of CHO clones and raised interesting questions. FGPCs were seen to possess similar levels of oxidative metabolism, while differences could be seen in the glycolytic metabolism of such clones. On the other hand, SGPCs showed enormous differences in both oxidative and glycolytic metabolism.

3.2.1.6.Summary of the analysis performed in the panel of CHO clones.

During this analysis of the selected panel of CHO clones in standard conditions, interesting information about the phenotype, behavior, and metabolism of the clones was collected.

First, the FGPC clones, CHO-520F and CHO-513 were observed to possess small differences despite being in the same phenotype growth. CHO-513F was observed to grow to higher cell densities than CHO-520F, despite both clones having the same cell growth rate, CHO-513F was also observed to remain viable slightly longer, containing a relatively higher number of mitochondria and having a lower recombinant protein production than CHO-520F. On the other hand, CHO-520F demonstrated higher levels of glycolytic metabolism than CHO-513F. While heteroplasmy could explain some of these differences, both clones showed similar COX2 and CYTB transcript levels. Therefore, the influence of heteroplasmy in these clones, if any, was hypothesized to be likely related to the protein expression.

Sadly, due to the previously commented difficulties in finding a suitable antibody, no reliable data related to the mitochondrial protein expression of the CHO clones were generated during this study. For this reason, whether heteroplasmy was causing differences in the protein expression levels of the clones remained unknown.

Secondly, clone CHO-596S peak growth density, recombinant protein titer, and viability were lower than in the rest of the clones from the panel. The metabolic analysis also revealed the oxidative and glycolytic metabolism of CHO-596S to be diminished in comparison with the rest of the clones from the panel. It is worth noting that, despite everything described above, CHO-596S growth rate and mitochondria content levels were equal to those from other clones such as CHO-111S. The decrease observed in peak growth density was likely to be related to the low viability of CHO-596S, as this clone was observed to have a higher growth rate, but a lower peak cell density than CHO-111S. Additionally, the transcript levels of the CYTB gene were greatly increased in CHO-596S with respect to the other clones. This data suggested a link between the low performance showed by CHO-596S and the high levels of heteroplasmy found in the CYTB mitochondrial gene in this clone. However, more robust evidence and protein expression data would be needed before making a strong statement about this relationship.

Finally, the data collected in clone CHO-111S showed very different results from CHO-596S, despite both clones being originally classified as Slow Growth Phenotype Clones. While CHO-111S showed a lower growth rate and reached lower peak cell densities than any FGPC. However, high levels of both oxidative and glycolytic metabolism and also recombinant protein titer were observed in CHO-111S compared with the other ``slow´´ clone, CHO-596S. CHO-111S was noted to perform similarly to CHO-520F in mitochondrial content, specific productivity of r-protein, CYTB expression, and oxidative metabolism. Notably, CHO-111S showed the highest levels of glycolytic metabolism, which did not seem to correspond to increased growth.

On the other hand, observations made in CHO-111S were the very opposite of CHO-596S. CHO-111S was observed to have increased metabolism, specific productivity, and protein titer compared with CHO-596S, despite both being SGPCs. Additionally, CHO-111S metabolic values were observed to be higher than any other clone, and possessed a protein titer, specific productivity, and mitochondrial content equal to that of clone CHO-520F, despite the differences in growth phenotype.

On a first view, a relationship between the heteroplasmy levels and the phenotype observed in the evaluated panel of CHO cell clones was not evident. However, FGPCs were observed to possess heteroplasmic variants in both the COX2 gene and CYTB that may influence their higher growth and viability compared to the SGPCs.

Several studies in CHO literature have highlighted the changes in the metabolism induced by a specific shift in the temperature of incubation. According to these publications, shifting the temperature of CHO cells from 37ºC down to 31ºC can induce growth arrest in CHO cells.

During growth arrest, CHO cells' growth is considerably diminished, but their protein titer is significantly increased. The protein titer has been reported to be closely linked to the levels of oxidative metabolism in the cells. For this reason, it was hypothesized that CHO cells with different heteroplasmic variants may respond differently to the temperature shift. It is worth mentioning that after the temperature shift, the life span of the CHO cells has also been reported to increase.

The next section of this chapter, **section 3.2.3**, is dedicated to the results obtained from a temperature shift experiment performed in a panel of 4 CHO cell clones containing relevant heteroplasmic variants which may impact the oxidative metabolism of the cell.

3.2.2 Temperature shift influence in the metabolism of CHO cell clones with different heteroplasmy variants.

The results described in the previous section (**Section 3.2.2.**) suggested a potential between the heteroplasmy reported in the set of CHO cell clones and the phenotype observed in the clones but did not provide a definite conclusion. For this reason, a new and different approach was taken.

One of the most popular methods of achieving proliferation control in CHO cells is temperature shift. In normal conditions, CHO cells are grown at 37ºC in a shaking incubator. If the temperature of the incubator is decreased from 37ºC to a temperature between 28ºC and 33ºC, often 31ºC, CHO cells will undergo cell growth arrest.

During this ``cell growth arrest´´ state, CHO cells grow slower, but their recombinant protein titer is increased, as the cells will commit their resources to protein production rather than proliferation. The life span of the cells has been reported in the literature to be increased during the cell growth arrest.

The protein titer has been reported to be closely linked to the levels of oxidative metabolism in the cells. Therefore, it was hypothesized that CHO cells with different heteroplasmic variants may respond differently to the temperature shift.

This section describes how a temperature shift experiment was performed in a panel of 4 different selected CHO cell clones containing different heteroplasmy variants. The goal of this experiment was to determine if heteroplasmy can affect the metabolic changes caused by the temperature shift. To this end, the growth, viability, and metabolism of the clones were evaluated.

3.2.2.1. Growth arrest and long-term viability increases in a panel of CHO cell clones after the temperature shift.

The selected CHO cell clones for the temperature shift experiment included CHO-520F, CHO-111S, CHO-513F, and CHO-596S. Clones were seeded at a cell density of $2x10^5$ and culture in 5mL of media. For every clone, six 5mL tubes were seeded as described.

All the tubes were grown at 37ºC in a shaker incubator for 48hours. After 48hours, all the tubes' cell content was measured using a cytometer as previously described. Samples were taken from each tube and used in an extracellular flux analysis, as will be described later.

At this point, and for every clone, 3 tubes were moved into a new shaker incubator, which temperature was set to 31ºC. The other 3 tubes were maintained at 37ºC in the same shaker incubator. Other than temperature, the conditions in the two shaking incubators were identical (humidity, CO2, etc).

The cells were then incubated for an additional 24 hours. Then, all tubes were again counted with Guava Viacount, and samples were collected to be used in an extracellular flux analysis as previously described.

The first analysis of the growth density of the clones was made after 48 hours of culture before the temperature shift happened. (**Figure 3.11 A**). Growth of both CHO-520F and CHO-111S appeared similar, while CHO-513F growth was diminished compared to the other clone's observations, being similar to the growth of CHO-596S. To make sure this observation was not due to neither experimental error nor cross-contamination, the experiment was repeated three times using newly recovered cells. The result was observed to be similar every time. **Figure 3.11** corresponds with the most representative attempt. These results were similar to the results previously shown in this chapter in the growth of the clones after 48 hours.

After 72 hours of culture, 24 hours after the temperature shift, the growth, and viability of most shifted samples from the clones were demonstrated to be similar to those of the non-shifted. The sole exception was CHO-111S, which shifted samples were observed to reach significantly higher cell densities than the unshifted. Interestingly, the growth data

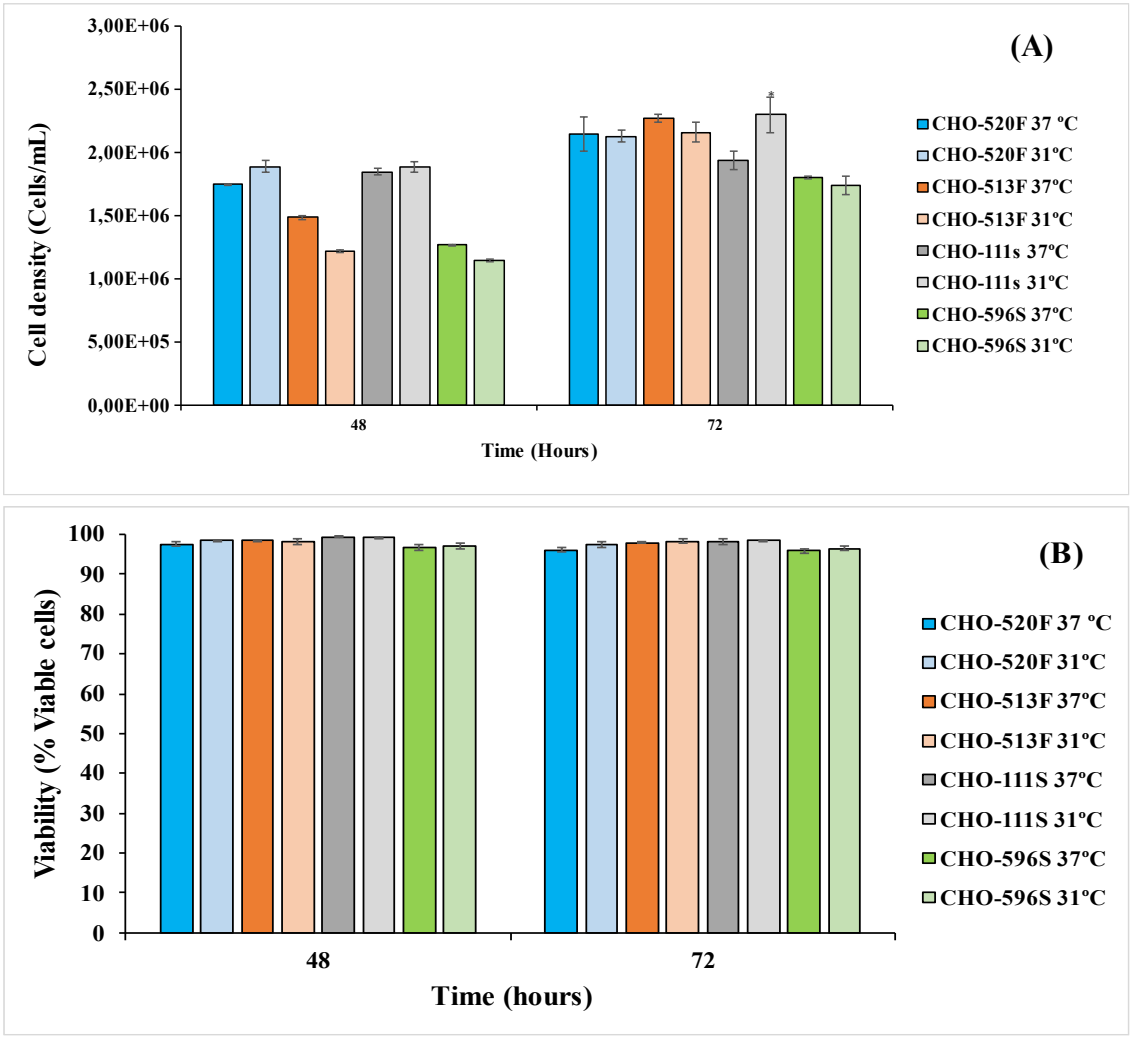

Figure 3. 11. (A) Viable cell density of CHO clones after 48 (left) and 72 (right) hours of culture. Cells were culture in suspension culture in a shaker incubator in 5mL of CHO-SFMII media at 37ºC or 31ºC respectively. Each column represents the average viable cell density of biological triplicates measured in triplicates using Guava Easycite cytometer ± SD. Significance was tested using a one-way ANOVA with α <0,05, marked with * in the figure.

(B) Viability of CHO clones after 48 (left) and 72 (right) hours of culture. Cells were culture in suspension culture in a shaker incubator in 5mL of CHO-SFMII media at 37ºC or 31ºC respectively. Each column represents the average viability of biological triplicates measured in triplicates using Guava Easycite cytometer ± SD. Significance was tested using a one-way ANOVA with α <0,05, marked with * in the figure.

obtained for the clones at 96 hours of culture showed CHO-111S cell density to be diminished compared to CHO-520F and CHO-513F when grown at 37ºC but to be increased when grown at 31ºC.

The data collected in the viability of the cells showed the viability of all clones being similar after both 48 and 72 hours of culture (**Figure 3.11 B**).

Given the apparent lack of response of the cells, and to ensure that the cells have enough time to adapt to the temperature shift from 37ºC to 31ºC, an additional experiment was performed in which the cells were incubated for an additional 48 hours after the temperature shift (up from 24 hours). This change gave the cells more time to shift their behaviour towards the expected phenotype previously described in the literature. After performing the corresponding analysis at 96 hours, cells were left to grow in their current conditions for an additional 48 hours.

Analysis of the growth of the clones after this change was introduced revealed differences in the growth of the cells after 96 hours of culture and onwards (**Figure 3.12 A**). The cells grown at 31ºC temperature show a significant decrease in growth when compared with their counterparts who grew at 37ºC. Although the growth of all the clones from the panel was affected by the shift, this decrease was especially acute in both CHO-520F and CHO-513F, with an approximate decrease of 1 million cells /mL after being grown at 31ºC. The differences observed between clones grown at 37ºC and 31ºC respectively were also observed after 144 hours of culture. The differences became more acute in clones CHO-111S and CHO-513F. Due to low viability issues in the samples cultured at 37ºC, these differences were not appreciated in both clones CHO-596S and CHO-520F, as both clones showed a sharp decrease in viability after 144 hours of culture at 37ºC.

Moreover, at 144 hours of growth, the cells that were grown at 37ºC show a drastic decline in viability, while those cells that were grown at 31ºC still showed a high percentage of viable cells (**Figure 3.12 B**). As commented before, the decrease in viability was less pronounced in clones CHO-111S and CHO-513F than in clones CHO-520F and CHO-596S. With the cell growth arrest finally observed in the panel of selected clones, and in addition to the growth and viability profile of the CHO cell clones, extracellular flux assays were performed before and after the temperature shift, aiming to capture potential changes in the metabolism of the cells caused by the temperature shift.

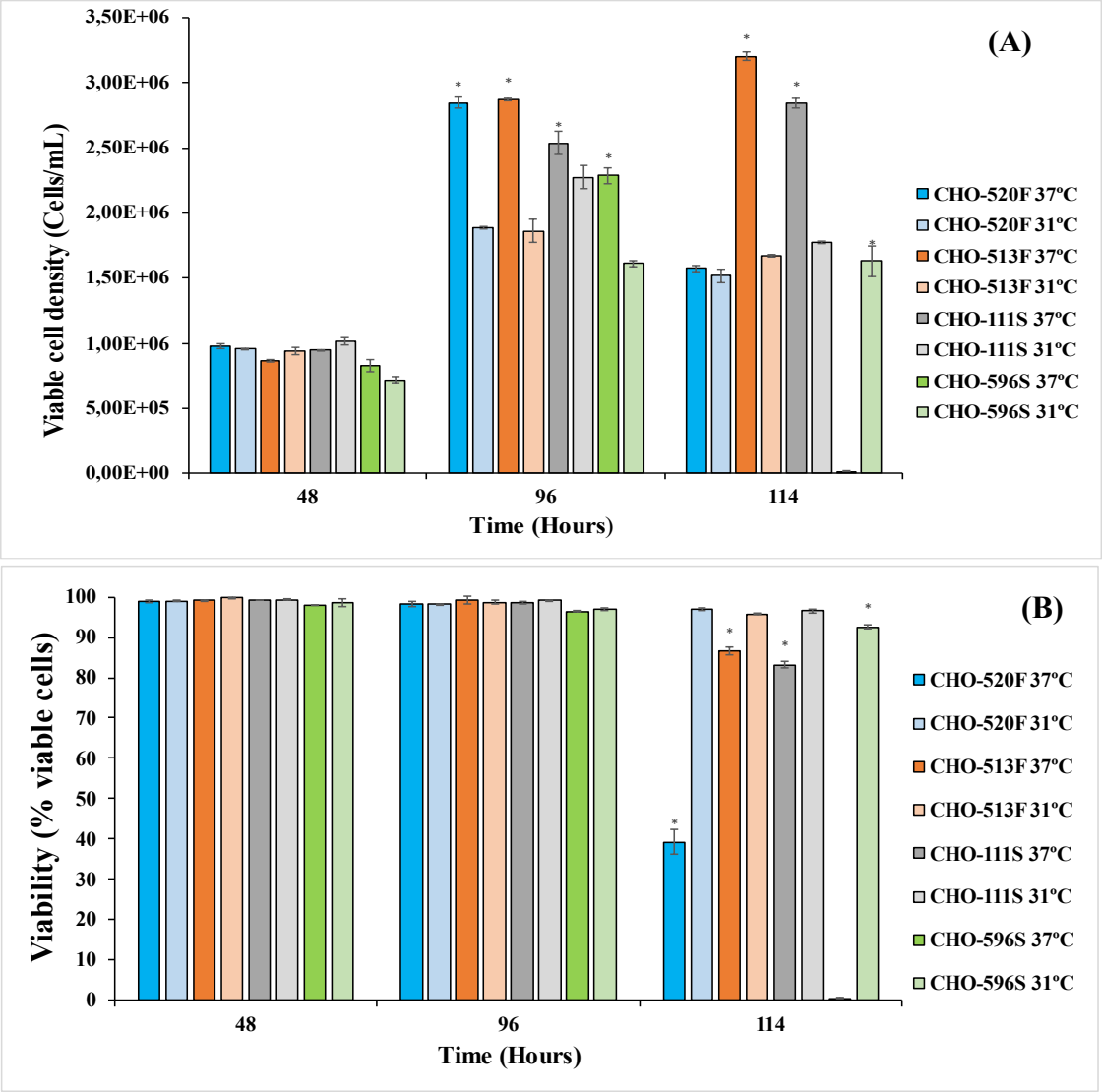

Figure 3. 12. (A) Viable cell density of CHO clones after 48 (left), 96 (centre) and 144 (right) hours of culture. Cells were cultured in suspension culture in a shaker incubator in 5mL of CHO-SFMII media at 37ºC or 31ºC respectively. Each column represents the average viable cell density of biological triplicates measured in triplicates using Guava Easycyte cytometer ± SD. Significance was tested using a one-way ANOVA with α <0,05, marked with * in the figure.

(B) Viability of CHO clones after 48 (left), 96 (centre) and 144 (right) of culture. Cells were culture in suspension culture in a shaker incubator in 5mL of CHO-SFMII media at 37ºC or 31ºC respectively. Each column represents the average viability of biological triplicates measured in triplicates using Guava Easycyte cytometer ± SD. Significance was tested using a one-way ANOVA with α <0,05, marked with * in the figure.

These extracellular flux analyses were performed using the Seahorse XF-96. The results of these experiments are described in detail in the next sub-section of this chapter.

3.2.2.2.Post-temperature shift metabolic analysis of the metabolism reveals changes in the metabolism of SPGCs from the panel of CHO clones.

As previously described, the effects of shifting the incubation temperature of CHO cells from 37ºC to 31ºC include cell growth arrest and viability increase. These phenotypical changes are likely to reflect a metabolic change inside the cells.

Temperature shift has been previously reported in the literature to positively impact the recombinant protein titer of CHO cells (*Barron N., Kumar N, et al 2011*) while diminishing cell growth, one effect of temperature shift is to cause a metabolic shift towards the oxidative metabolism, similar to the shift most cultured cell lines and cancer cells undergo during the late exponential phase of growth. However, the mechanisms of the changes induced in CHO cells by the temperature shift are not fully understood.

In this study, cell samples were collected before and after the temperature shift. The metabolism of those cell samples was measured ``In vivo´´ using a Seahorse XF-96 extracellular flux analyzer to perform an Extracellular Flux assay (XF-assay). The Extracellular Flux performed was the ``Metabolic phenotype assay´´, a basic assay that allows the measurement of both oxidative and glycolytic metabolism of the cells. The data obtained from this assay can be used to compare the metabolism of the cell grown at different temperatures.

The first XF assay was performed with samples collected from the cells grown as seen in **Figure 3.11.** Analysis of the data obtained from the samples cultured during 48 hours showed no significant differences between samples labelled as ``37º´´ and samples marked as ``31º´´ in any of the CHO clones from the panel. (**Figure 3.13**). This was the expected outcome of the first assay, as both batches of cells were grown identically (at 37ºC) up to this point.

This metabolic analysis showed differences with the previously performed analyses, described in previous sections. The most notable difference observed concerned the behaviour of clone CHO-596S. Previously, this clone was repeatedly observed to be the worst-performing clone in both oxidative and glycolytic metabolism terms. However, during this XF-assay, both OCR and ECAR levels from this clone were observed to be

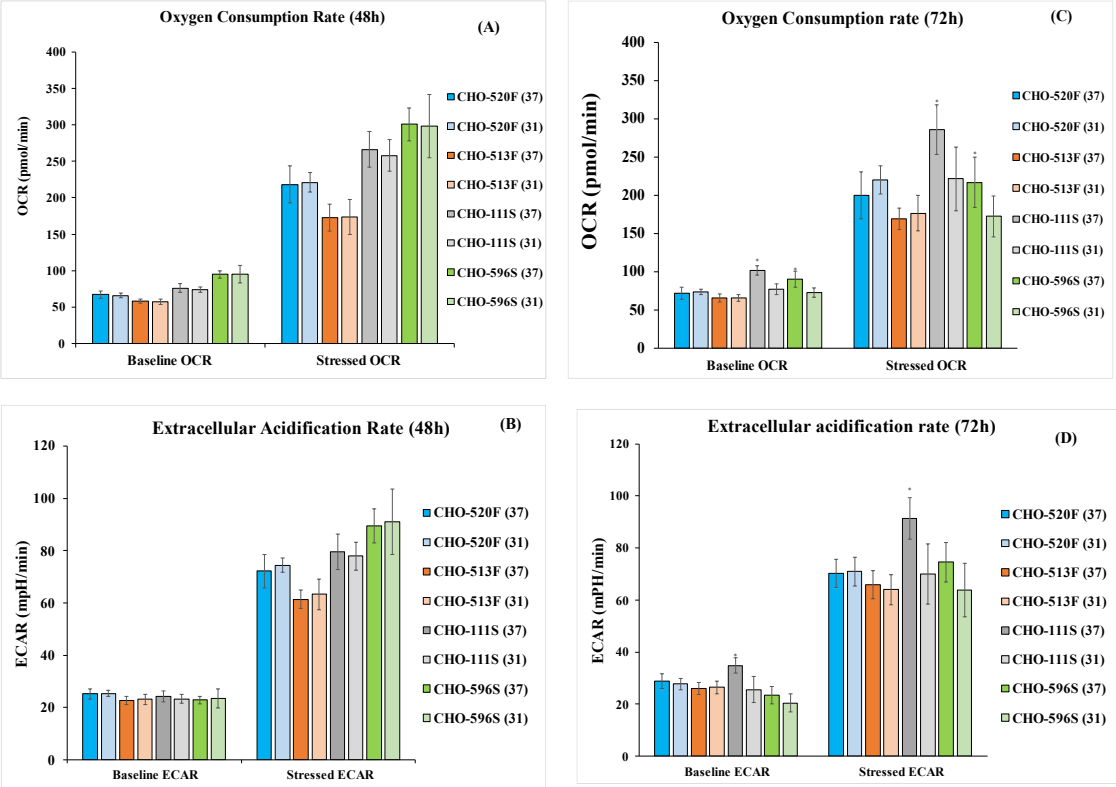

Figure 3. 13. (A) Oxygen consumption rate (OCR) from CHO cell clones after 48 hours of culture. Each bar represents the average OCR level of biological triplicates measured in 7 technical replicates using Seahorse XF-96 analyser ± SD. Significance was tested using one-way ANOVA with $\alpha<0.05$, represented by * in the figure.

(B) Extracellular Acidification Rate (ECAR) from CHO cell clones after 48 hours of culture. Each bar represents the average ECAR level of biological triplicates measured in 7 technical replicates using Seahorse XF-96 analyser ± SD. Significance was tested using one-way ANOVA with $\alpha<0.05$, represented by * in the figure.

(C) Oxygen consumption rate (OCR) from CHO cell clones after 72 hours of culture. Each bar represents the average OCR level of biological triplicates measured in 7 technical replicates using Seahorse XF-96 analyser ± SD. Significance was tested using one-way ANOVA with $\alpha<0.05$, represented by * in the figure.

(D) Extracellular Acidification Rate (ECAR) from CHO cell clones after 72 hours of culture. Each bar represents the average ECAR level of biological triplicates measured in 7 technical replicates using Seahorse XF-96 analyser ± SD. Significance was tested using one-way ANOVA with $\alpha<0.05$, represented by * in the figure.

higher than the rest of the clones from the panel, reaching an ECAR score of 90 mpH/min in the stressed state after 48 hours of culture, 20 mpH /min higher than the closer clone, CHO-111S, and an OCR score of 300 pmol/min in the same conditions, 50 pmol higher than the closer clone, which was again CHO-111S.

The metabolic levels of CHO-596S seemed to decrease with time, as both OCR and ECAR levels were observed to be similar to those of clone CHO-520F after 72 hours of culture, ranging around 200mPH/min for OCR and 74 mpH/min for ECAR. Despite the decrease, these results still show an increase in the metabolism of CHO-596S with respect to the previously available data

Oppositely, the metabolism of clone CHO-513F appeared to be decreased in comparison to the previous data obtained, being the clone with the lowest performance in b OCR and both 72 hours of culture. On average, CHO-513 OCR levels were 40 pmol/min lower than the levels of the closest clone, CHO-520F. ECAR levels were not observed to be significantly different between these two clones.

Finally, CHO-111S showed a significant increase in both ECAR in OCR levels after 72 hours of culture at 37ºC with respect to the other clones. This increase was not previously observed in the previous data.

While these data seem to contradict the results previously obtained from the Metabolic phenotype assays previously performed in the panel of CHO cell clones, it must be taken into account that the previous data was obtained after 96 hours of culture, and therefore the data previously obtained corresponded to another point in time in the metabolic cycle of the clones.

Finally, the data obtained from this extracellular flux analysis experiment did not show any clear differences between cells grown at 37ºC and cells grown at 31ºC. While some differences can be observed in some cases, which are especially pronounced in the case of the SGPCs CHO cell clones CHO-111S and CHO-596S, the high variability makes these differences unclear.

To ensure that the cells had had enough time to adapt to the temperature shift from 37ºC to 31ºC, a new assay was performed. This new assay included a metabolic assay after 96 hours, which allowed the comparison with the results previously obtained. Cell samples were taken for this experiment correspond with the cells grown as seen in **Figure 3.12.**

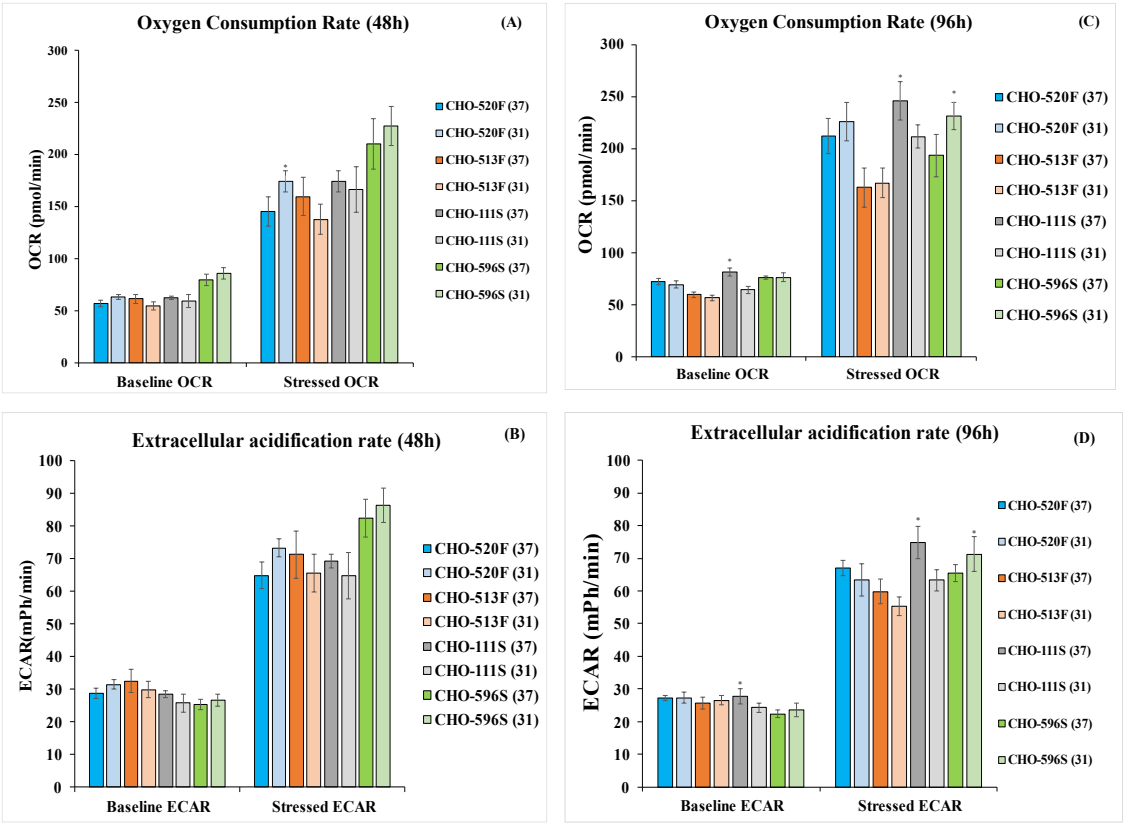

Figure 3. 14. (A) Oxygen consumption rate (OCR) from CHO cell clones after 48 hours of culture. Each bar represents the average OCR level of biological triplicates measured in 7 technical replicates using Seahorse XF-96 analyser ± SD. Significance was tested using one-way ANOVA with $\alpha<0.05$, represented by * in the figure.

(B) Extracellular Acidification Rate (ECAR) from CHO cell clones after 48 hours of culture. Each bar represents the average ECAR level of biological triplicates measured in 7 technical replicates using Seahorse XF-96 analyser ± SD. Significance was tested using one-way ANOVA with $\alpha<0.05$, represented by * in the figure.

(C) Oxygen consumption rate (OCR) from CHO cell clones after 96 hours of culture. Each bar represents the average OCR level of biological triplicates measured in 7 technical replicates using Seahorse XF-96 analyser ± SD. Significance was tested using one-way ANOVA with $\alpha<0.05$, represented by * in the figure.

(D) Extracellular Acidification Rate (ECAR) from CHO cell clones after 96 hours of culture. Each bar represents the average ECAR level of biological triplicates measured in 7 technical replicates using Seahorse XF-96 analyser ± SD. Significance was tested using one-way ANOVA with $\alpha<0.05$, represented by * in the figure.

This new analysis of the metabolism of the clones demonstrated similar results to the previous one after the first 48 hours of culture (**Figure 3.18**). Once again, no major differences between samples labelled as ``37 º´´ and samples marked as ``31´´ (cultured at 37 and 31ºC respectively) were observed at any of these clones at this point. Again, this was the expected outcome of the first assay, as both batches of cells were grown at 37ºC up to this point.

The differences between clones observed at this point in the assay previously described were hinted at but were not found to be statistically significant, during this analysis due to the high variability. Most CHO cell clones showed similar OCAR (160 pmol/min at the stressed state) and ECAR (70mPH/min at the stressed state) values in both basal and stressed states. However, clone CHO-596S showed again significantly higher values than the rest of the CHO cell clones at both basal and stressed states at this time. OCAR value for clone CHO-596S in the stressed state ranged around 200 pmol/min, 50 pmol/min higher than the rest of the CHO cell clones. ECAR value of clone CHO-596S, on the other hand, was only slightly higher than the rest of the CHO cell clones, being only 10 mph/min higher than the ECAR values of the other CHO cell clones.

However, after 96 hours of total incubation time, the results from the extracellular flux assay showed a different picture. The oxygen consumption was again similar for most of the clones with OCAR values around 240 pmol/min. However, this time the OCAR values of CHO-596S were observed to be similar to those of clone CHO-520F and CHO-111S, while the OCAR values of clone CHO-513 fall behind the rest, showing an OCAR score of around 150 pmol/min.

ECAR values also reflected this change. However, while clones CHO-520F, CHO-513F, and CHO-111S showed values of approximately 70 mph/min, clone CHO-596S showed slightly higher values, scoring more than 80 mph/min in cells incubated at 37ºC.

Despite having observed differences in cell growth on the cells shifted to 31ºC (**Figure 3.16.**), these differences were not reflected in the general metabolism of the shifted cells. Clones CHO-520F and CHO-513F were observed to have almost identical OCAR and ECAR scores regardless of which temperature they were grown. The only differences between cells grown at 37ºC and cells that grew at 31ºC were observed in clones CHO-111S and CHO-596s.

For clone CHO-111S, the cells grown at 37ºC were observed to have higher OCAR (240 pmol/min at 37ºC and 210 pmol/min at 31ºC) and ECAR scores than those grown at 31ºC.

CHO-596S, in the other hand, show the opposite results: the cells grown at 31ºC showed higher OCAR (240 pmol/min at 31ºC and 200 pmol/min at 37ºC) and ECAR (74 mph/min at 37ºC and 60 mph/min at 31ºC) than the cells grown at 37ºC. These differences were observed to be relatively small, compared with the differences observed in CHO-111S, but were found to be statistically significant.

The results demonstrated that differences in the metabolism of the cells after being shifted to a lower temperature were mainly observed in clones CHO-111S and CHO-596S, both classified as SGPCs.

Additionally, differences between the different clone's metabolism were observed to be more apparent when samples were taken at later time points. However, the viability of the cells cultured at 37ºC became greatly diminished after 114 hours of culture, making it impossible to compare the metabolism of cells cultured at different temperatures at this particular point in time.

Overall, it was observed that this panel of CHO cell clones has diminished growth and increased viability after being shifted to 31ºC while in culture. Nonetheless, these changes in phenotype were seemingly not reflected in the metabolism of clones CHO-520F and CHO-513F, which metabolism remained similar regardless of which temperature was used during the culture. Clone CHO-111S was one of the exceptions, showing a decrease in both oxidative and glycolytic metabolism levels after being shifted to 31ºC. Oppositely, Clone CHO-596S showed an increase in both oxidative and glycolytic metabolism after being shifted to 31ºC. Clone CHO-596S seems to benefit more from the temperature shift than all the other clones from the panel.

The results obtained were surprising, as previous studies reported the growth arrest induced by the temperature shift to increase the recombinant protein titer of the cells. Therefore, an increase in oxidative metabolism and a reduction of glycolytic metabolism was expected to be seen in the cells. From the panel of clones, only CHO-596S showed an increase in OCR after being shifted to 31ºC. Moreover, only CHO-111S showed a decrease in ECAR after being shifted. These results suggested that the temperature shift

can induce changes in the phenotype of the cells without having a strong impact on the metabolism of the cells.

Interestingly, both CHO-111S and CHO-596S metabolism were shown to change differently with the shift. This result again raises the question about the influence of the heteroplasmic variants of these clones in the metabolism, in this particular case, in the response to the shift. The CYTB *m.14136delA* variant had a much lower frequency in CHO-596S than in CHO-111S. This may have, for example, prevented CHO-596S from reaching a metabolic threshold which provided this clone with a better adaptative response to environmental changes. Potential implications of heteroplasmy will be discussed later.

Looking into more insight into the adaptative capabilities of the clones to change their metabolism when exposed to new environments, a new experiment was planned. A common, popular way to change the behaviour of the CHO cells when they are grown in a Bioreactor is to grow them in media with different formulations. The availability of nutrients and metabolites in the media is a major factor in the metabolic behaviour of the cells, which may change drastically.

Therefore, the set of 4 CHO cell clones was grown in two different media to observe differences in behaviour and/or metabolism that may be related to the heteroplasmy variants previously observed in them. These experiments are described in the next section of this chapter.

3.2.3. Influence of the growth media used in the metabolism and growth of CHO cell clones with different heteroplasmy variants.

3.2.3.1. The influence of the growth media on max viable cell density and viability is significantly more acute in SGPCs from the CHO clone panel.

As stated at the end of the previous section, a widely used way to influence the metabolic behaviour of the CHO cells when they are grown in a Bioreactor is to change the formulation of the media used.

The literature widely describes the effect of different growth media, different supplements, etc on the general cell behaviour. Commercial media are frequently designed to stimulate the immortalized cell lines' metabolism in a specific direction. For

example, the media used in the previous experiments, CHO-S-SFMII media, is a Serum-Free media designed specifically to stimulate the protein titer, but the viability of the CHO cells used in this study was observed to quickly decline when the cells are cultured in this media.

The heteroplasmic variants previously reported in the set of four CHO clones can potentially affect oxidative metabolism, as the genes affected encode mitochondrial subunits of two complexes of the electron transport chain. This means the heteroplasmy mutations have the potential to influence the general metabolism of these CHO clones and, consequently, the ability of these cells to adapt their metabolism to different growth media.

The media used in the experiments described in the previous sections was CHO-S-SFMII media. This media favours oxidative metabolism over glycolytic metabolism to improve the recombinant protein yield. Therefore, all the CHO cell clones previously exanimated in this media were potentially reaching the maximum oxidative metabolism state, masking potential differences related to their heteroplasmy variants.

CHO BalanCD media is a commercial media chemically formulated to increase the recombinant protein yield of CHO cells. This is achieved by increasing the viability of the cells in this media, therefore elongating time cells produce the recombinant protein before dying. CHO cells grown in BalanCD media normally show increases in viability and cell growth. This may imply that BalanCD media composition favours the glycolytic metabolism over the oxidative metabolism, which will lead to an increase in cell growth and viability.

Therefore, BalanCD media was theorized to potentially be a better testing media for differences in metabolism caused by heteroplasmy, as differences at the oxidative metabolism, theoretically diminished, will be easier to observe.

For this experiment, Clones CHO-520F, CHO-111S, CHO-513F, and CHO-596S were grown in both CHO-S-SFMII media and CHO BalanCD media for 96 hours total time. Cells were evaluated after 72 and 96 hours of incubation using the Seahorse XF Mito stress assay to evaluate the potential changes and differences in oxidative metabolism between the clones in the most accurate way possible.

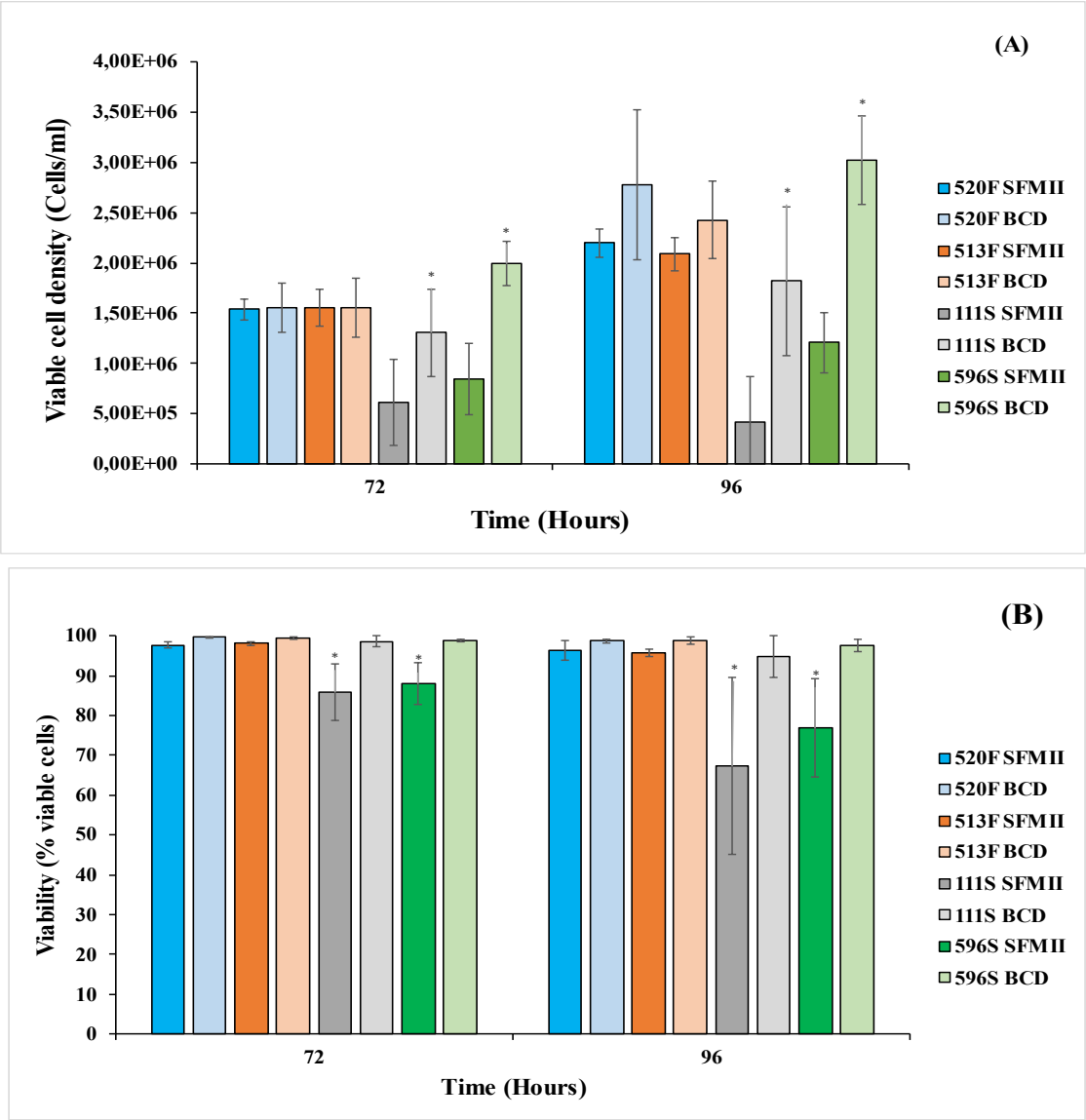

Figure 3. 15. (A) Viable cell density of CHO clones after 72 (left) and 96 (right) hours of culture. Cells were culture in suspension culture in a shaker incubator at 37ºC in 5mL of either CHO-SFMII media or CHO-BalanCD media respectively. Each bar represents the average viable cell density of biological triplicates measured in triplicates using Guava Easycite cytometer ± SD. Significance was tested using a one-way ANOVA with α <0,05, marked with * in the figure.

(B) Viability of CHO clones after 72 (left) and 96 (right) hours of culture. Cells were culture in suspension culture in a shaker incubator at 37ºC in 5mL of either CHO-SFMII media or CHO-BalanCD media respectively. Each bar represents the average viability of biological triplicates measured in triplicates using Guava Easycite cytometer ± SD. Significance was tested using a one-way ANOVA with α <0,05, marked with * in the figure.

The first insight into the growth of Clones CHO 520F and CHO 513F showed similar growth at both CHO-S-SFMII media and CHO-BalanCD media after 72 hours of incubation, with approximately 1,5 million cells per mL of media (**Figure 3.15 A**).

CHO 111S and CHO 596S showed, on the other hand, a decrease in cell density in CHO-S-SFMII when compared with CHO-BalanCD after 72 hours of incubation. However, it must be noted that the Viability of both clones CHO 111S and CHO 596S was slightly diminished when growth in CHO-S-SFMII media (**Figure 3.15 B**). dropping to 85% in the case of CHO-111 and 89% in the case of CHO 596S. Viability was equal for all clones (nearly 100%) when grown in BalanCD.

Additionally, clones CHO 520F and CHO 513F maintained good viability, nearly 100% in both CHO-S-SFMII media and CHO-BalanCD media. Therefore, the differences in the response to a new media demonstrated by FCPCs and SCPCs growth clones were likely to be a consequence of differences in viability.

After 96 hours of incubation, the data showed a different picture. Clone CHO-596S showed an increase in cell density when grown in BalanCD media. The growth of the clones CHO-520F and CHO-513F, on the other hand, showed no significant differences regardless of the media employed. It is worth noting that the differences in the growth of SCPCs CHO cell clones CHO-111S and CHO-596S may have been overestimated in **Figure 3.15**, due to the acute decrease in viability observed in these clones at the time of the experiment.

In summary, the clones CHO-111S and CHO-596S were observed to grow to higher cell densities in BalanCD media compared with CHO-S-SFMII media after 96 hours of incubation in this media. These differences in growth were observed in neither CHO-520F nor CHO-513F. Additionally, CHO-111S and CHO-596S showed lower viabilities than the rest of the clones when grown in CHO-S-SFMII media.

3.2.3.2.Influence of the growth media in the metabolism of the panel of CHO cell clones.

To determine the effects of the different media in the metabolism, aiming to observe differences between clones potentially caused by heteroplasmy, an extracellular flux analysis experiment was conducted.

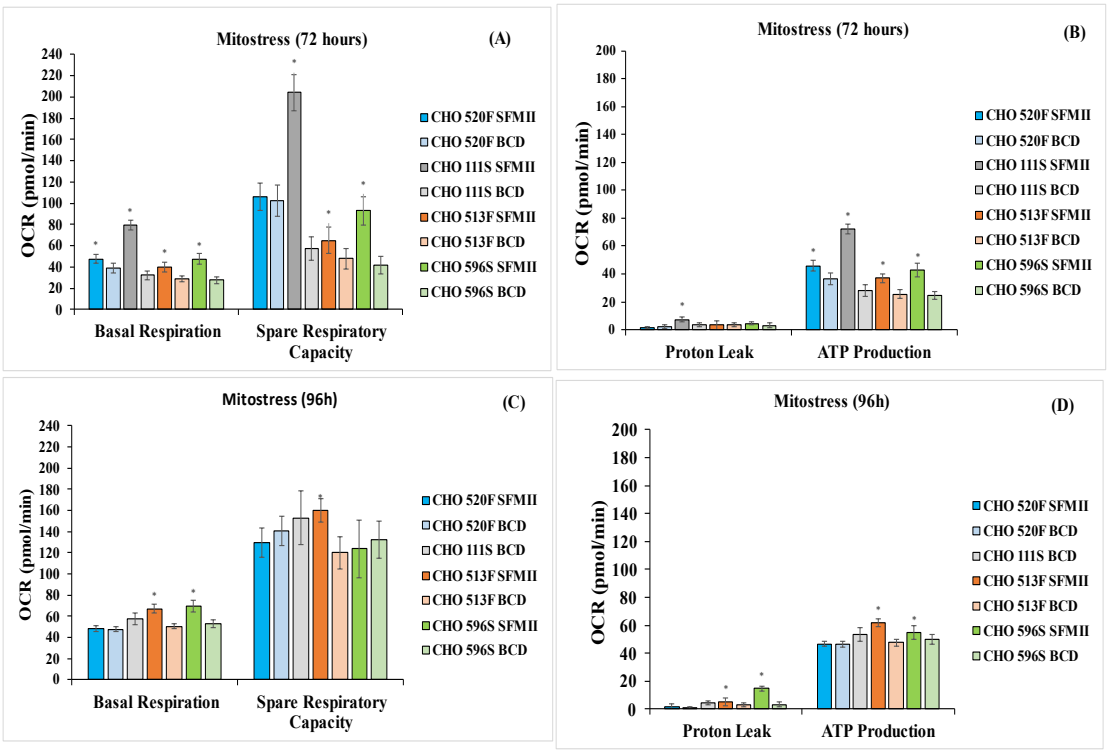

Figure 3. 16. (A) Oxygen consumption rate (OCR) from CHO cell clones after 72 hours of culture. Each bar represents the average OCR levels during basal and spare respiration of biological triplicates measured in 7 technical replicates using Seahorse XF-96 analyser mitochondrial stress assay kit ± SD. Significance was tested using one-way ANOVA with $\alpha<0.05$, represented by * in the figure.

(B) Oxygen consumption rate (OCR) from CHO cell clones after 72 hours of culture. Each bar represents the average OCR levels during proton leak and average ATP production of biological triplicates measured in 7 technical replicates using Seahorse XF-96 analyser mitochondrial stress assay kit ± SD. Significance was tested using one-way ANOVA with $\alpha<0.05$, represented by * in the figure.

(C) Oxygen consumption rate (OCR) from CHO cell clones after 96 hours of culture. Each bar represents the average OCR levels during basal and spare respiration of biological triplicates measured in 7 technical replicates using Seahorse XF-96 analyser mitochondrial stress assay kit ± SD. Significance was tested using one-way ANOVA with $\alpha<0.05$, represented by * in the figure.

(D) Oxygen consumption rate (OCR) from CHO cell clones after 96 hours of culture. Each bar represents the average OCR levels during proton leak and average ATP production of biological triplicates measured in 7 technical replicates using Seahorse XF-96 analyser mitochondrial stress assay kit ± SD. Significance was tested using one-way ANOVA with $\alpha<0.05$, represented by * in the figure.

The XF analysis was conducted using a Seahorse XF-96 together with a Seahorse Mitostress kit, to have an accurate picture of the oxidative metabolism of the studied clones. The assay was performed twice: first, after 72 hours of incubation, and once again after 96 hours of incubation, matching the growth curve results previously seen in **Figure 3.15.**

On the Mitostress analysis, both clones CHO-111S and CHO-596S showed an increase in oxygen consumption ratio after 72 hours of being grown in CHO- S-SFMII media compared with their oxygen consumption in CHO-BalanCD (**Figure 3.16**).

This increase was observed for both basal and spare respiration and was also reflected in ATP production. This difference is especially acute in CHO-111S, showing an OCR of 200 pmol/min at spare respiration when grown in CHO-S-SFMII but an OCR of only 50 pmol/min at spare respiration when grown in CHO-BalanCD, equally to a 4-fold increase of the OCAR score at spare respiration when grown in SFMII.

Clone CHO-596S also showed an increase in the OCAR score when grown of CHO-S-SFMII when compared to BalanCD, the increase was not as dramatic as the one observed in CHO-111S, being an increase of roughly 1-fold at spare respiration state.

The clone CHO-513 showed a significant increase in oxidative metabolism when grown in CHO-S-SFMII, compared to CHO-BalanCD in all levels bar the proton leak respiration. This increase in oxidative activity was also translated into higher ATP production levels. Similar to CHO-596S, these differences were far more discrete than the differences observed in clone CHO-111S.

Finally, clone CHO-520F was observed to have an increase in oxygen consumption when grown in CHO-S-SFMII media compared to CHO-BalanCD. However, these differences were observed only in the basal state, and not during the uncoupled state. Regardless, ATP production was also observed to be higher in CHO-S-SFMII media for this particular clone.

After 96 hours of incubation, the previously described characteristics of the cell metabolism were observed to change slightly. Clones CHO-520F and CHO-596S general metabolism did not demonstrate any differences regardless of the media used in the incubation.

The differences in the general metabolism of clone CHO-513F already observed after 72 hours of culture, became more apparent on the assay performed after 96 hours of culture. At basal, spare respiration, and ATP production levels, CHO-513F OCR levels were observed to increase slightly when grown at CHO-S-SFMII compared with CHO-BalanCD. This difference was observed to amount about 50pmol/min at Spare respiration level (160 pmol/min in CHO-S-SFMII versus 110 pmol/min in CHO-BalanCD), but only a modest increase in OCR at both Basal level and ATP production of the cells.

Finally, differences in the CHO cell clone CHO-111S metabolism in different media could not be completely assessed due to the cells` growth in CHO-S-SFMII media rapid decline in viability, which ultimately resulted in not enough cells being available for the experiment. However, it is worth noting that at 96 hours of incubation, CHO-111S grown in BalanCD showed a similar metabolism at all levels to the rest of the CHO cell clones regardless of the growth media. The only exception was CHO cell clone CHO-513F, which showed higher oxidative metabolism than the rest of the CHO cell clones when grown in CHO-S-SFMII.

The data seemingly showed how as the growth of the cell diverges, after 96 hours of incubation, the oxidative metabolism becomes more similar in all the clones regardless of the media used, with the sole exception of CHO-513F, which oxidative metabolism appeared as higher when growth in CHO-S-SFMII.

Generally, differences in oxidative metabolism and /or growth are directly tied with differences in glycolytic metabolism. Glycolytic metabolism data were obtained during the experiment as ``Extracellular Acidification ratio´´ (ECAR).

After 72 hours of culture, ECAR data showed clones CHO-520F, CHO-513F, and CHO-596S to experience a significant increase in ECAR when grown in CHO-S-SFMII media. (**Figure 3.17**). in CHO-520F, this increase was only made evident after 75 minutes into the assay. Other clones, like clone CHO-111S, this increase in ECAR score was dramatically faster and higher, showed a 2-fold increase in ECAR when grown in CHO-S-SFMII media when compared to BalanCD media after only 15 minutes in the assay.

After 96 hours of incubation, ECAR data showed clones CHO-520F and CHO-513F were observed to have overall similar ECAR levels regardless of which growth media was used to grow them.

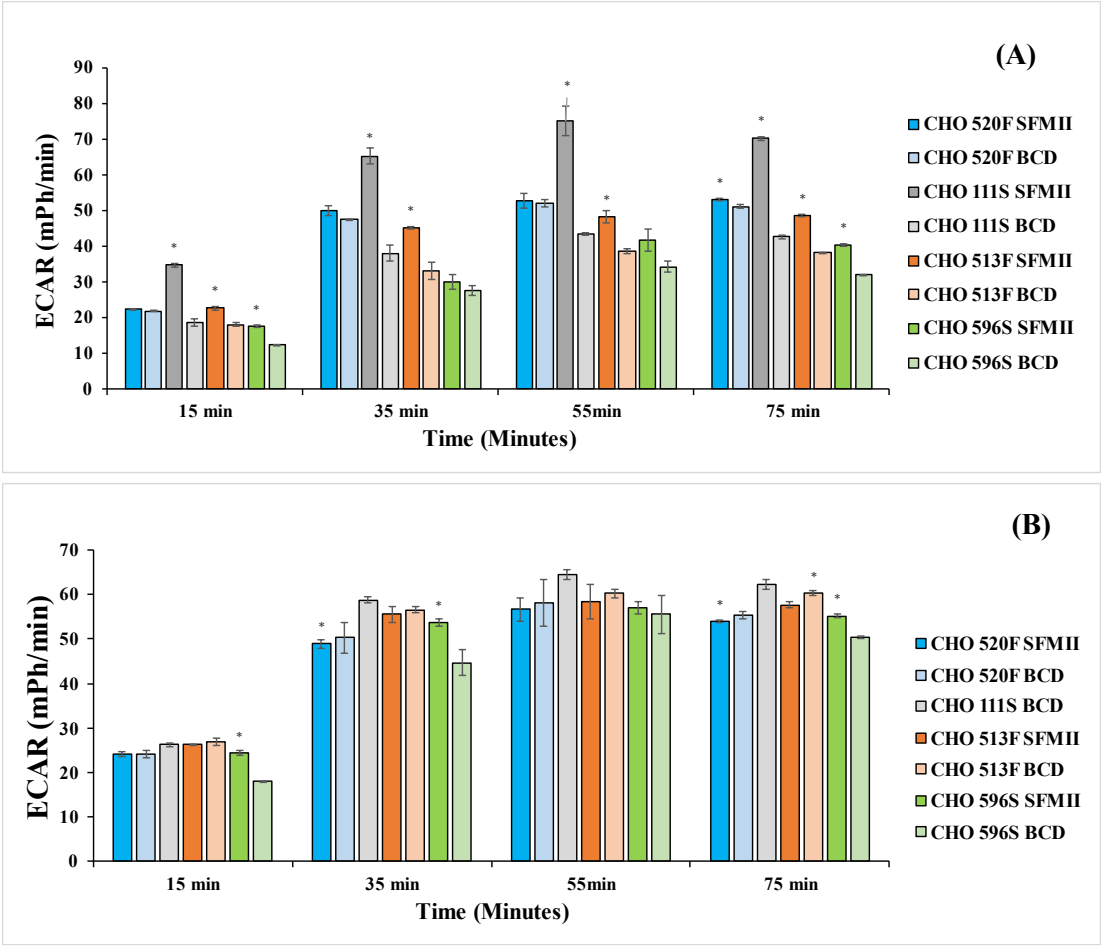

Figure 3. 17. (A) Extracellular Acidification Rate (ECAR) from CHO cell clones after 72 hours of culture over the course of the analysis. Each bar represents the average ECAR level of biological triplicates measured in 7 technical replicates using Seahorse XF-96 analyser glycolytic stress assay ± SD. Significance was tested using one-way ANOVA with $\alpha<0.05$, represented by * in the figure.

(B) Extracellular Acidification Rate (ECAR) from CHO cell clones after 96 hours of culture over the course of the analysis. Each bar represents the average ECAR level of biological triplicates measured in 7 technical replicates using Seahorse XF-96 analyser glycolytic stress assay ± SD. Significance was tested using one-way ANOVA with $\alpha<0.05$, represented by * in the figure.

The ECAR score for clone CHO-520F grown in CHO-S-SFMII media was shown to diminish after the addition of Oligomycin to the media (which is needed to measure the proton leak and uncouple ATP synthase), corresponding with the period of the 35 minutes mark. Additionally, clone CHO-513F was shown to have a slightly higher level of ECAR when grown in BalanCD media after 75 minutes into the assay. This is the only observed instance of a clone having higher ECAR when grown in CHO-BalanCD media.

Differences in the clone CHO-111S glycolytic metabolism in different media could not be assessed due to the cells grown in CHO-S-SFMII media's rapid decline in viability, which ultimately resulted in not enough cells being available for the experiment. However, Clone CHO-111S ECAR scores were observed to be like the ECAR scores of the rest of the clones, regardless of the media used to grow them.

Finally, the Clone CHO-596S ECAR score was observed to be significantly decreased when grown in BalanCD after both 72 and 96 hours of culture.

3.2.3.3.Summary of media adaptability experiment results.

As can be seen, most of the CHO cell clones showed a dramatic increase in growth after 96 hours of being grown in BalanCD, with the only exception being the clone CHO-513F, which growth remains equal in all cases. Additionally, this difference in growth in favour of BalanCD was observed at an earlier time point (72 hours) in the SGPCs CHO-111S and CHO-596S. CHO-BalanCD media was observed to greatly benefit the growth of clone CHO-520F, CHO-111S, and CHO-596S after 96 hours of culture. Meanwhile, clone CHO-513F remained largely unaffected by the growth media, growing to similar numbers in both media used.

Oppositely, CHO-S-SFMII media seems to induce an increase in both OCR and ECAR ratio of most clones after 72 hours of incubation. OCAR scores were observed to be generally higher for all the clones after 72 hours of culture. The oxidative metabolism of most clones, represented by OCR, was observed to be increased for all clones after 72 hours of incubation in CHO-S-SFMII. However, after 96 hours of incubation in CHO-S-SFMII, this increase will only be observed at clone 513F and CHO-596S. This shows behavioural differences that cannot be attained to the growth phenotype of the clones.

Finally, glycolytic metabolism, represented by ECAR, was observed to be increased in clones CHO-111S and CHO-513F after 72 hours of incubation in CHO-S-SFMII media

and clone CHO-596S after 96 hours of incubation in CHO-S-SFMII media. Interestingly, in the first case, this case higher ECAR was not corresponded with an increase in growth, with clone CHO-111S growing less in CHO-S-SFMII than in its BalanCD counterpart. On the other hand, the decrease in ECAR observed in clone CHO-596S after 96 hours of incubation in BalanCD did not seem to correlate with a dramatic increase in growth.

The results obtained in this experiment do not show a strong correlation of heteroplasmy variants with the observed response to different growth media. As the growth and metabolism of the cells seemingly tended to normalize, it was hypothesized that the heteroplasmy may tend to disappear from the CHO cell clones with time. For this reason, an experiment in heteroplasmy variance with time in CHO cell clone 520F was performed, as described in the next chapter.

3.3 Discussion

The work performed in the first sections of this chapter aimed to establish whether the different heteroplasmy variants previously observed in the different CHO clones could impact the metabolism of the cell and, consequently, the phenotype of these CHO cells.

Initially, when the first three CHO clones from the group of clones containing the heteroplasmy variants of interest (CHO-520F, CHO-111S, and CHO-513F) were evaluated, their growth rate, maximum viable cell density, and viability were found to be similar, despite the previous classification of such clones into ``Fast clones´´ or FGPCs and ``Slow clones´´ or SGPCs. Given the previous classification of the clones was based on ranges of growth ratio (**Table 3.1**) and the use of a growth media different from the media originally used, due to the unavailability of the former, it was deemed possible that the different clones may have adapted to the new growth media, CHO-S-SFMII, in a similar way as CHO cells are known for their adaptability and response to environmental changes (*Fischer, Handrick and Otte, 2015*). Equally, the mitochondrial content, evaluated by fluorescent dye, was similar in all clones. Interestingly, the variation of the levels mitochondrial content over the days drew a curve which was the reserve of the growth curve of the cells, with mitochondrial content levels going down during the first stages of growth and then experiencing a sharp, drastic increase after 120 hours of culture. This change in the mitochondrial levels suggested that the CHO clones being evaluated possessed a Warburg-like metabolism, commonly found in immortalized cell lines such

as CHO (*Young, 2013*) and the metabolic shift occurring at some point after 96 hours of cell culture.

The re-evaluation of the cells, after thawing a new stock of cells and which included additional SGPC clones 792S and 596S, showed the clones having growth phenotypes much closer to the original classification. Interestingly, clone 792S max viable cell density was similar to that of FGPCs, while its growth rate was closer to the other SPGCs. Once again, this is a consequence of a pre-existing classification based on growth rate ranges. Clone 596S was overall the worst-performing clone, with low viable cell densities and a quicker decline in viability than the rest of the clones. Despite this, clone 596S was the SGPC with the highest growth rate.

The mitochondria content of the clones was again evaluated, this time at 96 and 120 hours of culture, which correspond with points in time believed to be, according to the previous results, before and after the metabolic shift towards the oxidative metabolism correspondingly. A general increase in mitochondrial content occurred, which further supports the hypothesis of the metabolic shift occurring between 96 and 120 hours of culture in this panel of clones. At 96 hours of culture, the mitochondrial content of SGPCs was significantly lower than the content FGPCs, which was hypothesized to have different potential explanations: The first hypothesis pointed to the possibility of the FGPCs higher mitochondrial content, and therefore OXPHOS activity, promoting growth as these cells would have more energy available than its SGPC counterparts and the dye used, Mitotracker Green, is only able to enter active mitochondria. While this first hypothesis contradicts the widely reported inverse relationship between OXPHOS and growth (with the reduction in OXPHOS favoring the glycolytic pathway), normally found in cells with Warburg-like metabolism, previous studies using metabolite analysis pointed to a potential relationship between higher oxidative activity and faster growth, making this hypothesis feasible (*Edros, McDonnell and Al-Rubeai, 2013)*.

A second hypothesis will be related to the heteroplasmy levels previously reported in these clones, while FGPCs showed lower levels of the *m.14136delA* frameshift variant in the CYTB gene than SGPCs, making it unlikely that this mutation surpasses the necessary metabolic threshold to exert an effect in the mitochondria, both FGPCs possessed an *m.14378G>A* stop codon variant with high frequencies, which has the potential to produce non-functional copies of the Cytochrome b subunit encoded by this gene. In the

presence of non-functional mtDNA copies, mitochondria have been previously reported to increase their numbers and, with it, the total number of mtDNA copies within the cell, in an attempt to increase the total number of wild-type, functional mtDNA copies to compensate the presence of the mutant copies. (*Chinnery and Samuels, 1999; van den Ameele et al., 2020*). Therefore, the presence of these heteroplasmy variants within both FGPCs could be causing an increase in the cells' mitochondrial content.

The mitochondrial outcome observed after 120 hours, and after the metabolic shift, showed the mitochondrial content increasing in all the clones. This was expected, as the cells will increase their mitochondria numbers as they shift towards oxidative metabolism. The mitochondrial content of clones 520F, 111S, and 596S became similar at this stage, which came as curious due to their different growth behaviour. Clone 513F stood out as the clone with the highest mitochondria content, which supported the hypothesis of the higher mitochondria content of the clone supporting a better culture performance. Oppositely, clone 792S showed the lowest mitochondrial content among the clones. This lower level of mito-content did not seem to impact the performance of clone 792S, which showed similar culture performance to both 520F and 111S, which correlates well with pre-existing literature, in which no correlation between mito-content and culture performance was found, performance being driven by mitochondrial efficiency instead (*O'Callaghan et al., 2015*). However, the levels of mtDNA in cells are known to impact the metabolism and oxidative stress of the cells (*Jeng et al., 2008*), so it is possible that the variants contained in clone 513F have accelerated the mitochondria fusion/fusion process, creating more mitochondria and more mtDNA copies (*Reznik et al., 2016)*. This data was interesting, as it hints at a potential relationship between the *m.6996G>A* variant in the COX2 gene and the higher performance of clone 513F, as it is the clone with the highest frequency of this variant. Additionally, this data suggested the *m.14136delA* frameshift variant did not have an impact on the general performance of the clones, as the clones with the highest frequency (50%) of this variant, 792S, performed better than clone 596S, which has a frequency of approximately 20% for this variant, while the fast clones had much lower frequencies (7 and 15% respectively) and performed better in culture. Curiously, clone 792S have lower mitochondrial content than the rest of the clones after 120 hours of culture, while the expected content for a clone containing a high-frequency, potentially critical mutation will be to have a higher number of mitochondria, similarly to clone 513F, compensating the mutation by increasing mtDNA

levels and, with it, mitochondria content *(Jeng et al., 2008; Kandul et al., 2016; Reznik et al.,* 2016). Despite this, this data was insufficient by itself to establish a clear relationship between the heteroplasmy and the phenotypes, so more assays were performed to evaluate the potential influence of heteroplasmy at the transcriptomic, proteomic and metabolic level as previously described.

The expression analysis revealed differences between the transcript levels of COX2 and CYTB among the 5 selected clones from the CHO panel. Levels of COX2 transcription were higher in clone 513F compared with both 520F and 111S. Higher transcript levels of COX2 could be related to the higher growth rate, viable cell density, and mitochondrial content previously observed in clone 513F, as high levels of heteroplasmy are known to induce mitochondrial fusion/fission mechanisms, aiming to clear the mtDNA of mutation (*Tam et al., 2015; Kandul et al., 2016)*, and COX2 has been previously reported to be a regulator of apoptosis (*Xiang et al., 2019)*. It must be noted that clone 513F contained an initiator codon variant in the mitochondrial COX2 gene at a frequency of 26%, higher than the other FGPC, clone 520F. Additionally, transcript levels of the mitochondrial COX1 gene were also higher in 513F compared with the other CHO clones. Therefore, these results suggest a certain frequency of the *m.6996G>A* variant may potentially be beneficial for the culture performance of CHO cells. The levels of expression of mitochondrial genes CYTB and NaD5 showed by the clones also point in this direction, as 513F had the highest transcript levels of both COX genes among the clones, but showed similar transcript levels of both CYTB and NaD5 genes to those of other clones. The highest transcript levels of CYTB were observed in clone 596S, which showed the worst culture performance, as previously commented , higher transcripts of CYTB have been related in literature with higher levels growth, oxidative phosphorylation and glycolytic metabolism. (*Dasgupta et al., 2008; Śmiech et al., 2019*). However, overexpression of mitochondrial CYTB has also been related to the generation of excessively high levels of ROS, which may explain the poor performance of clone 596S. Despite this, a clear relationship between the higher levels of CYTB and heteroplasmy was considered not established, as the frequency of the *m.14136delA* frameshift variant in clone 596S was lower than in clone 792S, which had higher frequencies. Therefore, a linear relationship between heteroplasmy and transcript levels was not observed in these CHO clones.

The protein expression levels of both COX2 and CYTB could not be evaluated due to the unavailability of effective, commercial antibodies targeting the CHO version of both mitochondrial genes. The design of a new, specific antibody targeting these genes, should enough resources be available, could be interesting in future work regarding CHO heteroplasmy.

The metabolic data was obtained from the Seahorse XF-96 metabolic flux analyzer, as previously described. Due to time, assay, and space constraints regarding this assay and problems with the stock cells, clone 792S could not be evaluated in the subsequent assays. The OCR and ECAR obtained with the XF-96 analyzer for each clone included showed a different picture to that of respirometry. Most clones showed similar OCAR ratios after 96 hours of culture, while differences in the ECAR ratio were observed in several metabolic assays, which included the glycolytic rate assay, designed to accurately measure the glycolytic ratio. Clones 111S, 520F, and 513F had different proton efflux levels, which may indicate that FGPCs had already shifted oxidative metabolism at this stage, while the SPGCs had not or were in the process of shifting. Alternatively, this may mean that clone 513F high growth ratio and viable cell density were related to the oxidative metabolism rather than the glycolytic metabolism, as previously discussed. However, this hypothesis seems unlikely, as the OCR ratios shown by the clones 520F, 513F, and 111S were similar despite their differences in mitochondria content, which hints at an absence of a relationship between higher mitochondrial content and the oxidative metabolism, which has been previously discussed in the literature (*O'Callaghan et al., 2015*). Clone 596S was again the worst-performing clone in both OCAR and ECAR ratios. Overall, the results of the metabolic assay did not establish a relationship between the heteroplasmic variants detected in the clones and the metabolic phenotypes observed. Despite the *m.6996G>A* initiator variant being apparently able to increase COX2 transcription levels and mitochondrial content, this overexpression did not translate into significant metabolic differences, which may mean that either the overexpression of COX2 is not, by itself, able to increase the efficiency of the electron transport chain, due to the existence of other limiting steps, such as the levels of expression of other COX subunits (Schägger, 2001; Kovářová *et al.*, 2012; Geldon, Fernández-Vizarra and Tokatlidis, 2021), or, alternatively, that the mRNA generated from the initiator codon variant generates non-functional protein due to the slightly displaced position of the initiator codon, which is unable to participate in the assembly of

the COX complex (*Bourens et al., 2014; Bourens and Barrientos, 2017*). Due to the absence of further proteomic data for COX2, currently, this cannot be refuted. Similarly, no clear relationship between the variants observed in CYTB mitochondrial gene and metabolic phenotype was observed, as clones with significantly different frequencies showed similar metabolic phenotypes and vice versa. Overall, the metabolism of the clones could not be related to the heteroplasmy alone, so alternative approaches were attempted.

CHO cells have been previously reported to undergo growth arrest after a temperature shift from 37ºC to 31ºC, improving the longevity of the cells in culture and the r-protein production (*Barron et al., 2011; Kelly et al., 2017; Torres et al., 2021*). The four clones previously analyzed were used to conduct a temperature shift experiment, aiming to determine if the heteroplasmy variants these clones contain could influence their response to the temperature shift. Surprisingly, growth arrest was observed in the clones only after 48 hours of post-shift culture while most CHO literature reports the shift occurring after only 24 hours. As expected, long-term viability was significantly increased in all the clones from the panel while maximum viable cell density was decreased in cells shifted to 31ºC. Curiously, clones 520F and 592S were the clones which most benefit from the shift long term, as both viable cell density and viability were much higher for both clones when cultured 114h at 31ºC, despite belonging to different growth groups and not sharing similarities in any other assay. The XF-analysis of the clones showed significant differences between cells grown at 37ºC and 31ºC respectively in the metabolism of clones 596S and 111S, both SGPCs, after 96 hours of culture. Clone 111S showed a decrease in both OCR and ECAR levels when grown at 31ºC. Oppositely, clone CHO 596S showed an increase in both OCR and ECAR in the same conditions. Clones 520F and 513F showed no changes in metabolism despite the shift. The differences between 111S and 596S could potentially be related to the CYTB *m.14136delA* frameshift variant which both possess in different degrees of frequency. Clone 111S possessed a higher frequency for this variant than 596S, which may imply, as previously seen, that CHO-596S has been unable to reach a significant metabolic threshold that 111S reached, which can explain the previously observed poor performance of 596S in SFMII. The temperature shift to 31ºC seems to improve the metabolic performance of clone 596S while slightly hindering the performance of clone 111S, which may be due to the growth constraints diverting more energy towards the oxidative metabolism (*Yoon, Song and Lee,*

2003; Torres et al., 2021), improving the previously seen clone 596S low levels but hindering clone 111S, which already had high OCR levels, due to an excess of oxidative stress caused by high expression of mitochondrial CYTB, leading to excessive generation of ROS in clone 111S (*Dasgupta et al., 2008)*. This suggests a relationship between the response of CHO cells to the temperature shift and high frequencies of the *m.14136delA* frameshift variant, as both FGPCs, which showed lower frequencies of this variant, showed no differences in the metabolism. It is also possible that the other variants found on the FGPCs can somehow compensate for the effects of the temperature shift.

To further investigate the potential influence of the heteroplasmy in the adaptative response of CHO cells, the cells were culture in two different growth media: the standard CHO-S-SFMII, in which the stocks were normally grown, and BalanCD CHO growth A medium. The SGPCs were observed to benefit especially from BalanCD media, experiencing a significant increase in both viable cell density and viability compared to the cells grown in SFMII media. An apparent increase in viable cell density was also observed in FGPCs after 96 hours of culture in BalanCD, although these differences were not statistically significant. Metabolic analysis showed both OCR and ECAR levels to be diminished in cells grown in BalanCD, compared to SFMII media, after 72 hours of culture. These differences were notably higher in clone 111S for both OCR and ECAR. Surprisingly, despite the increase in growth observed for SGPCs in BalanCD media, the ECAR levels were observed to be higher in CHO-S-SFMII for both clones, which seemed to contradict the well-known relationship between glycolytic metabolism and growth normally observed in Warburg-like cells. Notably, a decrease in OCR levels after 96 hours of culture in BalanCD was noted in clones 513F and 596S but not in clone 520F, which showed differences between clones belonging to the same group. Finally, differences between the metabolism of clone 111S after 96 hours of culture in each media could not be evaluated due to the cells cultured in SFMII media dying abruptly at this point of the experiment, leaving only the cells cultured in BalanCD media to be evaluated. Overall, these results suggest, in conjunction with the data acquired from the temperature shift experiment, the existence of differences between the adaptative response of FGPCs and SGPCs, which may be related to the *m.14136delA* frameshift variant, explaining the differences between clones, or with the variants in mitochondrial COX2 gene (like the *m.6996G>A* variant), which are exclusive to FGPCs. However, differences among clones from the same group, as well as inter-group similarities, have also been noted during these

experiments. Additionally, r-protein titre and specific productivity data were missing for the adaptability experiments due to technical and time constrains, as the XF-analyser instrument was only available for a limited time and all the efforts were concentrated in the metabolic profile of the cells. For this reason, different explanations for the observed differences between clones could not be ruled out. Therefore, a strong correlation between heteroplasmy and adaptative response in CHO cells was not found in this study, although the results provided some evidence that pointed at the possibility of such a relationship existing.

CHAPTER 4

Evolution of heteroplasmy in clonal CHO cell populations

4.1 Introduction:

As summarized at the end of the previous chapter, a panel of CHO cell clones with different heteroplasmic mutations were observed to differ to various extents in their behavior in terms of their phenotype in culture, mitochondrial content, and metabolic profiling.

These clonal cell lines were all derived from the same mixed, stable population of producer cells after an industrial cell line development project (transfection). It was therefore of interest to understand whether the difference in heteroplasmy was simply reflecting the cloning process, i.e., separating individual cells with different heteroplasmic profiles, or whether heteroplasmy changes over time in a cloned population. Literature reports have described major changes in mitochondrial DNA heteroplasmy in the germline, caused by an unequal distribution of mutated and wildtype mitochondria after mitosis and meiosis processes. Consequently, the mitochondrial genome has been previously observed to tend to homogenize, either towards wild-type homoplasmy, losing all mutations, or to a metabolic shift in which the copies with the heteroplasmic variants become the majority copies in the mitochondria present in the cells.

This phenomenon is commonly known as ``the mitochondrial bottleneck´´ in the germline and can cause a sudden change of almost homoplasic mitochondria to heteroplasmic mutants due to the unequal distribution of the genome. These phenomena are the cause of a variety of human congenital mitochondria-related diseases manifesting suddenly in the offspring of healthy women (*Wallace, 2013*). The heteroplasmic drift caused by the bottleneck was originally believed to be limited to the germline, recent studies have shown evidence hinting that the bottleneck is present during different stages of the development, which is perhaps related to different levels of heteroplasmy appearing in different tissues from the same organism (*Wonnapinij, Chinnery and Samuels, 2008; Zhang, Burr and Chinnery, 2018*). While the unequal segregation of the heteroplasmy has not been studied in depth in continuous cell lines such as CHO, the processes of single-cell clone, which distribute cells from a population contained mixed degrees of heteroplasmy, could theoretically represent a ``bottleneck´´ similar to meiosis in cell lines, causing dramatic changes in the heteroplasmy degree. This could lead to new

phenotypes related to heteroplasmy surfacing from the cloning process, as heteroplasmy in the cells is known to drift towards homoplasy (*Uusimaa et al., 2007*), regardless of this homoplasy being a new type of homoplasy, composed by the new mutant mtDNA copies or a return to the old, wild-type homoplasy.

The cloning step is a critical part of the cell line development process. Most regulatory agencies, including the European Medicines Agency (EMA) and the American Food and Drug Administration (FDA), include in their regulations regarding cell-based medicinal products the need for definitive proof that any producer cell line has been derived from a single cell and that their stability is fully determined. There is considerable debate in the community regarding the relationship between consistent product quality and the clonality of the producer cell considering the number of studies reporting on how CHO cells accumulate SNPs in their nuclear genome, the plasticity of the epigenome, and other molecular genetic profiles that vary over relatively short periods. (*Wurm and Wurm, 2021)*. Comparatively, it normally takes around 1 year to develop a new cell line from single-cell clone to master, and it could take even more time to escalate it to a 1000L bioreactor and to complete all the stability studies and get approval in your cell line. For this reason, the industry needs to consider sources of potential change in CHO cell lines not only to use them to improve the cell phenotype but also to ensure that the phenotype of the cells remains stable over time.

Efforts to identify heteroplasmy in different cell lines have been performed over the last years. Kelly and collaborators (*Kelly et al., 2017*) sequenced a panel of 24 CHO clones to identify the heteroplasmy variants contained within the clones. This study highlighted the variability of the mt-genome in closely related CHO clones, which could impact the metabolism of the cell, and therefore the productivity and stability of such clones. This study suggested that the comprehension of mt-genome dynamics can be of potential use to engineering more productive metabolic phenotypes.

To date, no reports have been published reporting on whether heteroplasmy in different clones derived from a parental cell population could potentially influence the phenotypic stability of those clones. Understanding this better might therefore influence either clone selection strategies in industrial cell line development projects. To this end, an experiment was planned to attempt to measure the variability of the heteroplasmy within the set of

CHO cell clones newly derived from one of the cell lines used in the previous experiments, which was previously sequenced by Kelly and collaborators.

4.2. Evaluation of evolution of heteroplasmy in CHO clones derived from CHO-520F

4.2.1. Generation of new clones by limited dilution cloning results in changes in heteroplasmy over 20 passages.

A panel of 24 new CHO cell clones was created from CHO-520F by limited dilution cloning, as described in Section 2.1.9. CHO-520F was chosen as parental among the previously evaluated clones mainly due to two factors:

1. CHO-520F possess both the *m.6996G>A* COX2 and *m.14136delA* CYTB variants, making possible to evaluate the evolution over time of both these high-frequency variants of interest.
2. CHO-520F in-culture performance was generally good and consistent.

The panel of clones generated was then cultured for 20 passages (10 weeks in total), taking a sample for mitochondrial DNA analysis from every clone once per week.

Samples of mitochondrial DNA were then PCR amplified by using a High-Fidelity Polymerase. Due to the size of mitochondrial DNA, two different PCR reactions were performed per mitochondrial DNA sample, each of which contained approximately half of the total mitochondrial DNA sequence. The PCR products were checked, purified, and subsequently sequenced.

Additionally, the growth and recombinant protein titer of two of the clones were measured and compared with the parental line, CHO-520F, aiming to observe any differences in the phenotype of the new clones and parental line that could be related to heteroplasmy.

4.2.1.1.Amplification and purification of mtDNA.

As briefly mentioned in the introduction of this section, the mitochondrial DNA of the clones was first amplified by PCR using a high-fidelity polymerase. However, due to the relatively large size of the whole mtDNA sequence, 16,5 Kb, to ensure the maximum

fidelity, two reactions with overlapping products, corresponding with roughly half of the mtDNA sequence, were made per clone to amplify the totality of the mtDNA.

Samples of mtDNA were extracted using the method described in Quispe-Tintaya et al., 2013, described in more detail in section 2.2.10. Samples selected corresponded with Passage number 4 (2 weeks of cell culture since single-cell cloning) and Passage number 20 (10 weeks of cell culture single-cell cloning). Samples from Passage number 4 and Passage number 20 will be referred to in this section as P4 and P20 correspondingly. These two points were used to observe the changes that may occur to heteroplasmy over a time frame shorter than a typical cell line development campaign. Samples from Passage 4 were used instead of Passage 3 to give more time to the cells to adapt to growth in 24-well plates and to allow potential early heteroplasmy changes, if any, to be observable. The mtDNA obtained from these plates was then PCR amplified.

Figure 4.1. shows the primers used in the process and the logic behind this amplification process. These primers were the same ones used in *Kelly et al 2015*. Each reaction was intended to amplify approximately half of the mtDNA sequence as previously mentioned. Primers were designed to make the amplified sequences overlap, ensuring that no fragment of mtDNA was missing. The reaction with the bigger product (8814 bp) was named Reaction 1 or R1. The reaction with the smaller product (7702 bp) was therefore named Reaction 2 or R2.

After amplification, a small aliquot of the product was run in a 1% agarose gel to ensure the amplification has been successful and that the fragment size was correct. An example of such amplification can be seen in **Figure 4.2.** Overall, the process was successful for all the samples, although the bands obtained in Reaction 2 were generally lower yield than those obtained by Reaction 1. As both samples were processed with the same reagents and following the same procedure, this difference is likely to be due to primers from Reaction 2 being less efficient than those from Reaction 1.

With the amplification of all samples being successful, DNA samples were purified using AMPure magnetic beads to get rid of the other components of the PCR reaction, nucleotides, and the primers. After the purification process, these samples were also run in an agarose gel to ensure the purification was successful. **Figure 4.3** shows an example of a gel run with previously purified samples.

After ensuring the success of the purification process, the samples corresponding to the full mitochondrial sequence of 8 clones and the parental CHO clone were selected for sequencing. This number was selected to ensure a high depth of sequencing while using a broad enough panel of clones to capture sequence diversity. Additionally, time and resource limitations were taken into account.

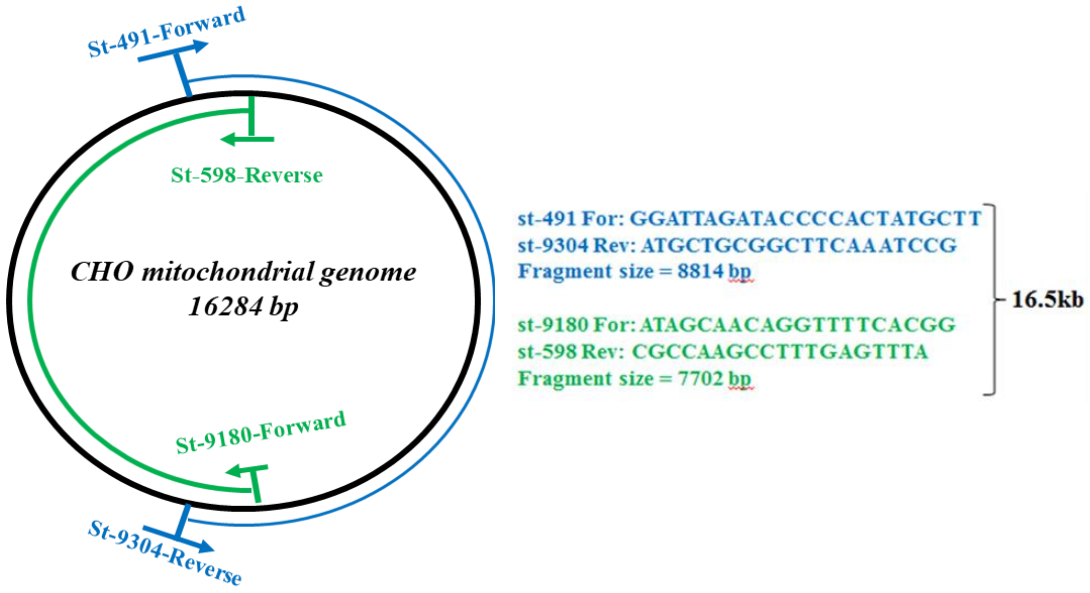

Figure 4. 1. The mitochondrial DNA amplification and the primers used. Primer sequence was obtained from *Kelly et al 2014*. Primers were designed to amplify overlapping sections of the mtDNA, ensuring that the total sequence is present in the final sample. Subsequently, the reaction with the biggest product (blue) was named Reaction 1 and the reaction with the smaller product (green) was named Reaction 2.

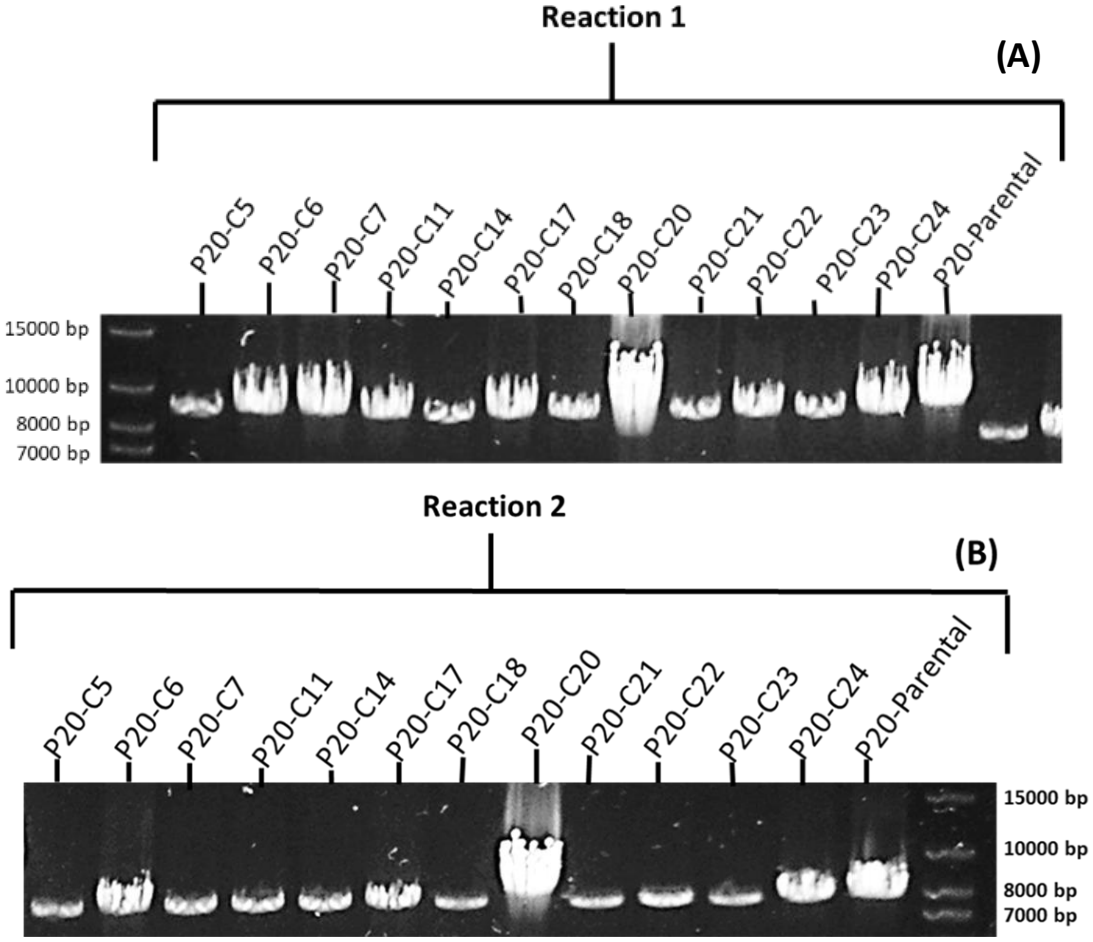

Figure 4. 2. (A) Agarose 1% gel containing the amplicons obtained from a High-fidelity PCR amplification of DNA samples from CHO clones using the primers correspondent with Reaction 1. Samples were run at 180V for a total time of 1 hour and 30 minutes to ensure proper run and separation.

(B) Agarose 1% gel containing the amplicons obtained from a High-fidelity PCR amplification of DNA samples from CHO clones using the primers correspondent with Reaction 2. Samples were run at 180V for a total time of 1 hour and 30 minutes to ensure proper run and separation.

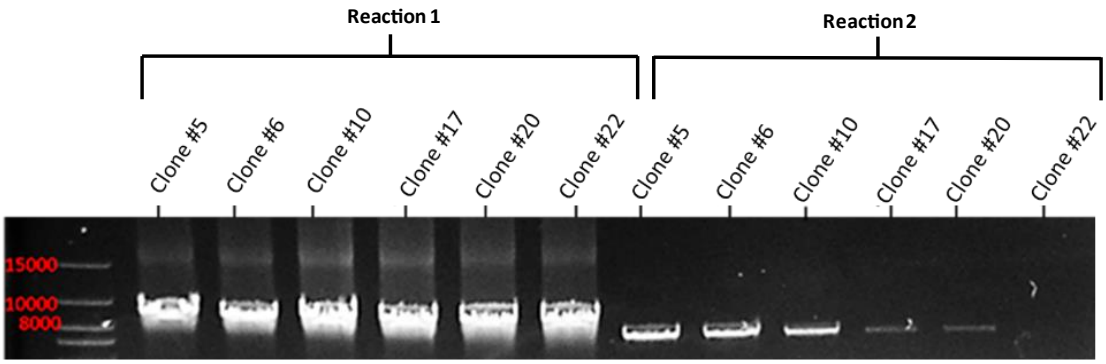

Figure 4. 3. PCR amplicons obtained from each clone after purification with magnetic beads. Reactions 1 and 2 should yield an amplicon of 8814bp and 7702 bp correspondingly. Samples were run in a 1% Agarose gel at 180V for a total time of 1 hour and 30 minutes to ensure proper run and separation. This figure shows only one example of the multiple gels that were run, specifically, samples from the fourth passage (P4).

The DNA content of selected samples (**Table 4.1)** was measured using Qubit to ensure accurate quantification. Samples were then normalized to a final concentration of 1ng/µl in 10 µl and processed with a Nextera XT DNA library prep kit according to the manufacturer's instructions.

After performing the tagmentation process, the PCR amplification and the tagmented DNA purification using AMPpure beads, as described in the Nextera XT DNA library prep Kit protocol, the samples were analyzed using a Tapestation DNA screentape system, which is a rapid electrophoresis-based system and facilitates size and quality analysis of the fragments (**Figure 4.4).**

Samples used on the sequencing experiment			
Passage #4 (2 weeks of culture)		**Passage 20 (10 weeks of culture)**	
Clone number	**Nomenclature**	**Clone number**	**Nomenclature**
Parental	P4-Parental	Parental	P20-Parental
Clone #5	P4-C5	Clone #5	P20-C5
Clone #6	P4-C6	Clone #6	P20-C6
Clone #10	P4-C10	Clone #10	P20-C10
Clone #14	P4-C14	Clone #14	P20-C14
Clone #15	P4-C15	Clone #15	P20-C15
Clone #17	P4-C17	Clone #17	P20-C17
Clone #18	P4-C18	Clone #18	P20-C18
Clone #20	P4-C20	Clone #20	P20-C20
Clone #21	P4-C21	Clone #21	P20-C21
Clone #22	P4-C22	Clone #22	P20-C22
Clone #24	P4-C24	Clone #24	P20-C24

Table 4. 1. Samples selected for the sequencing experiment. Each sample correspond to a whole mtDNA sequence obtained after mixing the two PCR reactions performed per clone, week and passage number. These samples were normalized to 1 ng/ µL and used to prepare the indexed mtDNA library using the Nextera XT DNA library prep Kit.

Samples were then pooled into an mtDNA library, which was loaded into a cartridge and analysed in an Illumina Iseq Sequencer following the manufacturer's instructions. This library of samples was run twice to increase the sequencing depth.

The mtDNA sequences corresponding to each reaction were observed to correspond with the expected size, with the fragment from Reaction 1 being bigger than the fragment from Reaction 2 (**Fig 4.5**). The samples were deemed appropriate to continue the sequencing process and a new library containing only the two parental samples was made and sequenced, aiming to ensure a higher depth of sequencing of these samples.

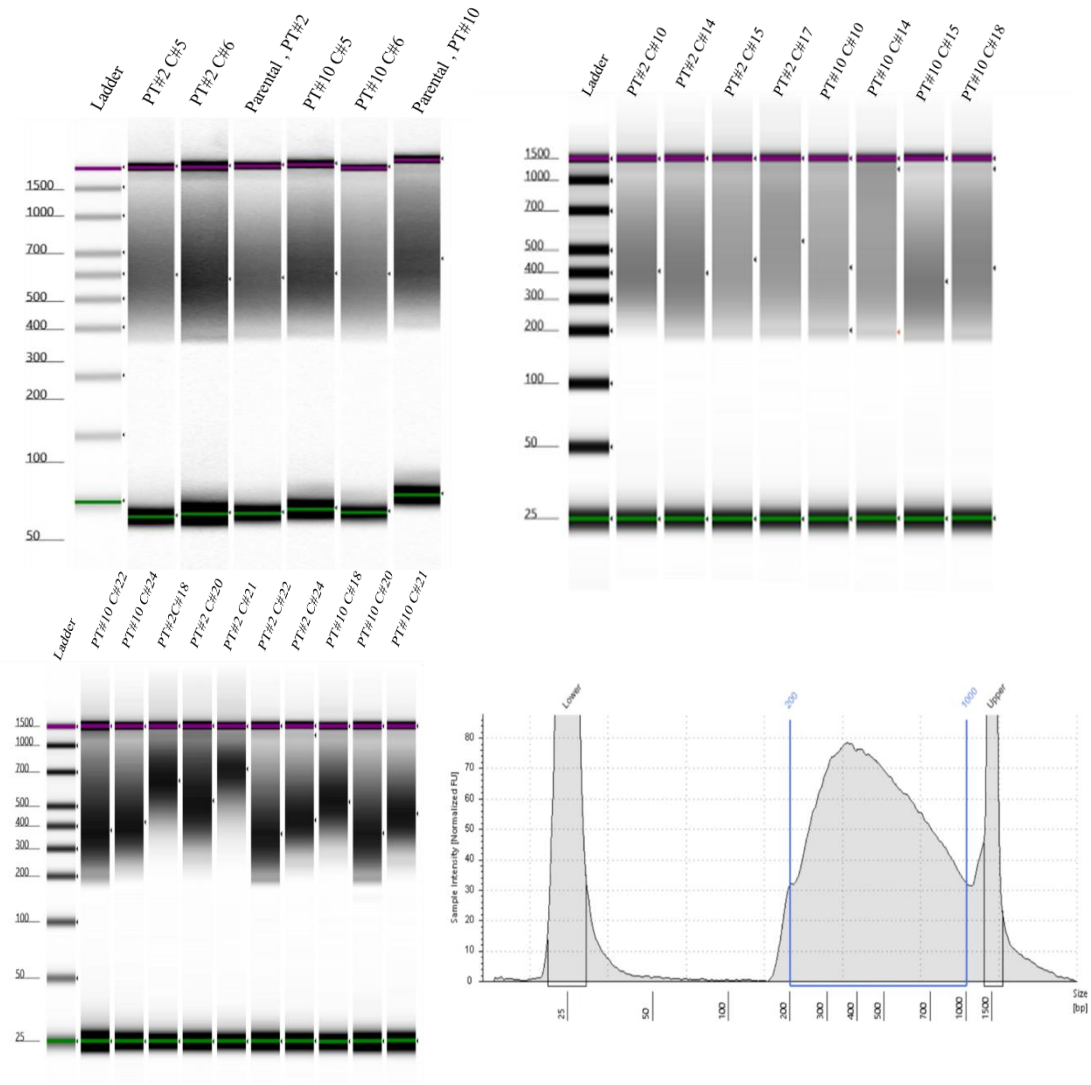

Figure 4. 4. mtDNA fragment analysis performed using a Tapestation DNA screentape system. The molarity and the average fragment size of the mtDNA samples obtained after tagmentation, amplification and purification of the DNA, calculated with the instrument, can be seen in the image. As required for the library generation, the analysis of fragment size and molarity was limited to those fragments between 200-1000 bp.

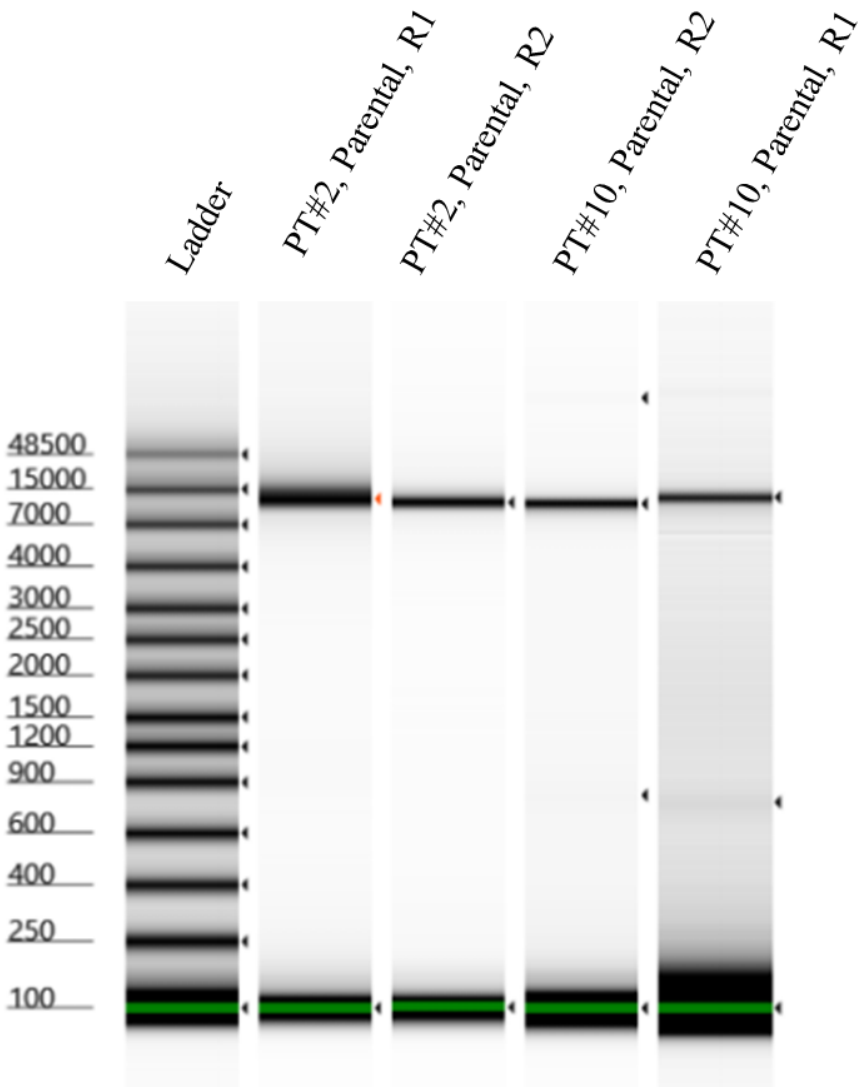

Figure 4. 5. mtDNA fragment analysis performed using a Tapestation DNA screentape system performed to ensure the presence of the mtDNA sequences corresponding to the high-fidelity PCR amplification previously performed in the samples.

4.2.1.2. Analysis of output from mtDNA library sequencing

As described in the previous section, a set of 24 samples, corresponding to 1 parental CHO cell line (CHO-520F) and 11 clones generated by limited dilution cloning, at two culture 'ages' (12 corresponding to samples collected after 2 weeks of culture and the same 12 collected after 10 weeks of culture). These samples were processed, pooled into a library, and then sequenced using an Illumina iSeq system (methods section 2.3.3).

Bioinformatic analysis was performed by Dr. Colin Clarke.

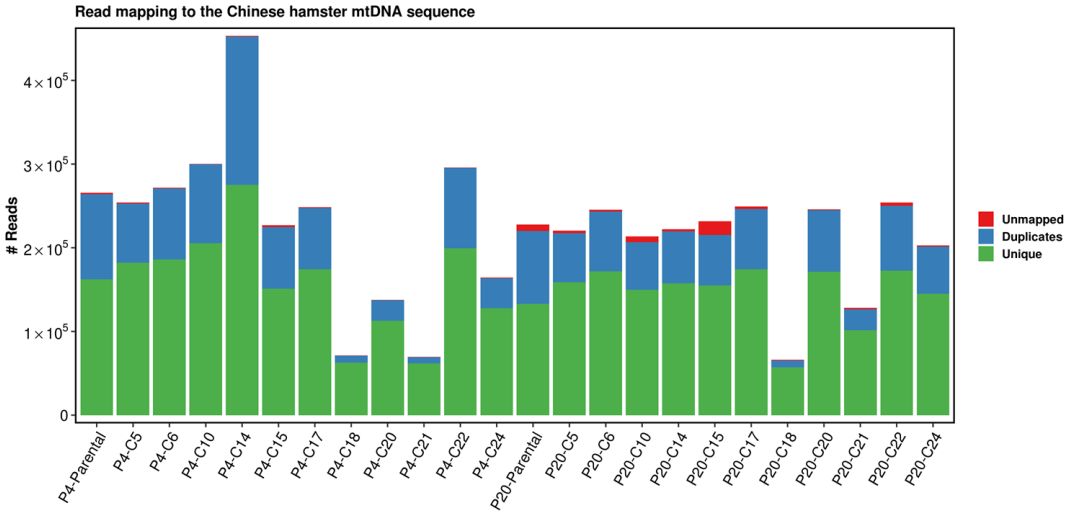

Figure 4. 6. Read mapping of CHO mtDNA sequence from samples of 12 different clones at two different timepoints (P4 or P20). Each bar represent the number of reads per sample, with a color code representing the unique (green), duplicate (blue) or unmapped sections read.

Figure 4.6 shows the reads obtained from the sequencing process. As seen in the figure, most of the samples had at least 1 x10^5 unique reads. The only exceptions to this were the samples related to clones 18 and 21, which had less than 1 x10^5 unique reads. The parental samples and clone 15 had a higher number of unmapped sections (failure to align with the reference sequence) than the other clones, but overall represented a very small proportion of the total reads. Duplicates, represented in blue, are a consequence of the

PCR step performed before the sequencing Duplicates may contain errors and mutations and/or interfere with the allele frequency analysis, and for this reason, were not taken into account during posterior analysis.

Besides the read counts, the depth of sequencing (number of times each base was sequenced) was examined during the initial analysis of the sequencing results. **Figure 4.7. A** show the average sequencing depth per sample. The average depth for most of the clones was higher than 1000X. This depth of sequencing should be sufficient to confidently identify heteroplasmy variants with an allele frequency of 2% (*Gonzalez et al 2020*). In the previous study (*Kelly et al 2017*) heteroplasmy variants with an allele frequency of 1% were identified. However, it must be noted that Kelly and collaborators only took into account those mutations with an allele frequency of 1% when the obtained depth of coverage for that particular position was equal or higher to 1500X. For this reason, as the depth of coverage obtained in this study was slightly lower, being closer to 1000X, the threshold for identification of heteroplasmic variants was instead set at 2% allele frequency.

As previously observed during the mapping process, Clones 18 and 21 had a lower sequencing depth than most of the other clones, at around 400X for these samples. This depth reduces our ability to confidently call variants with low allele frequencies, i.e., 2%. However, variants with higher frequencies (e.g., >10%) can still be confidently identified at 400X.

Figure 4.7.B and Figure 4.7.C also show the average depth of sequencing achieved, in both unshifted and shifted sequences respectively, for every nucleotide position of the mtDNA. For both sequences, the coverage of positions between 5000-7000 bp and 14000-15000 bp of the mitogenome was observed to be higher than average, being between depths of 1300X and 1500X. As two of the main mutations of interest are located in those regions (namely, *m.6996G>A* variant for COX2 gene and *m.14136delA* variant for CYTB gene), the depth of coverage achieved allowed identification of low-frequency heteroplasmic variants at these positions with high confidence.

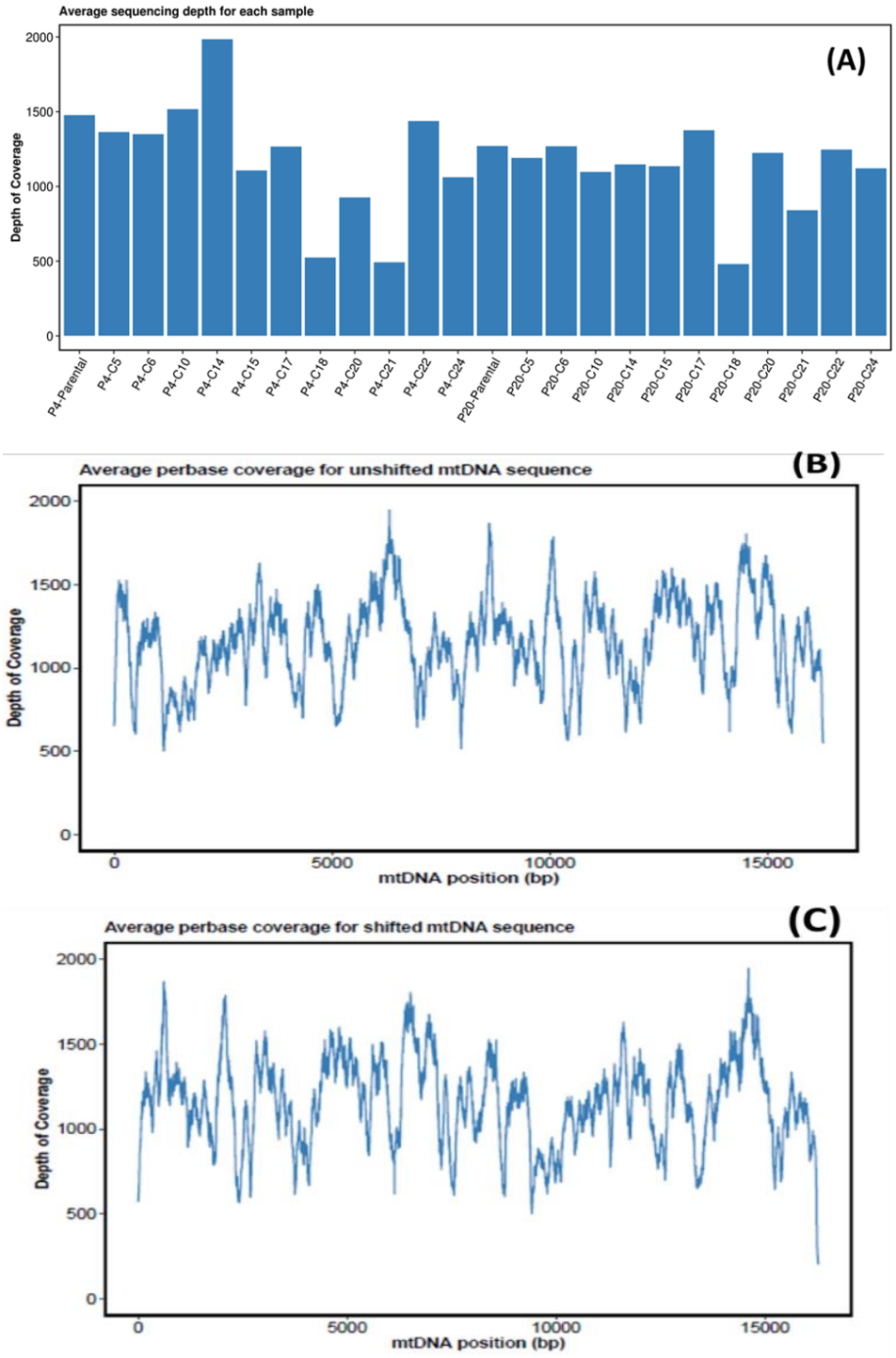

Figure 4. 7. (A) Average depth of sequencing, performed with Illumina iSeq for each CHO clone sample.

(B) Average per base coverage for unshifted DNA sequences for each CHO clone sample. Sequencing was performed with Illumina iSeq.

(C) Average per base coverage for shifted DNA sequences for each CHO clone sample. Sequencing was performed with Illumina iSeq.

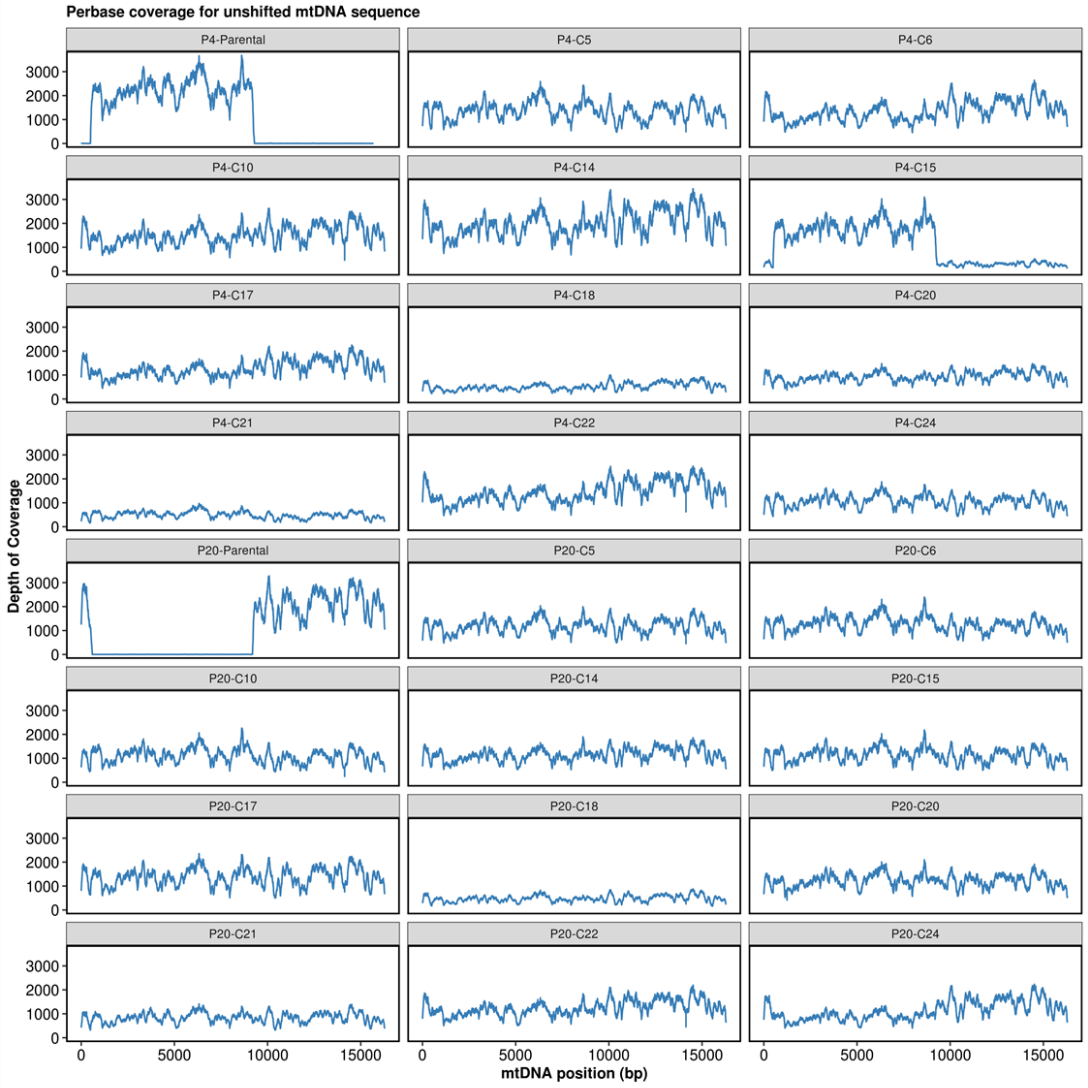

Figure 4. 8. Coverage per base of mtDNA sequence for each clone and timepoint

However, when the coverage per base of the sequences was evaluated in each sample, a region of no coverage in certain samples became evident. The samples corresponding with the parental cell lines (P4-Parental and P20-Parental), and the sample corresponding with Clone 15 at passage 4 (P4-C15) were observed to lack approximately half of the sequence. In the case of the parentals this sequence was seemingly totally absent, while in the case of Clone 15, the region seemed to have been partially sequenced, but with very low depth. This is shown in detail in **Figure 4.8.**

During the first two runs, half of the sequence of the Parental sample at both passage 4 and 20 (P4-Parental and P20 Parental correspondingly) was observed to have low coverage, as well as half of the sequence of P4-C15, observation of these results led us to re-sequence both the parental samples, this time making sure that both halves of the sequence were present in the sample before starting the process of the library preparation. On the other hand, the P4-C15 sample contained a very low concentration of DNA and was deemed unsuitable for inclusion in this new sequencing process, which aimed to achieve a good depth of sequencing of the parental samples as possible. Unfortunately, and for reasons yet to be determined, the re-sequencing effort yielded the same result.

To try to identify any heteroplasmic variants that may have arisen between the parent and the clones (clonal) and at the different time points (temporal), the gap in the sequence of the P4-Parental sample was imputed using the sequence for CHO-520F derived in a previous study (*Kelly et al 2017).* For P20-Parental, only the sequence from position 10000nt onwards was considered in subsequent analysis. Similarly, for P4-C15 only the sequence up to position 9000 was considered for analysis.

With the mapping and the depth of sequencing accounted for, the next point of the analysis was to establish the allele frequency distribution in the samples. The majority of the variants found had low allele frequencies, below 25% (**Figure 4.9**) A considerable number of variants were observed to have up to 25% allele frequency compared with previous CHO mtDNA sequencing studies, with some variants having allele frequencies around 50%.

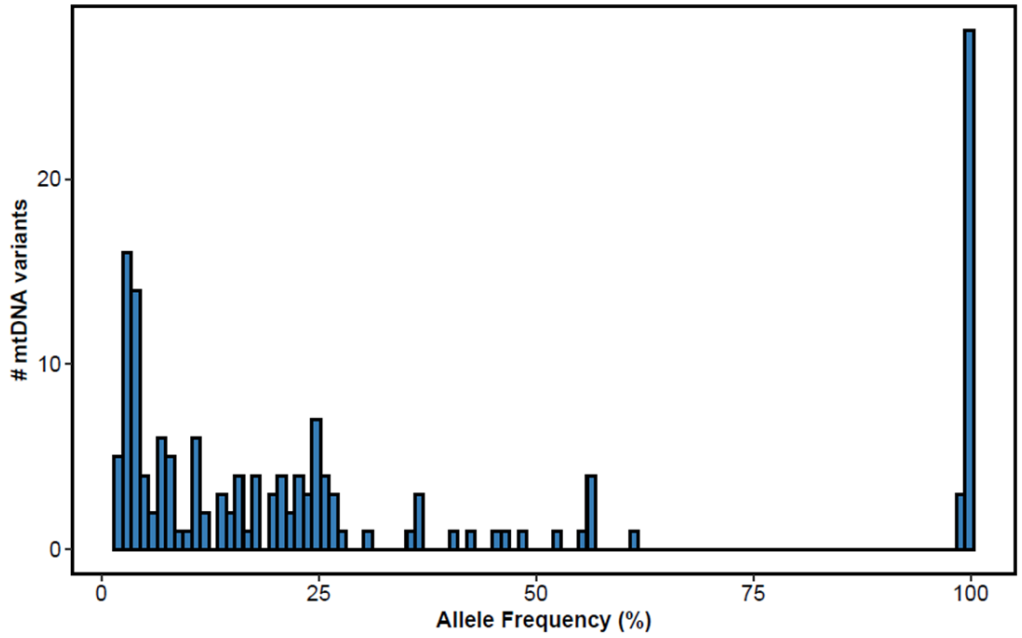

Figure 4. 9. Distribution of allele frequency in the CHO clones. The minimum allele frequency called was 2%.

Finally, over 20 variants were observed to be close to 100%, which was already observed in the previous study and raises interesting questions about these particular variants, such as if these variants are preserved because of their impact in the mitochondria or despite their lack of impact. This will be seen in detail later in this section.

To understand the potential impact of the variants found in cellular function, the SnpEff tool was employed. SnpEff is a bioinformatic tool, consisting of software that annotates and predicts the effects of genetic variants that could have an impact on the phenotype of the cells, such as amino-acid changes (*Cingolani et al., 2012*). The output of this analysis is illustrated in **Figure 4.10**.

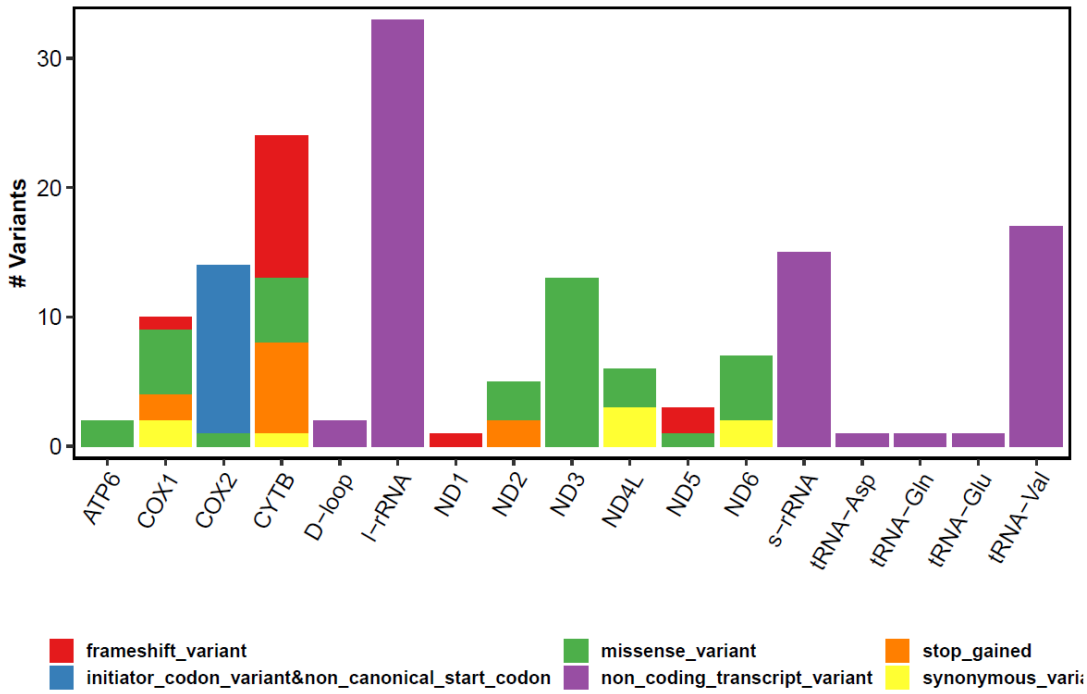

Figure 4. 10. Predicted number of impactful variants per gene in the CHO clones. Each bar represent the number of predicted variants for a given gene. Analysis performed using SnpEff analysis software.

Most of the heteroplasmic variants were found in the long-rRNA sequence. Followed by the sequences corresponding with *CYTB, s-rRNA, tRNA-Val*, *COX2*, *ND3,* and *COX1* from higher to lower number of variants.

Curiously, *tRNA-Val* has a high number, over 30, of non-coding variants, despite Valine being a fundamental amino acid in the mitochondria. This raises some interesting questions about the potential of the variants observed to impact mitochondrial function, the frequency of these variants, and if these variants affect the activity of tRNA-Val or not. These questions will be explored in the discussion section.

The Cytochrome B gene (*CYTB*) showed the greatest number of variants among the protein-encoding genes across all samples compared with the reference genome. However, given the results of the previous experiments, it is likely that a very high threshold must be met to meaningfully impact the metabolism of the cell. This means each of these individual variants would have to be represented in at least 70-90% of the mtDNA copies of the cell to have an actual effect on the phenotype. Therefore, *CYTB* could have been accumulating a high number of heteroplasmic variants because these variants are not frequent enough to be impactful for the mitochondria.

COX2 gene was observed to accumulate a high number of variants, most of them corresponding with the initiator codon variant previously identified in the fast growth phenotype clones, the only exception being a low-frequency missense variant found in C5.

After the evaluation of the overall incidence of variants in the clones compared to the reference, next the heteroplasmy variants found at different passages were investigated. The analysis was focused on specific sequences of interest, mainly genes identified in previous studies to present interesting heteroplasmy variants, but also in genes with a high number of variants that were predicted to be impactful, as seen in the SnpEff analysis previously. Therefore, attention was focused on analyzing genes that either display a high number of heteroplasmic variants or where heteroplasmic variants could potentially have a strong influence on mitochondrial function.

Firstly, the heteroplasmic variants located in sections of the mitochondrial DNA sequence encoding RNAs were analyzed, as these particular sequences were observed to accumulate a very large number of variants. In particular, the sequences encoding the

short ribosomal RNA, $tRNA^{val,}$ and the long Ribosomal RNA were observed to contain many heteroplasmic variants at very high allelic frequencies (**Fig 4.11).** A very high-frequency (>50%) non-coding variant (*m.1074C>T*) was observed at position 1074, corresponding with the sequence of $tRNA^{val}$. This variant was also observed to be present in most of the clones: At passage 4 all the samples from the clones except P4-C20 were observed to possess this variant; at passage 20, the variant was also observed in P20-C20 but was not observed anymore in P20-C24.

Valine is required for mitochondrial protein synthesis and the sequence encoding the tRNA is relatively short, giving this mutation the potential to significantly impact the use of valine in the mitochondria. Given the high frequency, the presence of this variant in most clones and its location in position 1074 of the mitochondrial genome, near the end of the sequence, is likely that this variant is not located in a critical region of the tRNA, such as the anticodon nor the aminoacyl site regions of the tRNA, and therefore does not have an impact in the tRNA function in the valine synthesis process.

Recent research in mitochondria ribosomes has highlighted $tRNA^{val}$ as one of the two tRNAs capable of being integrated into the mitochondrial ribosome (the other one being $tRNA^{Phe)}$, fulfilling a structural function in substitution of the 5S RNA of the long subunit. Therefore, the high-frequency variant observed in the $tRNA^{val}$ may be related to this alternative function. This will be discussed in the discussion section.

The non-coding variant (*m.2235C>T*) found at position 2235, within the long ribosomal RNA, is similar to the previous case: this variant is found throughout the panel of clones, has very high frequencies (>50%) and, with only one exception, does not change with time. The *m.2235C>T* was present in all the clone's samples at passage 4 except for P4-C20 and P4-C22. By passage 20, the variant was not present in the P20-C24 sample but remained observable in the rest of the clones. Both m.2235C>*T* and the previously seen *m.1074C>T* variant are caused by the same SNPs, a substitution of C to T (C >T).

	Non-coding variant
	Missing sequence

(A)

	mt-genome position									
Sample	105	575	591	915	1074	1243	1354	1719	2151	2235
P4-Parental					99%				15%	99%
P4-C5					>50%	15%	30%		30%	>50%
P4-C6	10%		2%		>50%			35%		>50%
P4-C10			2%		>50%				25%	>50%
P4-C14			5%		>50%				35%	>50%
P4-C15					>50%	25%			25%	>50%
P4-C17			5%		>50%				35%	>50%
P4-C20										
P4-C22			5%	15%	>50%				40%	
P4-C24					>50%					>50%
P20-C5					>50%		30%		30%	>50%
P20-C6	15%				>50%			35%		>50%
P20-C10			2%		>50%				25%	>50%
P20-C14			5%		>50%				35%	>50%
P20-C15			5%		>50%				15%	>50%
P20-C17					>50%				30%	>50%
P20-C20			2%		>50%					
P20-C22			5%	10%	>50%				40%	
P20-C24										
	rRNA-S				tRNA-Val	rRNA-L				

(B)

	mt-genome position									
Allele frequence variance	105	575	591	915	1074	1243	1354	1719	2151	2235
Parental										
Clone #5 (C5)	0	0	0	0	0	-15%	0	0	0	0
Clone #6 (C6)	5%	0	-2%	0	0	0	0	0	0	0
Clone #10 (C10)	0	0	0	0	0	0	0	0	0	0
Clone #14 (C14)	0	0	0	0	0	0	0	0	0	0
Clone #15(C15)					0	-25%	0	0	-10%	0
Clone #17 (C17)	0	0	-5%	0	0	0	0	0	-5%	0
Clone #20 (C20)	0	0	2%	0	50%	0	0	0	0	0
Clone #22 (C22)	0	0	0	-5%	0	0	0	0	0	0
Clone #24 (C24)	0	0	0	0	-50%	0	0	0	0	-50%
	rRNA-S				tRNA-Val	rRNA-L				

Figure 4. 11. (A) Frequency of heteroplasmy variants of mitochondrial rRNA-S, tRNA-Val and rRNA-L sequences found in the CHO clones using iSeq instrument after 4 passages) or 20 passages correspondingly. The colour of the highlighted positions indicates the predicted impact of the heteroplasmic mutation.

(B) Variance of heteroplasmy in the mitochondrial rRNA-S, tRNA-Val and rRNA-L sequences CHO clones after 16 passages. Frequency increases are highlighted in blue colour, while Frequency decreases highlighted in red colour.

The same applies to the non-coding variant (*m.2151C>T)* observed at position 2151. This variant was caused by the same C by T substitution, was widely spread among the panel of clones, and was not changed in the majority of the clones with time. Overall, it seems like this particular region of the mtDNA, encoding the three previously mentioned RNAs, tends to accumulate high-frequency variants. This result probably reflects the fact that DNA that does not encode proteins may be more tolerant of heteroplasmic mutations than the protein-encoding sequences.

Next, the protein-encoding genes with a high number of variants were observed. *NADH3* was the first good candidate. This gene seemed to accumulate many missense variants overall with high frequency. For this reason, a closer analysis was performed on this gene.

Figure 4.12 shows the heteroplasmic variants found at the NADH3 mitochondrial sequence and the allelic frequencies. A missense variant (*m.9704C>T*) caused by a substitution (C >T) was observed in many of the clones at Position 9704, which doesn't appear in the parental sequences. At passage 4, samples P4-C5, P4-C10, P4-C14, P4-C20, and P4-C24 were observed to have this variant in their mitochondrial sequence at a high frequency (30-40%). P4-C6 was also observed to hold this variant, but at a much lower frequency (2%).

The *m.9704C>T* variant changed considerably in frequency over the time of the experiment. This variant was absent from some of the clones, namely P20-C10, P20-C20, and P20-C24, at passage 20. Interestingly, the opposite phenomenon was also observed, with this variant detected at passage 20 at high frequencies in some of the clones that previously lacked it at passage 4. P20-C17 and P20-C22 samples showed high frequencies of this variant (30-40%). Additionally, this variant was also observed in the P20-Parental sample at a lower frequency degree (15%).

Similarly, Clone #14 showed a new missense variant (*m.9647C>A)* which does not appear in any other clone. This variant was observed at low frequency at the P4-C14 sample but was observed to have increased up to a 15% frequency in sample P20-C14.

The variants observed in NADH3 were present in most clones among the panel, despite being originally absent in the parental, and the frequency of these variants was observed to change dramatically over time. These results again demonstrate how the cloning process can potentially result in clones with variants that are present at a low (or high)

(A)

	mt-genome position	
Sample	9647	9704
P4-Parental		
P4-C5		*30%*
P4-C6		*2%*
P4-C10		*35%*
P4-C14	*2%*	*30%*
P4-C15		
P4-C17		
P4-C20		*30%*
P4-C22		
P4-C24		*40%*
P20-Parental		*15%*
P20-C5		*30%*
P20-C6		
P20-C10		
P20-C14	*15%*	*30%*
P20-C15		
P20-C17		*30%*
P20-C20		
P20-C22		*40%*
P20-C24		
	NADH3	

Missense Variant

(B)

Allele frequence variance	mt-genome 9647	
Parental	*0*	
Clone #5 (C5)	*0*	
Clone #6 (C6)	*0*	-2%
Clone #10 (C10)	*0*	-35%
Clone #14 (C14)	13%	*0*
Clone #15(C15)		
Clone #17 (C17)	*0*	30%
Clone #20 (C20)	*0*	-30%
Clone #22 (C22)	*0*	40%
Clone #24 (C24)	*0*	-40%

(B)

Figure 4. 12. (A) Frequency of heteroplasmy variants of mitochondrial NADH3 sequence found in the CHO clones using iSeq instrument after 4 passages or 20 passages correspondingly. The colour of the highlighted positions indicates the predicted impact of the heteroplasmic mutation.

(B) Variance of heteroplasmy in the mitochondrial NADH3 sequence in the CHO clones after 16 passages. Frequency increases are highlighted in blue colour, while Frequency decreases highlighted in red colour.

frequency in the original population but become more abundant in the resulting sub-culture. In saying that, if an individual cell is an outlier within a population – contributing to the overall heteroplasmy profile but very different from the 'average' – one might expect the subsequent clonal line to be 100% for that 'rare' variant. However, that does not seem to be the case not only for this variant but in general, which means that either the 'founder' cell had heteroplasmy within its mtDNA or, a change in variant frequency occurred during the first four passages after cloning. This question can only be resolved by resorting to single-cell mtDNA sequencing to discover the extent of heteroplasmy within individual cells rather than within cell populations in CHO cultures. These possibilities will be explored in the discussion section.

Another heteroplasmy variant of interest previously observed in CHO-520F was the initiator codon variant *m.6996G>A* in the *COX2* gene. This variant appears as one of the predicted functionally impactful variants in the SnpEff analysis, where *COX1* and *COX2* were observed to have 9 and 14 variants respectively. For this reason, the variants identified in these two genes were also analyzed.

Figure 4.13 shows the heteroplasmic mutations and variants found in both *COX1* and *COX2* and the allelic frequencies of those variants. The *m.6996G>A* variant was observed to be present in most of the clones after 4 passages. Moreover, in some samples, such as P4-C5, P4-C6, P4-C10, P4-C14, P4-C15, the allele frequency of this variant was observed to be higher than in the parental sample (roughly 10-15% higher). Samples P4-C20, P4-C22, and P4-C24 were an exception, as this variant was not observed in P4-C22 and P4-C24 samples and was slightly decreased (-5%) in the P4-C20 sample.

Additionally, P4-C17 was observed to have the same frequency for this variant as the P4-Parental sample.

After 20 passages, the *m.6996G>A* variant frequency was observed to be decreasing in most of the clones. This variant frequency showed a strong decrease in P20-C5 (-20%), P20-C15 (-30%), and P20-C17 (-15%) samples. A lower decrease was also noted in P20-C10 and P20-C14 samples (-5%).

On the other hand, this variant frequency was increased in the P20-C6 sample (+10%) and remained unchanged in P20-C20. These results suggest that the *m.6996G>A* variant is preserved in the short term, as it was observed in most of the clones after the cloning

	Sinonymous Variant
	Missense Variant
	Initiator codon variant
	Frameshift variant
	Stop codon variant

(A)

	mt-genome position							
Sample	5746	5779	5888	6085	6097	6552	6996	7295
P4-Parental							25%	
P4-C5					2%		40%	5%
P4-C6							30%	
P4-C10							35%	
P4-C14		25%	35%			10%	40%	
P4-C15	5%						30%	
P4-C17							25%	
P4-C20							20%	
P4-C22				20%				
P4-C24								
P20-C5							20%	
P20-C6							40%	
P20-C10							30%	
P20-C14		25%	35%			10%	35%	
P20-C15								
P20-C17							10%	
P20-C20							20%	
P20-C22				25%				
P20-C24								
	COX1						COX2	

(B)

	mt-genome position							
Allele frequence variance	5746	5779	5888	6085	6097	6552	6996	7295
Clone #5 (C5)	0	0	0	0	-2%	0	-20%	-5%
Clone #6 (C6)	0	0	0	0	0	0	10%	0
Clone #10 (C10)	0	0	0	0	0	0	-5%	0
Clone #14 (C14)	0	0	0	0	0	0	-5%	0
Clone #15(C15)	-5%	0	0	0	0	0	-30%	0
Clone #17 (C17)	0	0	0	0	0	0	-15%	0
Clone #20 (C20)	0	0	0	0	0	0	0	0
Clone #22 (C22)	0	0	0	5%	0	0	0	0
Clone #24 (C24)	0	0	0	0	0	0	0	0

Figure 4. 13. (A) Frequency of heteroplasmy variants of mitochondrial COX1 and COX 2 sequences found in the CHO clones using iSeq instrument after 4 passages or 20 passages correspondingly. The colour of the highlighted positions indicates the predicted impact of the heteroplasmic mutation.

(B) Variance of heteroplasmy in the mitochondrial COX1 and COX 2 sequences in the CHO clones after 16 passages. Frequency increases are highlighted in blue colour, while Frequency decreases highlighted in red colour.

process, even with higher frequency than in the parental clone in some clones. However, these results also show that this variant frequency tended to decrease after some time, rather than increase.

A missense variant (*m.7259G>A)* with a low frequency (5%) was also observed at position 7259 in the *COX2* gene in sample P4-C5. This variant corresponded to a G>A substitution, and was not observed in sample P20-C5.

In several clones from the panel, the *COX1* gene contained several variants in its sequence. Sample P4-C14, corresponding with Clone #14, included a stop codon variant *(m.5779C>A)* at position 5779 (25% frequency), a synonymous variant *(m.5888G>A*) at position 5888 (35%), and a missense variant (*m.6552G>A)* at position 6552 (10%); none of these variants was observed to change with time, as they were still present at the same frequencies at sample P20-C14.

Clone #15 was also observed to have a missense variant (*m.5746C>T)* with 5% frequency in sample P4-C15, which was undetected in sample P20-C15. Similarly, P4-C15 showed a low-frequency frameshift variant (*m.6097delA*) with 2% frequency at position 6097, which was not detected later in P20-C15.

Finally, P4-C22 showed a missense variant (*m.6085C>T)* with 20% frequency. Unlike the previously described variants, this particular variant was found to increase in frequency over time, going from 20% to 25% frequency in P10-C22.

Most of the variants observed in *COX1* were caused by different single nucleotide polymorphisms or SNPs, in which a single nucleotide substitution changed the aminoacid encoded by that codon, creating a mutation. The only exception was the low-frequency *m.6097delA* frameshift variant in P4-C15, which was the product of a GA>G deletion. The variants observed in Clone #14 were particularly interesting, as these variants were unique to this clone, correspond with three separated point mutation events of G>A substitution and they did not change over the following 16 passages. Clone #22 was similar, with a point C>T substitution event creating a new variant that not only persisted within the mitochondria but increased within the time frame from Passage 4 to Passage 20.

Whether these variants affect or not overall metabolism, they still constitute an interesting example of how random events can induce unique changes in the mitochondrial sequence

that may be preserved (or lost) over time. It is also possible that these small variants were previously present in the parental population at a low degree and have been distributed by the cloning process into different clones, as many of them appeared as unique to a single clone.

Finally, the heteroplasmic variants of the *CYTB* gene were evaluated, the *m.14136delA* frameshift variant previously seen in Kelly et al 2017 study was of great interest, but more variants were detected and considered. This can be seen in **Figure 4.14**, which shows the heteroplasmic variants found in the *CYTB* mitochondrial sequence and the allelic frequencies of such variants. The first thing that was noted was how the heteroplasmic frequency of the *m.14136delA* variant (which results in a frameshift mutation) was observed to change during the cloning process, apparently increasing compared to the parental. As previously mentioned, this could be due to the parent population (CHO-520F), even though was supposed to be a clone itself, likely contained a mixed population of cells with different levels of heteroplasmy, which during the single-cell clone process were isolated, potentially changing the heteroplasmy had already increased during the cloning process. However, it must be noted that the probability of picking a small number of cells from a population and finding them to be very different from the whole population average was considered low enough to consider that real heteroplasmy changes over a certain period were being observed.

At P4-Parental sample, this variant only had an allelic frequency of 8%, while in 5 of the clones, namely in samples P4-C5, P4-C14, P4-C17, and P4-C22 the frequency of this variant was observed to become higher than the parental, reaching levels of 30-40% frequency. On the other hand, several clones, namely P4-C6, P4-C20, and P4-C24, showed lower levels of this variant. P4-C6 have 3% less frequency compared to the parental, while P4-C10, P4-C20, and P4-C24, did not show this variant at all.

After 20 passages, the *m.14136delA* variant frequency was observed to increase in the Parental sample (+12% frequency) and in P20-C5 (+5%). On the other hand, this variant disappeared completely in P20-C6 (-5%) and P20-C10 (-40%) with a dramatic decrease in the latter. In the other clones, the *m.14136delA* variant frequency remained stable after 8 weeks of culture.

CYTB also contained another position of interest, noted in previous studies, i.e., to have an *m.14378G>A* variant at position 14378, which generates a new stop codon. In this

study, while the frequency of the *m.14378G>A* was high in the P4-Parental sample (approximately 35% frequency), this variant was observed to be dramatically lower in most of the clones. P4-C17 sample showed a frequency of 25% (-10% frequency

	Sinonymous Variant
	Missense Variant
	Initiator codon variant
	Frameshift variant
	Stop codon variant

(A)

	mt-genome position					
Sample	14136	14171	14378	14820	14994	15127
P4-Parental	8%		36%			
P4-C5	35%		5%			
P4-C6	5%		2%			
P4-C10	40%		2%			
P4-C14	30%				5%	
P4-C15						
P4-C17	30%	2%	25%			
P4-C20						
P4-C22	40%					
P4-C24						
P20-Parental	20%		10%			2%
P20-C5	40%					
P20-C6						
P20-C10						
P20-C14	30%				5%	
P20-C15			35%			
P20-C17	30%	5%	25%			
P20-C20						
P20-C22	40%					
P20-C24						
	CYTB					

(A)

(B)

	mt-genome position					
Allele frequence variance	14136	14171	14378	14820	14994	15127
Parental	12%	0	-26%	0	0	2%
Clone #5 (C5)	5%	0	-5%	0	0	0
Clone #6 (C6)	-5%	0	-2%	0	0	0
Clone #10 (C10)	-40%	0	-2%	0	0	0
Clone #14 (C14)	0	0	0	0	0	0
Clone #15(C15)						
Clone #17 (C17)	0	3%	0	0	0	0
Clone #20 (C20)	0	0	0	0	0	0
Clone #22 (C22)	0	0	0	0	0	0
Clone #24 (C24)	0	0	0	0	0	0

(B)

Figure 4. 14. (A) Frequency of heteroplasmy variants of mitochondrial CYTB sequence found in the CHO clones using iSeq instrument after 4 passages or 20 passages correspondingly. The colour of the highlighted positions indicates the predicted impact of the heteroplasmic mutation.

(B) Variance of heteroplasmy in the mitochondrial CYTB sequence in the CHO clones after 16 passages. Frequency increases are highlighted in blue colour, while Frequency decreases highlighted in red colour.

compared with the parental sample); in P4-C5, P4-C6, and P4-C10, this variant showed a dramatic allele frequency reduction compared with the parental: 5%, 2%, and 2% respectively (Approximately 30% frequency reduction compared with the parental sample). Additionally, this variant was not found in the rest of the clones sequenced. The changes in heteroplasmy at this position observed in the clones compared to the parental were notable.

Following this trend, after 10 weeks of culture, this heteroplasmy variant was observed to have almost disappeared from all the clones of the panel. The variant was only observed at this point in the P20-Parental sample at a frequency of 10% (-25%) and in the P20-17 sample, where it remained unchanged at a frequency of 25%.

Other minor variants were noted in the *CYTB* sequence. An *m.14171G>A*, predicted to cause a missense, was observed in the P4-C17 sample, which went up from 2% frequency at passage 4 to 5% frequency at the P20-C17 sample. Similarly, a missense-inducing variant (*m.14994T>C)* was noted in P4-C14 at position 14994. However, the *m.14994T>C* variant was observed to remain unchanged over time, remaining detectable at 5% frequency in the P20-C14 sample. Finally, the detection of a low-frequency synonymous variant in the P20-Parental (2% Frequency), which was not detected at passage 4, was also noted.

Overall, these results showed changes in heteroplasmy after the cloning process and, additionally, changes in the heteroplasmy observed in the clones from passage 4 to passage 20. Many of the changes observed in the clones at passage 4 could be as a result of heterogeneity in the parental 520F cell line (even though it was a cloned line itself) and simply reflect the random nature of cloning single cells from it. However, the dramatic differences in heteroplasmy being observed at positions 14136 and 14378 for example, in several of the clones doesn't appear to reflect what should essentially be a random sampling of the original population. Therefore, this result may hint at significant changes in heteroplasmic frequency happening very quickly, maybe to a redistribution of heteroplasmy taking place even during or soon after the cloning process itself.

Heteroplasmy was also observed to vary significantly with both the cloning process and time as potential factors of change. The *m.14136delA* variant showed different tendencies

to change in frequency depending on the clone. The frequency of this variant increased in 4 clones and decreased in 3 clones compared with the parental at Passage 4. Later, at passage 20, the *m.14136delA* was observed to increase in the parental and one clone and to decrease until a non-observable level in two of the clones. Conversely, the *m.14378G>A* variant appeared to have a strong tendency to decrease and/or disappear in most of the clones at both Passage 4 and Passage 20, with the sole exception of Clone #17.

4.2.2. Phenotypical differences found in clones #5 and #6 after 24 passages.

With the sequencing data at hand and knowing the differences found in the mtDNA of all the clones from the panel, the growth and recombinant protein titer of two of the clones sequenced, namely, Clone #5 and Clone #6, were evaluated after 24 passages (12 weeks of culture time). It must be noted that passages from 21st to 24th were performed in a vented cap tube in 5mL of cell culture media, instead of the 24-well plate. This evaluation was performed to observe if there were any differences in phenotype that could be related to the changes in heteroplasmy. The parental clone, CHO-520F, thawed and passaged 2 times, was used as a reference.

The analysis of cell growth and viability revealed differences in growth manifesting after 96 hours of culture. (**Figure 4.15 A**) The viable cell density of Clone #5 started to quickly decline from 96 hours of culture and onwards, and was observed to be considerably lower than the densities reach by both Clone #6 and the parental. Clone #6 was observed to reach maximum viable cell densities similar to those of the parental until 120 hours of culture. After this point, the growth of Clone #6 seemed to stall and differences between clone #6 and the parental started to become evident, with the viable cell density of Clone #6 declining much faster than the parental. The viability (**Figure 4.15 B**) remained equal for both clones and the parental for most of the culture, with clone #5 viability declining slightly faster after 144 hours of culture, which normalizes to the levels of the other clones shortly afterward. It must be noted that the growth rate of these clones was also changed (**Figure 4.15 C**), with clone #6 having a higher and clone #5 having a lower growth rate than the parental sample, respectively.

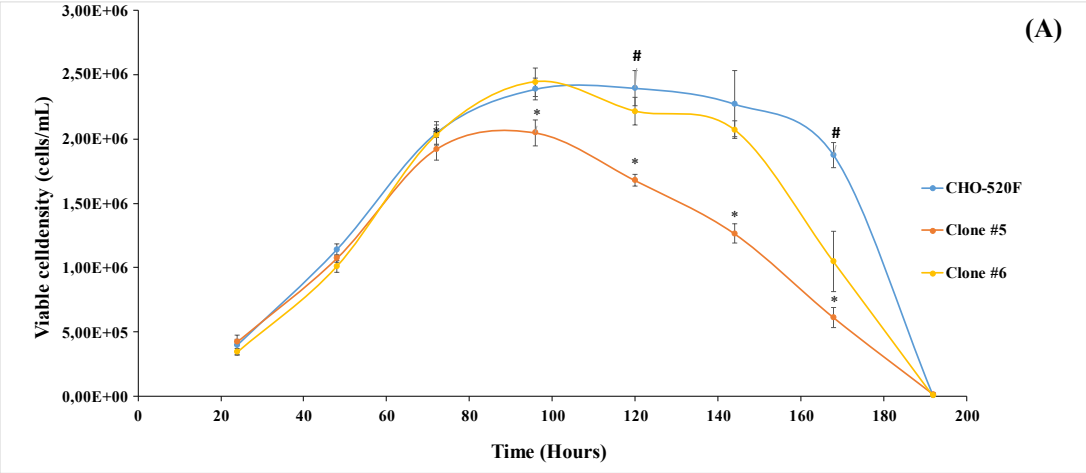

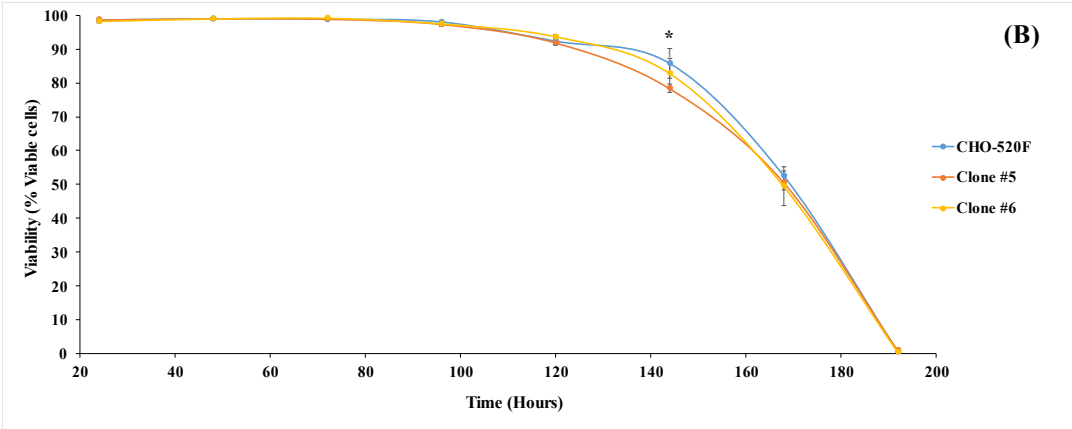

(C)

	μ (1/h)
CHO-520F	0,0248246
Clone #5	0,0219062
Clone #6	0,0270782

Figure 4. 15. (A) Viable cell density of the CHO clones over the course of 196 hours. Cells were cultured in suspension culture in 5mL of CHO-SFMII media. Each line represent the average viable cell density of biological triplicates measured in triplicates using Guava Easycite cytometer ± SD. Significance was tested using a one-way ANOVA with α <0,05.

(B) Viability of the CHO clones over the course of 196 hours. Cells were cultured in suspension culture in 5mL of CHO-SFMII media. Each line represent the average viability cell density of biological triplicates measured in triplicates using Guava Easycite cytometer ± SD. Significance was tested using a one-way ANOVA with α <0,05.

(C) Average growth rate of the CHO clones over time over the course of 196 hours

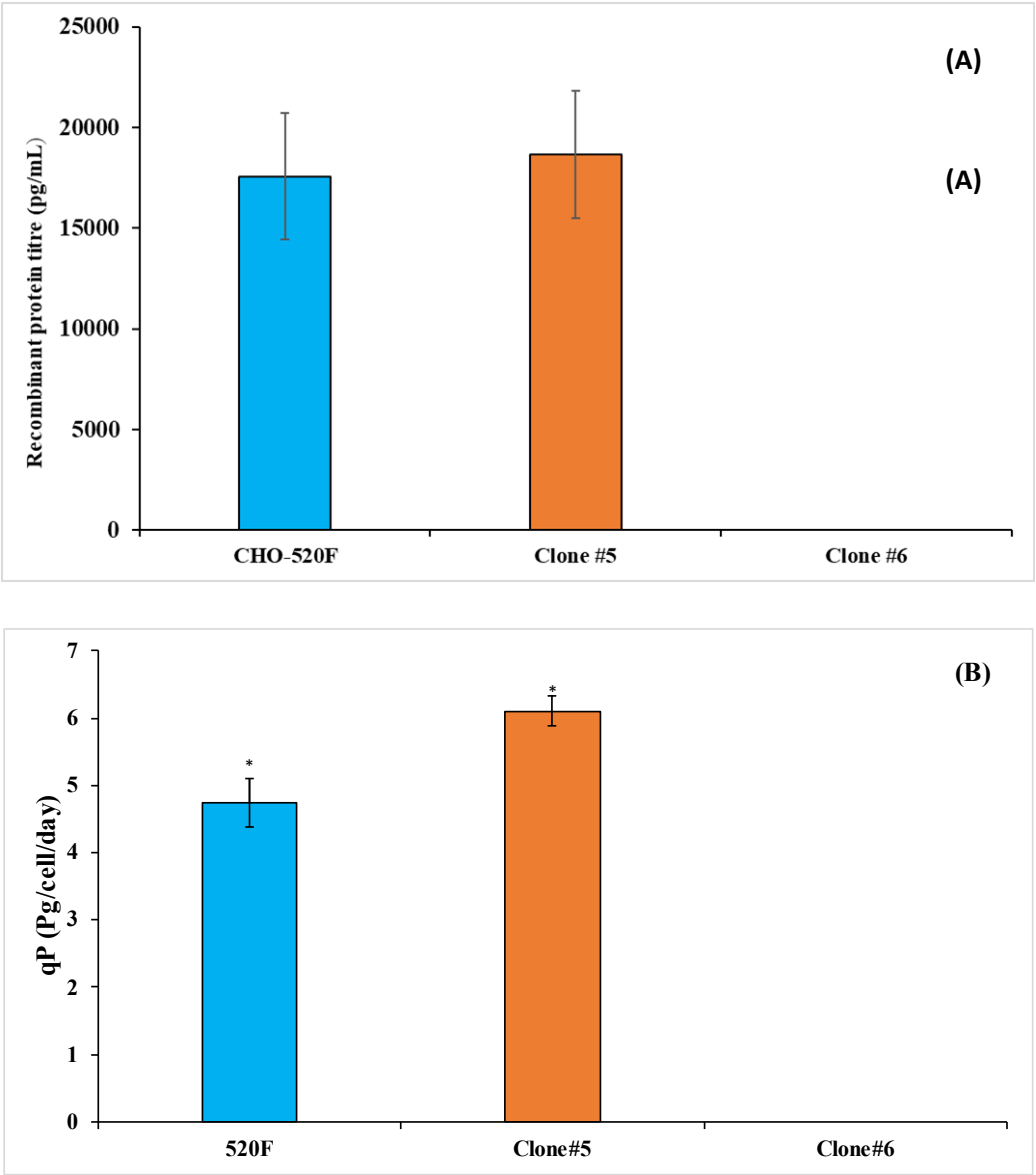

Figure 4. 16. (A) Protein titre from clones after 96 hours in culture. Each bar represent the average protein titre of biological triplicates measured in duplicate by ELISA ± SD. Significance was tested using 1-way ANOVA with $\alpha < 0,05$.

(B) Specific productivity (qP) of the clones measured over 96 hours of culture. Each bar represent the average qP of biological triplicates measured in duplicate by ELISA ± SD. Significance was tested using 1-way ANOVA with $\alpha < 0,05$.

Recombinant protein titer was also evaluated to obtain the full picture of the phenotype of the clones. The analysis of titer by ELISA showed differences between the clones, mainly between Clone #6 and the two others (**Figure 4.16 A**). Clone #6 had no detectable levels of IgG at all in any of the samples. On the other hand, the mAb levels for both parental CHO-520F and Clone #5 were similar, despite the differences in viable cell density.

CHO-520F clone was able to grow to high densities and produce an average of 17,5 µg/mL of protein. Clone #5 was observed to grow to much lower densities but was still able to produce a similar amount of IgG, 18 µg/mL to clone CHO-520F, which might be due to a higher level of oxidative metabolism in Clone #5 compared to the parental. Specific productivity (qP) data (**Figure 4.16 B**) supports this hypothesis, as Clone #5 showed higher productivity (6.1 pg/cell/day) than Parental CHO-520F (4.7 pg/cell/day). Finally, Clone #6 demonstrated similar growth to the parent, but the IgG production of this clone could not be detected.

The results obtained in the phenotype showed differences in growth and recombinant protein titer, in which the different heteroplasmy variants found in the clones could potentially have a role. This will be further elaborated in the discussion.

4.3. Discussion

The work described in this section of the thesis aimed to investigate the levels of variance of heteroplasmy in individual CHO cell clones over time, the direction of these changes, and to check if these changes influenced the phenotype of the cells in a significant way. As described in the previous result section (4.2.2), the heteroplasmy within the 9 clones analysed (plus the parental samples) changed over time in some clones and specific positions, while some heteroplasmic variants were widely conserved in the clone panel showing very high frequencies, suggesting a shift towards homoplasy of those specific mutations has already taken place in these cells.

Most of the clones possessed the *m.1074C>T* non-coding variant in the mitochondrial $tRNA^{Val}$ gene, which had a very high frequency (higher than 50%). $tRNA^{Val}$ is not only a fundamental tRNA for the synthesis of the 13 mitochondrially encoded proteins, but also a main component of the large subunit of the mitochondrial ribosome (LSU) together with the mitochondrial 16S rRNA (*Brown et al., 2014; Hock, Robinson and Stroud, 2020)*.

Given the important role of 16S $tRNA^{Val,}$ it is likely that this mutation has either no significant effect on the mitochondria and for this reason has been maintained, or it confers some kind of advantage to the cells. Cases of known human mitochondrial diseases have been linked with heteroplasmic mutations in the mitochondrial $tRNA^{Val}$ sequence, such as an m.1616A>G mutation inducing MELAS (*Toyoshima, Tanaka and Satomi, 2017),* an m.1640 G>A mutation inducing similar symptoms to LHON, which became worse in different patients at increasing frequency of the mutation (*Fraidakis et al., 2014*) or an m.1606 G>A mutation reported to cause several neurological disorders due to the loss of stability of the $tRNA^{Val}$ stem hairpin structure (*Tiranti et al., 1998*). The defects in mitochondrial activity caused by these mutations are believed to be related to the secondary structure of the $tRNA^{Val}$, leading to loss of translational or structural activity. However, $tRNA^{Val}$ defects in the hairpin which impair mitochondrial protein production are known to lead to high levels of lactic acidosis and poor cell growth in cultured human cells (Hock, Robinson and Stroud, 2020), which is lethal for cells in culture. Two explanations for such an extended, conserved mutation in the panel of clones could be: the mutation is not located in a region critical for $tRNA^{Val}$ structure, meaning this mutation has no effect and thus allows passive accumulation over time in the cells. The second potential explanation is related to the role of $tRNA^{Val}$ in the mitochondrial ribosome LSU. The mitochondrial ribosome has been reported in humans to be able to recruit $tRNA^{Phe}$ instead of $tRNA^{Val}$ when $tRNA^{Val}$ levels are limiting. *(Chrzanowska-Lightowlers, Rorbach and Minczuk, 2017).* If the *m.1074C>T* non-coding variant had a negative effect on the structural role of $tRNA^{Val}$ in the ribosome, but not in its protein synthesis role, it is possible that the mitochondria would use another tRNA, such as $tRNA^{Phe}$, in its place, allowing the potentially defective mutation to accumulate without any pernicious effects to the cells. Interestingly, this mutation was not only limited to the clones derived from CHO-520F, as it was also reported in the sequencing performed by Kelly and collaborators (*Kelly et al., 2017*) in 17 different CHO clones from the CHO-K1 lineage, which means this non-coding variant has become a homoplasic mutation characteristic of this lineage, as it was conserved over the cloning process and 20 additional passages. However, whether the presence of this mutation has a positive, negative, or no effect on the metabolism of these CHO clones remains unknown.

Another heteroplasmic mutation observed in the majority of the clones was the *m.9704C>T* variant at mitochondrial gene NAD3 or ND3, which is part of the ND2

subcomplex of Complex I from the mitochondrial respiratory chain. While this mutation was not observed in the parental clone at passage 4 (P4), it must be noted that the parental P4 sample was not fully sequenced and half of the sequence was missing, including position 9074 where the mutation is located. Moreover, the presence of the mutation in most clones, added to the presence of the mutation at the parental P20 sample point to the likelihood of the mutation being present in the parental P4 sample, despite the lack of actual empirical data. The literature describes missense heteroplasmic variants in the NAD3 gene (as well as any mitochondrially encoded subunit of ND2 subcomplex) as the cause of several neurological diseases such as Leigh syndrome, LHON, and ataxia (*Wang et al., 2009; Vodopivec et al., 2016)*. Given that those mutations in the ND3 gene that have an impact on protein expression are normally caused by genetic diseases (*Hock, Robinson and Stroud, 2020)*, it was considered unlikely that a common mutation like the NAD3 missense, present in most CHO clones sequenced, had a frequency high enough to exert an influence over NAD3 protein expression. Moreover, the frequency of this particular *m.9704C>T* variant declined after 16 additional passages (P20) in all the clones in which it was present, indicating this mutation may be either negatively selected or subjected to random somatic heteroplasmic drift (*Barrett et al., 2020)*.

Both COX1 and COX2 were found to have heteroplasmic variants in their sequence. While COX 1 showed a wide variety of variants, most of them were clone specific and their impact on the metabolism was most likely neutral, as the mutations were not observed to change throughout the passages. The case of COX2 was different, as this gene sequence also showed a high number of variants in the clone panel, but most of them corresponded with the m.6996G>A initiator codon variant, predicted by SnpEff software to potentially impact protein expression, and with it, the metabolism of the clones containing this variant. Moreover, this variant was reported in the previous sequencing study (*Kelly et al., 2017*) to be present only in FGPC. As described in chapter 3, only FGPC clones possessed this variant, which weakly correlated with increased growth rate and maximum viable cell density. However, the exact influence of this mutation in the metabolism remained unclear. The results obtained in the sequencing experiments showed a tendency of this variant to decrease in frequency over the passages in most clones, except for clone #6 in which this variant frequency was slightly increased, which cast doubts about the m.6996G>A initiator codon variant being somehow beneficial for CHO metabolism, as such mutations will be more prone to be preserved over time. It is

possible that the potential positive effects of COX2 overexpression caused by this variant are somehow limited by the levels of expression of other proteins necessary for the assembly of Complex IV, some examples include COX20 and COX18, which are necessary for the insertion in the mitochondrial inner membrane (*Bourens et al., 2014; Bourens and Barrientos, 2017)*, the SCO1 and 2 assembly factors (*Morgada et al., 2015)* and the incorporation of more subunits, such as the aforementioned COX1 module, but also including other nuclear-encoded COX subunits such as COX5B, COX6C, and COX8A (*Vidoni et al., 2017; Hock, Robinson and Stroud, 2020)* and the corresponding COX 3 module.

Finally, CYTB was reported to be the mitochondrial protein-encoding gene with the most significant heteroplasmic mutations (*Kelly et al., 2017*). CYTB, together with the nuclearly encoded subunits CYC1 and UQCRFS1 are the only subunits in Complex III capable of participating in the electron transport chain (*Fernández-Vizarra and Zeviani, 2015)*. Therefore, mutations changing the expression or function of the CYTB gene could potentially exert a strong impact on the oxidative metabolism of the cell. The SnpEff analysis confirmed that CYTB also had the highest number of variants among all the genes in the clones derived from CHO-520F. Once again, the *m.14136delA* frameshift variant was the most extensive mutation in the panel, showing high frequencies in most clones. Additionally, this variant was mostly unchanged throughout 16 passages in most of the clones in which it was present, the only exception being clone #6, where it was present at a low frequency (5%) at P-4 and was not observed to be present at P-20. Changes in CYTB expression related to heteroplasmic mutations have been previously reported to depend significantly on the load of mutant DNA. The mutant variants of CYTB in human disease are known to cause mild symptoms, like exercise intolerance related to myopathy, when the load of mutant DNA is relatively low (*Legros et al., 2001; Sallevelt et al., 2016; Rugolo, Zanna and Ghelli, 2021)*. Other, more pernicious manifestations of CYTB mutations as human disease included classic LHON or encephalopathies (*Johns and Neufeld, 1991; Protasoni and Zeviani, 2021)*. Curiously, mutations in CYTB normally have their impact limited to muscle tissue (*Hock, Robinson and Stroud, 2020)*, while changes in other subunits of the complex, such as UQCC2, were reported to impact other tissues, like skin (*Tucker et al., 2013*). This may explain the apparent lack of impact of the different CYTB mutation frequencies in the different clones, as CHO cells did not originate from muscle tissue. The *m.14136delA* frameshift

variant was conserved in most of the clones derived from 520F, and the variations observed over the passages in both the parental clone and clones' number #5 and #6 are likely to correspond with random heteroplasmic drifting. Another variant, an *m.14378G>A* stop codon variant, was found to be quite extensive in the clones from the panel.

However, oppositely to the previously described variant, the *m.14378G>A* stop codon variant tended to diminish over time. Even at early passages, this variant frequency was greatly diminished for most of the clones, while remaining high in the parental clone. At P-20, the frequency of this variant was also observed to have diminished greatly in the parental sample, and disappeared completely from most clones, remaining only in clones #15 and #17. It may be that *m.14378G>A* has a higher potential to impact oxidative metabolism, as mutations that negatively impact the activity of Complex III in a significant way are known to also impact Complex I activity indirectly (*Acín-Pérez et al., 2004; Hock, Robinson and Stroud, 2020)*. Therefore, this mutation would likely end up being negatively selected over time (*Stewart and Chinnery, 2015; van den Ameele et al., 2020)*.

The growth, viability, and r-protein titer of clones #5 and #6 were evaluated after 20 passages to see if these phenotypes had changed and could be attributed to changes in heteroplasmy. Compared with the parental clone, CHO-520F, the maximum viable cell density achieved by these clones was diminished after 96 hours of culture and onwards, with clone #5 cell density being significantly lower than clone #6. The viability, however, was similar for the three samples evaluated. On the other hand, while the r-protein titer of CHO-520F and clone#5 was nearly identical, the specific productivity of clone #5 was higher than in the other clones. Additionally, clone #6 did not yield detectable levels of recombinant IgG. Clone #5 had the highest frequency of the three evaluated clones for the *m.9704C>T* variant in NAD3 gene (30%), and the *m.14136delA* frameshift variant in CYTB (40%), while clone #6 had the lowest frequencies for those two mutations, possessing only the m.6996G>A initiator codon variant in COX 2 but at 40% frequency, the highest among the panel. Perhaps the combination of variants in NAD3 and CYTB caused higher levels of oxidative metabolism in Clone #5 cells, increasing ROS generation but also allowing high and effective production of r-protein. Therefore, the reduction in max viable cell density observed in clone #5 and the corresponding increase

in specific productivity will be related to either oxidative stress or a drastic reduction of glycolysis in favor of OXPHOS. The parental CHO-520 showed lower frequencies for both the NAD3 and CYTB variants while performing better in culture than both clones #5 and #6, but had lower specific productivity than clone #5, which suggest the heteroplasmy differences observed in clone #5 may be increasing the oxidative metabolism of this clone at the expense of growth. However, this evidence is circumstantial and more evidence and insight into different clones will be needed to make a strong claim about the influence of heteroplasmy in these clones. Therefore, a relationship between changes in the phenotype of the different clones and changes in heteroplasmic frequencies could not be clearly established from these experiments.

However, these experiments were useful to determine the relative speed of the changes in the frequency of different heteroplasmic mutations, which overall were observed to change quite quickly, over only a few passages. The rapid changes observed in the heteroplasmy of these clones may reflect the heterogeneity observed in CHO cells in general. Currently, some researchers have been questioning the actual definition of CHO lineages, citing their high mutation rate, the ability to adapt, and the antiquity of some lineages (*Wurm and Wurm, 2021*). Taking into account the heteroplasmic mutations and the potential changes in phenotype that these mutations can generate could add a new layer of complexity to the definition of CHO cell 'lines'. The redistribution of heteroplasmy observed in the cells after a few passages show a certain degree of heterogeneity even within a population of the same clone. Such heterogeneity has been reported in the mitochondrial transcriptome at the cell-to-cell level (*Ogata et al., 2021)*. As the samples used in this study came from mixed populations of clones derived from 520F single cells using limited dilution cloning, the next natural step would be to generate new clones from one single cell using advanced systems such as Fluorescent Activated Cell Sorting (FACS) system and study the variability of the heteroplasmy within those cells. As the control of heteroplasmy constitutes nowadays a promising genetic engineering tool for both therapeutic and industrial processes *(Nissanka and Moraes, 2020*), understanding heteroplasmic drift and underlaying mechanism could become increasingly important, as, without the ability to predict the potential results of heteroplasmic drift, the heteroplasmic changes engineered into the cells may be quickly lost throughout a few passages.

CHAPTER 5

CHO CELL MITOCHONDRIAL ENGINEERING THROUGH NUCLEAR-ENCODED GENES.

5.1. Introduction.

Engineering CHO cell metabolism towards a more productive phenotype has been the subject of a considerable number of research studies in the last decade. As previously mentioned, this often involves changes in the culture conditions, such as media composition (*Ritacco, Wu and Khetan, 2018)* or temperature (*McHugh et al., 2020*) However, these changes in the culture conditions can potentially lead to the generation in culture of undesirable waste products, such as ammonia and lactate (*Karengera et al., 2018)* which may compromise the quality of the final product. Additionally, the culture conditions normally need to be tailored to each production cell line.

Another common approach to engineer CHO cell metabolism is genetic manipulation. Certain genes, normally related to the growth, metabolism, or viability of the cells are good candidates for engineering. Stable overexpression, silencing or knockdown of these genes can potentially generate new CHO cell lines with advantageous phenotypes towards recombinant protein production, such as increased protein titre (Templeton *et al.*, 2013; Kelly, Breen, *et al.*, 2015), extended lifespan (*Cost et al., 2010*) or faster growth (*Wlaschin and Hu, 2007)*.

This project focused on mitochondrial-related metabolic changes in CHO cells. However, the editing of mitochondrial genome-encoded genes has proven to be both challenging and expensive. Although some studies have described the editing of mitochondrial DNA using CRISPR/Cas9 as being possible (*Jo et al., 2015*), controversy remains as to whether it is possible to import RNAs successfully into the mitochondria, such as the gRNA needed by the CRISPR system to target specific sequences. A recent overview on the editing of mtDNA stated the following concerning results reported by *Jo et al 2015* (*Jo et al., 2015*): ``(they) fall well short of providing reasonable evidence that CRISPR/Cas9 technology can be used to edit the mitochondrial genome in mammalian systems´´ (*Gammage, Moraes and Minczuk, 2018*). Protein-only nucleases, such as Zinc-Finger nucleases (ZFN) (*Sandra R. Bacman, Sion L. Williams, Milena Pinto, 2014*) or TALE-nucleases (TALENS) (*Reddy et al., 2015*) have been successfully used for mtDNA editing, but these systems are both expensive and complicated to develop.

Therefore, in considering ways to engineer CHO mitochondrial metabolism, several genes known to influence mitochondrial metabolism were chosen as candidates to engineer CHO cells towards a more productive phenotype. All the genes chosen were nuclear-encoded and were previously reported in the literature to influence mitochondrial metabolism.

1.PGC1α:

Peroxisome proliferator-activated receptor-gamma coactivator-1 α (PGC1 α) is a member of the PGC1 family. Together with PGC1β, PGC1α is highly expressed in high-energy demanding tissues, like the heart, brain, skeletal muscle, and kidney (*Dillon, Rebelo and Moraes, 2012*). PGC1α is associated with mitochondrial respiration, activating nuclear respiratory factors, promoting fatty acid oxidation and inducing mitochondrial biogenesis under stress conditions (such as exercise or similar stimuli) (*Scarpulla, Vega and Kelly, 2012)*. For this reason, transfection of murine PGC1α gene was performed in selected CHO cells to explore whether its overexpression would increase oxidative metabolism and mitochondrial biogenesis and in doing so, potentially improve recombinant protein production.

2.DRP1: Dynamin-related Protein 1, also known as Dynamin-1-like protein, is involved in the process of mitochondrial fission. The DRP1 gene encodes a protein belonging to the superfamily of GTPases. It mediates membrane fission through the oligomerization of tubular structures that wrap around the fission site. (Elena Smirnova *et al.*, 2001). Overexpression of DRP1 promotes the mitochondrial fission process and prevents cellular ageing processes in young *Drosophila* cells (*Rana et al., 2017*). According to this study, the midlife induction of DRP1 prolonged the lifespan and healthspan of *Drosophila melanogaster* individuals. Additionally, mitochondrial metabolism was also observed to increase. However, it must be noted the same effect was not observed in older flies. According to this study, the overexpression of DRP1 promotes mitochondrial fission, which prevents the accumulation of mitochondrial damage caused by ROS, leading to a healthier phenotype. The increased mitochondria numbers also manifested in an increase in OXPHOS. In this work, we set out to examine whether overexpression of DRP1 in CHO cells would lead to increased mitochondrial fission. Theoretically, this increase should lead to an increase in viability and oxidative metabolism, as described above.

3.ANT1: ANT1 (Adenine Nucleotide Translocator isoform 1) is a gene member of the mitochondrial carrier subfamily, which is expressed in skeletal/heart muscle and brain. Its function is to translocate ADP from the cytoplasm into the mitochondrial matrix and ATP from the mitochondria matrix into the cytoplasm *(Brenner et al., 2011; Pan et al., 2015).* It is also known as SLC25A4 (Solute Carrier Family 25 member 4). Knock-down of ANT1 in skeletal muscle has been reported to lead to mitochondria hyperproliferation in diabetic mice (*Morrow et al., 2017)*. During this process Subunit V of the respiratory chain, ATPase, partially uncouples from the electron transport chain through not well-understood means, leading the cell to a constant maximum ETS state but partially inhibiting ATP production. In this study, we examined the potential applications of inhibiting ANT1 in CHO cells. The knockdown of ANT1 was theorized to produce an increase in mitochondria numbers and oxidative metabolism, which theoretically could support an increase in recombinant protein production. However, the partial uncoupling of the ATPase from the chain, observed in the previously described study, may cause instead of a limitation in ATP production and, therefore, a limitation of the recombinant protein production.

For the experiments described in this section, mouse PGC1α and DRP1 genes were transfected into the CHO cells using a pcDNA 3.1 plasmid as a vector. The plasmid included a Neomycin resistance gene as a selection marker. Transient transfections were performed as described in section 2.1.6. ANT1 knockdown was also performed as described in **section 2.1.6** using a siRNA designed specifically to target ANT1 mRNA.

5.2. Overexpression of PGC1a and DRP1 in CHO-K1-EPO cells.

CHO-K1-EPO is a subclone of CHO-K1 cells modified to express human Erythropoietin (EPO). EPO expression was maintained by incubating the cells with puromycin. CHO-K1-EPO cells were chosen for the overexpression of PGC1α and DRP1 due to their ability to express a therapeutic protein of interest. Both PGC1α and DRP1 were hypothesized to affect the mitochondrial population in the cells. Consequently, the effects of PGC1α and DRP1 on the oxidative metabolism of CHO-K1-EPO cells may benefit EPO production by the cells.

The first step of this experiment was the transfection of the plasmids. Briefly, 4 plasmids were transfected into CHO-K1-EPO cells. 500ng of plasmid per million cells were transfected using *Mirus Trans-it XT* kit according to the manufacturer's instruction (Section 2.1.6).

The following plasmids were transfected into the CHO-K1-EPO cells:

- pcDNA 3.1- PGC1α
- pcDNA 3.1- DRP1
- pcDNA 3.1 (control)
- pcDNA 3.1-eGFP
- No plasmid (Mirus only)

All the resulting CHO-K1-EPO cell lines were split to a density of $2x10^5$ cells/mL into three 50mL vented cap spin tubes in 5mL of media. Samples were taken every 24 hours approximately to measure growth and productivity.

5.2.1. Transient transfection of PGC1a and DRP1 impacts the growth of CHO-K1-EPO cells.

The evaluation was focused on growth, viability, and mitochondrial content. Samples were also taken to perform ELISA assay, to measure any changes in EPO expression, and qPCR assays to confirm the overexpression of the transfected genes.

Fluorescence was measured in the cells to evaluate the transfection efficiency of the plasmid, using GFP as a marker, and mitochondrial content. The process was done as described in Section 2.2.4.

The number of eGFP positive cells was used as a measurement of plasmid transfection efficiency into CHO-K1-EPO cells. Measuring this daily throughout the duration of the culture gave an indication of how long transgene overexpression could be expected to last and thus influence cell behaviour.

The initial transfection efficiency, after 24 hours, was observed to be approximately 86%. (**Figure 5.1**). The percentage of fluorescent cells decreased by 10-15% approximately every 24 hours till 96 hours, after which it decreased more abruptly. It should be noted that this decline can not only be attributed to the dilution of the plasmid due to cell division but also due to the short half-life of the eGFP protein.

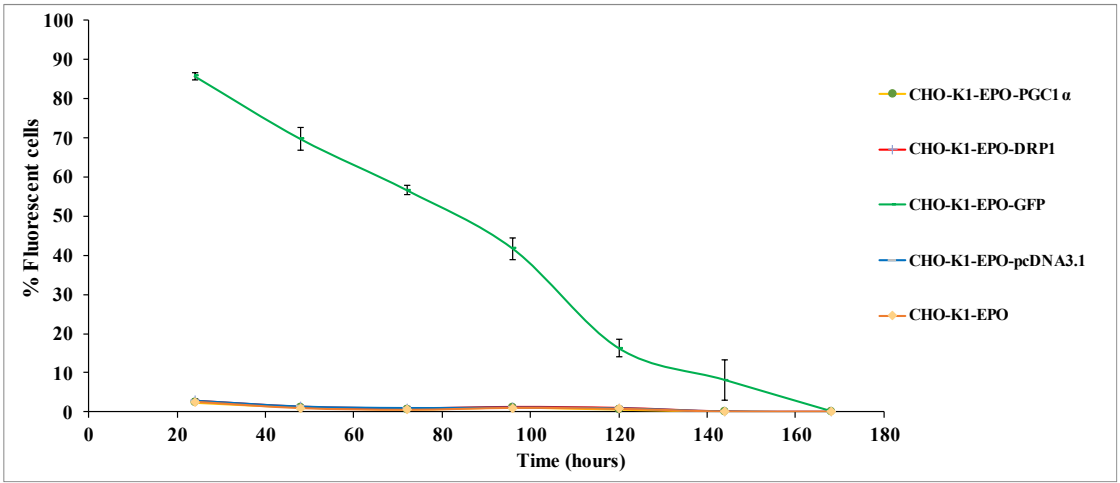

Figure 5. 1. Percent of fluorescent CHO-K1-EPO cells after transfection. Each line represent the average green fluorescence of biological triplicates measured in triplicate using Guava Easycyte cytometer and Expressplus software.

Growth profiles were similar across the panel of transfected CHO-K1-EPO cells. Cell growth was practically identical for the first 96 hours of culture. (**Figure 5.2 A**). However, after 120 hours of culture, both CHO-K1-EPO-PGC1α and CHO-K1-EPO-DRP1 showed higher viable cell densities ($2.7x10^6$ and $2.5\ x10^6$ cells/ml respectively) than control cell lines. Additionally, the DRP1 line showed a viable cell density of $3.1\ x10^6$ cells/mL after

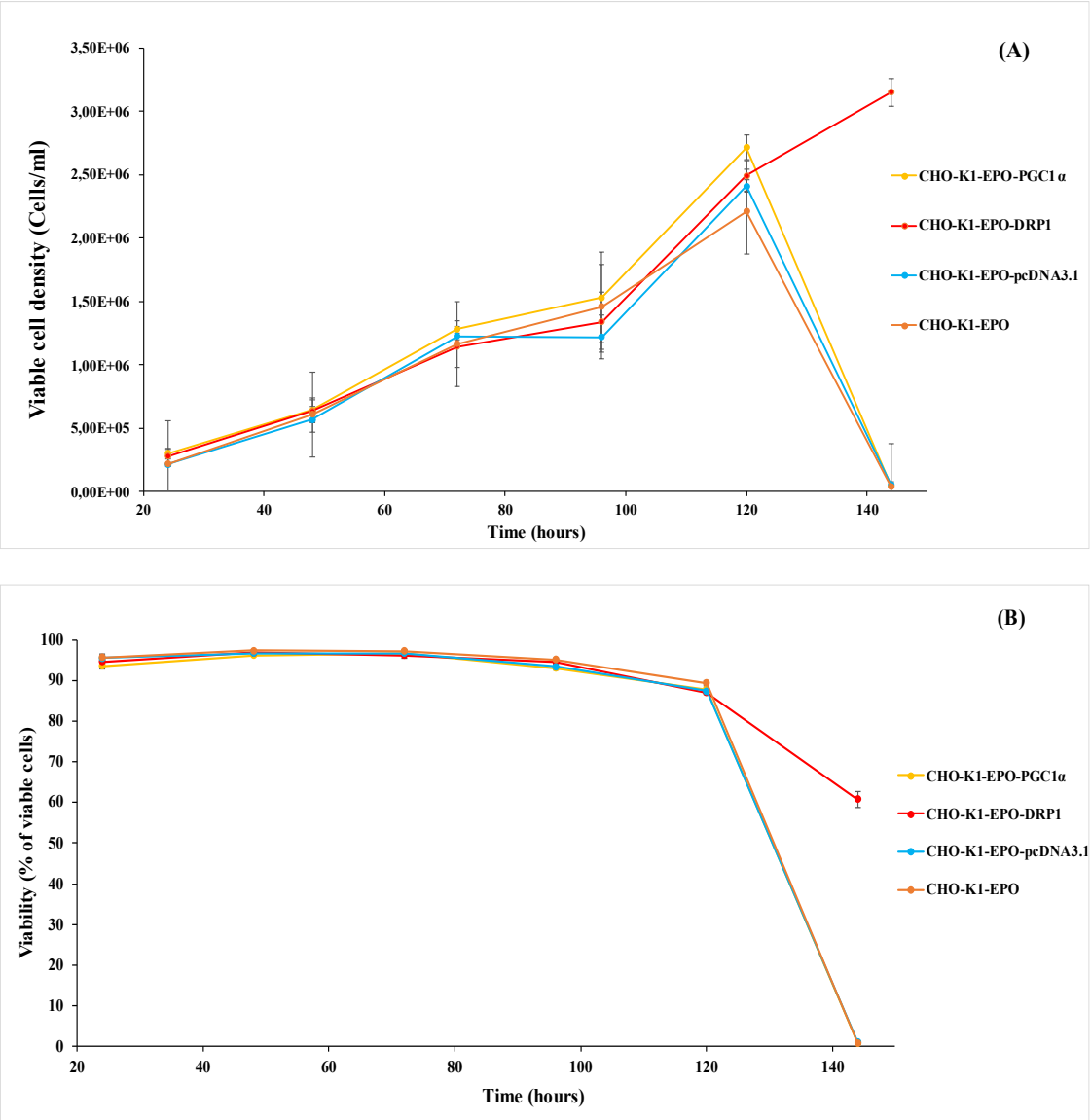

Figure 5. 2. (A) Viable cell density of the transiently transfected CHO cells over the course of 144 hours. Cells were cultured in suspension culture in 5mL of CHO-SFMII media. Each line represent the average viable cell density of biological triplicates measured in triplicates using Guava Easycite cytometer ± SD. Significance was tested using a one-way ANOVA with α <0,05.

(B) Viability of the transiently transfected CHO cells over the course of 144 hours. Cells were cultured in suspension culture in 5mL of CHO-SFMII media. Each line represent the average viability of biological triplicates measured in triplicates using Guava Easycite cytometer ± SD. Significance was tested using a one-way ANOVA with α <0,05.

144 hours of culture, much higher than the rest of the CHO-K1-EPO lines, which were observed to decline abruptly to very low numbers after 144 hours of culture (**Figure 5.2 B**). CHO-K1-EPO-DRP1 was also observed to decline, but at a much slower pace, with a decrease of 20% in viability observed after 144 hours of culture. These results suggested a potential small increase in growth caused by PGC1α overexpression and a potential increase in viability over time caused by DRP1 transfection.

Having seen this effect in transient transfection, the next step taken was to generate stably transfected CHO-K1-EPO cell lines.

5.2.2 Generation of CHO-K1-EPO cell lines stably overexpressing PGC1a and DRP1.

The cells were transfected and put under selective pressure in suspension culture by supplementing CHO-S-SFMII media with 500µg/ml of G418 (Neomycin) Neomycin selection acts by interfering with the function of 80S ribosome and inhibiting the protein synthesis of the cells, eventually leading to the death of the non-resistant cells. However, this proved to be slow and not very efficient in suspension culture, as the non-transfected control cells experienced a decrease in viability, but ultimately survive. Therefore, the cells were moved to attached culture in DMEM-F12 media supplemented with 5% FBS and 1mg/mL of G418 (Neomycin) for the selection process, which proved to be much more efficient, as the non-transfected control cells were observed to be completely eradicated by G418 after 10 days of culture. The cells were grown in attached culture for a total of 10 days. In this way the generation of stable CHO-K1-EPO-PGC1α, CHO-K1-EPO–DRP1, and CHO-K1-EPO-pcDNA 3.1 was successful. After the selection was complete, the CHO-K1-EPO -PGC1α, CHO-K1-EPO –DRP1, and CHO-K1-EPO -pcDNA 3.1 cell lines were moved back to suspension culture in CHO-S-SFMII media. The stock culture for these stable cell lines was from this point onwards permanently maintained with 500µg/mL of G418 to ensure stable selection. Cells were only moved to CHO-S-SFMII media without neomycin to prepare them for subsequent experiments, allowing them to grow for one week without Neomycin to prevent the drug from interfering with the experiments. Subsequently, a set of assays was performed to check the phenotypic effects of the transfection.

This set of assays included:

- A growth curve to check the effects of the overexpression of the genes of interest.
- Mitochondrial content analysis.
- An ELISA assay, to check the potential effects of the transfected genes on the recombinant protein titre.
- PCR and qPCR analysis to confirm the stable overexpression of PGC1α and DRP1.

5.2.3 Stable overexpression of DRP1 and PGC1a influences growth, viability, and mitochondrial content of CHO-K1-EPO cells.

An evaluation of the stably transfected CHO-K1-EPO cell lines was performed over 96 hours of culture. Culture flasks were set up as before. Evaluation of mitochondrial content was performed using Mitotracker Green™.

All the CHO-K1-EPO lines showed a similar growth pattern during the first 72 hours. (**Figure 5.3 A**). However, CHO-K1-EPO-PGC1α cell numbers started declining quicker than the other lines, with a small decline after 72 hours of incubation and a total and rapid decline after 96 hours. The rest of the CHO-K1-EPO lines doubled their numbers every 24 hours approximately before stabilizing between 2 x 10^6 and 2.5 x 10^6 cells/mL after 96 hours.

Similar differences were observed in viability, where CHO-K1-EPO-PGC1α cells showed an approximately 5% lower viability than the rest of CHO lines during the first 72 hours (**Figure 5.3 B**), experiencing a rapid decline in viability to nearly 0% beyond this point. This correlates with the previously observed decrease in CHO-K1-EPO-PGC1α viable cell density, suggesting a detrimental effect of PGC1α stable expression in CHO-K1 cells.

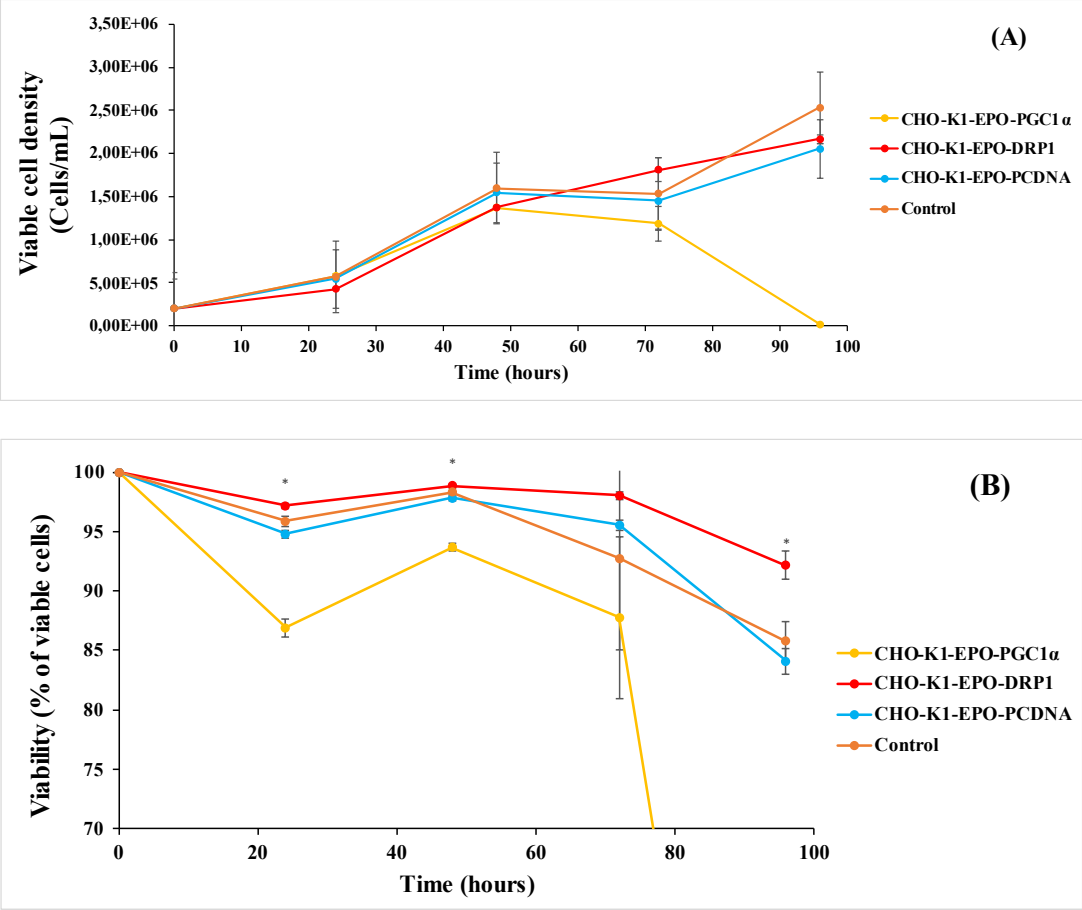

Figure 5. 3. (A) Viable cell density of the stably transfected CHO cells over the course of 144 hours. Cells were cultured in suspension culture in 5mL of CHO-SFMII media. Each line represent the average viable cell density of biological triplicates measured in triplicates using Guava Easycyte cytometer ± SD. Significance was tested using a one-way ANOVA with $\alpha < 0,05$ (* in the figure).

(B) Viability of the stably transfected CHO cells over the course of 144 hours. Cells were cultured in suspension culture in 5mL of CHO-SFMII media. Each line represent the average viability of biological triplicates measured in triplicates using Guava Easycyte cytometer ± SD. Significance was tested using a one-way ANOVA with $\alpha < 0,05$ (* in the figure).

This sharp decline in CHO-K1-EPO-PGC1α cells viability was observed repeatedly over time, both in the cell stock (under Neomycin selection) and while performing experiments. Conversely, the viability of the CHO-K1-DRP1 cells remained consistently higher than the rest of the CHO-K1 lines, despite the peak cell density being similar to the controls later in culture.

The final step consisted of a mitochondrial content analysis of the CHO-K1-EPO cell lines. $1x10^6$ cells were taken after 72 hours and incubated in CHO-S-SFMII media containing Mitotracker green dye. Fluorescence was then quantified on a Guava Easycyte cytometer and ExpressPlus software.

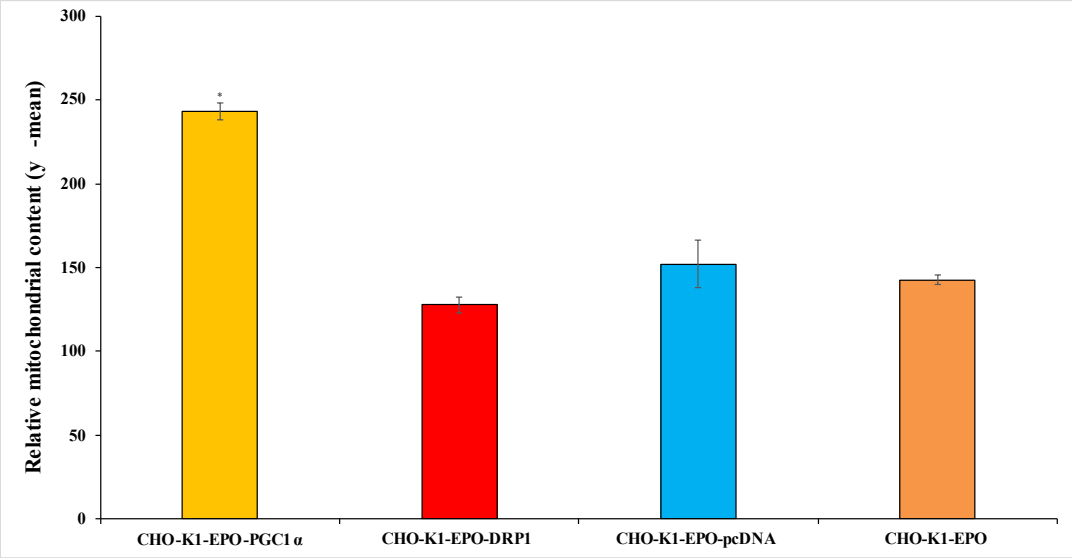

Figure 5. 4. Relative mitochondrial content of CHO clones after 72 hours of culture. Each bar represent the average mitochondrial content of biological triplicates measured with a flow cytometer (Guava Easycyte) after being incubated with Mitotracker Green dye. Significance was tested using a one-way ANOVA with α <0,05 (* in the figure).

The results of the assay revealed both CHO-K1-EPO-pcDNA 3.1 and CHO-K1-EPO cells showed similar mitochondrial content (**Figure 5.4**). This was expected as, essentially, the only difference between them is the presence of a pcDNA 3.1 plasmid transfected in CHO-K1-EPO-pcDNA 3.1. Therefore, these are both considered control cell lines, and their behaviour was expected to be similar.

CHO-K1-EPO-PGC1α was observed to have higher mitochondrial content than CHO-K1-EPO-pcDNA 3.1 and CHO-K1-EPO. The average fluorescence score for CHO-K1-EPO-PGC1α was approximately 250, while the average signal for both CHO-K1-EPO-

pcDNA 3.1 and CHO-K1-EPO was approximately 150. This result demonstrated that CHO-K1-EPO-PGC1α had significantly higher mitochondrial content than any other of the CHO K1 lines. Finally, CHO-K1-EPO-DRP1 showed slightly lower mitochondrial content than the control cell lines. The average fluorescence score for CHO-K1-EPO-DRP1 was 120, slightly lower than the control cell lines value.

Next, PCR and qPCR experiments were performed to confirm the overexpression of both PGC1α and DRP1 genes into CHO-K1-EPO cells. For this purpose, mRNA was extracted from the cells, digested with DNase I to avoid DNA contamination, and reverse transcribed to cDNA. Samples were then amplified and run on a gel. The first PCR assay was performed in samples obtained from CHO-K1-EPO- PGC1α and CHO-K1-EPO-pcDNA 3.1. cells. Oddly, PGC1α expression was not detected in any of the CHO-K1-EPO-PGC1α samples (**Supplementary Figure 2**). Subsequently, it was concluded that PGC1α gene expression was lost in these CHO-K1-EPO- PGC1α cells, which had somehow retained the Neomycin resistance gene included in the plasmid.

DRP1 expression was measured in CHO-K1-EPO- DRP1 and CHO-K1-EPO-pcDNA 3.1. A band of the expected size appeared in the positive control (pcDNA 3.1-DRP1 plasmid) samples, proving the primers were effective and specific. (**Supplementary Figure 3**).

The results obtained for growth, viability, and mitochondrial content seemed to differ from what was observed in transiently transfected clones, especially in the case of CHO-K1-EPO-PGC1α. However, the oscillations observed in viability and the subsequent fast decline in both cell density and viability may be explained by the higher active mitochondria number. The high mitochondria numbers and, consequently, the increase in oxidative metabolism may lead to the fast accumulation of Reactive Oxygen Species (ROS), which are detrimental for the cell integrity, potentially leading to a decrease in viability.

The slight decrease in active mitochondria content observed in CHO-K1-EPO-DRP1 cells can also potentially explain the slight increase in viability observed. DRP1 promotes mitochondrial fission, leading to an increase in mitochondrial numbers and delaying ageing related to the accumulation of ROS. However, this may also lead to the accumulation of smaller, non-functional mitochondria, which will not be stained by Mitotracker dye, which can only permeate and become fluorescent in active

mitochondria. The loss of active mitochondria and mitochondrial fission itself will then lead to a decrease in ROS accumulation, allowing the cells to remain viable for a longer time.

The PCR results confirmed the expression of DRP1 in the CHO-K1-EPO-DRP1 cells. However, PCG1α was not detected in CHO-K1-PCG1α cells. This led to us generating new CHO-K1-PCG1α cells.

5.2.4 Generation of new CHO-K1-EPO-PGC1α cells to ensure the stable overexpression of PGC1α.

CHO-K1-EPO-PGC1α cells previously generated were suspected to not be overexpressing the PGC1α gene after the previously described PCR experiment. The point at which these cells may have lost the overexpression of PGC1α remained unclear. For this reason, a decision was made to generate a brand-new CHO-K1-EPO- PGC1α cell line, ensuring the overexpression of the PGC1α gene for future experiments.

The process used was once again the Mirus Trans-IT XT system as previously described, following the manufacturer's instructions.CHO-K1-EPO cells were once again transfected with pcDNA 3.1-PGC1α plasmid. To avoid confusion with the old CHO-K1-EPO cell line, the new CHO-K1-EPO cell line was assigned a new name: CHO-K1-EPO -PGC1α-AT#4.

After 72 hours of culture, cells samples were collected to perform PCR experiments in the newly transiently transfected CHO-K1-EPO cells. A qPCR experiment was then performed using the cDNA samples obtained from the transiently transfected CHO-K1-EPO cells.

The expression levels of the PGC1α gene detected in CHO-K1-EPO-PGC1α-AT#4 was much higher than the expression detected in CHO-K1-EPO-pcDNA 3.1, which was near zero. (**Figure 5.5**).

These results demonstrated the overexpression of PGC1α in the newly transfected CHO-K1-EPO-PGC1α-AT#4 cells. Subsequently, CHO-K1-EPO-PGC1α-AT#4 was chosen to be the subject of future experiments once stable CHO-K1-EPO -PGC1α-AT#4 cells are generated.

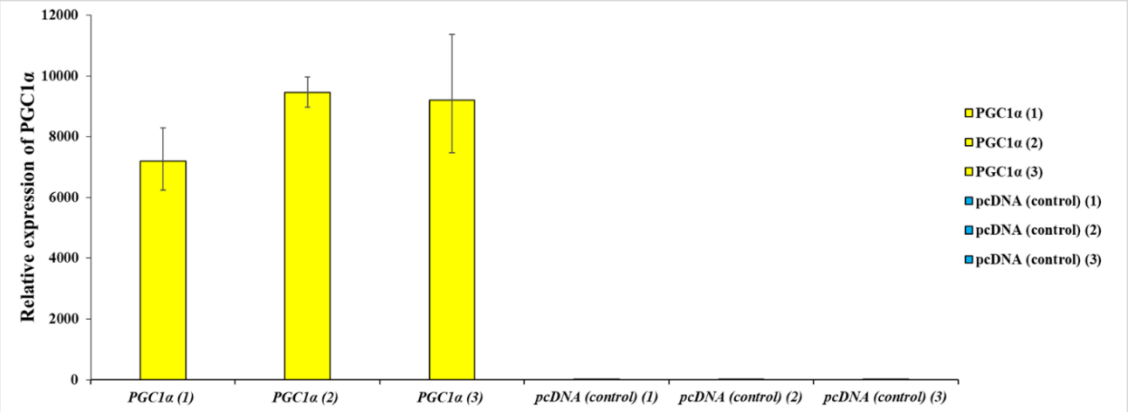

Figure 5. 5. Relative expression PGC1α in the transfected CHO cells. Each bar represents the RQ for given sample, calculated using the 2ΔΔcT formula. For each sample, biological triplicates were measured in triplicates.

With the overexpression of PGC1α confirmed in CHO-K1-EPO-PGC1α-AT#4, generation of stable CHO-K1-EPO-PGC1α-AT#4 cells was next to be performed as described in section 2.4.3 from the Materials and Methods section of this study. After the stable clones were generated, growth profiles were once again investigated.

5.2.5 Stable overexpression of DRP1 leads to extended viability in CHO-K1-EPO cells in CHO-S-SFMII media, but not in CHO-BalanCD media.

The following stable CHO-K1-EPO cell lines were grown in two different culture media:

- CHO-K1-EPO-PGC1α-AT#4
- CHO-K1-EPO-DRP1
- CHO-K1-EPO-pcDNA 3.1

The cells were grown in CHO-S-SFMII media and CHO-BalanCD media (which contains high glucose concentration) to test the effects of PGC1α and DRP1 in the growth and viability of the cells when exposed to different growth media.

Due to the different characteristics of the culture media, the growth was evaluated for different periods. Cells cultured in CHO-S-SFMII media were grown for 120 hours. After this time, the viability of CHO-K1-EPO cells suffered a drastic decline and the experiment was terminated (**Figure 5.6**). However, CHO-BalanCD media is designed to support cell viability for a longer time. For this reason, cells cultured in BalanCD were grown for a total time of 264 hours.

CHO-K1-EPO-PGC1α-AT#4 and CHO-K1-EPO-pcDNA 3.1 showed a very similar growth pattern when grown in CHO-S-SFMII media for 120 hours. (**Figure 5.6 A**). Meanwhile, CHO-K1-EPO-DPR1 showed a slightly diminished growth when compared to the other two clones during the first 48 hours, in which the viable cell density was around $1{,}35 \times 10^6$ cells/mL for CHO-K1-EPO-DPR1 while the other lines reached densities of approximately $1{,}55 \times 10^6$ cells/mL. CHO-K1-EPO-PGC1α-AT#4 cells behaved similarly to the control over the culture time. CHO-K1-EPO-DPR1 cell proliferation stopped at 72 hours and the viable cell density remained stable after that.

After 72 hours of culture, CHO-K1-EPO-PGC1α-AT#4 cells behaved similarly to CHO-K1-EPO-pcDNA 3.1 over the culture time. CHO-K1-EPO-DPR1 cell proliferation stopped at 72 hours and the viable cell density remained steady for the duration of the culture.

The viability was observed to be similar in all CHO-K1-EPO lines for the first 96 hours of culture, after which both CHO-K1-EPO-PGC1α-AT#4 and CHO-K1-EPO-pcDNA 3.1 cells experience a drastic decrease in viability while CHO-K1-EPO-DPR1 cells remained more viable, presumably due to its lower viable cell density (**Figure 5.6 B).**

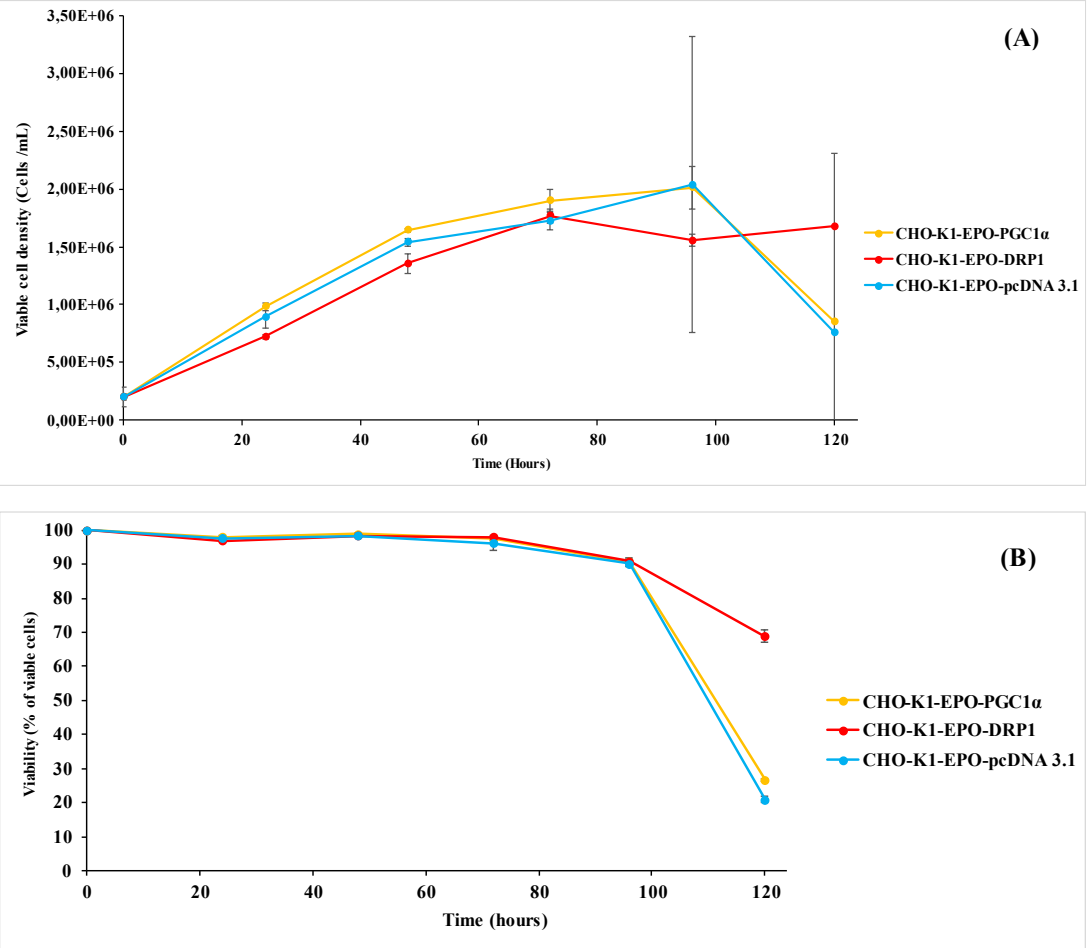

Figure 5. 6. (A) Viable cell density of the stably transfected CHO cells over the course of 120 hours. Cells were cultured in suspension culture in 5mL of CHO-SFMII media. Each line represent the average viable cell density of biological triplicates measured in triplicates using Guava Easycyte cytometer ± SD. Significance was tested using a one-way ANOVA with $\alpha < 0,05$ and highlighted with * in the figure.

(B) Viability of the stably transfected CHO cells over the course of 120 hours. Cells were cultured in suspension culture in 5mL of CHO-SFMII media. Each line represent the average viability of biological triplicates measured in triplicates using Guava Easycyte cytometer ± SD. Significance was tested using a one-way ANOVA with $\alpha < 0,05$ and highlighted with * in the figure.

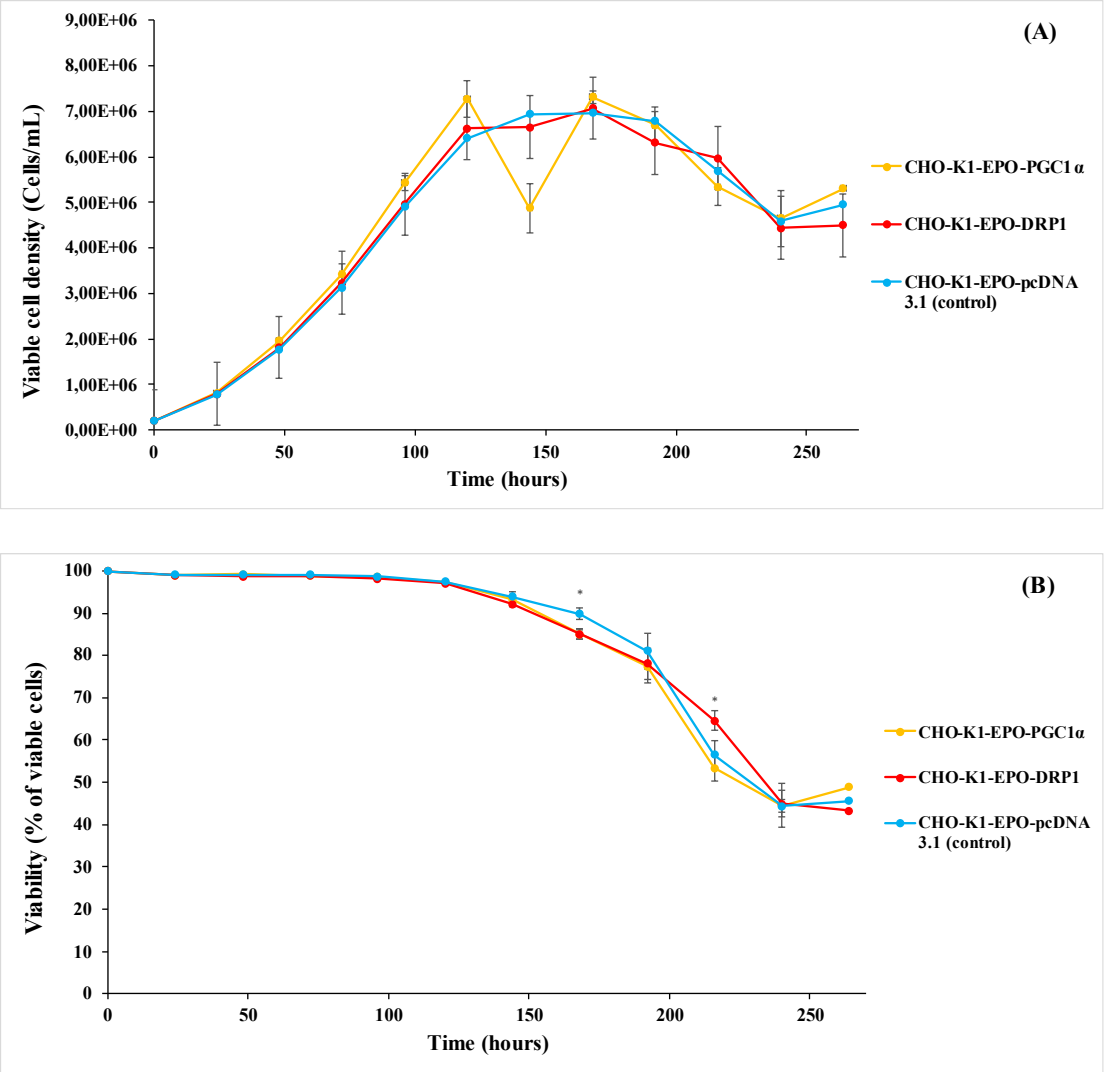

Figure 5. 7. (A) Viable cell density of the stably transfected CHO cells over the course of 264 hours. Cells were cultured in suspension culture in 5mL of CHO BalanCD media. Each line represent the average viable cell density of biological triplicates measured in triplicates using Guava Easycyte cytometer ± SD. Significance was tested using a one-way ANOVA with $\alpha < 0,05$ and highlighted with * in the figure.

(B) Viability of the stably transfected CHO cells over the course of 264 hours. Cells were cultured in suspension culture in 5mL of CHO BalanCD media. Each line represent the average viability of biological triplicates measured in triplicates using Guava Easycyte cytometer ± SD. Significance was tested using a one-way ANOVA with $\alpha < 0,05$ and highlighted with * in the figure.

Therefore, results demonstrated the DRP1 line to grow to lower densities, but maintain higher viability over time, than the other cell lines when grown in CHO-S-SFMII media. The PGC1α line and the control (pcDNA 3.1) line demonstrated similar behaviour in both growth and viability over time in the same growth media.

The stable transfected CHO-K1-EPO cell lines were also grown in CHO-BalanCD culture media to check if more differences between the different transfected CHO-K1 lines arise in different conditions. The analysis of the growth pattern and the viability of the cells of all CHO-K1-EPO cell lines cultures in BalanCD media showed both be almost identical for all the lines over 264 hours of culture. (**Figure 5.7**)

During this growth curve performance, samples were collected to perform qPCR and ELISA assays to confirm the overexpression of PGC1α and DRP1 in the stable cell lines and to compare the effects of the genes in the recombinant protein titre.

A new qPCR assay was performed to compare the levels of expression of both PGC1α and DRP1 genes in the stably transfected CHO-K1-EPO cells.

CHO-K1-EPO-PGC1α-AT#4 samples showed considerably higher levels of PGC1α expression than CHO-K1-EPO-Empty (pcDNA 3.1) samples. (**Figure 5.8 A**) The difference in expression levels observed amounted to approximately 25-fold, which is not as big as the difference observed in the transient version of CHO-K1-EPO-PGC1α-AT#4, which demonstrated expression levels 6000 times higher than the control sample. Still, stable overexpression was confirmed by this result, PGC1α was observed to be 25 times more expressed in CHO-K1-EPO-PGC1α-AT#4 than in CHO-K1-EPO-Empty

In contrast, only a small (2-fold) increase in DRP1 expression was observed in CHO-K1-DRP1 when compared to CHO-K1-EPO-Empty (pcDNA 3.1) (**Figure 5.8 B**). However, this difference was determined to be statistically significant. Endogenous DRP1 expression was high in CHO-K1-EPO cells. Therefore, transfecting additional DRP1 may be the reason for the subtle effect in the transcript levels, as measured.

In summary, the results demonstrated successful overexpression of PGC1α, but overexpression of DRP1 caused a significant, yet modest increase of DRP1 transcript levels. To further explore this qPCR assays were performed to quantify genes that are either downstream from or related to both PGC1α and DRP1.

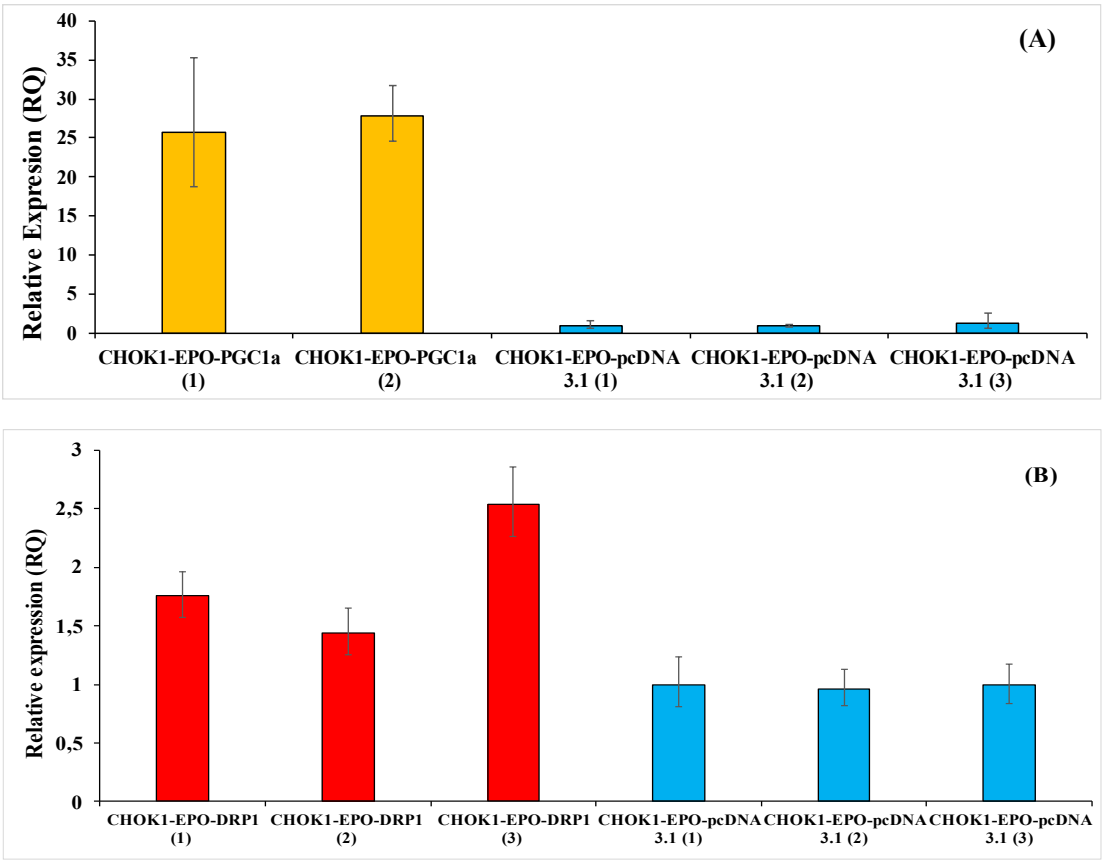

Figure 5. 8. (A) Relative expression of PGC1α in the transfected CHO cells (CHO-K1-EPO-PGC1α-AT#4). Each bar represents the RQ for given sample, calculated using the 2ΔΔcT formula. For each sample, biological triplicates were measured in triplicates. Numbers in brackets represent these different cell populations.

(B) Relative expression of DRP1 α in the transfected CHO cells. Each bar represents the RQ for given sample, calculated using the 2ΔΔcT formula. For each sample, biological triplicates were measured in triplicates. Numbers in brackets represent these different cell populations.

Several genes were selected for this set of assays. For PGC1α, both genes downstream and genes whose products interact with PGC1α were chosen. The transcript levels of the selected genes did not change significantly despite the overexpression of PGC1α (**Figure 5.9**). PPARD, NRF1, and TFAM transcript levels in the CHO-K1-EPO-PGC1α line were nearly identical, with no significant differences to the transcript levels found in CHO-K1-EPO-pcDNA 3.1, the control cell line.

This result might explain why no differences were observed between the CHO-K1-EPO-PGC1α line during the previous assays. The overexpression of PGC1α by itself did not seem to alter significantly the levels of related genes, which may mean there is another limiting step in the gene network controlled by PGC1α, currently unknown. This will be discussed in detail in the discussion section of this chapter.

Similarly, MNF1 and MNF2, genes downstream DRP1, were measured aiming to clarify if there was significant overexpression of DRP1 and, if this overexpression was exerting an influence over the cells.

Significant differences in the levels of both MNF1 and MNF2 were not observed between the cell lines CHO-K1-EPO-DRP1 and CHO-K1-EPO-pcDNA 3.1 (**Figure 5.10**). This result seemed to confirm that either the overexpression of DRP1 was not successfully achieved or rather the endogenous levels of DRP1 were already high enough to perform their maximum function and nothing further was achieved with the overexpression.

To conclude, ELISA assays were performed to compare the recombinant protein production of the different cell lines.

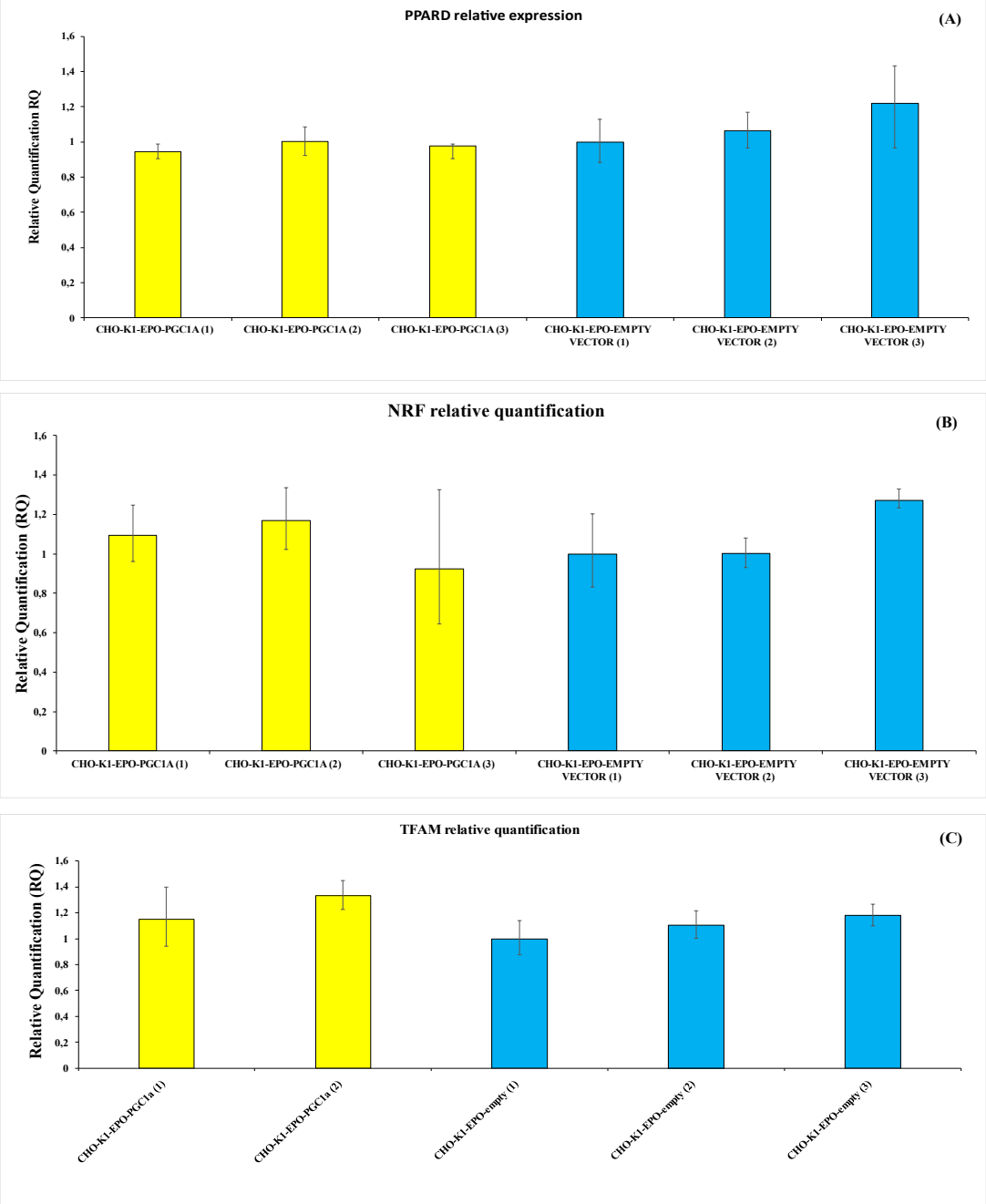

Figure 5. 9. (A) Relative expression of PPARD in the transfected CHO cells. Each bar represents the RQ for given sample, calculated using the 2ΔΔcT formula. For each sample, biological triplicates were measured in triplicates.

(B) Relative expression of NRF in the transfected CHO cells. Each bar represents the RQ for given sample, calculated using the 2ΔΔcT formula. For each sample, biological triplicates were measured in triplicates.

(C) Relative expression of TFAM in the transfected CHO cells. Each bar represents the RQ for given sample, calculated using the 2ΔΔcT formula. For each sample, biological triplicates were measured in triplicates.

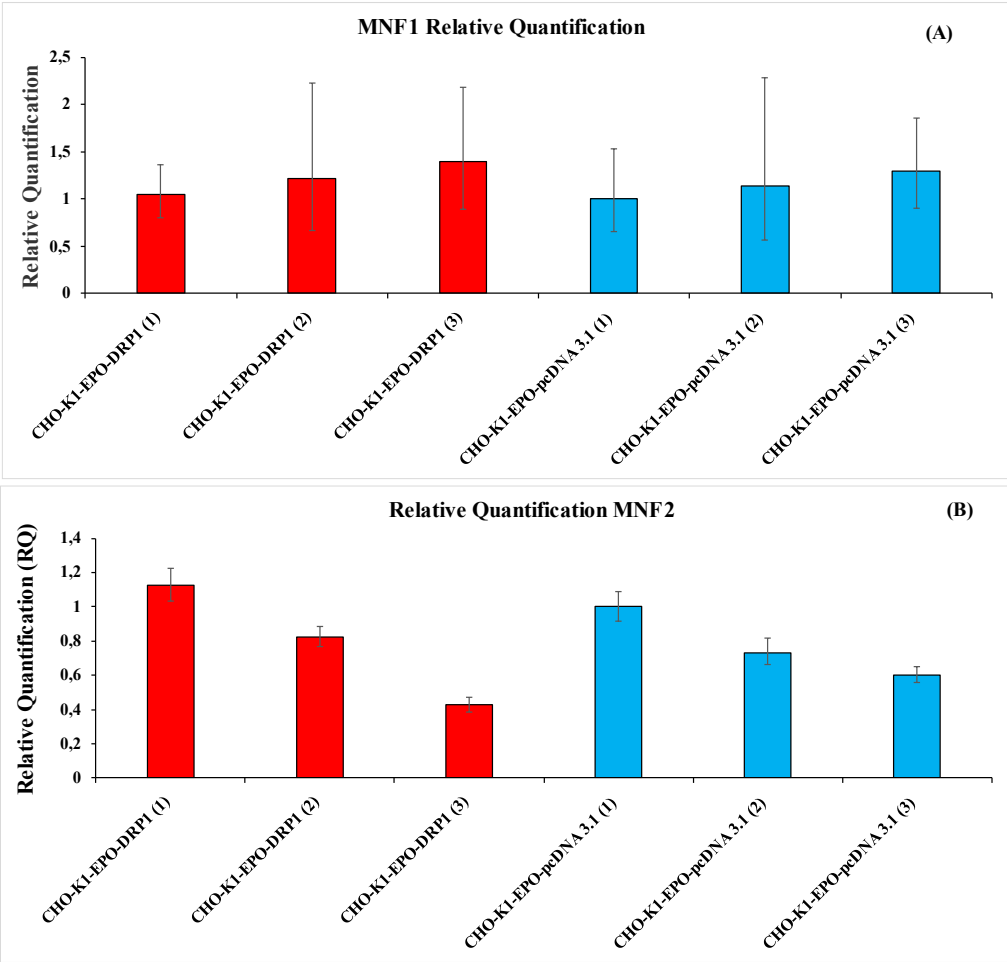

Figure 5. 10. (A) Relative expression of MNF1 in the transfected CHO cells. Each bar represents the RQ for given sample, calculated using the 2ΔΔcT formula. For each sample, biological triplicates were measured in triplicates.

(B) Relative expression of MNF2 in the transfected CHO cells. Each bar represents the RQ for given sample, calculated using the 2ΔΔcT formula. For each sample, biological triplicates were measured in triplicates.

5.2.6. PGC1α and DRP1 overexpression induce changes in the recombinant protein titre of transfected CHO-K1-EPO cells.

The main goal of this project was to increase the recombinant protein titre of CHO cells. For this purpose, CHO-K1-EPO cells were transfected with different mitochondria-related genes, aiming to engineer the mitochondrial metabolism of the cells by overexpressing genes that promote mitochondrial biogenesis, fission, and oxidative metabolism. An ELISA was performed to check if EPO yield was affected by this increase or decrease, correspondingly, in mitochondrial activity, which may translate into a higher recombinant protein titre from CHO-K1 cells. The recombinant protein titre was evaluated by using a sandwich EPO ELISA. Samples were collected from two different media (CHO-S-SFMII and CHO-BalanCD) to check potential differences in the recombinant protein titre of the transfected clones when grown in different cultures. The recombinant protein titre was measured by using a Sandwich ELISA using two primary antibodies, following the manufacturer's instructions.

The assay revealed the EPO titre to be similar in PGC1α-AT#4 and DRP1 (approximately 17 µg/mL for both), but significantly higher in pcDNA 3.1-Plasmid (NC), when cultured in CHO-S-SFMII. (**Figure 5.11 A)**. As expected, the protein titre was significantly lower in BalanCD media compared with the samples taken from cells cultured in CHO-S-SFMII. It must be mentioned that, despite these differences, the PGC1α and DRP1 lines maintained a similar recombinant protein titre, approximately 7 µg/mL, regardless of the media used in the culture, while the pcDNA 3.1 control line demonstrated a dramatic decrease in recombinant protein titre when cultured in BalanCD, tending to almost 0. The calculation of Specific Productivity (qP) for these cells after 96 hours of culture (**Figure 5.11 B)** confirmed the previous observations.

The ELISA assay results suggested that the transfection of both PGC1α and DRP1 could have hindered the recombinant protein production. As PGC1α-AT#4 was previously observed to grow to higher densities than the other cell lines during the first stages of the culture, this could translate into lower protein production, as resources are diverted to growth.

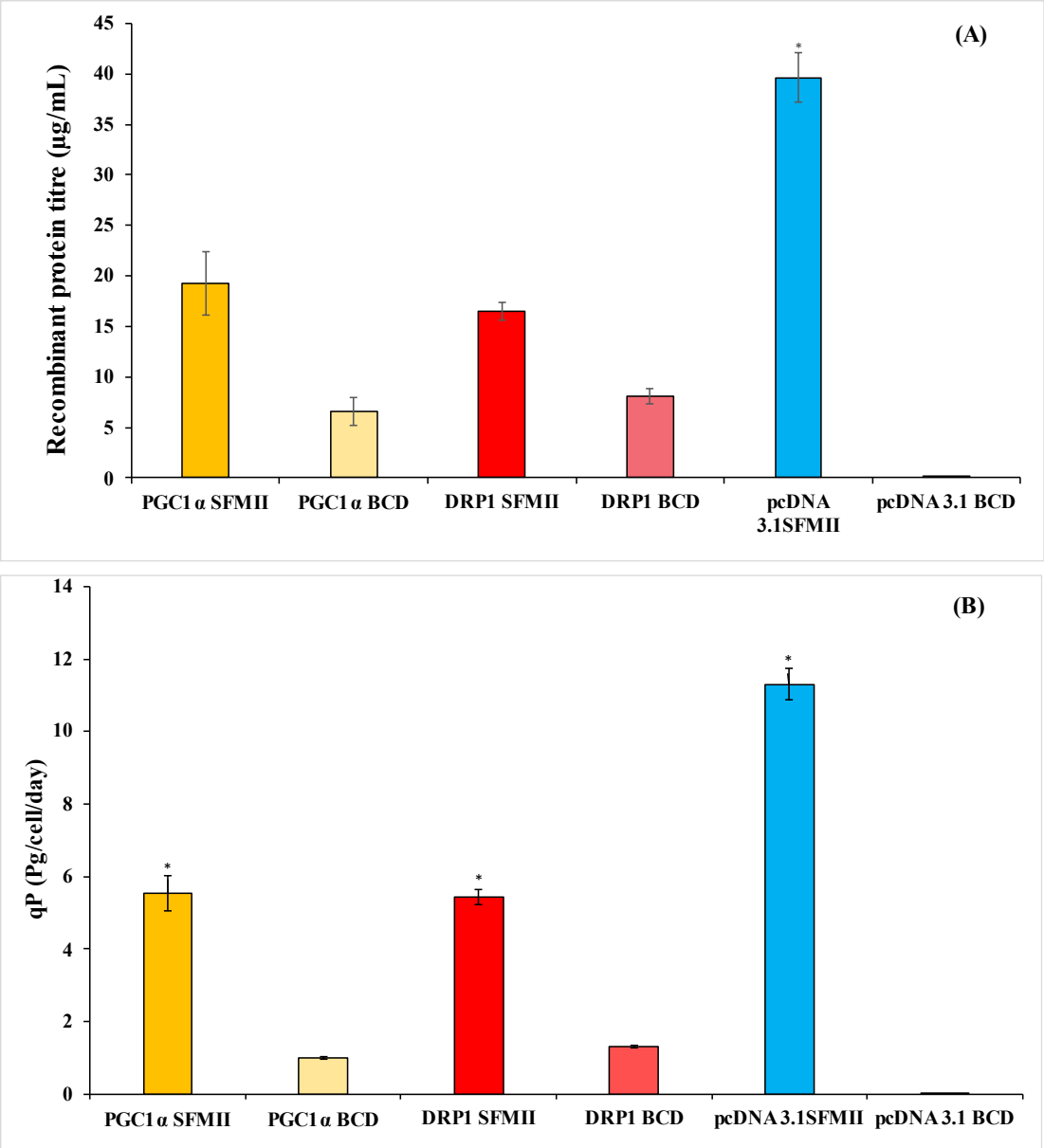

Figure 5. 11. (A) Protein titre from stably transfected CHO-K1 cells. Each bar represent the average protein titre of biological triplicates measured in duplicate by ELISA ± SD. Significance was tested using 1-way ANOVA with $\alpha < 0,05$ and highlighted with * in the figure.

(B) Specific productivity (qP) from stably transfected CHO-K1 cells. Each bar represent the average qP of biological triplicates measured in duplicate by ELISA ± SD. Significance was tested using 1-way ANOVA with $\alpha < 0,05$ and highlighted with * in the figure.

In the case of DRP1, the increased viability observed during the late stages of culture in SFMII media could be related to the lower recombinant protein. However, it is important to remember that the overexpression of DRP1 has not been proven in these cells.

To finish this set of experiments, a different approach to engineering the mitochondria was taken: instead of overexpressing a mitochondrial-related gene, the gene in question was be silenced using a siRNA. This last experiment is described in the next section.

5.3. ANT1 silencing in CHO-K1-EPO cells.

ANT1 gene knockdown was performed in CHO-K1-EPO cells by using a siRNA designed specifically to target ANT1 miRNA.

Briefly, siRNA was introduced into the cell by using Mirus Trans-IT transit according to the manufacturer's instructions. 1 million cells were plated in 1mL of media containing the siRNA complexed with Mirus and incubated at a shaker incubation at 37ºC for 48 hours.

During the transfection process, two more siRNA were transfected into CHO-K1-EPO cells:

- siRNA-eGFP: this siRNA targets eGFP miRNA. However, CHO-K1-EPO cells do not include that gene naturally. Therefore, this siRNA acted as a negative control sample.
- siRNA-VCP: This siRNA silences the expression of a critical component of the cells, which eventually kills them. Therefore, this siRNA acted as a positive control, as the cells successfully transfected with this siRNA will start dying about 48 hours after the transfection.

After this, samples were collected to perform PCR and qPCR and confirm the silencing of the ANT1 gene, and cDNA was produced as described in Section 2.2. ANT1 primers were successful in amplifying the ANT1 gene in the control (CHO-K1-EPO-sieGP) cells, while no band was observed in the ANT1 (-) sample. (**Supplementary Figure 4**). The transfection of siRNA-VCP in the cells was successful, quickly reducing the cell viability levels. No RNA was extracted from the CHO-K1-EPO-siVCP cells.

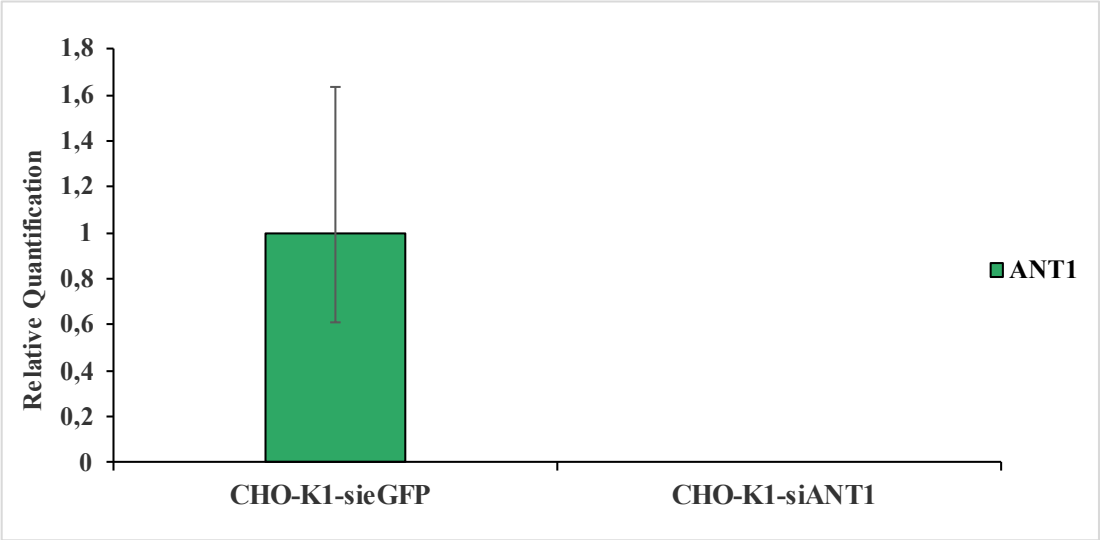

Figure 5. 12. (A) Relative expression of ANT1 in the CHO cells transfected with siRNA. Each bar represents the RQ for given sample, calculated using the 2ΔΔcT formula. For each sample, biological triplicates were measured in triplicates.

qPCR was performed to quantify the downregulation of ANT1 by the corresponding siRNA. This analysis confirmed the silencing of ANT1 in CHO-K1-EPO cells, as ANT1 was only amplified in the control sample transfected with siRNA against eGFP (**Figure 5.12**). The results showed that the ANT1 gene had a very low expression level in CHO-K1-EPO cells even before the transfection of the siRNA.

With the downregulation of ANT1 demonstrated in the CHO-K1-EPO-siANT1 cells, the next step taken was to culture the cells to observe any differences in cell growth that could be related to ANT1 dysregulation.

ANT1 downregulation has been reported in the literature to lead to an uncoupling of ATP synthesis from the electron transport chain in transgenic mice, making the cells engage in a ``wasteful´´ incomplete oxidative phosphorylation process, which produces no ATP and quickly depletes the available glucose (*Morrow et al., 2017)*. Therefore, an experiment to check if the ANT1 downregulation in CHO cells could change both metabolism and/or recombinant protein titre of the cells was performed. The ANT1-depleted cells grew more rapidly and reached a higher maximum cell density than the cells transfected with the control siRNA, reaching densities of 1,8x10 ^{6} cells/mL in 72 hours (**Figure 5.13 A**).

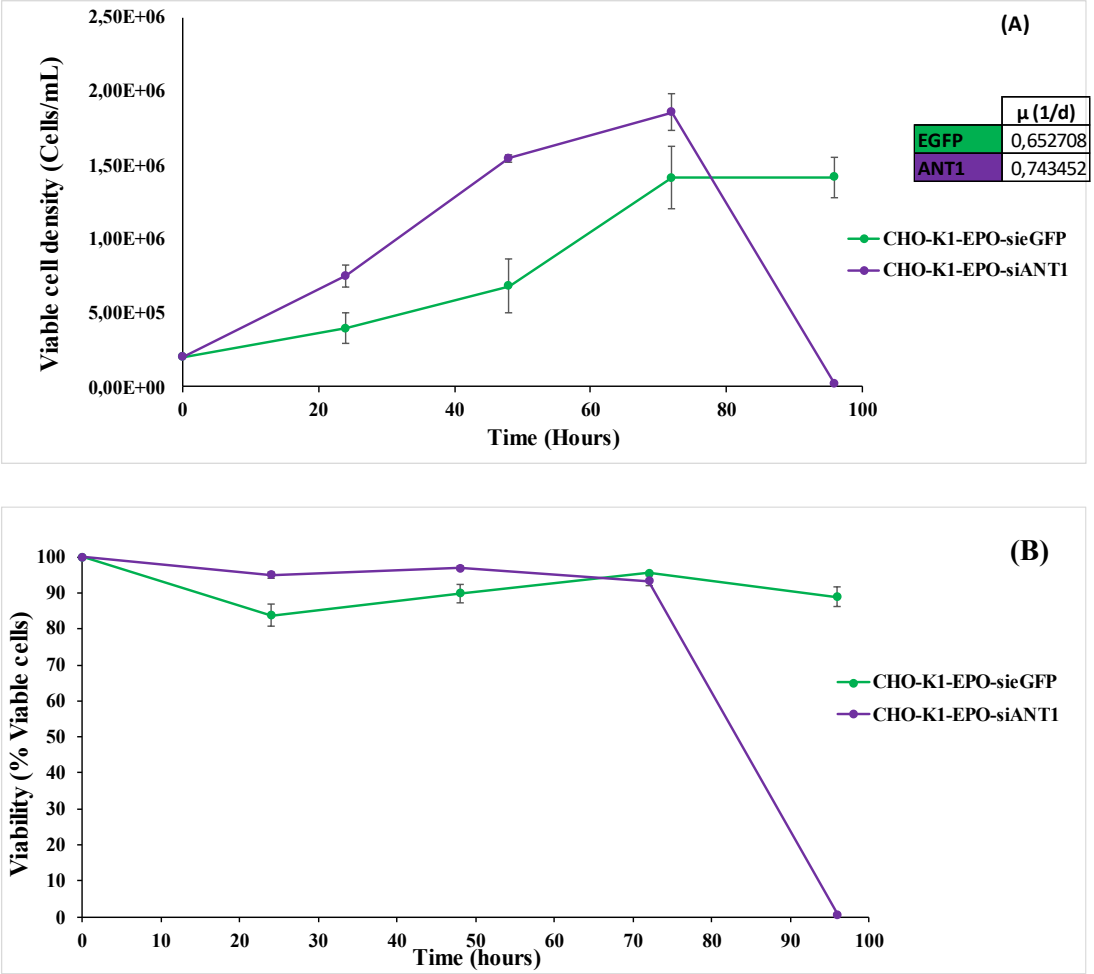

Figure 5. 13. (A) Viable cell density of the siRNA transfected CHO cells over the course of 96 hours. Cells were cultured in suspension culture in 5mL of CHO SFMII media. Each line represent the average viable cell density of biological triplicates measured in triplicates using Guava Easycyte cytometer ± SD. Significance was tested using a one-way ANOVA with α <0,05 and highlighted with * in the figure.

(B) Viability of the siRNA transfected CHO cells over the course of 96 hours. Cells were cultured in suspension culture in 5mL of CHO SFMII media. Each line represent the average viability of biological triplicates measured in triplicates using Guava Easycyte cytometer ± SD. Significance was tested using a one-way ANOVA with α <0,05 and highlighted with * in the figure.

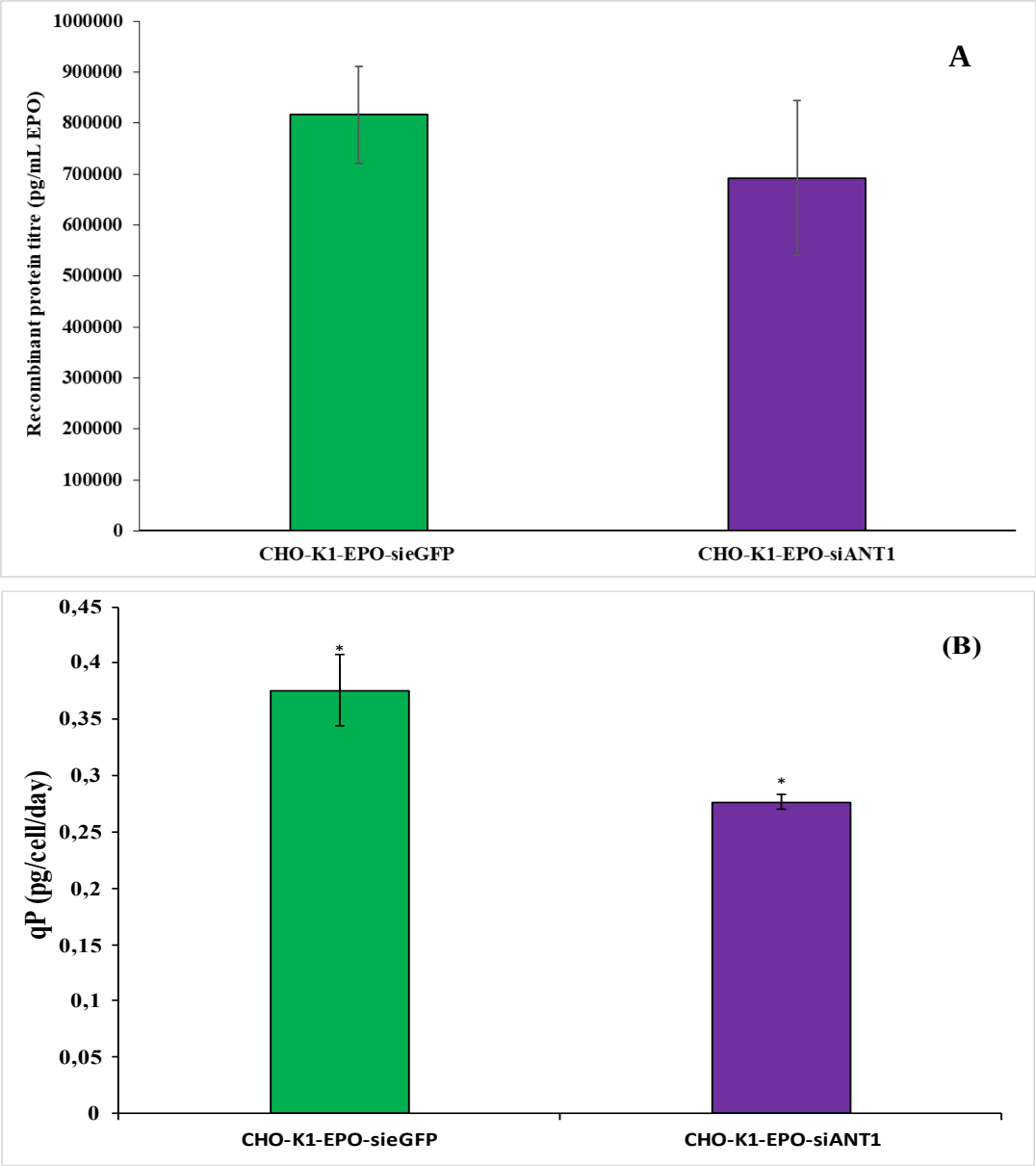

Figure 5. 14. (A) Protein titre from siRNA transfected CHO-K1 cells. Each bar represent the average protein titre of biological triplicates measured in duplicate by ELISA ± SD. Significance was tested using 1-way ANOVA with $\alpha < 0,05$ and highlighted with * in the figure.

(B) Specific productivity (qP) from siRNA transfected CHO-K1 cells. Each bar represent the average qP of biological triplicates measured in duplicate by ELISA ± SD. Significance was tested using 1-way ANOVA with $\alpha < 0,05$ and highlighted with * in the figure.

After this point, CHO-K1-sieGFP cell density plateaued, while CHO-K1-EPO-siANT1 cells density plummeted to nearly 0. The viability of the CHO-K1-EPO-sieGFP initially decreased and then remained steady for the duration of the culture (**Figure 5.13 B**). On the other hand, the viability of the CHO-K1-EPO-siANT1 cells remained steadily high for the first 72 hours of culture, dropping to nearly zero after this point in time.

These results demonstrated that the downregulation of ANT1 in CHO-K1-EPO cells promoted cell growth during the first 72 hours of culture, allowing those cells without ANT1 to reach higher peaks of viable cell density. However, this high cell density presumably resulted in depletion of the media leading to a decline in viability before the control culture.

5.3.1. Silencing of ANT1 CHO-K1-EPO cells does not significantly change the recombinant protein titre.

Supernatant samples were collected after 72 hours of culture and an ELISA assay was performed to check the recombinant protein levels of both cell lines. The recombinant protein titre was similar in CHO-K1-EPO cells transfected with either siANT or sieGFP (control siRNA) after 72 hours of culture (**Figure 5.14A**). However, the specific productivity was higher in the cells transfected with sieGFP (**Figure 5.14B**). Depleting ANT1 benefits cell density but at the expense of specific productivity with a significantly lower yield of protein from a lot more cells.

5.4. Discussion.

The work performed in this chapter aimed to alter the phenotype of CHO-K1 cells by targeting nuclear genes related to the mitochondria. The chosen genes were either important regulators of mitochondrial activity and numbers, such as PGC1α (*Andersson and Scarpulla, 2001; Scarpulla, Vega and Kelly, 2012)* and DRP1 (*Frank et al., 2001; Wang et al., 2012)*, or played an important role in the regulation of mitochondria metabolism, such as ANT1.

PGC1α overexpression was expected to upregulate the mitochondrial metabolism and biogenesis while protecting the mitochondria from ROS damage, as previously reported in the literature (Dinulovic *et al.*, 2016; Cheng, Ku and Lin, 2018; Ascenzi *et al.*, 2019; Karlsson *et al.*, 2019). These effects are normally achieved by the interaction of

transcription factors such as ERRα, NRF-1, NRF2, and TFAM genes, with a special focus on NFR-1.

Initially, PGC1α transient transfection did not have an observable effect in CHO-K1 cells, with both the PGC1α cells maximum viable cell density and viability being similar to those of control cells. However, after stable transfection of both genes was achieved, the outcome was slightly changed. PGC1α stable transfection was observed to reduce the viability of CHO-K1 cells. This reduction was also reflected in the maximum viable cell density of PGC1α cells, which was negatively impacted by the reduction in viability. PGC1α has been previously reported to upregulate cell division in some kind of tumours such as pancreatic or breast tumours, while it downregulates the cell proliferation in other tumours, such as renal or prostate tumours (*Torrano et al., 2016; Zhang et al., 2017; Ascenzi et al., 2019; Valcarcel-Jimenez et al., 2019*). For this reason, the effects of PGC1α in cell proliferation are considered tissue-specific, being also very highly dependent on the presence of the ERRα transcription factor (*Valcarcel-Jimenez et al., 2019)*. Therefore, it is possible that, in the context of CHO cells, PGC1α has a detrimental effect on cell division. Moreover, it is possible that the influence of PGC1 could differ even among CHO cells, as subsequent transfections created CHO-K1 PGC1α cells with a maximum cell density and viability similar to those of control cells. Other potential explanations include previously reported the ability of PGC1α to shift the cells towards oxidative metabolism (*Dinulovic et al., 2016)*, in this context, PGC1α may promote the mitochondrial biogenesis and/or the oxidative metabolism to levels too high for the anti-ROS effect of PGC1α to be able to cope with the ROS level. In this topic, it must be considered that the PGC1α transfected into the CHO cells was the mouse version of the protein, which means the transfected protein may be unable to properly interact with some of the transcription factors that it is supposed to activate. As the anti-ROS response depends on the interaction between PGC1α and NRF2 *(Dobrowolny et al., 2005; Ascenzi et al., 2019)*, it is possible that the transfected PGC1α was unable to protect the cell against ROS, leading to a decrease in viability.

While the CHO-K1 cells transfected with PGC1α showed higher levels of mitochondrial content, as expected given the role of PGC1α in mitochondrial biogenesis (*Dillon, Rebelo and Moraes, 2012; Ihsan, Watson and Abbiss, 2014; Garcia et al., 2018)*, the higher mitochondrial content did not translate into higher r-protein production. Moreover, the r-

protein titre showed the cells were observed to be significantly lower than in control cells. Previous studies had reported a lack of relationship between the number of mitochondria within cells and their oxidative metabolism levels (*O'Callaghan et al., 2015*), which may explain why the r-protein production, closely related to oxidative metabolism (*Templeton et al., 2013*) was non impacted. Despite this, PGC1α is also known to stimulate OXPHOS, so an increase in r-protein production was nonetheless expected. PGC1α overexpression was proven in CHO-K1 cells. Moreover, the PGC1α expression levels became very high compared with the controls. However, the transcription levels of the evaluated transcription factors PPARD, NRF1, and TFAM, which are transcription factors co-activated by PGC1α, remained equal in both PGC1α and control cells. Additionally, NRF1, which expression is known to be promoted by PGC1α (*Cheng, Ku and Lin, 2018*), did not show increased transcript levels in the cells overexpression PGC1α. These results again suggested the possibility of the mouse PGC1α protein not being able to interact with the CHO version of the transcription factors. It is also possible that the levels of expression of the transcription factors constitute a limiting step for PGC1α to exert any effect in the mitochondrial metabolism, resulting in the phenotype of the PGC1α cells being identical to the controls cells, or even in a detrimental effect of the PGC1α overexpression, due to the accumulation in the mitochondria of unnecessary protein. While the reason behind it is subjected to speculation, the results obtained clearly point to the overexpression of PGC1α being detrimental to the r-protein production in CHO cells.

DRP1 overexpression was expected to increase the number and general health of the mitochondria by increasing the mitochondrial fission process (*E. Smirnova et al., 2001*). The mitochondrial fission process is known to exert a protective effect against ROS in the cells, and it has an integral role in the apoptosis and mitophagy induction in the cells (*Dulac et al., 2020; Pascucci et al., 2021*). DRP1 is, due to its role in the process, a fundamental component of the mitochondria. DRP1 overexpression was reported in the literature to increase the lifespan of midlife *Droposhila* individuals (*Rana et al., 2017*).

CHO-K1 cells transfected with DRP1 in this study showed increased viability compared with control cells. This increased viability resulted in an increase of the cell lifespan and maximum viable cell density at late stages of growth compared with the control. This was the expected outcome as reported by Rana and collaborators (*Rana et al., 2017)*, with

DRP1 promoting mitochondrial fission. However, the mitochondrial content of the cells was found to be slightly diminished in DRP1 cells compared with control cells. This is likely due to the mitochondrial fission process resulting in rounded, temporarily inactive mitochondria, especially if an excessively high number of mitochondria accumulates inside the cell, already observed by Rana and collaborators. The dye used to observe the mitochondria content, Mitotracker dye, is only able to enter and stain only those mitochondria actively performing the oxidative phosphorylation process. This means the mitochondrial fission process induced by DRP1 could have created many inactive mitochondria, which are not detected by this assay, explaining the relatively low reported mitochondrial content of DRP1 cells.

Increased DRP1 transcript levels were achieved in CHO-K1 cells. However, actual overexpression of DRP1 in the cells remained unclear, as the related genes MFN1 and MFN2 did not show increased transcript levels in DRP1 cells compared with the control sample. It was theorized that DRP1 transcript levels are already quite high in wild-type cells, and therefore the introduction of an exogenous DRP1 gene may not increase the actual process of mitochondrial fission. Like in the case of PGC1α, it is possible that the mouse version of DRP1 is not able to upregulate the CHO versions of MFN1 and MFN2. Regardless, changes in the phenotype of CHO-K1 cells transfected with DRP1 compared with control cells were observed, hinting at the DRP1 overexpression having an actual, observable effect despite the transcriptomic data obtained. Finally, the r-protein titre of CHO-K1-DRP1 cells was reduced compared with the control cells. This makes sense, as previously commented, the reduction in size and the change of shape in the newly generated mitochondria could have interfered with their ability to effectively produce r-proteins. Additionally, no relationship between mitochondrial content and r-protein production has been previously established (*O'Callaghan et al., 2015)*. Overall, the results suggest the overexpression of DRP1 in CHO cells is useful to increase the lifespan and viability of the cells, probably by protecting the cells from ROS (*Jin et al., 2020),* resulting in a long-term increase of viable cell density, with the drawback of causing a reduction in r-protein titre. This makes the DRP1 gene an interesting target for mitochondrial engineering, as the effects of DRP1 overexpression in CHO cells can be helpful depending on the specific CHO cell line to be engineered.

ANT1 downregulation, achieved using a siRNA targeting ANT1 gene (si-ANT), has been reported in the literature to lead to mitochondria hyperproliferation in diabetic mice (*Morrow et al., 2017*). During this state, the ATPase partially uncouples from the electron transport chain, leading to a constant ETS state in the cell, but partially inhibiting the ATP production. While this state was previously believed to be a mitochondrial disfunction, recent studies had described it as a natural, regulatory state of the cells (*Demine, Renard and Arnould, 2019)*.

The downregulation of ANT1 transcript levels in CHO-K1 cells was successfully achieved. During the assay, it was noted that basal ANT1 transcript levels were already quite low in control cells, hinting ANT1 to be a relatively low expressed gene in CHO cells. This makes sense as ANT1 is known to be mainly expressed in skeletal and heart muscle tissue (*Karch et al., 2019)*. ANT (-) cells maximum viable cell density was higher than the control during the first 72 hours of culture, after which it dropped to almost 0. The viability of ANT (-) cells followed a similar pattern to growth, being high and stable for the first 72 hours of culture and suddenly dropping to near 0. Low levels of ANT1 expression in cancer cells have been reported to increase cell proliferation and resistance to stress-induced death (*Vial et al., 2020*). Therefore, it is possible that fully eliminating ANT1with the siRNA has led to the eventual death of these cells. This may be caused by an accumulation of aberrant, caused by the quick mitochondrial hyperproliferation caused by ANT1 know down, previously reported in the literature (*Hoshino et al., 2019*). It is also possible that the sudden drop in viability is caused by an excess of ROS being generated due to the constant max ETS state of the ANT1 (-) cells. The r-protein titre of ANT1 (-) was also observed to be similar to control cells, but specific productivity was negatively impacted. As in ANT1 (-), the ATPase is uncoupled from the electron transport chain, and therefore the ATP production of the cell is partially inhibited, cells with ANT1 knockdown will also divert resources to the glycolytic pathway, relying upon lactic fermentation to generate ATP (*Subramaniam et al., 2008; Karch et al., 2019)*. This need for ATP and subsequent increase in lactic fermentation, together with the maintenance of a constant max ETS, will result in the cells constantly demanding glucose, lactic acidification of the media, and a quick accumulation of ROS inside the cells, which could explain the quick death of the cells compared with control and their incapability to produce similar r-protein levels to the control as they have a reduced capability to resort to the oxidative metabolism for ATP production.

Overall, the knockdown of ANT seemed to have mainly negative effects in CHO-K1 cells, shortening their lifespan and reducing their r-protein production.

CHAPTER 6

ALTERNATIVE ENVIRONMENTAL AND GENOMIC APPROACHES TO IMPROVE CHO CELL METABOLISM.

6.1. Reducing leachables and extractables in Single-use bioreactors

6.1.1.Introduction:

The process of manufacturing biopharmaceutical products, such as recombinant proteins, presents several difficulties widely addressed in the literature. One of these concerns is the accumulation of wasteful by-products produced by the cells while in the bioreactor, such as ammonia or lactate.

On that note, recent studies have raised concern about the possible presence of leachables and extractables derived from the materials used in single-use bioreactors. Leachables and extractables (E&Ls) from plastics, also known as Non-Intentionally Added Substance (NIAS) are defined as substances released from plastic to the media unintentionally. These substances are not only potentially dangerous for health if mixed with the final product, but they have also been observed to have detrimental effects on the growth of the producer cell line (*Hammond et al., 2013*)

Additionally, the exact nature or composition of the Single-use bioreactors (SUBs) is not always well-known, as the information is not made available from the manufacturers. Therefore, many potential side effects of the extractables and leachables (E&L) may have been overlooked in SUBs. For this reason, the manufacturing companies have recently developed safer materials, which release less, if any, leachable into the media during the recombinant protein manufacturing process.

As mentioned before, the detrimental effects of leachables on CHO cell growth have been previously described in the literature. A previous study described the effects of bDtBPP (tris 2,4-di-tert-butyl phenyl-phosphite), a well-known E&L, on CHO-K1 and CHO-DP12 lines observing a reduction of the cell growth and r-protein titer in both cell lines at very low bDtBPP concentrations, even before reaching cytotoxic concentrations (*Kelly et al., 2016*). However, the quality and glycosylation patterns of the r-protein product were not affected by the presence of leachables. However, the effects of the bDtBPP on the metabolism of the cells were not investigated in this study.

In this section, the effect of the use of newer materials in single-use bioreactors was evaluated. The results described in this section were published in 2019 as part of a collaboration with Kelly and co-authors (*Kelly et al., 2019*). The study was performed to elucidate if a new generation SUB (F2 model), designed with a lower level of Irgafos 168, with the ultimate goal of reducing the release of E&L compared to its predecessor SUB (F1 model). This study was the perfect chance to assess the effects of E&L on the metabolism of the cells and, more specifically, on mitochondrial function. Cell growth arrest and the reduction in recombinant protein production, previously reported to be caused by the presence of E&Ls in the media, were believed to be likely reflected in the metabolic profile of the cells.

The three different media used for these experiments were generated by Paul Kelly, the first author of the study. As outlined in the materials and methods section of the paper, chemically defined BalanCD media was incubated in each one of the SUBs (F1 and F2 models correspondingly) for a total time of seven days at 37°C. The purpose of this incubation process was to allow any E&Ls to accumulate in the media. The media obtained from these incubation processes was labeled as Bio 10 media (F1) or Bio 11 media (F2). A negative control was generated by incubating BalanCD® CHO Growth A media in autoclaved grade A glass bottles that were not exposed to any SUB material. Subsequently, these three sets of growth media samples were used to culture CHO cells and observe their behavior. Two different CHO cell lines were used: CHO-DP12 and CHO-K1. The cells were incubated for a total of 96 hours after which growth, viability, and metabolic activity were evaluated.

6.2. Different SUB materials impact in CHO-K1 and CHO-DP12 cells.

6.2.1 The different E&L released by SUBs have different impacts on CHO cell growth and viability.

Firstly, the growth of the cells in the differently conditioned media was evaluated. Cells were grown for a total of 96 hours in Bio 10, Bio 11, or control media. For each media, three tubes of 5mL media were seeded with $2x10^5$ cells, either CHO-DP12 or CHO-K1. After 96 hours, cell density was calculated and samples were collected to perform an extracellular flux analysis to measure the metabolism of the cells.

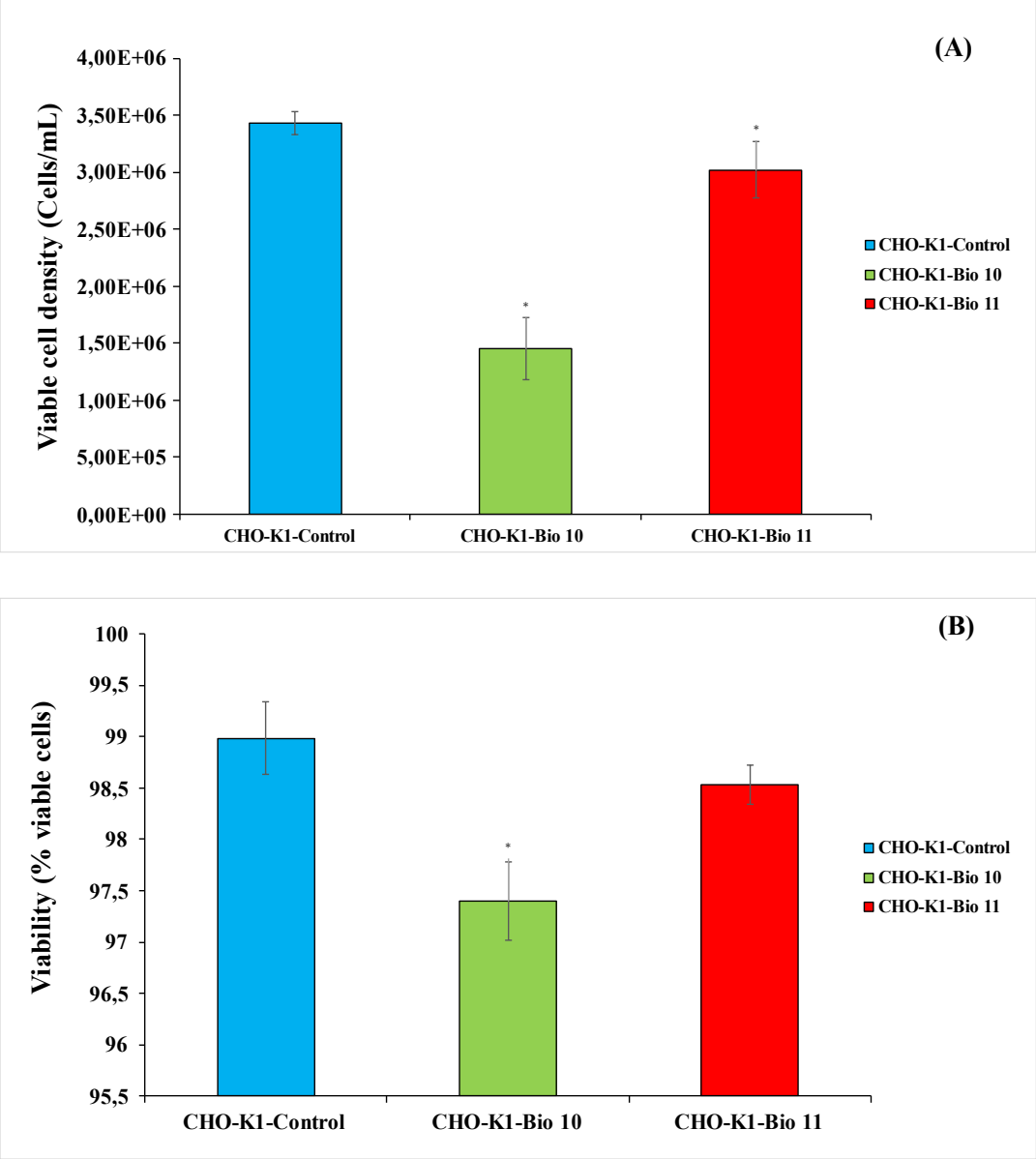

Figure 6. 1. (A) Viable cell density of CHO-K1 cells after 96 hours of culture. Cells were cultured in suspension culture in 5mL of the corresponding media. Each line represent the average viable cell density of biological triplicates measured in triplicates using Guava Easycyte cytometer ± SD. Significance was tested using a one-way ANOVA with α <0,05 and highlighted with * in the figure.

(B) Viability of CHO-K1 cells after 96 hours of culture. Cells were cultured in suspension culture in 5mL of the corresponding media. Each line represent the average viability of biological triplicates measured in triplicates using Guava Easycyte cytometer ± SD. Significance was tested using a one-way ANOVA with α <0,05 and highlighted with * in the figure.

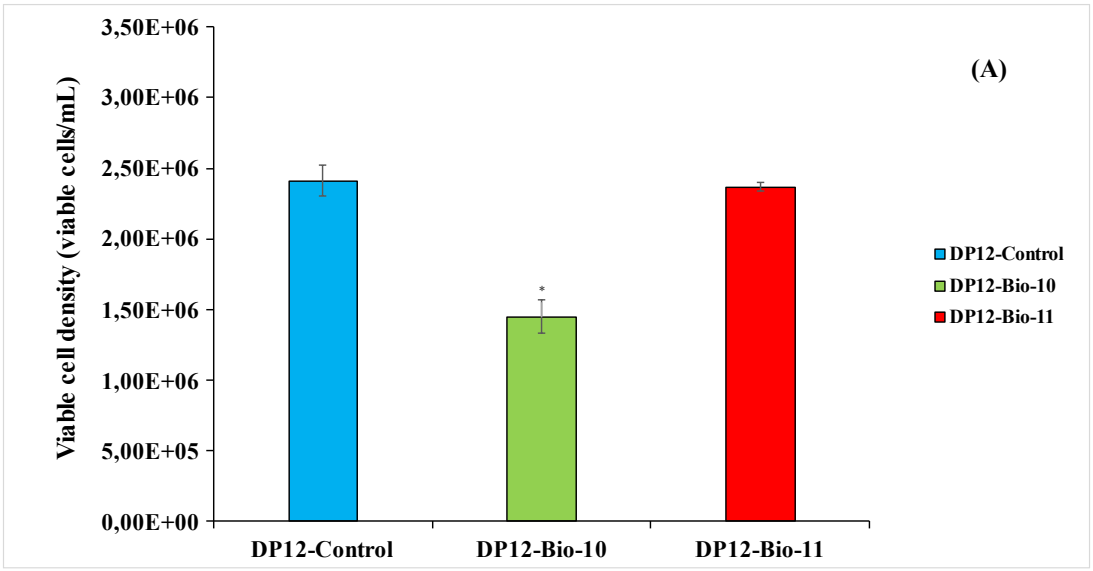

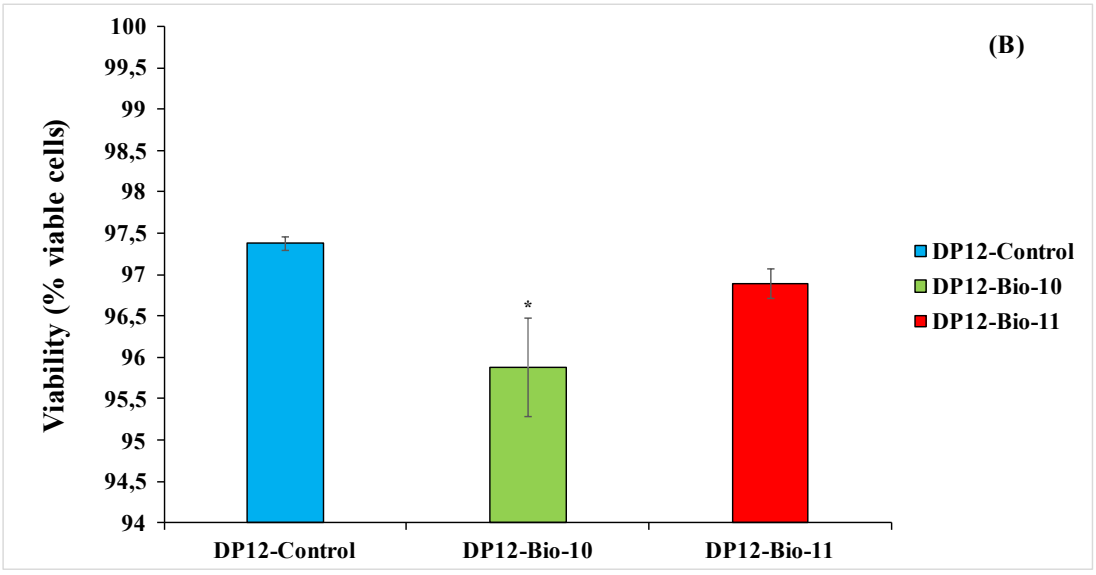

Figure 6. 2. (A) Viable cell density of CHO- DP12 cells after 96 hours of culture. Cells were cultured in suspension culture in 5mL of the corresponding media. Each line represent the average viable cell density of biological triplicates measured in triplicates using Guava Easycyte cytometer ± SD. Significance was tested using a one-way ANOVA with $\alpha < 0,05$ and highlighted with * in the figure.

(B) Viability of CHO-DP12 cells after 96 hours of culture. Cells were cultured in suspension culture in 5mL of the corresponding media. Each line represent the average viability of biological triplicates measured in triplicates using Guava Easycyte cytometer ± SD. Significance was tested using a one-way ANOVA with $\alpha < 0,05$ and highlighted with * in the figure.

CHO-K1 cell growth in control media reached an average cell density of $3.4x10^6$ cells/ml, while CHO-K1 cells growth in Bio 11 media reached an average cell density of $3.0x10^6$ cells/ml (**Figure 6.1**). CHO-K1 cells grown in Bio 10 media grew considerably less, reaching an average cell density of $1.50x10^6$ cells/ml. This density is not only considerably lower than the cell density observed in CHO-K1 cells grown in the control media, but it is also considerably lower than the cell density observed in CHO-K1 cells grown in Bio 11 media. To confirm these results, the same experiment was performed with a different CHO cell line, specifically, CHO-DP12. CHO-DP12 cell growth in the different media was similar to the pattern previously observed for CHO-K1 cells where growth in control media reached a peak cell density of $2.4x10^6$ cells/ml (**Figure 6.2**). Cells that were grown in Bio 11 media also achieved high cell density, reaching a peak of $2.4x10^6$ cells/ml, similar to the control cells. These results showed the Bio 10 media to have a detrimental effect on the growth of both CHO-K1 cells and CHO-DP12 cells, which reach lower viable cell densities when cultured at this media compared with culture in both control and Bio 11 media. The difference in cell density was more evident on CHO-K1 media, where this parameter was reduced to roughly half of the amount reached by cells cultured in control media. On the other hand, CHO-DP12 cells decreased in viable cell density, but the decrease was significantly less pronounced than in CHO-K1 cells. This data could imply either a resistance of CHO-DP12 cells to the E&Ls or higher sensitivity of CHO-K1 to these chemicals. The next step was to investigate the effects of the media on the metabolism of the cells with an XF-analyser.

6.2.2 The different E&L released by SUBs have different impacts on CHO cell metabolism.

After evaluating the changes in growth phenotype caused by the different media, the impact on cell metabolism was evaluated using the Seahorse XF-96 analyzer. Briefly, cell samples were taken from each culture, resuspended in Seahorse XF-96 conditioned media, and plated in a 96-well Seahorse plate at a cell density of 20,000 cells /well.

For CHO-K1 cells, both oxidative and glycolytic metabolism was drastically reduced after incubation in Bio-10 media (**Figure 6.3**) in both the basal and stressed states. In the stressed state, the OCR for cells grown in Bio 10 media was 100 oxygen pmol/min, while the OCR observed in CHO-K1 cells incubated in Bio 11 media and Control media reached approximately 175 pmol/min. (**Figure 6.3 A**) Similarly, cells grown in Bio 10 media

showed reduced ECAR scores compared to the control. It must be noted that CHO-K1 cells grown in Bio 11 media also showed a decrease in ECAR compared to the control, although this decrease was not as pronounced as the decrease observed in Bio 10 incubated cells (**Figure 6.3 B**).

The ECAR score for cells grown in Bio 10 media during the stressed state was approximately 70 mph/min, while ECAR for cells grown in control media was approximately 102 mph/min. Therefore, incubation of the CHO-K1 cells in Bio 10 media reduced the non-oxidative metabolism to 70% of its normal capacity. Similarly, the ECAR of cells grown in Bio 10 media during the stressed state was 80 mph/min. Therefore, Bio 11-conditioned media was concluded to reduce the non-oxidative metabolism to 80% of its normal capacity.

The experiments performed in CHO-DP12 cells showed similar results. Again both oxidative and glycolytic metabolism was observed to be drastically reduced after incubation in Bio-10 media (**Figure 6.4.**) at both basal and stressed states. In the stressed state, the OCR for CHO-DP12 cells grown in Bio 10 media was 133 pmol/min, while the OCR in CHO-DP12 cells incubated in Bio 11 media and Control media reached OCR values of approximately 220 pmol/min (**Figure 6.4 A**). As in the case of CHO-K1 cells, CHO-DP12 cells grown in Bio 10 media showed reduced ECAR values compared to the control. However, CHO- DP12 cells grown in Bio 11 media and Control media had similar ECAR values of approximately 110 mph/min. CHO-DP12 cells grown in Bio 10 media had an ECAR of 82 mph/min. (**Figure 6.4 B**). Therefore, incubation of the CHO-DP12 cells Bio 10 media reduced the non-oxidative metabolism to approximately 70% of its normal capacity.

In conclusion, CHO cells grown in Bio 10 media had reduced metabolic activity when compared with CHO cells incubated in either the control media or Bio 11 media. This data further confirmed a higher content of E&L in Bio 10 media compared with Bio 11 media, which was expected given the absence of Irgafos 168 in the composition of the F-2 bioreactor material. To further confirm whether Bio 10 media was inducing changes in glycolytic metabolism or if the observed changes were induced by the oxidative metabolism introducing a bias, i.e. the CO_2 produced as a by-product of OXPHOS acidifying the media as previously described in Chapter 3. For this reason, an additional glycolytic stress assay was chosen to assess this.

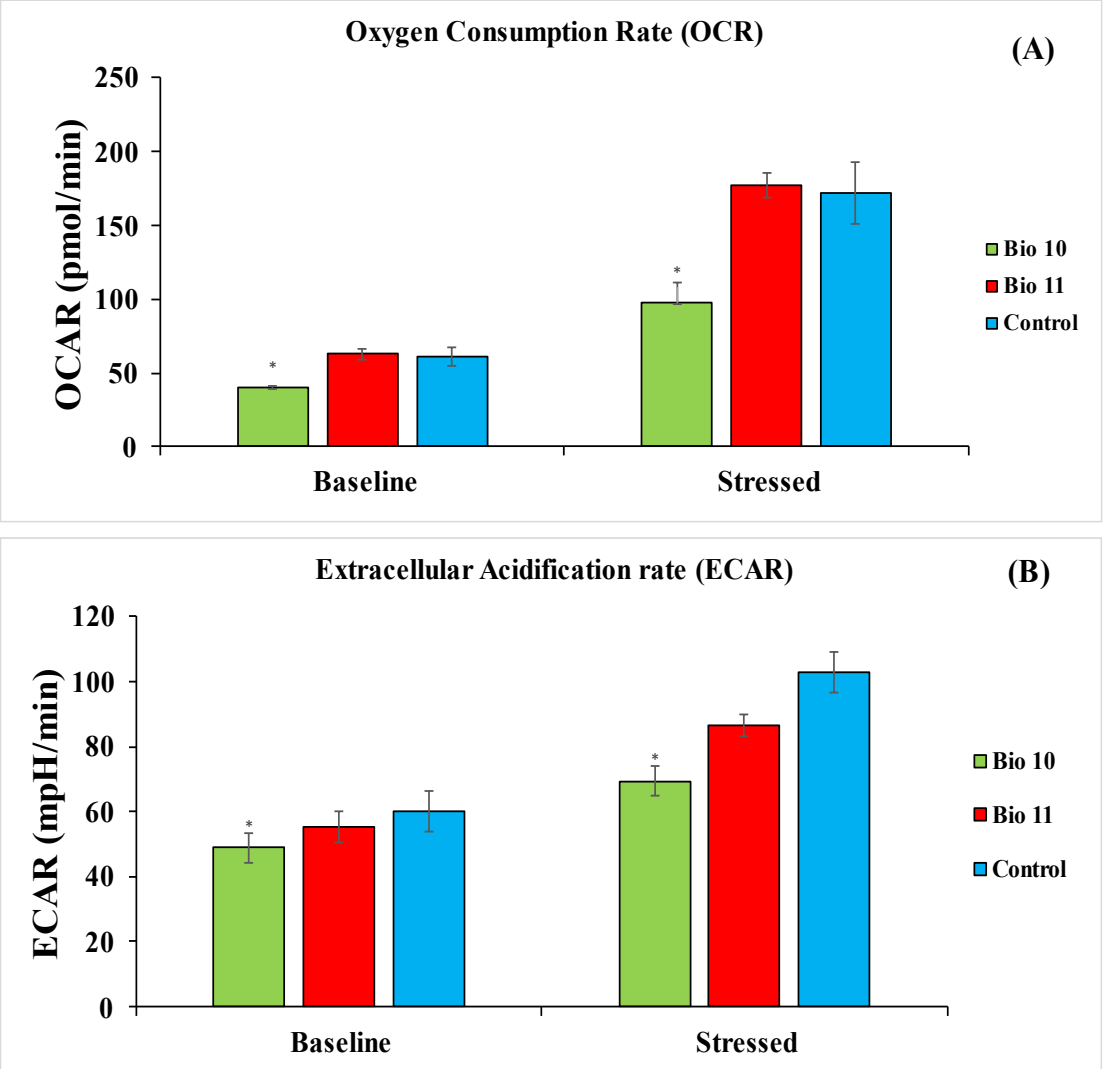

Figure 6. 3. (A) Oxygen consumption rate (OCR) from CHO-K1 after 96 hours of culture in each of the three different media tested. Each bar represents the average OCR level of biological triplicates measured in 9 technical replicates using Seahorse XF-96 analyser ± SD. Significance was tested using one-way ANOVA with $\alpha<0.05$, represented by * in the figure.

(B) Extracellular Acidification Rate (ECAR) from CHO-K1 after 96 hours of culture in each of the three different media tested. Each bar represents the average ECAR level of biological triplicates measured in 9 technical replicates using Seahorse XF-96 analyser ± SD. Significance was tested using one-way ANOVA with $\alpha<0.05$, represented by * in the figure.

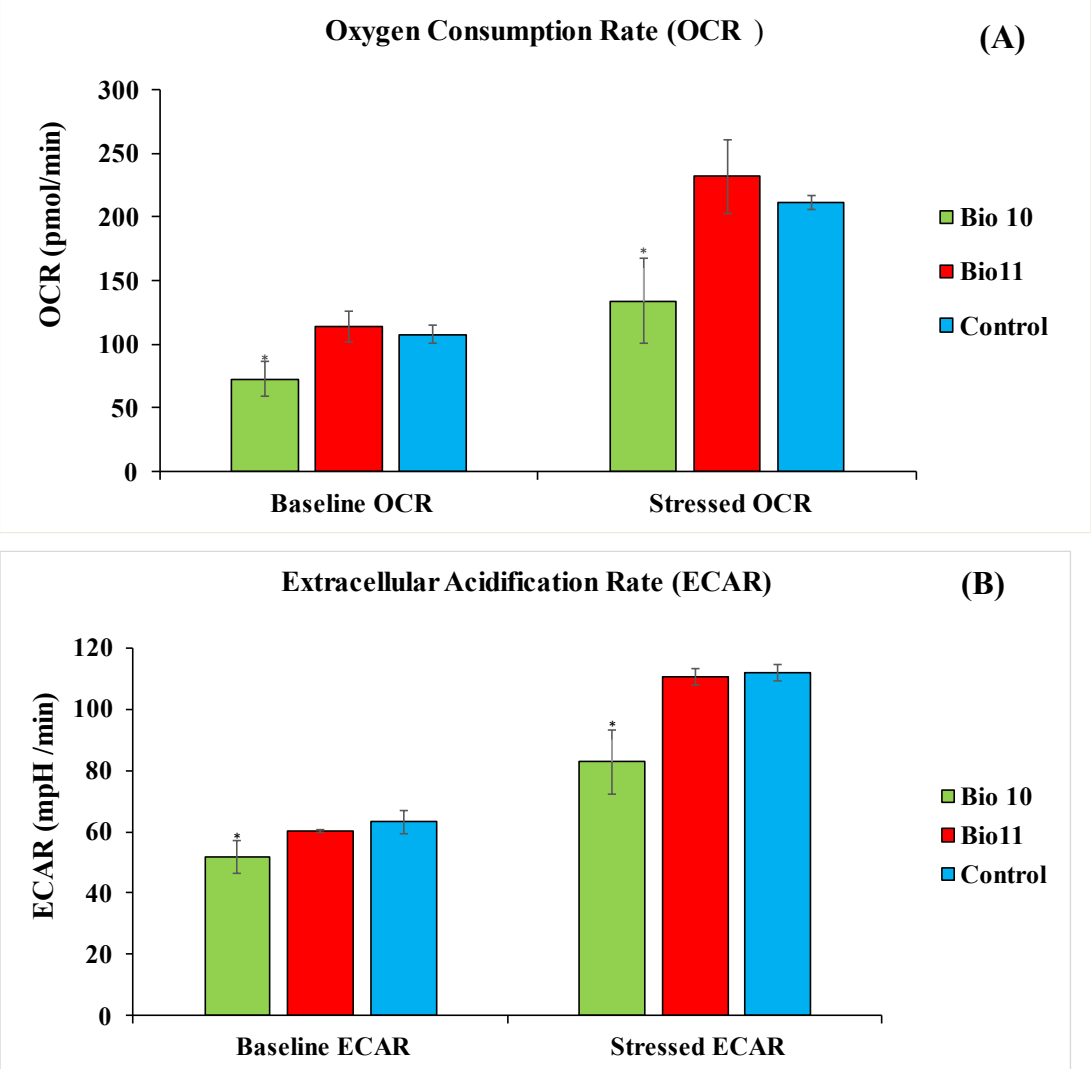

Figure 6. 4. (A) Oxygen consumption rate (OCR) from CHO-DP12 after 96 hours of culture in each of the three different media tested. Each bar represents the average OCR level of biological triplicates measured in 9 technical replicates using Seahorse XF-96 analyser ± SD. Significance was tested using one-way ANOVA with $\alpha<0.05$, represented by * in the figure.

(B) Extracellular Acidification Rate (ECAR) from CHO-DP12 after 96 hours of culture in each of the three different media tested. Each bar represents the average ECAR level of biological triplicates measured in 9 technical replicates using Seahorse XF-96 analyser ± SD. Significance was tested using one-way ANOVA with $\alpha<0.05$, represented by * in the figure.

6.2.3. The different E&L released by SUBs have different impacts on CHO cell glycolytic metabolism.

As described in the previous section, the data obtained with the XF analyzer suggested the cell culture media incubated in single-use Bioreactor ``Bio 10 ´´to cause a reduction of both glycolytic and oxidative metabolism in CHO cells. These results suggest that the higher levels of plastic E&L release to the media of SUB model F1 cause a reduction in both cell growth and the metabolism of CHO cells compared to model F2, which releases less E&L to the media. However, it must be noted that the XF Metabolic phenotype assay capacity to detect differences in extracellular acidification is known to be slightly biased. The CO_2 generated as a product of oxidative metabolism contributes to the acidification of the media. Therefore, the differences observed in the media acidification during the previous experiments may not correspond with differences in glycolytic metabolism levels, but rather can be a consequence of the differences observed in the oxidative metabolism of the cells, which also contributes to acidifying the media as explained below.

The samples showing higher levels of oxidative metabolism also showed higher glycolytic metabolism, but this difference may have been caused by higher levels of CO_2 being produced rather than by real differences in the glycolytic pathway. For this reason, the glycolytic stress assay was performed. As previously described in **Chapter 3, section 3.3.1** of this thesis, during this assay oxidative metabolism is inhibited, effectively overruling the role of the CO_2 produced during cellular respiration in the extracellular acidification levels.

Briefly, cell samples were taken from each tube, resuspended in Seahorse XF-96 conditioned media, and plated in a 96-well Seahorse plate at a cell density of 20000 cells /well. The plate was previously treated with Corning Cell-Tak cell adhesive to ensure the cells with fixating to the bottom of the well. Cells were first analyzed using the ``Glycolytic stress assay kit´´ as described by the manufacturer's instructions. The results of the Glycolytic stress assay in CHO-K1 cells showed a very similar picture to the one obtained during the metabolic phenotype assay (**Figure 6.5.A)**. Extracellular acidification, measured in this assay as the Proton Efflux Ratio (**PER)**, dependent in glycolysis (**GlycoPER**) was observed to be higher in the CHO-K1 cells grown in control

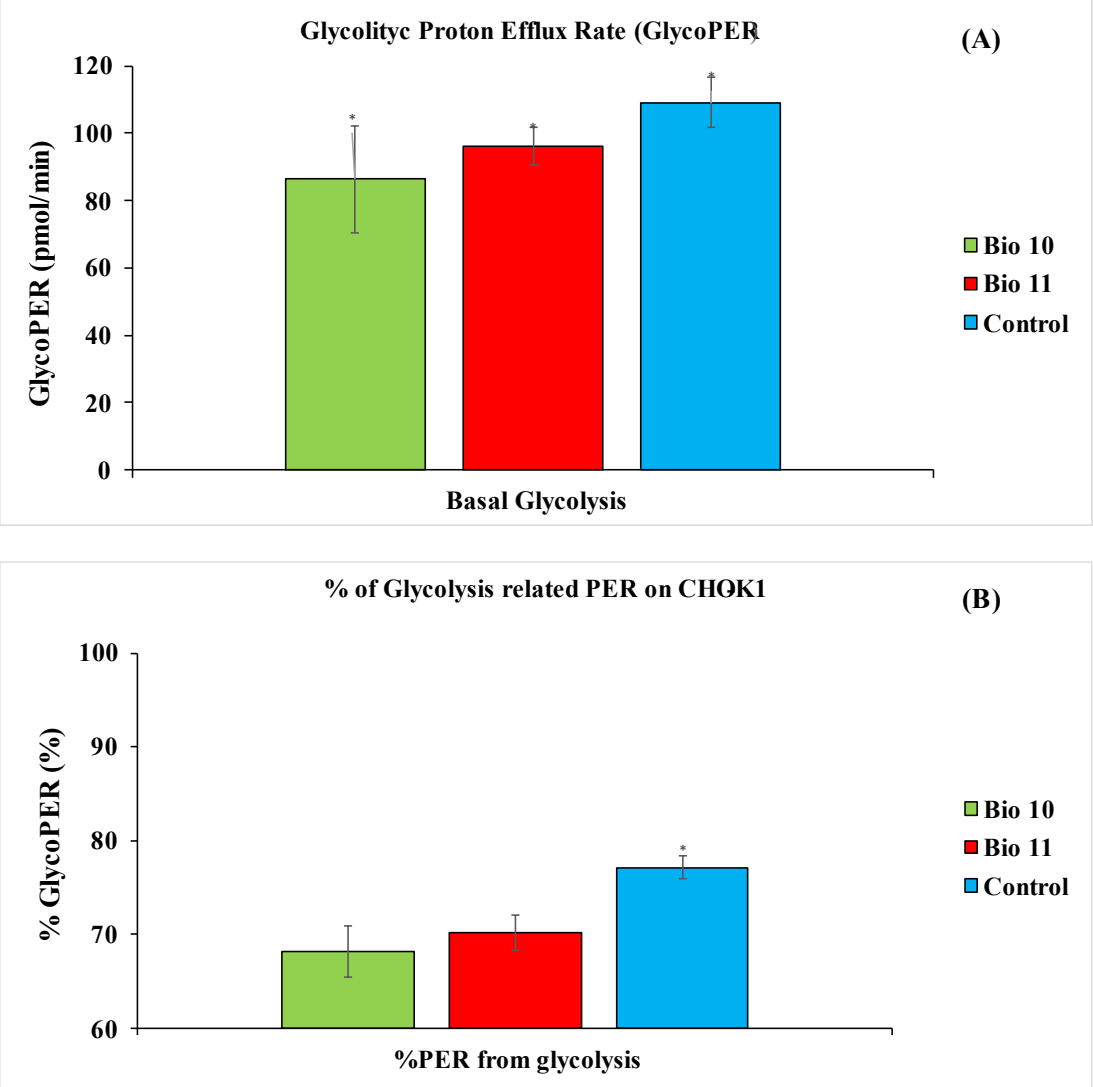

Figure 6. 5. (A) GlycoPER from CHO-K1 after 96 hours of culture in each of the three different media tested. Each bar represents the average GlycoPER level of biological triplicates measured in 9 technical replicates using Seahorse XF-96 analyser ± SD. Significance was tested using one-way ANOVA with $\alpha<0.05$, represented by * in the figure.

(B) Percent of glycolysis related PER from CHO-K1 after 96 hours of culture in each of the three different media tested. Each bar represents the average percent of Per-glycolysis of biological triplicates measured in 9 technical replicates using Seahorse XF-96 analyser ± SD. Significance was tested using one-way ANOVA with $\alpha<0.05$, represented by * in the figure.

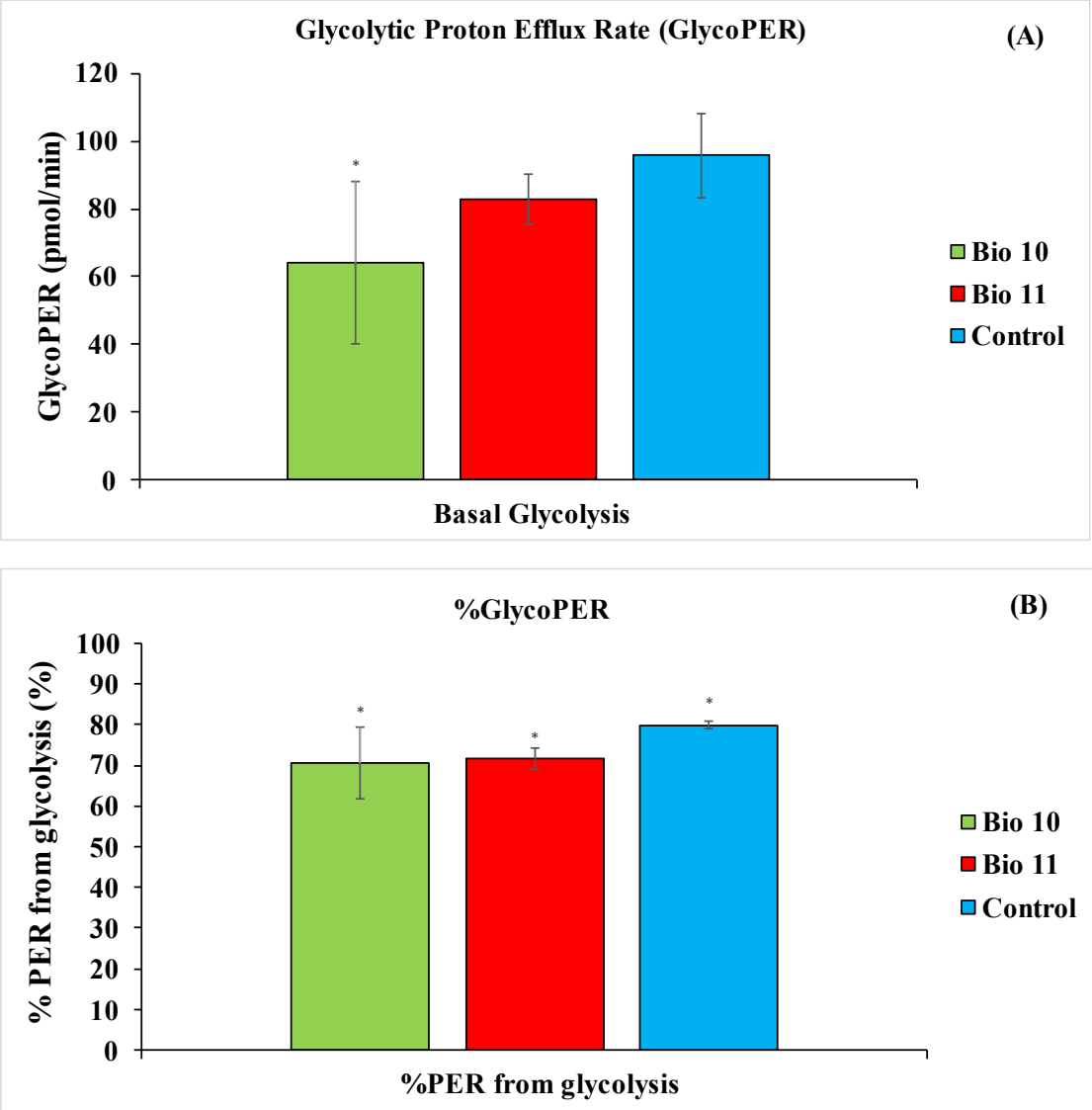

Figure 6. 6. (A) GlycoPER from CHO-DP12 after 96 hours of culture in each of the three different media tested. Each bar represents the average GlycoPER level of biological triplicates measured in 9 technical replicates using Seahorse XF-96 analyser ± SD. Significance was tested using one-way ANOVA with $\alpha<0.05$, represented by * in the figure.

(B) Percent of glycolysis related PER from CHO-DP12 after 96 hours of culture in each of the three different media tested. Each bar represents the average percent of Per-glycoliysis of biological triplicates measured in 9 technical replicates using Seahorse XF-96 analyser ± SD. Significance was tested using one-way ANOVA with $\alpha<0.05$, represented by * in the figure.

media compared to the cells grown in both Bio 10 and Bio 11 media. The percentage of **PER** related to glycolytic metabolism **(% GlycoPER**) was found to be approximately 76% of the total **PER** in CHO-K1 cells in control media (**Figure 6.5.B)**. However, the %GlycoPER was observed to decrease to 70% of the total **PER** when CHO-K1 cells were incubated in Bio11 media and to 66% of the total **PER** when CHO-K1 cells were incubated in Bio 10 media. The differences in %GlycoPER are also observed in the **GlycoPER** levels across the cells incubated in the different media. CHO-K1 cells grown in control media showed the highest GlycoPER value at approximately 110 pmol/min. Compared to the control media values, CHO-K1 cells showed a significant decrease in GlycoPER values when grown in either Bio 11 (98 pmol/min) or Bio 10 (78 pmol/min) media.

These results further confirm the influence of the media on the metabolism of CHO-K1 cells. The results strongly suggest a high presence of E&Ls in Bio 10 media and the presence of some E&Ls in Bio 11 media. These E&Ls seem to have an impact on both oxidative and glycolytic metabolism, which impacts the growth of CHO-K1 cells.

The results of the Glycolytic stress assay in CHO-DP12 cells (**Figure 6.6 A)** showed a very similar picture to the one obtained during the metabolic phenotype assay. The effects of the three different media in CHO-DP12 cells were similar to those observed in CHO-K1 cells. CHO-DP12 %GlycoPER was reduced in both Bio 10 and Bio11 media (**Figure 6.6 B)** by approximately 10%. These changes were also reflected in the GlycoPER value, where cells grown in Bio 10 media were observed to have significantly lower values, amounting to approximately 60 pmol/min, than cells grown in either Bio 11 or Control media, with values of approximately 80 and 97 pmol/min respectively. In summary, these results illustrate the impact of using the older SUB model (F-1) to incubate culture media (referred here as Bio 10 media), resulting in the release of more E&Ls into the media over 7 days than the newer SUB model (F-2). The data obtained shows an effect of these E&L in the growth of both CHO-K1 and CHO-DP12 cells, as previously reflected in the literature (*Hammond et al., 2013; Kelly et al., 2016)*, and in both the oxidative and the glycolytic metabolism in the CHO clones exanimated.

These results suggest that the newer SUB model, F-2, (correspondent with Bio 11 media), is more efficient in preventing the contamination of media with E&Ls.

6.3. Combined knockdown of the four pyruvate dehydrogenase complexes and LDHA eliminates lactate production by CHO cells.

6.3.1. Introduction:

The recombinant-protein production process is often hindered by the accumulation of lactate in the media. Lactate production in CHO cells is related to the Warburg effect, that is, aerobic glycolysis during the early stages of growth followed by a switch to normal oxidative metabolism during the late exponential phase of growth. *(Heiden, Cantley and* Thompson, 2009). During aerobic glycolysis, the pyruvate produced after glycolysis is mostly diverted from the tricarboxylic acid (TCA) cycle into lactic acid fermentation via lactate dehydrogenase (LDH) to generate lactate and ATP, even in the presence of abundant oxygen. Lactate accumulates in the media and contributes to its acidification causing several detrimental effects in cell growth and protein production. For this reason, several studies over the years have focused efforts on preventing the accumulation of lactate in the media, many of them through direct control of the Warburg effect in recombinant protein producer cells. Several of these strategies were focused on eliminating the enzymes regulating the destiny of pyruvate and/or the conversion of pyruvate to lactate. However, these efforts have been largely unsuccessful. Knockdown of LDH isoforms alone did not stop lactate from being generated and knockdown of pyruvate dehydrogenase isoforms, another key enzyme in glycolytic metabolism, was reported to be lethal for the cells (*Yip et al., 2014)*.

Despite these unsuccessful attempts, a collaborating research group from the University of California, San Diego, was able to generate a CHO cell line that doesn't produce any lactate. This feat was achieved through the combined knockdown of the LHDA isoform and four pyruvate dehydrogenase complexes. The cells were kindly provided by this group as part of a collaboration (Prof.Nathan Lewis). In this chapter, metabolic analyses of the newly generated Zero Lactate (ZeLa) CHO cells using a Seahorse XF-96 analyzer are described. The results of these experiments were also provided to the UCSD research group for publication (manuscript in preparation).

6.4. Analysis of the phenotype and metabolism of Zero Lactate (ZeLa) CHO cells.

6.4.1. ZeLa CHO cells exhibit increased oxidative metabolism and diminished glycolytic metabolism compared with wild-type CHO cells.

Cell proliferation experiments were set up as previously described. The viable cell density demonstrated by both ZeLa and WT CHO cells was similar (**Figure 6.7 A**). No significant differences were observed between the two cell lines, despite their metabolism being engineered to be different. Similarly, the viability observed for both groups of cells was nearly identical (**Figure 6.7 B**). These results showed that ZeLa cells were able to maintain a similar growth and viability to the wild-type cells despite being exclusively reliant on oxidative metabolism as an energy source. This suggests the CHO cells do not need Warburg metabolism to support their growth. The next analysis of their metabolism was performed using a Seahorse XF-96 Analyser.

The metabolism of the ZeLa cells and the wild-type CHO was evaluated using the Seahorse Xf-96 analyzer and the metabolic phenotype kit as described in **Chapter 2, section 2.3.2.** The Oxygen Consumption Rate (OCR) was significantly higher in ZeLa cells compared with the wild-type cells (**Figure 6.8 A**). On the other hand, the Extracellular Acidification Rate (ECAR) indicated lower levels of glycolytic activity in ZeLa cells compared with the WT cells (**Figure 6.8.B**). The results of the metabolic analysis confirmed what might be expected when the LDH pathway is blocked in growing cells. Without it, the ZeLa cells could not perform lactate fermentation, instead of relying practically entirely on oxidative metabolism. Curiously, the differences between the ECAR of ZeLa and WT cells were much bigger than the differences in OCR. This is likely due to the difference in energy output obtained from these processes. Comparatively, OXPHOS produces nearly 20 times more energy, in the form of ATP, than glycolytic metabolism. Therefore, a dramatic decrease in ECAR levels could theoretically be compensated by a small increase in OCR levels.

As mentioned earlier, the metabolic phenotype assay doesn't measure ECAR levels completely accurately, due to a part of the media acidification coming from the CO_2

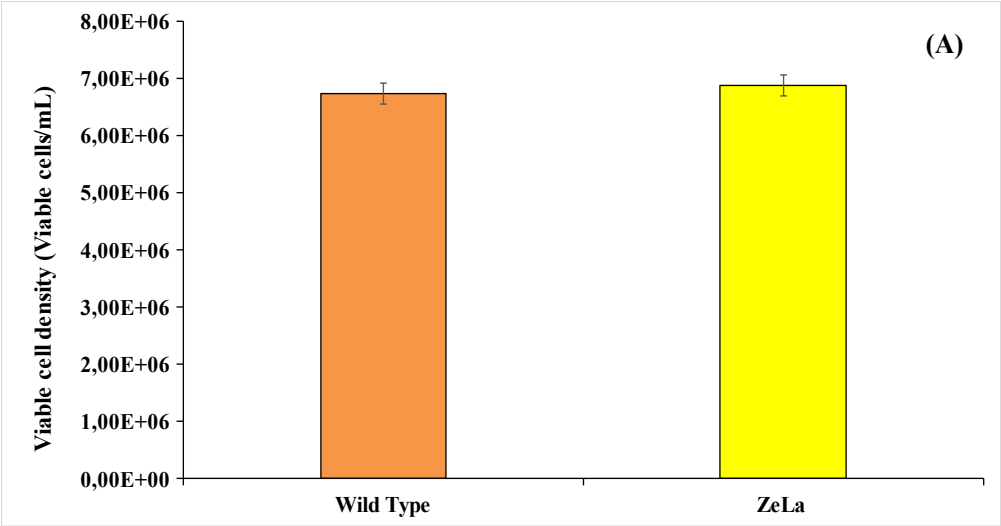

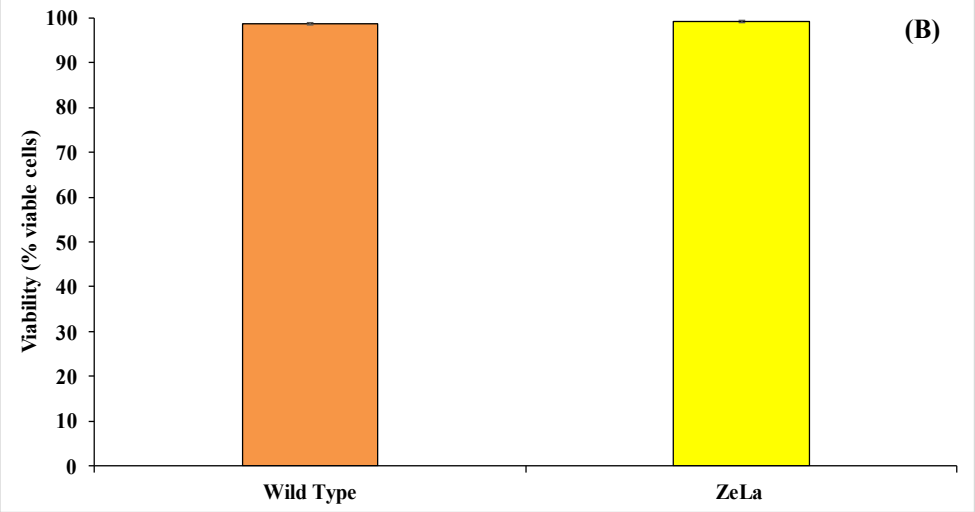

Figure 6. 7. (A) Viable cell density of Zero Lactate (ZeLa) and WT CHO cells after 96 hours of culture. Cells were cultured in suspension culture in 5mL of CD-CHO media. Each bar represent the average viable cell density of biological triplicates measured in triplicates using Guava Easycyte cytometer ± SD. Significance was tested using a one-way ANOVA with α <0,05 and highlighted with * in the figure.

(B) Viability of Zero Lactate (ZeLa) and WT CHO cells after 96 hours of culture. Cells were cultured in suspension culture in 5mL of CD-CHO media. Each bar represent the average viability of biological triplicates measured in triplicates using Guava Easycyte cytometer ± SD. Significance was tested using a one-way ANOVA with α <0,05 and highlighted with * in the figure.

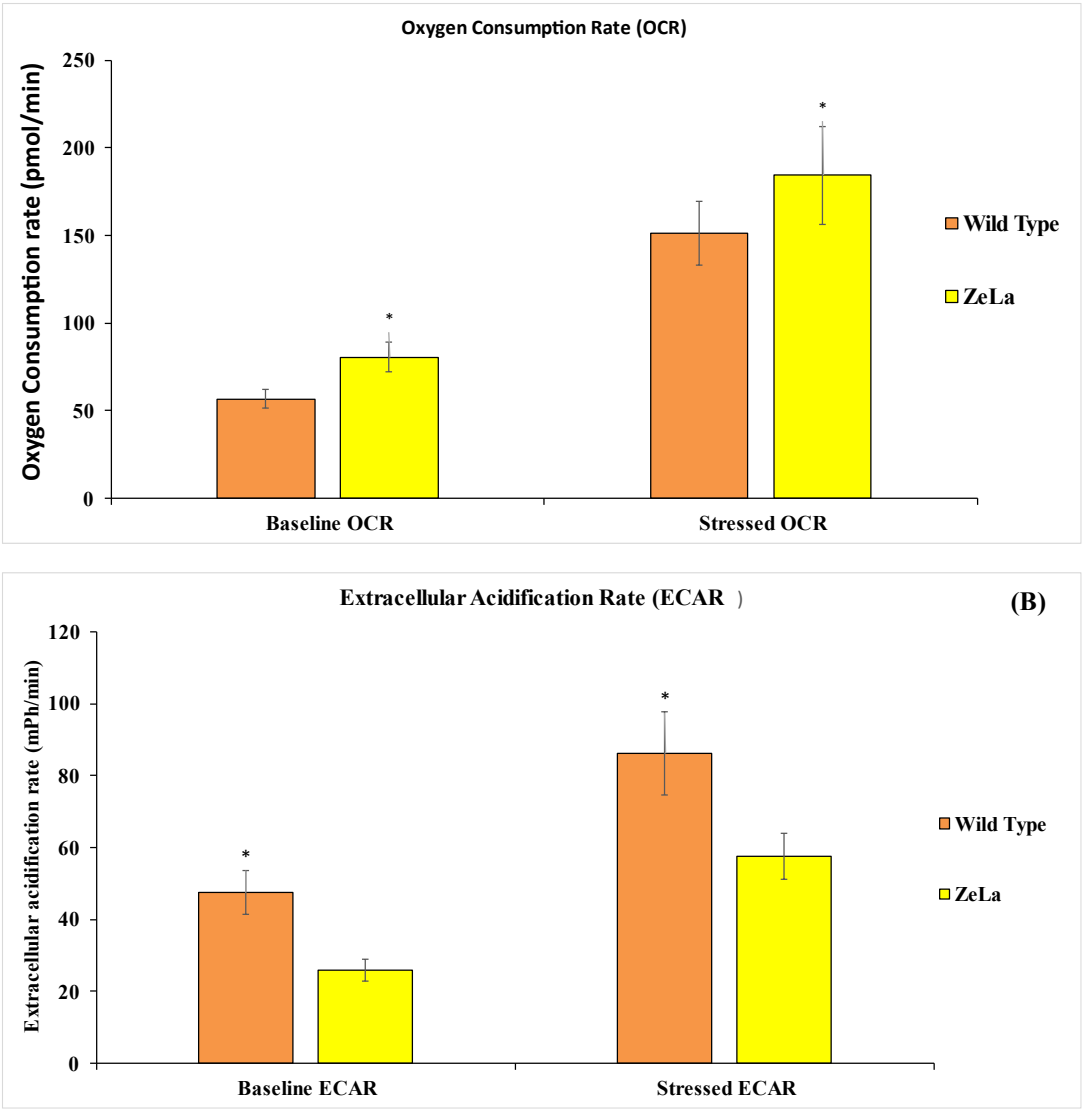

Figure 6. 8. (A) Oxygen consumption rate (OCR) from Zero Lactate (ZeLa) and WT CHO cells after 96 hours of culture. Each bar represents the average OCR level of biological triplicates measured in 15 technical replicates using Seahorse XF-96 analyser ± SD. Significance was tested using one-way ANOVA with $\alpha<0.05$, represented by * in the figure.

(B) Extracellular Acidification Rate (ECAR) from Zero Lactate (ZeLa) and WT CHO cells. Each bar represents the average ECAR level of biological triplicates measured in 15 technical replicates using Seahorse XF-96 analyser ± SD. Significance was tested using one-way ANOVA with $\alpha<0.05$, represented by * in the figure.

generated as a waste product during oxidative metabolism. For this reason, to ensure that the decrease in ECAR levels observed in ZeLa cells was a result of reduced/no lactate production, an additional analysis was conducted using the glycolytic rate assay.

6.4.2. Glycolytic metabolism of the ZeLa CHO cells is confirmed to be diminished compared with the wild-type CHO cells.

As previously described in Chapter 3, section 3.3.1, during this assay oxidative metabolism is inhibited, effectively overruling the role of the CO_2 produced during cellular respiration in the extracellular acidification levels. The Glycolytic stress analysis performed in ZeLa and WT cells showed a very similar picture to the one obtained during the metabolic phenotype assay (**Figure 6.9.A**). The extracellular acidification, measured in this assay as the Proton Efflux Ratio (**PER)**, dependent on glycolysis (**GlycoPER**) was significantly higher in the WT cells than in the ZeLa cells. Specifically, the average GlycoPER in WT cells was approximately 69 pmol/min, while the average GlycoPER of ZeLa cells was approximately 13 pmol/min, i.e. nearly 7 times lower than the control. This result suggested that blocking the lactate pathway was successful in switching the metabolism towards the oxidative route. This hypothesis was further confirmed by the analysis of the percentage of **PER** related to glycolytic metabolism **(% GlycoPER**) (**Figure 6.9.B**). The percent of GlycoPER was 78% of the total **PER** in WT cells while being only 30% of the total **PER** in ZeLa cells, again demonstrating that the knockout of LDH and the PDC enzymes caused a dramatic decrease in glycolytic metabolism and created a shift towards oxidative metabolism.

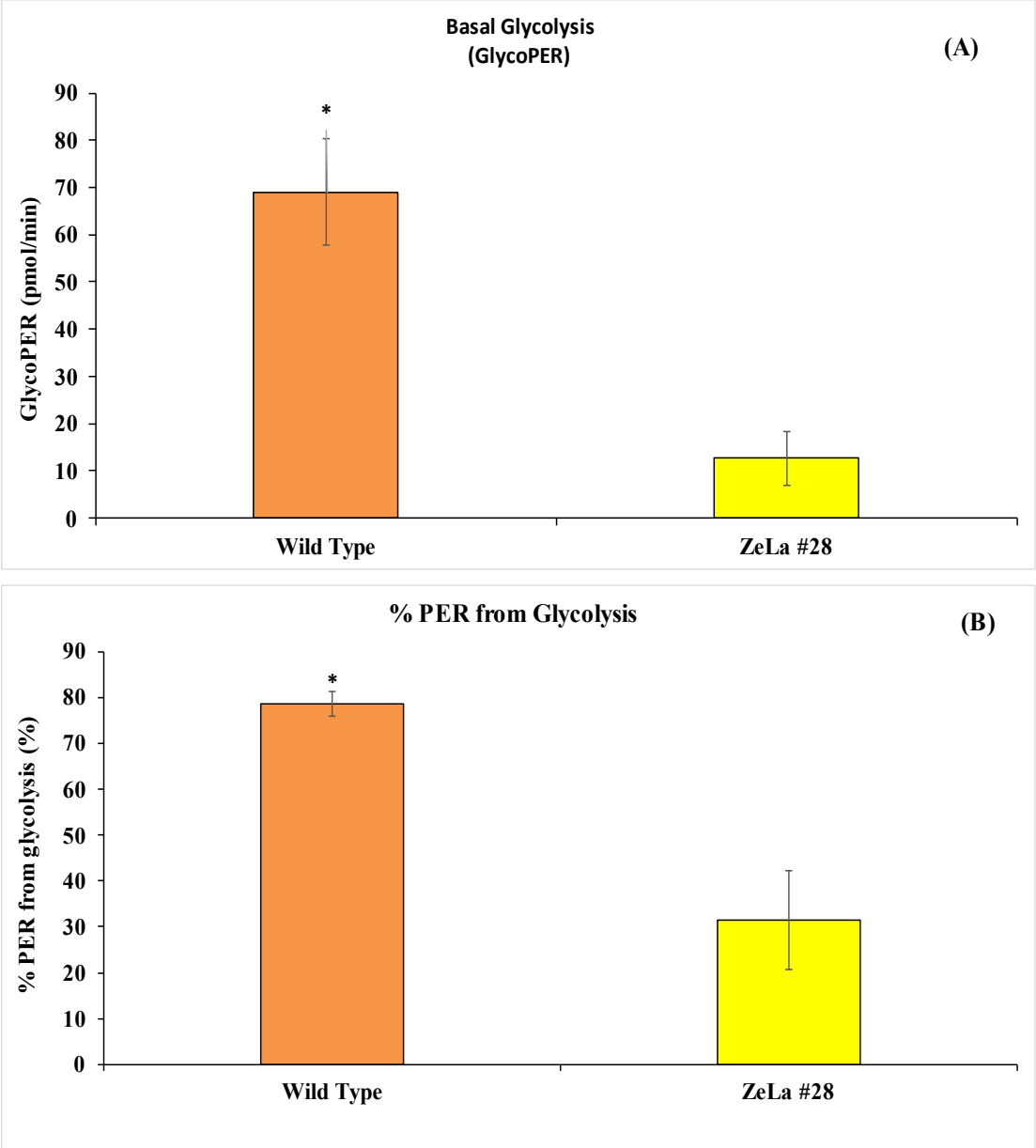

Figure 6. 9. (A) GlycoPER from Zero Lactate (ZeLa) and WT CHO cells after 96 hours of culture. Each bar represents the average GlycoPER level of biological triplicates measured in 15 technical replicates using Seahorse XF-96 analyser ± SD. Significance was tested using one-way ANOVA with $\alpha<0.05$, represented by * in the figure.

(B) Percent of PER associated with the glycolysis from Zero Lactate (ZeLa) and WT CHO cells. Each bar represents the average percent of PER associated with the level of biological triplicates measured in 15 technical replicates using Seahorse XF-96 analyser ± SD. Significance was tested using one-way ANOVA with $\alpha<0.05$, represented by * in the figure.

6.5. Discussion

6.5.1. The different E&L released by SUBs negatively impact the growth, viability, and metabolism of CHO cells.

The increased application of single-use plastics in Biopharmaceutical production – particularly in the bioreactor vessel – has led to some concerns related to E&Ls derived from those materials and their potential impact on patient safety as well as the behaviour of the producer cells in the vessel. This study demonstrated the impact of improved material design in the newer F-2 bioreactor model. The effect of these E&L on the growth and specific productivity of CHO cells was previously reported in the literature (*Hammond et al., 2013; Kelly et al., 2016; Shah et al., 2016*). However, more detailed metabolic profiling had not been performed. This study sought to fill an important gap in knowledge, illustrating how the effects of E&L on culture performance are likely a result of cell metabolism being impaired by the presence of these compounds.

Additionally, these results highlight how the improvement in SUB design can overall help to improve the culture performance of CHO cells. The F-2 model was designed with lower levels of Irgafos 168 in its composition, aiming to reduce the release of E&L to the media. Irgafos 168 is a secondary antioxidant commonly used in polyethylene-film-based plastic bags (*Kelly et al., 2016*), which breakdown releases bDtBPP, a cytotoxic compound, known to inhibit CHO cell growth *(Hammond et al., 2013; Shah et al., 2016*). The levels of both glycolytic and oxidative metabolism were increased when the media was incubated in the F-2 model to levels nearing the control media. Two different CHO lineages, DP12 and K1 essentially reacted in the same way to the presence of bDtBPP in the media, demonstrating that the detrimental effects caused by E&L in CHO cells are not limited to a specific lineage of cells. These results were included in a wider study, published in 2019 (*Kelly et al., 2019),* where higher levels of bDtBPP were confirmed in the F-1 model. However, the absence of the Irgafos 168 compound was noted for both SUB models F-1 and F-2. Nonetheless, the results obtained confirmed the materials used in the manufacturing of SUB model F-2 to release lower levels of E&L compared to model F-1 and demonstrate the necessity to further study and address the issue of cytotoxic E&L released by plastic bioreactors to improve the safety and efficiency of bioprocesses.

6.5.1. The Zero Lactate Cells (ZeLa) show increased oxidative metabolism and reduced media acidification.

All the results obtained in the analysis of CHO ZeLa cells compared with CHO WT cells for growth, viability, oxidative and glycolytic metabolism suggested a major change caused by the deactivation of LDHA activity achieved through several key knockouts. The growth and the viability of the cells remained similar. However, several changes in the metabolism of ZeLa cells were noted compared with the control. The ZeLa cells showed a slight increase in the oxygen consumption levels and, consequently, in oxidative metabolism compared to the control cells. Apart from this increase, the ZeLa cells demonstrated a dramatic decrease in glycolytic metabolism due to the knockout of the necessary enzymes required to convert pyruvate to lactate, thus being forced to shift to oxidative phosphorylation to generate ATP.

The Warburg effect, which causes aerobic lactate production, is a widely observed phenomenon in proliferative eukaryotic cells such as CHO cells. For this reason, as previously commented, the Warburg effect has been widely studied in the last decades in an attempt to understand the reasons and mechanisms behind this phenomenon (*Liberti and Locasale, 2016; Potter, Newport and Morten, 2016)*. As a result of aerobic glycolysis, lactate is produced as a wasteful product and released out of the cells, where it becomes lactic acid, contributing to media acidification which can negatively impact cell viability. Consequently, lactate levels are often monitored during bioprocesses (*Rafferty et al., 2020*) and many strategies have been developed to reduce the lactate levels in culture. To this end, numerous studies have tried to inhibit lactate production by different means, such as siRNAs, genomic editing via CRISPR, or chemical inhibitors targeting different LDH and/or PDHK complex subunits (*Jeong et al., 2001; Le et al., 2010; Calvaresi et al., 2013; Lewis et al., 2013; Yip et al., 2014; Martínez-Monge et al., 2019; Wilkens et al., 2019; Mazzio et al., 2020*). To date, most of the Warburg-null (or Zero Lactate) phenotypes achieved were hindered by the reduction or total absence of cell proliferation associated with these phenotypes. These reports were supported by the theories supporting the Warburg Effect as a fundamental part of the immortalized proliferative cells metabolism, which is highly dependent on the glycolytic route. Aerobic glycolysis is useful to produce energy, in the form of ATP, more rapidly than the oxidative route, supporting cell growth, maintenance, and general activities that may require energy in the cell (*Liberti and Locasale, 2016; Potter, Newport and Morten, 2016; Epstein,*

Gatenby and Brown, 2017). Additionally, the increased glycolytic flux in Warburg cells has been theorized to be necessary to produce higher levels of biomass precursors, allowing to increase the rate of proliferation during early culture phases (*Locasale and Cantley, 2011; Lunt and Vander Heiden, 2011; Liberti and Locasale, 2016*).

However, this data demonstrates that the generation of a Warburg-Null phenotype (Zero Lactate cells) is possible. While LDHA knockout resulted in a dramatic decrease of glycolytic metabolism, the increase observed in oxidative metabolism suggests the cells channel more glucose into the oxidative route. Therefore, the cells were not as dependant on aerobic fermentation of lactate to maintain their energy levels. Moreover, the elimination of the Warburg effect did not reduce the proliferation levels of the cells, which remained equal to the wild-type control. Therefore, the elimination of the Warburg effect with no detrimental effects to the cells was found to be feasible. The previously observed lethal effects of LDHA knockdown (*Yip et al., 2014*) was due to its involvement in several negative feedback loops, which can be removed if the involved genes are knocked down simultaneously. This highlights how the study of gene networks via genome editing screens and multiplex genome editing strategies (*Le et al., 2015; Hefzi et al., 2016; Najm et al., 2018*) could be used to engineer seemingly vital but ultimately unnecessary traits of CHO cells. As these zero lactate cells do not release lactic acid to the media as a waste product, the addition of bases to neutralize media acidification becomes unnecessary. Therefore, Zero Lactate is a valuable phenotype for industry, with the potential to be introduced into existing producing cell lines to improve their performance without causing drawbacks.

CHAPTER 7

CONCLUSIONS AND FUTURE WORK

7.1. Conclusions:

This study's main goal was to study the effects of heteroplasmy in the mitochondria, and subsequently, the metabolism of CHO cells. A sequencing experiment was then performed to assess the evolution of heteroplasmy throughout a few passages, to investigate the stability of these mitochondrial mutations within the clones. Additionally, the mitochondria were engineered through the transfection of several mitochondria-related genes in an attempt to improve the performance in culture of CHO cells. Finally, the effect of relatively new approaches on the metabolism of CHO cells was evaluated. The conclusions of this study are the following:

7.1.1: Evidence of the influence of heteroplasmy in the metabolism of the evaluated CHO clones was not obtained.

During this study, differences in the behavior of the evaluated CHO clones were observed. More specifically, several of the clones showed a growth phenotype corresponding with the previous classification as stated by Kelly and collaborators (*Kelly et al., 2017*). Additionally, differences in the mitochondrial content level, transcript levels, r-protein levels, and both oxidative and glycolytic metabolism were observed among the different clones evaluated.

Intra-group differences in the growth performance of CHO clones were noted, with clone CHO 513F being the clone with the higher growth ratio and mitochondrial content of the panel and clone CHO 596S showing a poor growth a metabolism performance. Curiously, CHO 513F showed higher levels of COX2 transcript compared to other clones from the panel, which may be related to the high frequency of the *m6996G>A* variant found only in FGPCs. However, it must be noted that this higher expression did not translate into significant metabolic changes, which may mean the expression of COX2 protein did not change despite the higher transcription. However, CHO 513F metabolism was shown to be similar to those of CHO 111S and CHO 520F despite the higher expression of both COX genes. Similarly, CHO 596S showed poor culture and metabolic performance despite showing much higher levels of CYTB transcripts than the rest of the clones. This may be due to higher CYTB levels being detrimental to the cells, as previously discussed, or simply due to an increase of CYTB transcripts, but not protein expression, due to the presence of non-functional copies of the transcript.

While an effect of heteroplasmy was suggested by these experiments, a clear relationship between the heteroplasmy and the metabolic phenotype of the cells could not be clearly established by these experiments alone, especially considering the lack of proteomic data.

Similarly, differences in response to a temperature shift caused by different heteroplasmy were suggested in clones 111S and 596S. The heteroplasmic mutation 14136*del*A may positively influence the response to temperature shift of CHO cells, allowing slow-growing cells to improve their culture performance. However, an actual relationship could not be proven. Finally, the response to a different growth media was different for each clone regardless of their previous phenotype group or the heteroplasmy present in them and was therefore considered non-related to heteroplasmy.

It must be noted that all the clones from the panel were observed to adapt in a similar fashion to the culture media if grown over a high number of passages. The clones' behaviour and growth phenotype and mitochondrial content became similar. This may be due to the cells adapting to the new media, as in previous studies a media provided by Pfizer which was not available anymore, was used to grow the cells. This adaptation phenomenon also raised the question about the clones' heteroplasmy be potentially changing over time, which lead to the evaluation of the evolution of heteroplasmy over time.

7.1.2: Heteroplasmy of CHO cells was observed to change throughout passages.

This part of the study aimed to study the variability of the heteroplasmy throughout 20 passages and check the potential effects of such changes, if any, in a panel of clones generated from the clone CHO 520F used in the previous part of the study. As described in the corresponding chapter (**Chapter 4**), the heteroplasmy was observed to change in all the 9 newly generated clones throughout 20 passages and even in the parental cell line.

Changes in different heteroplasmic variants previously reported in the clones were observed throughout 20 passages, as described below:

Some of these mutations were located in non-protein-coding sequences, such as tRNAVal sequence, containing the *m.1074C>T* non-coding variant showed high frequencies in most of the clones of the panel, this mutation was observed to be preserved in most clones

after 20 passages, meaning it either has a positive or a neutral effect in the metabolism and behavior of the cells, as previously discussed. Therefore, this mutation tends to become the dominant variant over time.

Some new mutations, which were not previously detected in the parental cell line, were also detected in this study, this was the case of the *m.9704C>T* variant at mitochondrial gene NAD3. This variant appeared to disappear in most of the clones after 20 passages, meaning it was either randomly drifting to disappearance or that this mutation had a negative effect on the metabolism of the cells. The latter hypothesis could be supported by reports in the literature reporting mutations in the NADH3 gene to be related to mitochondrial diseases, as discussed in section 4.3.

The case of COX2 m.6996G>A initiator codon variant, one of the mutations of interest as highlighted in the previous chapter, was curious, as it tends to disappear throughout 20 passages except in clone #6, in which its frequency was observed to increase over time. These results suggest that either this mutation had no effect on the cells and drifted randomly. An alternative hypothesis may be related to this mutation causing either the overexpression of non-functional COX2 proteins or overexpression of functional COX2 copies whose activity may be limited by the absence of other Complex IV COX subunits necessary to perform the role of COX protein in the respiratory chain complex.

Finally, CYTB was previously reported to be the mitochondrial protein-encoding gene with the most significant heteroplasmic mutations. Firstly, it contained the *m.14136delA* frameshift variant. This variant was the most extensive mutation in the panel, showing high frequencies in most clones, the only exception being clone #6, in which it showed a tendency to quickly diminished and eventually disappear. This variant was not varied in a significant way in most clones throughout 20 passages, which points to this mutation having a neutral effect on the metabolism of the cells, even at relatively high frequencies. Oppositely, the *m.14378G>A* stop codon variant tended to quickly diminish over time, even in early passages such as passage 4, this may be that *m.14378G>A* has a higher potential to impact oxidative metabolism, as mutations that negatively impact the activity of Complex III in a significant way are known to also impact Complex I activity indirectly. Therefore, if that was the case, the *m.14378G>A* stop codon variant will be negatively selected and will tend to disappear over time.

The evaluation of growth and r-protein titre of clones #5 and #6 and parental CHO-520F after a total of 20 passages showed differences in the phenotype which may be attributable to the differences in the heteroplasmy observed after the 20 passages. Clone #5 showed lower maximum viable cell density than the 520F parental, but similar specific productivity. Oppositely, clone #6 showed a similar maximum viable cell density to the parental but was not observed to yield an amount of r-protein observable by the assay used in this study. These results suggested the different evolution of heteroplasmy in these three cell lines to cause phenotypical differences. However, to further prove this relationship between heteroplasmy and phenotype changes, it will be desirable to collect more evidence at the proteomic, transcriptomic, and metabolic levels before being able to make strong assertions.

Overall, these results showed quick changes in heteroplasmy throughout a few passages, with the potential to influence the phenotype of the cells. These results can also help to explain the previously commented phenomenon of the CHO clones adopting a similar in-culture behavior after a high number of passages. This variation of heteroplasmy over a relatively short time may add another layer of complexity, previously unaccounted, to the problem of clone stability.

7.1.3: Overexpression of DRP1 improved CHO cells culture performance, while overexpression of PGC1α or ANT1 knockdown was detrimental.

The results highlighted and discussed in **Chapter 5** of this study showed the overexpression of the DRP1 gene in CHO cells being helpful to improve the lifespan of CHO cells in culture. As the DRP1 gene was previously reported in the literature to increase the mitochondrial fission process, protecting the mitochondria from excessive ROS damage (*E. Smirnova et al., 2001*) these results suggest the increase in mitochondrial fission was indeed occurring. However, a decrease in mitochondrial content was also reported, which was hypothesized to be a product of the mitochondria becoming briefly inactive after fission, which made them unable to be detected by the Mitotracker dye assay and could also explain the reduction in r-protein titre observed, as the oxidative metabolism will be also reduced in comparison with control cells. While these results were backed by an increase in DRP1 transcription, more experiments to determine the DRP1 protein expression and the changes in the metabolic activity of CHO-K1-DRP1

cells will be needed to determine without a doubt the influence of DRP1 overexpression in the metabolism of CHO cells.

Oppositely, the overexpression of PGC1α increased mitochondrial content, which was expected as PGC1α was known to increase mitochondrial biogenesis and promote OXPHOS metabolism. However, PGC1α overexpression also resulted in a reduced lifespan of CHO-K1 cells, with their viability quickly decreasing after 3 days of culture unless the media was promptly replaced every 48 hours of culture. It is possible that the PGC1α overexpression and subsequent increase in mitochondrial numbers generated an enormous amount of ROS in the cells, causing oxidative damage and being detrimental to viability. Additionally, these increases in mitochondrial numbers did not translate into an increase in r-protein titre. Both these occurrences were theorized by the mouse PGC1α not being able to interact with the corresponding CHO transcription factors, which expression was observed to not change. However, the lack of proteomic and metabolic data prevented reaching a strong conclusion about the influence of mouse PGC1α overexpression in CHO cells.

Finally, the knockdown of ANT1 in CHO-K1-EPO cells using a siRNA caused an increase in maximum viable cell density, but an early, sharp decrease in viability and r-protein specific productivity compared with control cells. ANT1 knockdown was previously reported in the literature to cause mitochondrial hyperproliferation and max ETS state, uncoupled from ATP synthesis, in the cells. Like in the case of PGC1α, the increase of the ETS can lead to a quick accumulation of ROS, causing a sharp decrease in viability. Additionally, like in the case of DRP1, the hyperproliferation of mitochondria can potentially lead to the presence of aberrant, non-functional mitochondria, making the cells resort to glycolytic metabolism, promoting the proliferation of the cells but reducing their specific productivity. Like in the previous cases, more data will be needed to make a strong statement about the effects of ANT1 knockdown on CHO-K1-EPO cells, more specifically, proteomic and metabolic data.

In summary, data suggest DRP1 overexpression is beneficial for CHO-K1-EPO cells viability, while both overexpression of PGC1α and ANT1 knockdown seemed detrimental for both viability and r-protein specific productivity. However, the collection of proteomic and metabolic data on these clones could help further clarify whether these observations are accurate.

7.1.4: New model plastic bioreactors can improve the general culture performance of CHO cells.

The increased application of single-use plastic bioreactors in the generation of biopharmaceutical products led to concerns about the safety of these bioreactors, related to the potential release of E&L, which detrimental effect on cell culture has already been reported in the literature (*Hammond et al., 2013; Kelly et al., 2016; Shah et al., 2016*).

The results described in section 6.1 of this study suggest the possibility of improving the CHO cell culture performance by using materials that break down releases bDtBPP, a cytotoxic compound, in the plastic bioreactors. Cells grown in media previously cultured in the newer F-2 bioreactor models, designed to contain lower levels of bDtBPP, demonstrated similar levels of growth and viability to those of the control cells, while the cells grown in media previously cultured in an older model of a plastic bioreactor, F-1, which contained higher levels of bDtBPP, showed reduced growth and viability. Similarly, the metabolic profile of cells grown in F-2 cultured media was more similar to the control cells than the metabolic profile of cells grown in F-1 cultured media, which showed a reduction in both oxidative and metabolic metabolism.

These results, which were part of a wider study, confirmed the materials used in the manufacturing of SUB model F-2 to release lower levels of E&L compared to model F-1 and demonstrate the necessity to further study and address the issue of cytotoxic E&L released by plastic bioreactors to improve the safety and efficiency of bioprocesses.

7.1.5: Warburg-Null CHO cells showed decreased lactate generation.

When engineering cell metabolism, Warburg metabolism constitutes one of the main metabolic phenomena of interest, as control over the metabolic shift to oxidative metabolism could reduce the accumulation of wasteful products in bioreactor culture, such as lactate while improving the r-protein productivity of the cells. For this reason, the generation of a CHO Warburg-Null cell line, unable to generate lactate as a wasteful product, has been repeatedly attempted to no avail. Recently, a research group generated a CHO Warburg-Null cell line by quadruple knockdown of PDHK and LDHA and kindly provided the cell to our laboratory to test the phenotype and metabolic profile.

The results obtained showed the CHO Warburg-Null cells' growth and viability to remain similar to those of control (CHO WT) cells. The metabolic profile of CHO Warburg-Null cells showed a slight increase in oxidative metabolism levels and a sharp decrease in glycolytic metabolism compared to control cells, probably due to the knockdowns performed in the cells effectively impeding the glycolytic route, making the cells fully dependent on the oxidative metabolism.

These results, which are part of a much wider study yet to be published, suggest that the generation of CHO Warburg-Null cells with no detrimental effects on culture performance or cell metabolism, previously thought impossible, can be done. Such cells will have the potential to produce valuable r-proteins at high efficiency without generating wasteful products such as lactate.

7.2. Future Work

7.2.1: Future work on heteroplasmy assessment:

The results obtained from the panel of CHO clones with different heteroplasmic variants suggested some degree of influence of the heteroplasmy in the metabolic phenotype of the clones. However, due to time and technical constraints, as well as the clones seemingly adapting to the media, the influence of heteroplasmy could not be clearly proven nor refuted. The next natural step in this line will be to obtain accurate proteomic data of COX2 and CYTB expression in the different clones to evaluate if the variability observed in transcript levels in the clones corresponds to the actual expression of the proteins.

Additionally, should proteomic data for COX2 and CYTB could be obtained, the temperature shift experiments could be repeated, this time performing an analysis of r-protein titre and specific productivity, which was not done in this study due to technical and time constraints.

7.2.2: Future work on heteroplasmy variability over passages :

The generation of a panel of CHO clones from clone CHO 520F showed differences in heteroplasmy among the panel of clones and the parental, which were observed to varied over time in different directions. Two clones, #5 and #6, plus the parental CHO 520F

clones were then evaluated to check the effects of these heteroplasmic changes on them. However, no proteomic or metabolic data from these clones could be generated, due to technical constraints. Therefore, the next logical step will consist in the obtention of this metabolic data, preferably using an XF-analyser system, to observe whether the observed changes correspond with changes in the metabolism.

In addition, while these clones originated from a single cell cloning process, the sequenced mtDNA was extracted after several passages from a population of cells, meaning the observed heteroplasmy represents the different mtDNA copies in a population of cells, ignoring the intra-population variation of heteroplasmy. Therefore, the next step could be the sequencing of heteroplasmy down to the single-cell level. Cells will be sorted by an advanced cell-sorting system, such as FACS, and then their mtDNA will be sequenced to figure out the intra-population variation of heteroplasmy, showing the variation of heteroplasmy cell to cell.

7.2.3: Future work on transfections :

Given the results obtained from the cells' overexpression of PGC1α and DRP1, and assuming the decline in viability observed by PGC1α was caused by ROS, the co-overexpression of PGC1α and DRP1 could be the next step in this direction, allowing to observe whether the theoretical increase in ROS caused by PGC1α overexpression is mitigated by the increased mitochondrial fission caused by DRP1.

As ANT1 was knockdown using a siRNA transfection, which did not allow the creation of a stable clone, a more accurate evaluation of ANT1 knockdown long-term effects could be performed by using genome editing systems, such as CRISPR-Cas9, to stably knockdown this gene, given the results obtained in this study showed the ANT- CHO-K1 cells are stable.

7.2.4: Future work on Bioreactor E&L :

This study and the corresponding publication highlighted the influence of the plastic bioreactors' composition on the cell culture performance. Two different CHO cell lines, namely CHO-K1 and CHO-DP12 were shown to be negatively impacted by the presence of plastic E&L in the media, such as bDtBPP. However, while detrimental, the effect of

the bDtBPP was slightly different for both cell lines. Subsequently, more experiments could be performed to determine how the metabolic profile of different CHO cell lines or even CHO cells from the same lineage expressing different types of r-protein are impacted by the presence of E&L in the media. In addition, further study on the potential E&L release by the bioreactors could be performed to further improve the in-culture performance of CHO cells without complex engineering processes.

7.2.5: Future work on Warburg-Null (Zero Lactate) cells :

The generation of Warburg-Null CHO cells could constitute an important milestone in biopharmaceutical production. The generation of Warburg-Null cells capable of producing r-protein products without generating wasteful products can improve the process efficiency and reduce cost by reducing the need for the product purification step. However, the generation of Warburg-Null CHO cells capable of generating high-quality, human-like, and hard-to-produce r-protein must be tested, as it is potentially possible that their dependency on the oxidative metabolism can reduce their r-recombinant producing capabilities.

Bibliography and references

Acín-Pérez, R. *et al.* (2004) 'Respiratory complex III is required to maintain complex I in mammalian mitochondria', *Molecular Cell*, 13(6), pp. 805–815. doi: 10.1016/S1097-2765(04)00124-8.

Alexeyev, M. *et al.* (2013) 'The maintenance of mitochondrial DNA integrity - Critical analysis and update', *Cold Spring Harbor Perspectives in Biology*, 5(5), pp. 1–17. doi: 10.1101/cshperspect.a012641.

Altamirano, C. *et al.* (2000) 'Improvement of CHO cell culture medium formulation: Simultaneous substitution of glucose and glutamine', *Biotechnology Progress*, 16(1), pp. 69–75. doi: 10.1021/bp990124j.

van den Ameele, J. *et al.* (2020) 'Mitochondrial heteroplasmy beyond the oocyte bottleneck', *Seminars in Cell and Developmental Biology*, 97(September), pp. 156–166. doi: 10.1016/j.semcdb.2019.10.001.

Andersson, U. and Scarpulla, R. C. (2001) 'PGC-1-Related Coactivator, a Novel, Serum-Inducible Coactivator of Nuclear Respiratory Factor 1-Dependent Transcription in Mammalian Cells', *Molecular and Cellular Biology*, 21(11), pp. 3738–3749. doi: 10.1128/mcb.21.11.3738-3749.2001.

Ascenzi, F. *et al.* (2019) 'Effects of IGF-1 isoforms on muscle growth and sarcopenia', *Aging Cell*, 18(3), pp. 1–11. doi: 10.1111/acel.12954.

Ayanga, B. A. *et al.* (2016) 'Dynamin-related protein 1 deficiency improves mitochondrial fitness and protects against progression of diabetic nephropathy', *Journal of the American Society of Nephrology*, 27(9), pp. 2733–2747. doi: 10.1681/ASN.2015101096.

Bacman, S. R. *et al.* (2013) 'Specific elimination of mutant mitochondrial genomes in patient-derived cells by mitoTALENs', *Nature Medicine*, 19(9), pp. 1111–1113. doi: 10.1038/nm.3261.

Barrett, A. *et al.* (2020) 'Pronounced somatic bottleneck in mitochondrial DNA of human hair', *Philosophical Transactions of the Royal Society B: Biological Sciences*,

375(1790). doi: 10.1098/rstb.2019.0175.
Barron, N. *et al.* (2011) 'Engineering CHO cell growth and recombinant protein productivity by overexpression of miR-7', *Journal of Biotechnology*, 151(2), pp. 204–211. doi: 10.1016/j.jbiotec.2010.12.005.
Battersby, B. J., Loredo-Osti, J. C. and Shoubridge, E. A. (2003) 'Nuclear genetic control of mitochondrial DNA segregation', *Nature Genetics*, 33(2), pp. 183–186. doi: 10.1038/ng1073.
Bender, A. *et al.* (2006) 'High levels of mitochondrial DNA deletions in substantia nigra neurons in aging and Parkinson disease', *Nature Genetics*, 38(5), pp. 515–517. doi: 10.1038/ng1769.
Berting, A., Farcet, M. R. and Kreil, T. R. (2010) 'Virus susceptibility of Chinese hamster ovary (CHO) cells and detection of viral contaminations by adventitious agent testing', *Biotechnology and Bioengineering*, 106(4), pp. 598–607. doi: 10.1002/bit.22723.
Besseiche, A. *et al.* (2015) 'Metabolic roles of PGC-1α and its implications for type 2 diabetes', *Diabetes and Metabolism*, 41(5), pp. 347–357. doi: 10.1016/j.diabet.2015.02.002.
Black, M. *et al.* (2020) 'FOXM1 nuclear transcription factor translocates into mitochondria and inhibits oxidative phosphorylation.', 31(13), pp. 1411–1424. doi: 10.1091/mbc.E19-07-0413.
Blakely, E. L. *et al.* (2014) 'Distal weakness with respiratory insufficiency caused by the m.8344A>G "MERRF" mutation', *Neuromuscular Disorders*, 24(6), pp. 533–536. doi: 10.1016/j.nmd.2014.03.011.
Bourens, M. *et al.* (2014) 'Human COX20 cooperates with SCO1 and SCO2 to mature COX2 and promote the assembly of cytochrome c oxidase', *Human Molecular Genetics*, 23(11), pp. 2901–2913. doi: 10.1093/hmg/ddu003.
Bourens, M. and Barrientos, A. (2017) 'Human mitochondrial cytochrome c oxidase assembly factor COX18 acts transiently as a membrane insertase within the subunit 2 maturation module', *Journal of Biological Chemistry*, 292(19), pp. 7774–7783. doi: 10.1074/jbc.M117.778514.
Brenner, C. *et al.* (2011) 'Adenine nucleotide translocase family: Four isoforms for apoptosis modulation in cancer', *Oncogene*, 30(8), pp. 883–895. doi: 10.1038/onc.2010.501.

Brown, A. *et al.* (2014) ‘Structure of the large ribosomal subunit from human mitochondria’, *Science*, 346(6210), pp. 718–722. doi: 10.1126/science.1258026.
Buchsteiner, M. *et al.* (2018) ‘Improving culture performance and antibody production in CHO cell culture processes by reducing the Warburg effect’, *Biotechnology and Bioengineering*, 115(9), pp. 2315–2327. doi: 10.1002/bit.26724.
Bulté, D. B. *et al.* (2020a) *Overexpression of the mitochondrial pyruvate carrier reduces lactate production and increases recombinant protein productivity in CHO cells*, *Biotechnology and Bioengineering*. doi: 10.1002/bit.27439.
Bulté, D. B. *et al.* (2020b) ‘Overexpression of the mitochondrial pyruvate carrier reduces lactate production and increases recombinant protein productivity in CHO cells’, *Biotechnology and Bioengineering*, 117(9), pp. 2633–2647. doi: 10.1002/bit.27439.
Calvaresi, E. C. *et al.* (2013) ‘Dual targeting of the warburg effect with a glucose-conjugated lactate dehydrogenase inhibitor’, *ChemBioChem*, 14(17), pp. 2263–2267. doi: 10.1002/cbic.201300562.
Capella Roca, B. *et al.* (2019) ‘Zinc supplementation increases protein titer of recombinant CHO cells’, *Cytotechnology*, 71(5), pp. 915–924. doi: 10.1007/s10616-019-00334-1.
Cassidy-Stone, A. *et al.* (2008) ‘Chemical Inhibition of the Mitochondrial Division Dynamin Reveals Its Role in Bax/Bak-Dependent Mitochondrial Outer Membrane Permeabilization’, *Developmental Cell*, 14(2), pp. 193–204. doi: 10.1016/j.devcel.2007.11.019.
Chakrabarti, L. *et al.* (2019) ‘Mitochondrial membrane potential identifies cells with high recombinant protein productivity’, *Journal of Immunological Methods*, 464, pp. 31–39. doi: 10.1016/j.jim.2018.10.007.
Chan, D. C. (2006) ‘Mitochondrial fusion and fission in mammals’, *Annual Review of Cell and Developmental Biology*, 22, pp. 79–99. doi: 10.1146/annurev.cellbio.22.010305.104638.
Cheng, C. F., Ku, H. C. and Lin, H. (2018) ‘Pgc-1α as a pivotal factor in lipid and metabolic regulation’, *International Journal of Molecular Sciences*, 19(11), pp. 1–21. doi: 10.3390/ijms19113447.
Chevallier, V., Andersen, M. R. and Malphettes, L. (2020) ‘Oxidative stress-alleviating strategies to improve recombinant protein production in CHO cells’, *Biotechnology and*

Bioengineering, 117(4), pp. 1172–1186. doi: 10.1002/bit.27247.
Chinnery, P. F. *et al.* (1997) 'Molecular pathology of MELAS and MERRF The relationship between mutation load and clinical phenotypes', pp. 1713–1721.
Chinnery, P. F. and Samuels, D. C. (1999) 'Relaxed replication of mtDNA: A model with implications for the expression of disease', *American Journal of Human Genetics*, 64(4), pp. 1158–1165. doi: 10.1086/302311.
Chinsomboon, J. *et al.* (2009) 'The transcriptional coactivator PGC-1α mediates exercise-induced angiogenesis in skeletal muscle', *Proceedings of the National Academy of Sciences of the United States of America*, 106(50), pp. 21401–21406. doi: 10.1073/pnas.0909131106.
Chrzanowska-Lightowlers, Z., Rorbach, J. and Minczuk, M. (2017) 'Human mitochondrial ribosomes can switch structural tRNAs–but when and why?', *RNA Biology*, 14(12), pp. 1668–1671. doi: 10.1080/15476286.2017.1356551.
Cingolani, P. *et al.* (2012) 'Using Drosophila melanogaster as a model for genotoxic chemical mutational studies with a new program, SnpSift', *Frontiers in Genetics*, 3(MAR). doi: 10.3389/fgene.2012.00035.
Clark, K. M., Bindoff, L. A., Lightowlers, R. N., Andrews, R. M., Griffiths, P. G., Johnson, M. A., … Turnbull, D. M. (1997) 'Reversal of a mitochondrial DNA defect in human skeletal muscle', *Nature Genetics*, 16(3), pp. 222–224. doi: doi:10.1038/ng0797-222.
Corral-Debrinski, M. *et al.* (1994) 'Marked changes in mitochondrial dna deletion levels in alzheimer brains', *Genomics*, pp. 471–476. doi: 10.1006/geno.1994.1525.
Cost, G. J. *et al.* (2010) 'BAK and BAX deletion using zinc-finger nucleases yields apoptosis-resistant CHO cells', *Biotechnology and Bioengineering*, 105(2), pp. 330–340. doi: 10.1002/bit.22541.
Cui, J. *et al.* (2014) 'FOXM1 promotes the warburg effect and pancreatic cancer progression via transactivation of LDHA expression', *Clinical Cancer Research*, 20(10), pp. 2595–2606. doi: 10.1158/1078-0432.CCR-13-2407.
Dasgupta, S. *et al.* (2008) 'Mitochondrial Cytochrome B gene mutation promotes tumor growth in bladder cancer', *Cancer Research*, 68(3), pp. 700–706. doi: 10.1158/0008-5472.CAN-07-5532.
Demine, S., Renard, P. and Arnould, T. (2019) 'Mitochondrial Uncoupling: A Key Controller of Biological Processes in Physiology and Diseases', *Cells*, 8(8), pp. 1–43.

doi: 10.3390/cells8080795.
Dillon, L. M., Rebelo, A. P. and Moraes, C. T. (2012) 'The role of PGC-1 coactivators in aging skeletal muscle and heart', *IUBMB Life*, 64(3), pp. 231–241. doi: 10.1002/iub.608.
Dinulovic, I. *et al.* (2016) 'PGC-1α modulates necrosis, inflammatory response, and fibrotic tissue formation in injured skeletal muscle', *Skeletal Muscle*, 6(1), pp. 1–11. doi: 10.1186/s13395-016-0110-x.
Diot, A. *et al.* (2016) 'Modulating mitochondrial quality in disease transmission: Towards enabling mitochondrial DNA disease carriers to have healthy children', *Biochemical Society Transactions*, 44(4), pp. 1091–1100. doi: 10.1042/BST20160095.
Dobrowolny, G. *et al.* (2005) 'Muscle expression of a local Igf-1 isoform protects motor neurons in an ALS mouse model', *Journal of Cell Biology*, 168(2), pp. 193–199. doi: 10.1083/jcb.200407021.
Druz, A. *et al.* (2013) 'Stable inhibition of mmu-miR-466h-5p improves apoptosis resistance and protein production in CHO cells', *Metabolic Engineering*, 16(1), pp. 87–94. doi: 10.1016/j.ymben.2012.12.004.
Dulac, M. *et al.* (2020) 'Drp1 knockdown induces severe muscle atrophy and remodelling, mitochondrial dysfunction, autophagy impairment and denervation', *Journal of Physiology*, 598(17), pp. 3691–3710. doi: 10.1113/JP279802.
Durham, S. E. *et al.* (2007) 'Normal levels of wild-type mitochondrial DNA maintain cytochrome c oxidase activity for two pathogenic mitochondrial DNA mutations but not for m.3243A→G', *American Journal of Human Genetics*, 81(1), pp. 189–195. doi: 10.1086/518901.
Edros, R., McDonnell, S. and Al-Rubeai, M. (2014) 'The relationship between mTOR signalling pathway and recombinant antibody productivity in CHO cell lines', *BMC Biotechnology*, 14, pp. 14–16. doi: 10.1186/1472-6750-14-15.
Edros, R. Z., McDonnell, S. and Al-Rubeai, M. (2013) 'Using Molecular Markers to Characterize Productivity in Chinese Hamster Ovary Cell Lines', *PLoS ONE*, 8(10). doi: 10.1371/journal.pone.0075935.
El-Hattab, A. W. *et al.* (2015) 'MELAS syndrome: Clinical manifestations, pathogenesis, and treatment options', *Molecular Genetics and Metabolism*, 116(1–2), pp. 4–12. doi: 10.1016/j.ymgme.2015.06.004.
Elliott, H. R. *et al.* (2008) 'Pathogenic Mitochondrial DNA Mutations Are Common in

the General Population', *American Journal of Human Genetics*, 83(2), pp. 254–260. doi: 10.1016/j.ajhg.2008.07.004.
Epstein, T., Gatenby, R. A. and Brown, J. S. (2017) 'The Warburg effect as an adaptation of cancer cells to rapid fluctuations in energy demand', *PLoS ONE*, 12(9), pp. 1–14. doi: 10.1371/journal.pone.0185085.
Erich Pfaff, Hans Walter Heldt, M. K. (1969) 'Adenine Nucleotide Translocation', *European J. Biochem*, 10, pp. 484–493.
Estrella, V. *et al.* (2013) 'Acidity generated by the tumor microenvironment drives local invasion', *Cancer Research*, 73(5), pp. 1524–1535. doi: 10.1158/0008-5472.CAN-12-2796.
Fan, W. *et al.* (2008) 'A mouse model of mitochondrial disease reveals germline selection against severe mtDNA mutations', *Science*, 319(5865), pp. 958–962. doi: 10.1126/science.1147786.
Fernández-Vizarra, E. and Zeviani, M. (2015) 'Nuclear gene mutations as the cause of mitochondrial complex III deficiency', *Frontiers in Genetics*, 6(APR), pp. 1–11. doi: 10.3389/fgene.2015.00134.
Fischer, S. *et al.* (2017) 'miRNA engineering of CHO cells facilitates production of difficult-to-express proteins and increases success in cell line development', *Biotechnology and Bioengineering*, 114(7), pp. 1495–1510. doi: 10.1002/bit.26280.
Fischer, S., Handrick, R. and Otte, K. (2015) 'The art of CHO cell engineering: A comprehensive retrospect and future perspectives', *Biotechnology Advances*, 33(8), pp. 1878–1896. doi: 10.1016/j.biotechadv.2015.10.015.
Floris, P. *et al.* (2020) 'Real-time characterization of mammalian cell culture bioprocesses by magnetic sector MS', *Analytical Methods*, 12(46), pp. 5601–5612. doi: 10.1039/d0ay01563f.
Fox, S. R. *et al.* (2005) 'Active hypothermic growth: a novel means for increasing total interferon-γ production by Chinese-hamster ovary cells', *Biotechnology and Applied Biochemistry*, 41(3), p. 265. doi: 10.1042/ba20040067.
Fraidakis, M. J. *et al.* (2014) 'Phenotypic diversity associated with the MT-TV gene m.1644G>A mutation, a matter of quantity', *Mitochondrion*, 15(1), pp. 34–39. doi: 10.1016/j.mito.2014.03.010.
Frank, S. *et al.* (2001) 'The Role of Dynamin-Related Protein 1, a Mediator of Mitochondrial Fission, in Apoptosis', *Developmental Cell*, 1(4), pp. 515–525. doi:

10.1016/S1534-5807(01)00055-7.
Freund, N. W. and Croughan, M. S. (2018) ‘A simple method to reduce both lactic acid and ammonium production in industrial animal cell culture’, *International Journal of Molecular Sciences*, 19(2). doi: 10.3390/ijms19020385.
Gagnon, M. *et al.* (2011) ‘High-End pH-controlled delivery of glucose effectively suppresses lactate accumulation in CHO Fed-batch cultures’, *Biotechnology and Bioengineering*, 108(6), pp. 1328–1337. doi: 10.1002/bit.23072.
Gammage, P. A., Moraes, C. T. and Minczuk, M. (2018) ‘Mitochondrial Genome Engineering: The Revolution May Not Be CRISPR-Ized’, *Trends in Genetics*, 34(2), pp. 101–110. doi: 10.1016/j.tig.2017.11.001.
Gao, P. *et al.* (2009) ‘C-Myc suppression of miR-23a/b enhances mitochondrial glutaminase expression and glutamine metabolism’, *Nature*, 458(7239), pp. 762–765. doi: 10.1038/nature07823.
Garcia, S. *et al.* (2018) ‘Overexpression of PGC-1α in aging muscle enhances a subset of young-like molecular patterns’, *Aging Cell*, 17(2), pp. 1–12. doi: 10.1111/acel.12707.
Geldon, S., Fernández-Vizarra, E. and Tokatlidis, K. (2021) ‘Redox-Mediated Regulation of Mitochondrial Biogenesis, Dynamics, and Respiratory Chain Assembly in Yeast and Human Cells’, *Frontiers in Cell and Developmental Biology*, 9(September), pp. 1–24. doi: 10.3389/fcell.2021.720656.
Gleyzer, N., Vercauteren, K. and Scarpulla, R. C. (2005) ‘Control of Mitochondrial Transcription Specificity Factors (TFB1M and TFB2M) by Nuclear Respiratory Factors (NRF-1 and NRF-2) and PGC-1 Family Coactivators’, *Molecular and Cellular Biology*, 25(4), pp. 1354–1366. doi: 10.1128/mcb.25.4.1354-1366.2005.
Grady, J. P. *et al.* (2018) ‘mtDNA heteroplasmy level and copy number indicate disease burden in m.3243A>G mitochondrial disease’, *EMBO Molecular Medicine*, 10(6), pp. 1–13. doi: 10.15252/emmm.201708262.
Graham, R. J. *et al.* (2021) ‘Effect of iron addition on mAb productivity and oxidative stress in Chinese hamster ovary culture’, *Biotechnology Progress*, (February), pp. 1–12. doi: 10.1002/btpr.3181.
Greaves, L. C. *et al.* (2006) ‘Mitochondrial DNA mutations are established in human colonic stem cells, and mutated clones expand by crypt fission’, *Proceedings of the National Academy of Sciences of the United States of America*, 103(3), pp. 714–719. doi: 10.1073/pnas.0505903103.

Gupta, S. K. *et al.* (2017) 'Metabolic engineering of CHO cells for the development of a robust protein production platform', *PLoS ONE*, 12(8), pp. 1–23. doi: 10.1371/journal.pone.0181455.
Gupta, S. K. and Shukla, P. (2017) 'Gene editing for cell engineering: trends and applications', *Critical Reviews in Biotechnology*, 37(5), pp. 672–684. doi: 10.1080/07388551.2016.1214557.
Gutierrez, J. M. *et al.* (2020) 'Genome-scale reconstructions of the mammalian secretory pathway predict metabolic costs and limitations of protein secretion', *Nature Communications*, 11(1), pp. 1–10. doi: 10.1038/s41467-019-13867-y.
Hammond, M. *et al.* (2013) 'Identification of a leachable compound detrimental to cell growth in single-use bioprocess containers', *PDA Journal of Pharmaceutical Science and Technology*, 67(2), pp. 123–134. doi: 10.5731/pdajpst.2013.00905.
Hartley, F. *et al.* (2018) 'Mechanisms driving the lactate switch in Chinese hamster ovary cells', *Biotechnology and Bioengineering*, 115(8), pp. 1890–1903. doi: 10.1002/bit.26603.
He, X. *et al.* (2012) 'Peri-implantation lethality in mice lacking the PGC-1-related coactivator protein', *Developmental Dynamics*, 241(5), pp. 975–983. doi: 10.1002/dvdy.23769.
Hefzi, H. *et al.* (2016) 'A Consensus Genome-scale Reconstruction of Chinese Hamster Ovary Cell Metabolism', *Cell Systems*, 3(5), pp. 434-443.e8. doi: 10.1016/j.cels.2016.10.020.
Heiden, M. G. V., Cantley, L. C. and Thompson, C. B. (2009) 'Understanding the warburg effect: The metabolic requirements of cell proliferation', *Science*, 324(5930), pp. 1029–1033. doi: 10.1126/science.1160809.
Hinterkörner, G. *et al.* (2007) 'Improvement of the energy metabolism of recombinant CHO cells by cell sorting for reduced mitochondrial membrane potential', *Journal of Biotechnology*, 129(4), pp. 651–657. doi: 10.1016/j.jbiotec.2007.02.002.
Hock, D. H., Robinson, D. R. L. and Stroud, D. A. (2020) 'Blackout in the powerhouse: Clinical phenotypes associated with defects in the assembly of OXPHOS complexes and the mitoribosome', *Biochemical Journal*, 477(21), pp. 4085–4132. doi: 10.1042/BCJ20190767.
Hock, M. B. and Kralli, A. (2009) 'Transcriptional control of mitochondrial biogenesis and function', *Annual Review of Physiology*, 71, pp. 177–203. doi:

10.1146/annurev.physiol.010908.163119.
Hoshan, L. *et al.* (2019) 'Effective bioreactor pH control using only sparging gases', *Biotechnology Progress*, 35(1), pp. 1–7. doi: 10.1002/btpr.2743.
Hoshino, A. *et al.* (2019) 'The ADP/ATP translocase drives mitophagy independent of nucleotide exchange', *Nature*, 575(7782), pp. 375–379. doi: 10.1038/s41586-019-1667-4.
Huang, T. Y. *et al.* (2017) 'Overexpression of PGC-1α increases peroxisomal activity and mitochondrial fatty acid oxidation in human primary myotubes', *American Journal of Physiology - Endocrinology and Metabolism*, 312(4), pp. E253–E263. doi: 10.1152/ajpendo.00331.2016.
Ihsan, M., Watson, G. and Abbiss, C. (2014) 'PGC-1α Mediated Muscle Aerobic Adaptations to Exercise, Heat and Cold Exposure', *Cellular and Molecular Exercise Physiology*, 3(1). doi: 10.7457/cmep.v3i1.e7.
Ikeda, M. *et al.* (2015) 'Overexpression of TFAM or twinkle increases mtDNA copy number and facilitates cardioprotection associated with limited mitochondrial oxidative stress', *PLoS ONE*, 10(3), pp. 1–19. doi: 10.1371/journal.pone.0119687.
Jacobi, F. K. *et al.* (2001) 'Segregation patterns and heteroplasmy prevalence in Leber's hereditary optic neuropathy', *Investigative Ophthalmology and Visual Science*, 42(6), pp. 1208–1214.
Jankauskaitė, E., Bartnik, E. and Kodroń, A. (2017) 'Investigating Leber's hereditary optic neuropathy: Cell models and future perspectives', *Mitochondrion*, 32, pp. 19–26. doi: 10.1016/j.mito.2016.11.006.
Jeng, J. Y. *et al.* (2008) 'Maintenance of mitochondrial DNA copy number and expression are essential for preservation of mitochondrial function and cell growth', *Journal of Cellular Biochemistry*, 103(2), pp. 347–357. doi: 10.1002/jcb.21625.
Jeong, D. won *et al.* (2001) 'Blocking of acidosis-mediated apoptosis by a reduction of lactate dehydrogenase activity through antisense mRNA expression', *Biochemical and Biophysical Research Communications*, 289(5), pp. 1141–1149. doi: 10.1006/bbrc.2001.6091.
Jeong, D. won *et al.* (2006) 'Effects of lactate dehydrogenase suppression and glycerol-3-phosphate dehydrogenase overexpression on cellular metabolism', *Molecular and Cellular Biochemistry*, 284(1–2), pp. 1–8. doi: 10.1007/s11010-005-9004-7.
Jiménez, N. E., Wilkens, C. A. and Gerdtzen, Z. P. (2011) 'Engineering CHO cell

metabolism for growth in galactose', *BMC Proceedings*, 5(Suppl 8), p. P119. doi: 10.1186/1753-6561-5-s8-p119.
Jiménez, N., Martínez, V. S. and Gerdtzen, Z. P. (2019) 'Engineering CHO cells galactose metabolism to reduce lactate synthesis', *Biotechnology Letters*, 41(6–7), pp. 779–788. doi: 10.1007/s10529-019-02680-8.
Jin, C. *et al.* (2020) 'Drp1-mediated mitochondrial fission induced autophagy attenuates cell apoptosis caused by 3-chlorpropane-1,2-diol in HEK293 cells', *Food and Chemical Toxicology*, 145(July), p. 111740. doi: 10.1016/j.fct.2020.111740.
Jin, L. H. and Wei, C. (2014) 'Role of microRNAs in the Warburg effect and mitochondrial metabolism in cancer', *Asian Pacific Journal of Cancer Prevention*, 15(17), pp. 7015–7019. doi: 10.7314/APJCP.2014.15.17.7015.
Jo, A. *et al.* (2015) 'Efficient mitochondrial genome editing by CRISPR/Cas9', *BioMed Research International*, 2015. doi: 10.1155/2015/305716.
Johns, D. R. and Neufeld, M. J. (1991) 'Cytochrome b mutations in Leber hereditary optic neuropathy', *Biochemical and Biophysical Research Communications*, 181(3), pp. 1358–1364. doi: 10.1016/0006-291X(91)92088-2.
Johnston, I. G. *et al.* (2015) 'Stochastic modelling, bayesian inference, and new in vivo measurements elucidate the debated mtDNA bottleneck mechanism', *eLife*, 4(JUNE2015), pp. 1–44. doi: 10.7554/eLife.07464.
Joost, H.-G. and Thorens, B. (2001) 'The extended GLUT-family of sugar/polyol transport facilitators: nomenclature, sequence characteristics, and potential function of its novel members', *Molecular Membrane Biology*, 18(4), pp. 247–256. doi: 10.1080/09687680110090.
Jossé, L. *et al.* (2016) 'MTORC1 signalling and eIF4E/4E-BP1 translation initiation factor stoichiometry influence recombinant protein productivity from GSCHOK1 cells', *Biochemical Journal*, 473(24), pp. 4651–4664. doi: 10.1042/BCJ20160845.
Just, R. S., Irwin, J. A. and Parson, W. (2015) 'Mitochondrial DNA heteroplasmy in the emerging field of massively parallel sequencing', *Forensic Science International: Genetics*, 18, pp. 131–139. doi: 10.1016/j.fsigen.2015.05.003.
Kandul, N. P. *et al.* (2016) 'Selective removal of deletion-bearing mitochondrial DNA in heteroplasmic Drosophila', *Nature Communications*, 7, pp. 1–11. doi: 10.1038/ncomms13100.
Kang, E. *et al.* (2016) 'Age-related accumulation of somatic mitochondrial DNA

mutations in adult-derived human ipscs', *Cell Stem Cell*, 18(5), pp. 625–636. doi: 10.1016/j.stem.2016.02.005.
Kao, F. T. and Puck, T. T. (1967) 'Genetics of somatic mammalian cells. IV. Properties of Chinese hamster cell mutants with respect to the requirement for proline.', *Genetics*, 55(3), pp. 513–524. doi: 10.1093/genetics/55.3.513.
Kao, F. T. and Puck, T. T. (1968) 'Genetics of Somatic Mammalian Cells , VII . Induction and Isolation of Nutritional Mutants in Chinese Hamster Cells Author (s): Fa-Ten Kao and Theodore T . Puck Source : Proceedings of the National Academy of Sciences of the United States of America , P', *Proceedings of the National Academy of Sciences of the United States of America*, 60(4), pp. 1275–1281. Available at: https://www.jstor.org/stable/59040.
Karch, J. *et al.* (2019) 'Inhibition of mitochondrial permeability transition by deletion of the ANT family and CypD', *Science Advances*, 5(8), pp. 1–7. doi: 10.1126/sciadv.aaw4597.
Karengera, E. *et al.* (2018) 'Concomitant reduction of lactate and ammonia accumulation in fed-batch cultures: Impact on glycoprotein production and quality', *Biotechnology Progress*, 34(2), pp. 494–504. doi: 10.1002/btpr.2607.
Karlsson, L. *et al.* (2019) 'Constitutive PGC-1α overexpression in skeletal muscle does not protect from age-dependent decline in neurogenesis', *Scientific Reports*, 9(1), pp. 1–11. doi: 10.1038/s41598-019-48795-w.
Katajisto, P. *et al.* (2015) 'Asymmetric apportioning of aged mitochondria between daughter cells is required for stemness', *Science*, 348(6232), pp. 340–343. doi: 10.1126/science.1260384.
Kaufman, R. J. and Malhotra, J. D. (2014) 'Calcium trafficking integrates endoplasmic reticulum function with mitochondrial bioenergetics', *Biochimica et Biophysica Acta - Molecular Cell Research*, 1843(10), pp. 2233–2239. doi: 10.1016/j.bbamcr.2014.03.022.
Kaushik, P. *et al.* (2020) 'LC-MS/MS-based quantitative proteomic and phosphoproteomic analysis of CHO-K1 cells adapted to growth in glutamine-free media', *Biotechnology Letters*, 42(12), pp. 2523–2536. doi: 10.1007/s10529-020-02953-7.
Kelly, P. S. *et al.* (2014) 'Bioprocess engineering: micromanaging Chinese hamster ovary cell phenotypes', *Pharmaceutical Bioprocessing*, 2(4), pp. 323–337. doi:

10.4155/pbp.14.28.
Kelly, P. S., Gallagher, C., *et al.* (2015) 'Conserved microRNA function as a basis for Chinese hamster ovary cell engineering', *Biotechnology Letters*, 37(4), pp. 787–798. doi: 10.1007/s10529-014-1751-7.
Kelly, P. S., Breen, L., *et al.* (2015) 'Re-programming CHO cell metabolism using miR-23 tips the balance towards a highly productive phenotype', *Biotechnology Journal*, 10(7), pp. 1029–1040. doi: 10.1002/biot.201500101.
Kelly, P. S. *et al.* (2016) 'Process-relevant concentrations of the leachable bDtBPP impact negatively on CHO cell production characteristics', *Biotechnology Progress*, 32(6), pp. 1547–1558. doi: 10.1002/btpr.2345.
Kelly, P. S. *et al.* (2017) 'Ultra-deep next generation mitochondrial genome sequencing reveals widespread heteroplasmy in Chinese hamster ovary cells', *Metabolic Engineering*, 41(January), pp. 11–22. doi: 10.1016/j.ymben.2017.02.001.
Kelly, P. S. *et al.* (2018) 'From media to mitochondria–rewiring cellular energy metabolism of Chinese hamster ovary cells for the enhanced production of biopharmaceuticals', *Current Opinion in Chemical Engineering*, 22, pp. 71–80. doi: 10.1016/j.coche.2018.08.009.
Kelly, P. S. *et al.* (2019) 'Improvements in single-use bioreactor film material composition leads to robust and reliable Chinese hamster ovary cell performance', *Biotechnology Progress*, 35(4), pp. 1–17. doi: 10.1002/btpr.2824.
Keogh, M. J. and Chinnery, P. F. (2015) 'Mitochondrial DNA mutations in neurodegeneration', *Biochimica et Biophysica Acta - Bioenergetics*, 1847(11), pp. 1401–1411. doi: 10.1016/j.bbabio.2015.05.015.
Kim, S. H. and Lee, G. M. (2007) 'Down-regulation of lactate dehydrogenase-A by siRNAs for reduced lactic acid formation of Chinese hamster ovary cells producing thrombopoietin', *Applied Microbiology and Biotechnology*, 74(1), pp. 152–159. doi: 10.1007/s00253-006-0654-5.
Kim, Y. G. *et al.* (2009) 'Effect of Bcl-xL overexpression on apoptosis and autophagy in recombinant Chinese hamster ovary cells under nutrient-deprived condition', *Biotechnology and Bioengineering*, 103(4), pp. 757–766. doi: 10.1002/bit.22298.
Klingenberg, M. (2008) 'The ADP and ATP transport in mitochondria and its carrier', *Biochimica et Biophysica Acta - Biomembranes*, 1778(10), pp. 1978–2021. doi: 10.1016/j.bbamem.2008.04.011.

Kou, T. C. *et al.* (2011) 'Detailed understanding of enhanced specific productivity in Chinese hamster ovary cells at low culture temperature', *Journal of Bioscience and Bioengineering*, 111(3), pp. 365–369. doi: 10.1016/j.jbiosc.2010.11.016.
Kovářová, N. *et al.* (2012) 'Adaptation of respiratory chain biogenesis to cytochrome c oxidase deficiency caused by SURF1 gene mutations', *Biochimica et Biophysica Acta - Molecular Basis of Disease*, 1822(7), pp. 1114–1124. doi: 10.1016/j.bbadis.2012.03.007.
Krasich, R. and Copeland, W. C. (2017) 'DNA polymerases in the mitochondria: A critical review of the evidence', *Frontiers in Bioscience - Landmark*, 22(4), pp. 692–709. doi: 10.2741/4510.
Larsson, N. G. *et al.* (1990) 'Progressive increase of the mutated mitochondrial DNA fraction in kearns-sayre syndrome', *Pediatric Research*, 28(2), pp. 131–136. doi: 10.1203/00006450-199008000-00011.
Le, A. *et al.* (2010) 'Inhibition of lactate dehydrogenase A induces oxidative stress and inhibits tumor progression', *Proceedings of the National Academy of Sciences of the United States of America*, 107(5), pp. 2037–2042. doi: 10.1073/pnas.0914433107.
Le, H. *et al.* (2015) 'Cell line development for biomanufacturing processes: recent advances and an outlook', *Biotechnology Letters*, 37(8), pp. 1553–1564. doi: 10.1007/s10529-015-1843-z.
Lee, J. S. *et al.* (2015) 'Site-specific integration in CHO cells mediated by CRISPR/Cas9 and homology-directed DNA repair pathway', *Scientific Reports*, 5, pp. 1–11. doi: 10.1038/srep08572.
Legros, F. *et al.* (2001) 'Functional characterization of novel mutations in the human cytochrome b gene', *European Journal of Human Genetics*, 9(7), pp. 510–518. doi: 10.1038/sj.ejhg.5200678.
Leong, D. S. Z. *et al.* (2017) 'Evaluation and use of disaccharides as energy source in protein-free mammalian cell cultures', *Scientific Reports*, 7(November 2016), pp. 1–10. doi: 10.1038/srep45216.
Leong, D. S. Z. *et al.* (2018) 'Application of maltose as energy source in protein-free CHO-K1 culture to improve the production of recombinant monoclonal antibody', *Scientific Reports*, 8(1), pp. 1–12. doi: 10.1038/s41598-018-22490-8.
Lewis, N. E. *et al.* (2013) 'Genomic landscapes of Chinese hamster ovary cell lines as revealed by the Cricetulus griseus draft genome', *Nature Biotechnology*, 31(8), pp. 759–

765. doi: 10.1038/nbt.2624.
Li, W. *et al.* (2016) 'MicroRNA-495 regulates starvation-induced autophagy by targeting ATG3', *FEBS Letters*, 590(6), pp. 726–738. doi: 10.1002/1873-3468.12108.
Liberti, M. V. and Locasale, J. W. (2016) 'The Warburg Effect: How Does it Benefit Cancer Cells?', *Trends in Biochemical Sciences*, 41(3), pp. 211–218. doi: 10.1016/j.tibs.2015.12.001.
Lim, S. F. *et al.* (2006) 'RNAi suppression of Bax and Bak enhances viability in fed-batch cultures of CHO cells', *Metabolic Engineering*, 8(6), pp. 509–522. doi: 10.1016/j.ymben.2006.05.005.
Locasale, J. W. and Cantley, L. C. (2011) 'Metabolic flux and the regulation of mammalian cell growth', *Cell Metabolism*, 14(4), pp. 443–451. doi: 10.1016/j.cmet.2011.07.014.
Logarušić, M. *et al.* (2021) 'Protein Hydrolysates from Flaxseed Oil Cake as a Media Supplement in CHO Cell Culture', *Resources*, 10(6), p. 59. doi: 10.3390/resources10060059.
Lunt, S. Y. and Vander Heiden, M. G. (2011) 'Aerobic glycolysis: Meeting the metabolic requirements of cell proliferation', *Annual Review of Cell and Developmental Biology*, 27, pp. 441–464. doi: 10.1146/annurev-cellbio-092910-154237.
Ma, H. and O'Farrell, P. H. (2016) 'Selfish drive can trump function when animal mitochondrial genomes compete', *Nature Genetics*, 48(7), pp. 798–802. doi: 10.1038/ng.3587.
Maekawa, M. *et al.* (1990) 'Molecular characterization of genetic mutation in human lactate dehydrogenase-A (M) deficiency', *Biochemical and Biophysical Research Communications*, 168(2), pp. 677–682. doi: 10.1016/0006-291X(90)92374-9.
Martinez-Lopez, J. E. *et al.* (2021) 'Transfection of miR-31* boosts oxidative phosphorylation metabolism in the mitochondria and enhances recombinant protein production in Chinese hamster ovary cells', *Journal of Biotechnology*, 333(November 2020), pp. 86–96. doi: 10.1016/j.jbiotec.2021.04.012.
Martínez-Monge, I. *et al.* (2019) 'Concomitant consumption of glucose and lactate: A novel batch production process for CHO cells', *Biochemical Engineering Journal*, 151. doi: 10.1016/j.bej.2019.107358.
Martínez, V. S. *et al.* (2013) 'Flux balance analysis of CHO cells before and after a metabolic switch from lactate production to consumption', *Biotechnology and*

Bioengineering, 110(2), pp. 660–666. doi: 10.1002/bit.24728.
Martínez, V. S. *et al.* (2015) 'Dynamic metabolic flux analysis using B-splines to study the effects of temperature shift on CHO cell metabolism', *Metabolic Engineering Communications*, 2, pp. 46–57. doi: 10.1016/j.meteno.2015.06.001.
Matthews, T. E. *et al.* (2016) 'Closed loop control of lactate concentration in mammalian cell culture by Raman spectroscopy leads to improved cell density, viability, and biopharmaceutical protein production', *Biotechnology and Bioengineering*, 113(11), pp. 2416–2424. doi: 10.1002/bit.26018.
Mazzio, E. *et al.* (2020) 'Whole-transcriptome analysis of fully viable energy efficient glycolytic-null cancer cells established by double genetic knockout of lactate dehydrogenase A/B or glucose-6-phosphate isomerase', *Cancer Genomics and Proteomics*, 17(5), pp. 469–497. doi: 10.21873/CGP.20205.
McDonald, S. A. C. *et al.* (2006) 'Clonal expansion in the human gut: Mitochondrial DNA mutations show us the way', *Cell Cycle*, 5(8), pp. 808–811. doi: 10.4161/cc.5.8.2641.
McDonnell, S. (2015) 'Production of Antibodies in Hybridoma and Non-hybridoma Cell Lines', *Animal Cell Culture. Cell Engineering*, 9, pp. 65–88. doi: 10.1007/978-3-319-10320-4_3.
McHugh, K. P. *et al.* (2020) 'Effective temperature shift strategy development and scale confirmation for simultaneous optimization of protein productivity and quality in Chinese hamster ovary cells', *Biotechnology Progress*, 36(3), pp. 1–11. doi: 10.1002/btpr.2959.
Meirhaeghe, A. *et al.* (2003) 'Characterization of the human, mouse and rat PGC1β (peroxisomeproliferator-activated receptor-γ co-activator 1β) gene in vitro and in vivo', *Biochemical Journal*, 373(1), pp. 155–165. doi: 10.1042/BJ20030200.
Meleady, P. *et al.* (2011) 'Sustained productivity in recombinant Chinese Hamster Ovary (CHO) cell lines: Proteome analysis of the molecular basis for a process-related phenotype', *BMC Biotechnology*, 11. doi: 10.1186/1472-6750-11-78.
Mirebeau-Prunier, D. *et al.* (2010) 'Estrogen-related receptor α and PGC-1-related coactivator constitute a novel complex mediating the biogenesis of functional mitochondria', *FEBS Journal*, 277(3), pp. 713–725. doi: 10.1111/j.1742-4658.2009.07516.x.
Möller, J. *et al.* (2021) 'Regulation of pyruvate dehydrogenase complex related to

lactate switch in CHO cells', *Engineering in Life Sciences*, 21(3–4), pp. 100–114. doi: 10.1002/elsc.202000037.
Monnot, S. *et al.* (2011) 'Segregation of mtDNA throughout human embryofetal development: M.3243A>G as a model system', *Human Mutation*, 32(1), pp. 116–125. doi: 10.1002/humu.21417.
Moore, A. *et al.* (1997) 'Effects of temperature shift on cell cycle, apoptosis and nucleotide pools in CHO cell batch cultues', *Cytotechnology*, 23(1–3), pp. 47–54. doi: 10.1023/a:1007919921991.
Moraes, C. T. *et al.* (1989) 'Heteroplasmy of mitochondrial genomes in clonal cultures from patients with Kearns-Sayre syndrome', *Biochemical and Biophysical Research Communications*, 160(2), pp. 765–771. doi: 10.1016/0006-291X(89)92499-6.
Morgada, M. N. *et al.* (2015) 'Loop recognition and copper-mediated disulfide reduction underpin metal site assembly of CuA in human cytochrome oxidase', *Proceedings of the National Academy of Sciences of the United States of America*, 112(38), pp. 11771–11776. doi: 10.1073/pnas.1505056112.
Morrow, R. M. *et al.* (2017) 'Mitochondrial energy deficiency leads to hyperproliferation of skeletal muscle mitochondria and enhanced insulin sensitivity', *Proceedings of the National Academy of Sciences of the United States of America*, 114(10), pp. 2705–2710. doi: 10.1073/pnas.1700997114.
Mou, C. *et al.* (2015) 'PGC-1-Related Coactivator (PRC) Is an Important Regulator of Microglia M2 Polarization', *Journal of Molecular Neuroscience*, 55(1), pp. 69–75. doi: 10.1007/s12031-014-0315-6.
Mulukutla, B. C. *et al.* (2015) 'Multiplicity of steady states in glycolysis and shift of metabolic state in cultured mammalian cells', *PLoS ONE*, 10(3), pp. 1–20. doi: 10.1371/journal.pone.0121561.
Murphy, M. P. (2009) 'How mitochondria produce reactive oxygen species', *Biochemical Journal*, 417(1), pp. 1–13. doi: 10.1042/BJ20081386.
Naciri, M., Kuystermans, D. and Al-Rubeai, M. (2008) 'Monitoring pH and dissolved oxygen in mammalian cell culture using optical sensors', *Cytotechnology*, 57(3), pp. 245–250. doi: 10.1007/s10616-008-9160-1.
Najm, F. J. *et al.* (2018) 'Orthologous CRISPR-Cas9 enzymes for combinatorial genetic screens', *Nature Biotechnology*, 36(2), pp. 179–189. doi: 10.1038/nbt.4048.
Nissanka, N. and Moraes, C. T. (2020) ' Mitochondrial DNA heteroplasmy in disease

and targeted nuclease-based therapeutic approaches ', *EMBO reports*, 21(3), pp. 1–12. doi: 10.15252/embr.201949612.

O'Callaghan, P. M. *et al.* (2015) 'Diversity in host clone performance within a Chinese hamster ovary cell line', *Biotechnology Progress*, 31(5), pp. 1187–1200. doi: 10.1002/btpr.2097.

Odet, F. *et al.* (2008) 'Expression of the gene for mouse lactate dehydrogenase C (Ldhc) is required for male fertility', *Biology of Reproduction*, 79(1), pp. 26–34. doi: 10.1095/biolreprod.108.068353.

Ogata, N. *et al.* (2021) 'Single-cell transcriptome analyses reveal heterogeneity in suspension cultures and clonal markers of CHO-K1 cells', *Biotechnology and Bioengineering*, 118(2), pp. 944–951. doi: 10.1002/bit.27624.

Pan, S. *et al.* (2015) 'Downregulation of adenine nucleotide translocator 1 exacerbates tumor necrosis factor-α-mediated cardiac inflammatory responses', *American Journal of Physiology - Heart and Circulatory Physiology*, 308(1), pp. H39–H48. doi: 10.1152/ajpheart.00330.2014.

Partridge, M. A., Davidson, M. M. and Hei, T. K. (2007) 'The complete nucleotide sequence of Chinese hamster (Cricetulus griseus) mitochondrial DNA', *DNA Sequence - Journal of DNA Sequencing and Mapping*, 18(5), pp. 341–346. doi: 10.1080/10425170601101287.

Pascucci, B. *et al.* (2021) 'Drp1 inhibition rescues mitochondrial integrity and excessive apoptosis in cs-a disease cell models', *International Journal of Molecular Sciences*, 22(13), pp. 1–18. doi: 10.3390/ijms22137123.

Pickles, S., Vigié, P. and Youle, R. J. (2018) 'Mitophagy and Quality Control Mechanisms in Mitochondrial Maintenance', *Current Biology*, 28(4), pp. R170–R185. doi: 10.1016/j.cub.2018.01.004.

Potter, M., Newport, E. and Morten, K. J. (2016) 'The Warburg effect: 80 years on', *Biochemical Society Transactions*, 44(5), pp. 1499–1505. doi: 10.1042/BST20160094.

Protasoni, M. and Zeviani, M. (2021) 'Mitochondrial structure and bioenergetics in normal and disease conditions', *International Journal of Molecular Sciences*, 22(2), pp. 1–55. doi: 10.3390/ijms22020586.

Puigserver, P. *et al.* (1998) 'A cold-inducible coactivator of nuclear receptors linked to adaptive thermogenesis', *Cell*, 92(6), pp. 829–839. doi: 10.1016/S0092-8674(00)81410-5.

Qian, Y. *et al.* (2011) 'Cell culture and gene transcription effects of copper sulfate on Chinese hamster ovary cells', *Biotechnology Progress*, 27(4), pp. 1190–1194. doi: 10.1002/btpr.630.
Rafferty, C. *et al.* (2020) 'Analysis of chemometric models applied to Raman spectroscopy for monitoring key metabolites of cell culture', *Biotechnology Progress*, 36(4), pp. 1–16. doi: 10.1002/btpr.2977.
Rahman, S. *et al.* (2001) 'Decrease of 3243 A→G mtDNA mutation from blood in MELAS syndrome: A longitudinal study', *American Journal of Human Genetics*, 68(1), pp. 238–240. doi: 10.1086/316930.
Rajasimha, H. K., Chinnery, P. F. and Samuels, D. C. (2008) 'Selection against Pathogenic mtDNA Mutations in a Stem Cell Population Leads to the Loss of the 3243A→G Mutation in Blood', *American Journal of Human Genetics*, 82(2), pp. 333–343. doi: 10.1016/j.ajhg.2007.10.007.
Rajendra, Y. *et al.* (2012) 'Reduced glutamine concentration improves protein production in growth-arrested CHO-DG44 and HEK-293E cells', *Biotechnology Letters*, 34(4), pp. 619–626. doi: 10.1007/s10529-011-0809-z.
Rana, A. *et al.* (2017) 'Promoting Drp1-mediated mitochondrial fission in midlife prolongs healthy lifespan of Drosophila melanogaster', *Nature Communications*, 8(1). doi: 10.1038/s41467-017-00525-4.
Reddy, P. *et al.* (2015) 'Selective elimination of mitochondrial mutations in the germline by genome editing', *Cell*, 161(3), pp. 459–469. doi: 10.1016/j.cell.2015.03.051.
Restelli, V. *et al.* (2006) 'The effect of dissolved oxygen on the production and the glycosylation profile of recombinant human erythropoietin produced from CHO cells', *Biotechnology and Bioengineering*, 94(3), pp. 481–494. doi: 10.1002/bit.20875.
Reznik, E. *et al.* (2016) 'Mitochondrial DNA copy number variation across human cancers', *eLife*, 5(FEBRUARY2016), pp. 1–20. doi: 10.7554/eLife.10769.
Ritacco, F. V., Wu, Y. and Khetan, A. (2018) 'Cell culture media for recombinant protein expression in Chinese hamster ovary (CHO) cells: History, key components, and optimization strategies', *Biotechnology Progress*, 34(6), pp. 1407–1426. doi: 10.1002/btpr.2706.
Robinson, N. J., Picken, A. and Coopman, K. (2014) 'Low temperature cell pausing: An alternative short-term preservation method for use in cell therapies including stem cell

applications', *Biotechnology Letters*, 36(2), pp. 201–209. doi: 10.1007/s10529-013-1349-5.

Roche, T. E. *et al.* (2001) 'Distinct regulatory properties of pyruvate dehydrogenase kinase and phosphatase isoforms', *Progress in Nucleic Acid Research and Molecular Biology*, 70. doi: 10.1016/s0079-6603(01)70013-x.

Rodriguez, J. *et al.* (2005) 'Enhanced production of monomeric interferon-β by CHO cells through the control of culture conditions', *Biotechnology Progress*, 21(1), pp. 22–30. doi: 10.1021/bp049807b.

Ross, J. M. *et al.* (2010) 'High brain lactate is a hallmark of aging and caused by a shift in the lactate dehydrogenase A/B ratio', *Proceedings of the National Academy of Sciences of the United States of America*, 107(46), pp. 20087–20092. doi: 10.1073/pnas.1008189107.

Rouzier, C. *et al.* (2012) 'The MFN2 gene is responsible for mitochondrial DNA instability and optic atrophy "plus" phenotype', *Brain*, 135(1), pp. 23–34. doi: 10.1093/brain/awr323.

Rugolo, M., Zanna, C. and Ghelli, A. M. (2021) 'Organization of the respiratory supercomplexes in cells with defective complex III: Structural features and metabolic consequences', *Life*, 11(4). doi: 10.3390/life11040351.

Salazar, A., Keusgen, M. and Von Hagen, J. (2016) 'Amino acids in the cultivation of mammalian cells', *Amino Acids*, 48(5), pp. 1161–1171. doi: 10.1007/s00726-016-2181-8.

Sallevelt, S. C. E. H. *et al.* (2016) 'De novo mtDNA point mutations are common and have a low recurrence risk', *Journal of Medical Genetics*, 54(2), pp. 114–124. doi: 10.1136/jmedgenet-2016-103876.

Sanchez, N. *et al.* (2014) 'CHO cell culture longevity and recombinant protein yield are enhanced by depletion of miR-7 activity via sponge decoy vectors', *Biotechnology Journal*, 9(3), pp. 396–404. doi: 10.1002/biot.201300325.

Sandra R. Bacman, Sion L. Williams, Milena Pinto, and C. T. M. (2014) 'The Use of Mitochondria-Targeted Endonucleases to Manipulate mtDNA', *Methods Enzymol.*, 547, pp. 373–397. doi: doi:10.1016/B978-0-12-801415-8.00018-7.

Sandri, M. *et al.* (2006) 'PGC-1α protects skeletal muscle from atrophy by suppressing FoxO3 action and atrophy-specific gene transcription', *Proceedings of the National Academy of Sciences of the United States of America*, 103(44), pp. 16260–16265. doi:

10.1073/pnas.0607795103.
Sarantos, K. and Cleo, K. (2013) ‘Analysis of the landscape of biologically-derived pharmaceuticals in Europe: Dominant production systems, molecule types on the rise and approval trends’, *European Journal of Pharmaceutical Sciences*, 48(3), pp. 428–441. doi: 10.1016/j.ejps.2012.11.016.
Scahill, S. J. *et al.* (1983) ‘Expression and characterization of the product of a human immune interferon cDNA gene in Chinese hamster ovary cells.’, *Proceedings of the National Academy of Sciences of the United States of America*, 80(15), pp. 4654–4658. doi: 10.1073/pnas.80.15.4654.
Scarpulla, R. C., Vega, R. B. and Kelly, D. P. (2012) ‘Transcriptional integration of mitochondrial biogenesis’, *Trends in Endocrinology and Metabolism*, 23(9), pp. 459–466. doi: 10.1016/j.tem.2012.06.006.
Schägger, H. (2001) ‘Respiratory chain supercomplexes’, *IUBMB Life*, 52(3–5), pp. 119–128. doi: 10.1080/15216540152845911.
Schmidt, C. *et al.* (2021) ‘Lactoyl leucine and isoleucine are bioavailable alternatives for canonical amino acids in cell culture media’, *Biotechnology and Bioengineering*. doi: 10.1002/bit.27755.
Seth, G. *et al.* (2006) ‘Engineering cells for cell culture bioprocessing - Physiological fundamentals’, *Advances in Biochemical Engineering/Biotechnology*, 101(June), pp. 119–164. doi: 10.1007/10_017.
Shah, R. R. *et al.* (2016) ‘Evaluating the toxicity of bDtBPP on CHO-K1 cells for testing of single-use bioprocessing systems considering media selection, cell culture volume, mixing, and exposure duration’, *Biotechnology Progress*, 32(5), pp. 1318–1323. doi: 10.1002/btpr.2322.
Shanware, N. P. *et al.* (2014) ‘Glutamine deprivation stimulates mTOR-JNK-dependent chemokine secretion’, *Nature Communications*, 5, pp. 1–13. doi: 10.1038/ncomms5900.
Shoubridge, E. A. and Wai, T. (2007) ‘Mitochondrial DNA and the Mammalian Oocyte’, *Current Topics in Developmental Biology*, 77(06), pp. 87–111. doi: 10.1016/S0070-2153(06)77004-1.
Smeitink, J., Van Den Heuvel, L. and DiMauro, S. (2001) ‘The genetics and pathology of oxidative phosphorylation’, *Nature Reviews Genetics*, 2(5), pp. 342–352. doi: 10.1038/35072063.
Śmiech, A. *et al.* (2019) ‘Heteroplasmic mutations and polymorphisms in the cyb gene

of mitochondrial DNA in canine mast cell tumours', *In Vivo*, 33(1), pp. 57–63. doi: 10.21873/invivo.11439.
Smirnova, Elena *et al.* (2001) 'Drp1 Is Required for Mitochondrial Division in Mammalian Cells', *Molecular Biology of the Cell*, 12(August), pp. 2245–2256. Available at: https://www.ncbi.nlm.nih.gov/pmc/articles/PMC58592/pdf/mk0801002245.pdf.
Smirnova, E. *et al.* (2001) 'Dynamin-related protein Drp1 is required for mitochondrial division in mammalian cells', *Molecular Biology of the Cell*, 12(8), pp. 2245–2256. doi: 10.1091/mbc.12.8.2245.
Spearman, M. *et al.* (2014) 'The bioactivity and fractionation of peptide hydrolysates in cultures of CHO cells', *Biotechnology Progress*, 30(3), pp. 584–593. doi: 10.1002/btpr.1930.
Stewart, J. B. and Chinnery, P. F. (2015) 'The dynamics of mitochondrial DNA heteroplasmy: Implications for human health and disease', *Nature Reviews Genetics*, 16(9), pp. 530–542. doi: 10.1038/nrg3966.
Subramaniam, V. *et al.* (2008) 'MITOCHIP assessment of differential gene expression in the skeletal muscle of Ant1 knockout mice: Coordinate regulation of OXPHOS, antioxidant, and apoptotic genes', *Biochimica et Biophysica Acta - Bioenergetics*, 1777(7–8), pp. 666–675. doi: 10.1016/j.bbabio.2008.03.015.
Sun, H. *et al.* (2019) 'Warburg Effects in Cancer and Normal Proliferating Cells: Two Tales of the Same Name', *Genomics, Proteomics and Bioinformatics*, 17(3), pp. 273–286. doi: 10.1016/j.gpb.2018.12.006.
Sun, M. J. *et al.* (2019) 'Changes in the PGC-1α and mtDNA copy number may play a role in the development of pelvic organ prolapse in pre-menopausal patients', *Taiwanese Journal of Obstetrics and Gynecology*, 58(4), pp. 526–530. doi: 10.1016/j.tjog.2019.05.017.
Sunley, K., Tharmalingam, T. and Butler, M. (2008) 'CHO cells adapted to hypothermic growth produce high yields of recombinant β-interferon', *Biotechnology Progress*, 24(4), pp. 898–906. doi: 10.1002/btpr.9.
Synoground, B. F. *et al.* (2021) 'Transient ammonia stress on Chinese hamster ovary (CHO) cells yield alterations to alanine metabolism and IgG glycosylation profiles', *Biotechnology Journal*, (February), pp. 1–13. doi: 10.1002/biot.202100098.
Tabuchi, H. *et al.* (2010) 'Overexpression of taurine transporter in Chinese hamster

ovary cells can enhance cell viability and product yield, while promoting glutamine consumption', *Biotechnology and Bioengineering*, 107(6), pp. 998–1003. doi: 10.1002/bit.22880.

Tabuchi, H. and Sugiyama, T. (2013) 'Cooverexpression of alanine aminotransferase 1 in Chinese hamster ovary cells overexpressing taurine transporter further stimulates metabolism and enhances product yield', *Biotechnology and Bioengineering*, 110(8), pp. 2208–2215. doi: 10.1002/bit.24881.

Takasu, T. *et al.* (2019) 'In Vitro Pharmacological Profile of Ipragliflozin, a Sodium Glucose Co-transporter 2 Inhibitor', *Biological and Pharmaceutical Bulletin*, 42(3), pp. 507–511. doi: 10.1248/bpb.b18-00728.

Tam, Z. Y. *et al.* (2015) 'Context-Dependent Role of Mitochondrial Fusion-Fission in Clonal Expansion of mtDNA Mutations', *PLoS Computational Biology*, 11(5), pp. 1–23. doi: 10.1371/journal.pcbi.1004183.

Taylor, R. W. *et al.* (2003) 'Mitochondrial DNA mutations in human colonic crypt stem cells', *Journal of Clinical Investigation*, 112(9), pp. 1351–1360. doi: 10.1172/JCI19435.

Templeton, N. *et al.* (2013) 'Peak antibody production is associated with increased oxidative metabolism in an industrially relevant fed-batch CHO cell culture', *Biotechnology and Bioengineering*, 110(7), pp. 2013–2024. doi: 10.1002/bit.24858.

Templeton, N. *et al.* (2014) 'The impact of anti-apoptotic gene Bcl-2Δ expression on CHO central metabolism', *Metabolic Engineering*, 25, pp. 92–102. doi: 10.1016/j.ymben.2014.06.010.

Thompson, L. H. and Baker, R. M. (1973) 'Isolation of mutants of cultured mammalian cells', *Methods in cell Biollogy*, 6(7), pp. 209–281. Available at: https://doi.org/10.1016/S0091-679X(08)60052-7.

Tiranti, V. *et al.* (1998) 'A novel mutation in the mitochondrial tRNA(Val) gene associated with a complex neurological presentation', *Annals of Neurology*, 43(1), pp. 98–101. doi: 10.1002/ana.410430116.

Torrano, V. *et al.* (2016) 'The metabolic co-regulator PGC1α suppresses prostate cancer metastasis', *Nature Cell Biology*, 18(6), pp. 645–656. doi: 10.1038/ncb3357.

Torres, M. *et al.* (2018) 'Mild hypothermia upregulates myc and xbp1s expression and improves anti-TNFα production in CHO cells', *PLoS ONE*, 13(3). doi: 10.1371/journal.pone.0194510.

Torres, M. *et al.* (2019) 'Metabolic flux analysis during galactose and lactate co-

consumption reveals enhanced energy metabolism in continuous CHO cell cultures', *Chemical Engineering Science*, 205, pp. 201–211. doi: 10.1016/j.ces.2019.04.049.
Torres, M. *et al.* (2021) 'Temperature Down-Shift Modifies Expression of UPR-/ERAD-Related Genes and Enhances Production of a Chimeric Fusion Protein in CHO Cells', *Biotechnology Journal*, 16(2), pp. 1–11. doi: 10.1002/biot.202000081.
Torres, M., Altamirano, C. and Dickson, A. J. (2018) 'Process and metabolic engineering perspectives of lactate production in mammalian cell cultures', *Current Opinion in Chemical Engineering*, 22, pp. 184–190. doi: 10.1016/j.coche.2018.10.004.
Toyoshima, Y., Tanaka, Y. and Satomi, K. (2017) 'MELAS syndrome associated with a new mitochondrial tRNA-Val gene mutation (m.1616A>G)', *BMJ Case Reports*, 2017(1), pp. 10–13. doi: 10.1136/bcr-2017-220934.
Trifunovic, A. *et al.* (2004) 'Premature ageing in mice expressing defective mitochondrial DNA polymerase', *Nature*, 429(6990), pp. 417–423. doi: 10.1038/nature02517.
Tucker, E. J. *et al.* (2013) 'Mutations in the UQCC1-Interacting Protein, UQCC2, Cause Human Complex III Deficiency Associated with Perturbed Cytochrome b Protein Expression', *PLoS Genetics*, 9(12). doi: 10.1371/journal.pgen.1004034.
Urlaub, G. *et al.* (1983) 'Deletion of the diploid dihydrofolate reductase locus from cultured mammalian cells', *Cell*, 33(2), pp. 405–412. doi: 10.1016/0092-8674(83)90422-1.
Urlaub, G. and Chasin, L. A. (1980) 'Isolation of Chinese hamster cell mutants deficient in dihydrofolate reductase activity', *Proceedings of the National Academy of Sciences of the United States of America*, 77(7 II), pp. 4216–4220. doi: 10.1073/pnas.77.7.4216.
Uusimaa, J. *et al.* (2007) 'Prevalence, segregation, and phenotype of the mitochondrial DNA 3243A>G mutation in children', *Annals of Neurology*, 62(3), pp. 278–287. doi: 10.1002/ana.21196.
Valcarcel-Jimenez, L. *et al.* (2019) 'PGC1a suppresses prostate cancer cell invasion through ERRA transcriptional control', *Cancer Research*, 79(24), pp. 6153–6165. doi: 10.1158/0008-5472.CAN-19-1231.
Valdés-Bango Curell, R. and Barron, N. (2018) 'Exploring the Potential Application of Short Non-Coding RNA-Based Genetic Circuits in Chinese Hamster Ovary Cells', *Biotechnology Journal*, 13(10), pp. 1–8. doi: 10.1002/biot.201700220.
Valvona, C. J. *et al.* (2016) 'The Regulation and Function of Lactate Dehydrogenase A:

Therapeutic Potential in Brain Tumor', *Brain Pathology*, 26(1), pp. 3–17. doi: 10.1111/bpa.12299.
Vial, J. *et al.* (2020) 'Low expression of ANT1 confers oncogenic properties to rhabdomyosarcoma tumor cells by modulating metabolism and death pathways', *Cell Death Discovery*, 6(1), pp. 1–13. doi: 10.1038/s41420-020-00302-1.
Vidoni, S. *et al.* (2017) 'MR-1S Interacts with PET100 and PET117 in Module-Based Assembly of Human Cytochrome c Oxidase', *Cell Reports*, 18(7), pp. 1727–1738. doi: 10.1016/j.celrep.2017.01.044.
Vodopivec, I. *et al.* (2016) 'Mitochondrial encephalopathy and optic neuropathy due to m.10158 MT-ND3 complex I mutation presenting in an adult patient: Case report and review of the literature', *Neurologist*, 21(4), pp. 61–65. doi: 10.1097/NRL.0000000000000084.
Wakabayashi, H. *et al.* (1996) 'Hereditary deficiency of lactate dehydrogenase H-subunit', *Internal Medicine*, 35(7), pp. 550–554. doi: 10.2169/internalmedicine.35.550.
Wallace, D. C. (2013) 'A mitochondrial bioenergetic etiology of disease', *Journal of Clinical Investigation*, 123(4), pp. 1405–1412. doi: 10.1172/JCI61398.
Walsh, G. (2018) 'Biopharmaceutical benchmarks 2018', *Nature Biotechnology*, 36(12), pp. 1136–1145. doi: 10.1038/nbt.4305.
Wang, K. *et al.* (2009) 'Mitochondrial ND3 as the novel causative gene for Leber hereditary optic neuropathy and dystonia', *Neurogenetics*, 10(4), pp. 337–345. doi: 10.1007/s10048-009-0194-0.
Wang, W. *et al.* (2012) 'Mitochondrial fission triggered by hyperglycemia is mediated by ROCK1 activation in podocytes and endothelial cells', *Cell Metabolism*, 15(2), pp. 186–200. doi: 10.1016/j.cmet.2012.01.009.
White, S. L. *et al.* (1999) 'Mitochondrial DNA mutations at nucleotide 8993 show a lack of tissue- or age-related variation', *Journal of Inherited Metabolic Disease*, 22(8), pp. 899–914. doi: 10.1023/A:1005639407166.
Wilkens, C. A. *et al.* (2019) 'An LDHa single allele CHO cell mutant exhibits altered metabolic state and enhanced culture performance', *Journal of Chemical Technology and Biotechnology*, 94(5), pp. 1488–1498. doi: 10.1002/jctb.5906.
Wilkens, C. A., Altamirano, C. and Gerdtzen, Z. P. (2011) 'Comparative metabolic analysis of lactate for CHO cells in glucose and galactose', *Biotechnology and Bioprocess Engineering*, 16(4), pp. 714–724. doi: 10.1007/s12257-010-0409-0.

Wilkens, C. A. and Gerdtzen, Z. P. (2015) ‘Comparative metabolic analysis of CHO cell clones obtained through cell engineering, for IgG productivity, growth and cell longevity’, *PLoS ONE*, 10(3), pp. 1–15. doi: 10.1371/journal.pone.0119053.
Wlaschin, K. F. and Hu, W. S. (2007) ‘Engineering cell metabolism for high-density cell culture via manipulation of sugar transport’, *Journal of Biotechnology*, 131(2), pp. 168–176. doi: 10.1016/j.jbiotec.2007.06.006.
Wonnapinij, P., Chinnery, P. F. and Samuels, D. C. (2008) ‘The Distribution of Mitochondrial DNA Heteroplasmy Due to Random Genetic Drift’, *American Journal of Human Genetics*, 83(5), pp. 582–593. doi: 10.1016/j.ajhg.2008.10.007.
Wurm, F. M. (2013) ‘CHO quasispecies-Implications for manufacturing processes’, *Processes*, 1(3), pp. 296–311. doi: 10.3390/pr1030296.
Wurm, F. M. and Wurm, M. J. (2017) ‘Cloning of CHO Cells, productivity and genetic stability-a discussion’, *Processes*, 5(2). doi: 10.3390/pr5020020.
Wurm, M. J. and Wurm, F. M. (2021) ‘Naming CHO cells for bio-manufacturing’, *Biotechnology Journal*, 16(7), p. 2100165. doi: 10.1002/biot.202100165.
Xiang, F. *et al.* (2019) ‘Tumor necrosis factor receptor-associated protein 1 regulates hypoxia-induced apoptosis through a mitochondria-dependent pathway mediated by cytochrome c oxidase subunit II’, *Burns and Trauma*, 7, pp. 1–11. doi: 10.1186/s41038-019-0154-3.
Xiong, K. *et al.* (2019) ‘Reduced apoptosis in Chinese hamster ovary cells via optimized CRISPR interference’, *Biotechnology and Bioengineering*, 116(7), pp. 1813–1819. doi: 10.1002/bit.26969.
Xu, S. *et al.* (2018) ‘Probing lactate metabolism variations in large-scale bioreactors’, *Biotechnology Progress*, 34(3), pp. 756–766. doi: 10.1002/btpr.2620.
Xu, X. *et al.* (2011) ‘The genomic sequence of the Chinese hamster ovary (CHO)-K1 cell line’, *Nature Biotechnology*, 29(8), pp. 735–741. doi: 10.1038/nbt.1932.
Yip, S. S. M. *et al.* (2014) ‘Complete knockout of the lactate dehydrogenase A gene is lethal in pyruvate dehydrogenase kinase 1, 2, 3 down-regulated CHO cells’, *Molecular Biotechnology*, 56(9), pp. 833–838. doi: 10.1007/s12033-014-9762-0.
Yoneda, M. *et al.* (1992) ‘Marked replicative advantage of human mtDNA carrying a point mutation that causes the MELAS encephalomyopathy’, *Proceedings of the National Academy of Sciences of the United States of America*, 89(23), pp. 11164–11168. doi: 10.1073/pnas.89.23.11164.

Yoon, S. K., Song, J. Y. and Lee, G. M. (2003) ‘Effect of low culture temperature on specific productivity, transcription level, and heterogeneity of erythropoietin in Chinese hamster ovary cells’, *Biotechnology and Bioengineering*, 82(3), pp. 289–298. doi: 10.1002/bit.10566.

Young, J. D. (2013) ‘Metabolic flux rewiring in mammalian cell cultures’, *Current Opinion in Biotechnology*, 24(6), pp. 1108–1115. doi: 10.1016/j.copbio.2013.04.016.

Yu, H. *et al.* (2012) ‘Gene delivery to mitochondria by targeting modified adenoassociated virus suppresses Leber’s hereditary optic neuropathy in a mouse model’, *Proceedings of the National Academy of Sciences of the United States of America*, 109(20). doi: 10.1073/pnas.1119577109.

Yuk, I. H. *et al.* (2014) ‘Effects of copper on CHO cells: Insights from gene expression analyses’, *Biotechnology Progress*, 30(2), pp. 429–442. doi: 10.1002/btpr.1868.

Zagari, F. *et al.* (2013) ‘Lactate metabolism shift in CHO cell culture: The role of mitochondrial oxidative activity’, *New Biotechnology*, 30(2), pp. 238–245. doi: 10.1016/j.nbt.2012.05.021.

Zboray, K. *et al.* (2015) ‘Heterologous protein production using euchromatin-containing expression vectors in mammalian cells’, *Nucleic Acids Research*, 43(16), pp. 1–14. doi: 10.1093/nar/gkv475.

Ždralević, M. *et al.* (2018) ‘Double genetic disruption of lactate dehydrogenases A and B is required to ablate the “Warburg effect” restricting tumor growth to oxidative metabolism’, *Journal of Biological Chemistry*, 293(41), pp. 15947–15961. doi: 10.1074/jbc.RA118.004180.

Zhang, F. *et al.* (2006) ‘Metabolic characteristics of recombinant Chinese hamster ovary cells expressing glutamine synthetase in presence and absence of glutamine’, *Cytotechnology*, 51(1), pp. 21–28. doi: 10.1007/s10616-006-9010-y.

Zhang, H., Burr, S. P. and Chinnery, P. F. (2018) ‘The mitochondrial DNA genetic bottleneck: Inheritance and beyond’, *Essays in Biochemistry*, 62(3), pp. 225–234. doi: 10.1042/EBC20170096.

Zhang, S. *et al.* (2017) ‘PGC-1 alpha interacts with microRNA-217 to functionally regulate breast cancer cell proliferation’, *Biomedicine and Pharmacotherapy*, 85, pp. 541–548. doi: 10.1016/j.biopha.2016.11.062.

Zhang, X. *et al.* (2018) ‘Enhanced production of anti-PD1 antibody in CHO cells through transient co-transfection with anti-apoptotic genes Bcl-xL and Mcl-1’,

Bioprocess and Biosystems Engineering, 41(5), pp. 633–640. doi: 10.1007/s00449-018-1898-z.

Zhang, X. *et al.* (2020) 'Feeding tricarboxylic acid cycle intermediates improves lactate consumption and antibody production in Chinese hamster ovary cell cultures', *Biotechnology Progress*, 36(4), pp. 1–9. doi: 10.1002/btpr.2975.

Zhang, Y. *et al.* (2018) 'PGC1β Organizes the Osteoclast Cytoskeleton by Mitochondrial Biogenesis and Activation', *Journal of Bone and Mineral Research*, 33(6), pp. 1114–1125. doi: 10.1002/jbmr.3398.

Zhou, M. *et al.* (2011) 'Decreasing lactate level and increasing antibody production in Chinese Hamster Ovary cells (CHO) by reducing the expression of lactate dehydrogenase and pyruvate dehydrogenase kinases', *Journal of Biotechnology*, 153(1–2), pp. 27–34. doi: 10.1016/j.jbiotec.2011.03.003.

Zinovkina, L. A. (2018) 'Mechanisms of Mitochondrial DNA Repair in Mammals', *Biochemistry (Moscow)*, 83(3), pp. 233–249. doi: 10.1134/S0006297918030045.

Annex A: Supplemental Figures

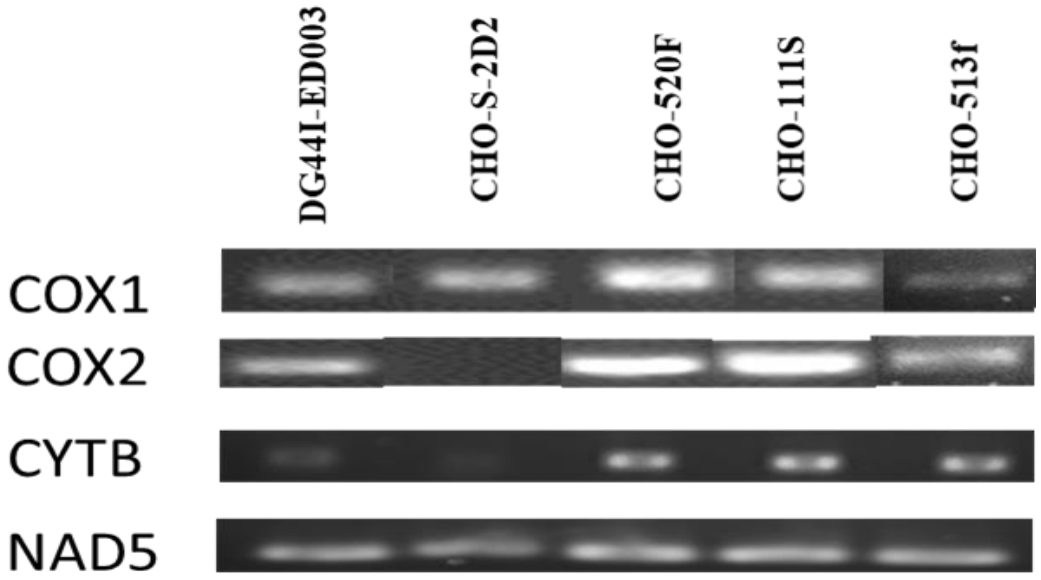

Supplementary Figure 1. PCR performed using CYTB, NAD5, COX1 and COX2 targeted primers using a standard PCR (MyTaq2x). Samples were run for 40 minutes in a 1% agarose gel. Primers were observed to work as expected in the samples in interest. The primers were observed to amplify bands of the expected size in most of the clones. Curiously, amplification of the samples from CHO-S-2D2, clones in which heteroplasmy variants for both COX2 and CYTB have not been observed, did not show a band for COX2 and only a very faint band was observed for CYTB. Regardless, the primers were proven to amplify the expected band size in the samples from the main clones of interest (520F, 111S, 513F), and therefore qPCR was performed.

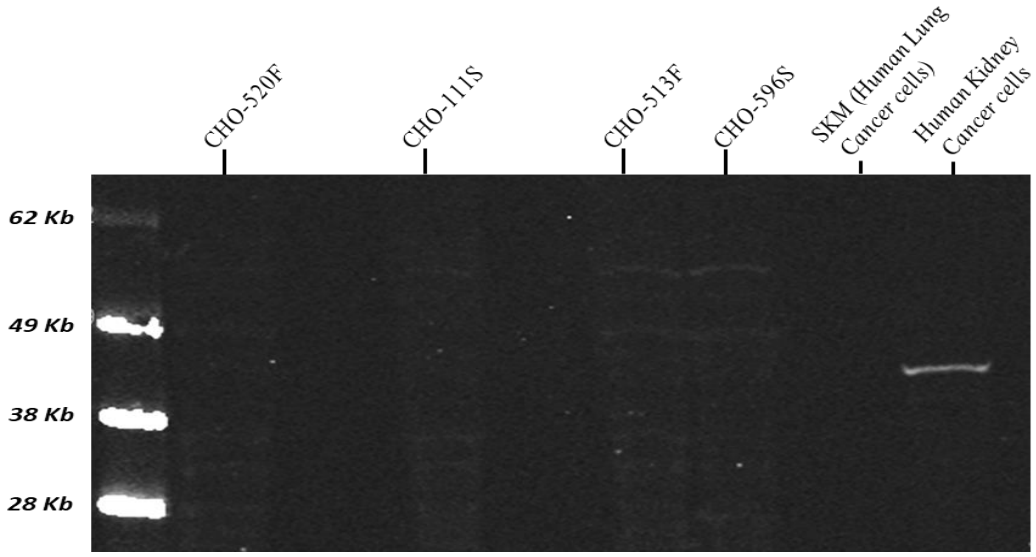

Supplementary Figure 3. Western blot performed using Anti-cytochrome b antibody c-terminal. Total lysis from CHO clones 520F, 111S, 513 and 596S. Human lung cancer derived cell lines lysate (SKMES) and human kidney cancer cell line lysate, were used as control samples in this assay. The CYTB protein expression was measured in CHO cell clones CHO-520F, CHO-111S, CHO-513F, and CHO-596S, looking for any differences potentially caused by these heteroplasmic mutations. CHO cell clone CHO-DG44i-ED003 was used as a control like in the transcriptomic experiments, as these cells did not show the heteroplasmic mutations in CYTB as seen in the previous sections. The OXPHOS cocktail antibody was previously shown to not work efficiently in CHO cells. For this reason, a more specific ``anti-cytochrome b antibody c-terminal´´ (Abcam #182330) which targets cytochrome b specifically, was used for this set of western blot experiments. The Anti-cytochrome b antibody was unable to detect hamster CYTB, despite both hamster and human mitochondrial CYTB protein being 90% identical. A specific band at the expected size of 45KD only appeared in a lysate of human kidney cells, which was used as an example in the Abcam website, but no band appeared when used in human lung cancer cell lysate. For this reason, due to the unavailability of reliable commercial antibodies targeting specifically the mitochondrially encoded subunit of CYTB in CHO cells, no reliable data could be obtained concerning the effects of heteroplasmy in mitochondrial CYTB protein expression. It is worth mentioning that the limited availability of detection antibodies with verified cross-reactivity is a common challenge when performing analysis of protein expression in CHO cells.

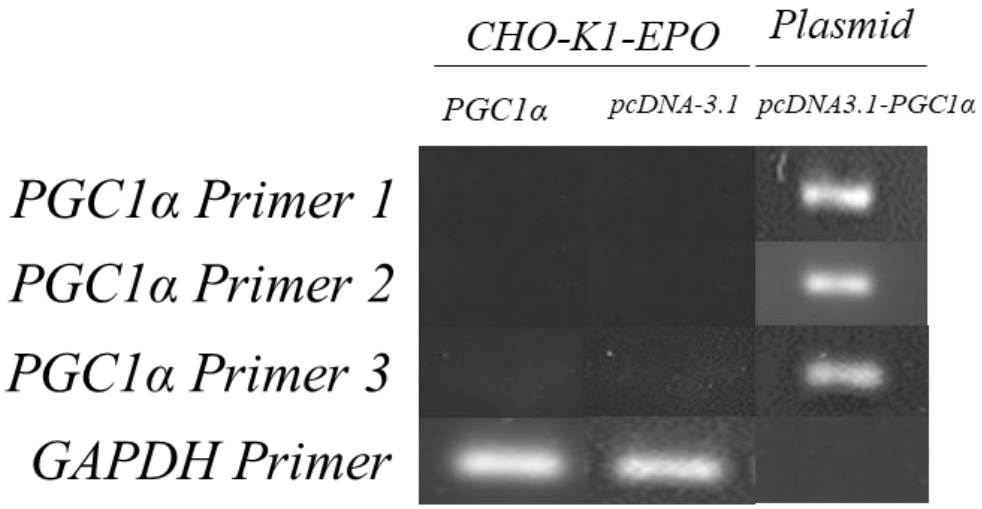

Supplementary Figure 4. Agarose gel (0,8%) containing the amplified PCR products of CHO-K1-EPO-PGC1α and CHO-K1-EPO-pcDNA 3.1 cell lines cDNA, which was produced by performing an RT-PCR in the mRNA extracted from the mentioned CHO-K1-EPO cell lines. Plasmid samples were included as positive control. GAPDH primers were also used to check the amount of DNA in the samples. 3 different sets of PGC1α primers were used, designed to target different sequences in both the mouse and the Chinese hamster versions of PGC1α gene.

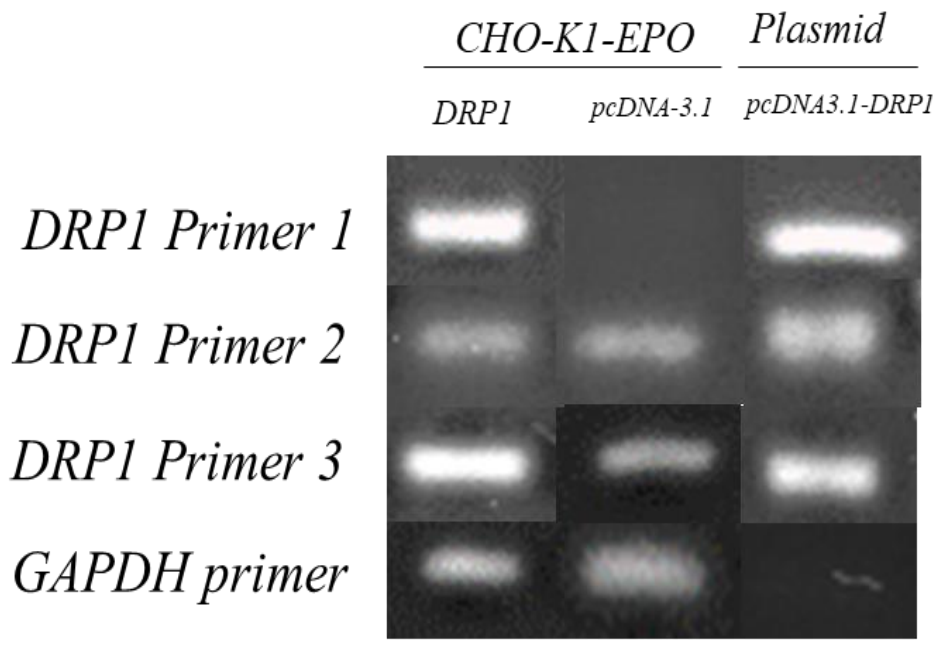

Supplementary Figure 5. Agarose gel (0,8%) containing the amplified PCR products of CHO-K1-EPO-DRP1 and CHO-K1-EPO-pcDNA 3.1 cell lines cDNA, which was produced by performing an RT-PCR in the mRNA extracted from the mentioned CHO-K1-EPO cell lines. Non-RT controls were included to rule out false positives. Plasmid samples were included as positive control. GAPDH primers were also used to check the amount of DNA in the samples. 3 different sets of DRP1 primers were used: DRP1 (P1) targeted both the mouse and the Chinese Hamster version of DRP1. DRP1 (P2) was also designed to target both mouse and Chinese hamster,but was directed towards a different point in the sequence. Finally, the final set of primers, DRP1 (P3) was designed to target only the mouse version of the sequence. All the primers were successful in detecting DRP1 expression in both the plasmid and the CHO-K1-EPO-DRP1 cells. However, DRP1 (P1) was unable to detect the endogenous DRP1 expression from pcDNA control cells, despite being designed to target both mouse and hamster sequences. Conversely, DRP1 (P3), despite being designed to detect only the mouse sequence, was able to pick up the endogenous hamster sequence. Regardless, these results showed DRP1 being expressed in CHO-K1-EPO-DRP1 cells, but also in CHO-K1-EPO-pcDNA 3.1 in an endogenous manner. Therefore, actual overexpression could not be confirmed without performing a qPCR experiment in CHO-K1-EPO-DRP1 samples.

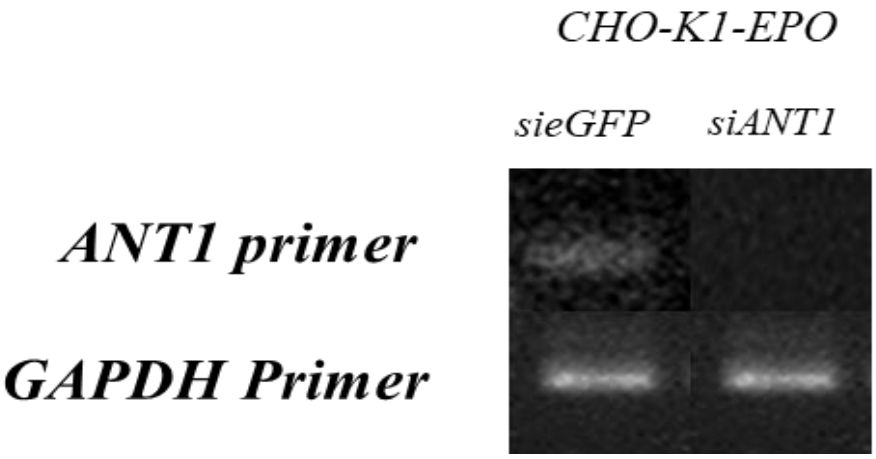

Supplementary Figure 6. Agarose 0,8% gel containing the PCR products of CHO-K1-EPO-siANT1 and CHO-K1-EPO-sieGFP amplified with ANT1 primers and GAPDH primers. GAPDH primers were also used to check the equal presence of DNA in the samples. It must be noted that, in the control cells, the ANT1 appeared as a faint band, which may be indicating a low base level of expression in CHO-K1-EPO cells.